Development of antibody-functionalised biomaterials for cancer immunotherapy

Karolina Dziemidowicz

A thesis submitted for the degree of
DOCTOR OF PHILOSOPHY

Department of Pharmaceutics
UCL School of Pharmacy
University College London

November 2020

Declaration

This thesis describes the research conducted in the UCL School of Pharmacy. I, Karolina Dziemidowicz, confirm that the work presented in this thesis is my own. Where information has been derived from other sources, I confirm that this has been indicated in the thesis.

……..

Karolina Dziemidowicz

Abstract

Protein-loaded biomaterials are generating considerable interest due to the growing importance of immunotherapy and tissue engineering in modern medicine. The complex and fragile structures of many therapeutic proteins require advanced delivery methods and careful optimisation of formulation and manufacturing conditions.

Electrohydrodynamic processes (EHD) are material fabrication techniques in which a polymer solution is drawn by the influence of an electrical field to produce solid micro-and nano scale fibres and particles. Multiple approaches have been proposed for the incorporation of therapeutic proteins in electrospun scaffolds, including surface functionalization and coaxial electrospinning. These concepts are introduced in **Chapter 1**.

This PhD thesis explores the EHD fabrication, functionalisation with therapeutically relevant proteins, and characterization of polycaprolactone (PCL) materials, with the aim of developing a platform protein delivery technology. Several protein loading methodologies were investigated on electrospun nanofibres and electrosprayed microparticles for applications relevant to regenerative medicine. The experimental procedures used are detailed in **Chapter 2**.

Chapter 3 explored the feasibility of surface functionalisation of electrospun PCL nanoscaffolds with proteins using perfluorophenyl azide chemistry. Examples of the conjugated biomolecules explored include bovine serum albumin, catalase and antibodies (infliximab and OKT3). The covalently conjugated catalase released from the fibres at a much slower rate than physically adsorbed catalase, revealing this approach to be suitable for safe and effective attachment of proteins to hydrocarbon-based biomaterials.

The next application explored is the fabrication of surface-functionalised anti-CD3 antibody-modified electrosprayed PCL microparticles, with the ultimate goal of achieving targeted T cell activation when the particles are injected intratumorally. Formulations were prepared by electrospraying PCL particles and subsequent surface functionalization using perfluorophenylazide chemistry (**Chapter 4**) and by using "click" chemistry to conjugate protein to azide-functionalised PCL (**Chapter 5**). The developed formulations were extensively characterised with *in vitro* T cell activation models. It was found that T cell activation can be achieved following stimulation with biomimetic electrosprayed microparticles prepared using either of the explored bioconjugation methods.

The final results chapter, **Chapter 6**, discusses the fabrication and characterisation of electrospun PCL patches loaded with a checkpoint inhibitor monoclonal antibody, ipilimumab. The coaxial electrospinning technology offers a simple solution for the fabrication of antibody-loaded biocompatible scaffolds that can be easily implanted at the desired site of action and release the therapeutic cargo in a sustained fashion. It was also found that electrospinning monoclonal antibodies near to their isoelectric point leads to improved process stability and enhanced protein encapsulation.

Impact statement

In recent years, increasing understanding of cancer immunology has led to greater interest in targeting the immune system in oncology therapies, leading to the emergence of a new therapeutic area – cancer immunotherapy. The field is rapidly developing, with many therapeutic agents in the drug discovery and development pipelines of major pharmaceutical companies.

Cancer immunotherapy can be broadly divided into two categories: cellular therapies and checkpoint inhibitor monoclonal antibodies. Although clinically promising, both treatment approaches possess inherent disadvantages. For example, high costs and the complexity of the manufacturing process of cellular therapies is a major limitation. The preparation of these highly personalised therapies is technically demanding and requires specialised centres. On the other hand, checkpoint inhibitors often cause serious immune-related side-effects due to the off-site toxicity.

The manufacturability issues associated with cell-based therapies may be addressed by employing scaffold-based delivery platforms capable of activating immune cells directly *in vivo*, without the need for multi-step *ex vivo* processing. It is also anticipated that biomaterials allowing more controlled and localised delivery of checkpoint inhibitors may be beneficial for minimising the off-target side-effects.

EHD offers a simple way of manufacturing drug-loaded implantable scaffolds, the properties of which can be tuned according to the therapeutic needs. One possible application of the EHD technology is the fabrication of antibody-loaded fibres for a localised delivery of checkpoint inhibitors. Moreover, electrosprayed or electrospun biomaterials can be surface-functionalised with proteins, for example with antibodies stimulating T cell activation in cancer immunotherapy applications.

It is anticipated that the platform technology generated in this research may provide researchers with new tools for surface immobilisation of proteins on polymeric

biomaterials, which may be beneficial for many biomedically relevant applications in tissue engineering and regenerative medicine. Moreover, the antibody-loaded scaffolds developed in this thesis could potentially widen the application of EHD processes into the cancer immunotherapy field.

Table of contents

List of figures

List of tables

List of abbreviations

aAPCs	Artificial antigen presenting cells
Ab	Antibody
ACT	Adoptive T cell therapy
AEO	2-(2-aminoethoxy)ethanol
ANOVA	Analysis of variance
APCs	Antigen presenting cells
bFGF	Basic fibroblast growth factor
BSA	Bovine serum albumin
BTS	NHS Blood and Transplant Service
CAR	Chimeric antigen receptor
CD	Cluster of differentiation
CFSE	Carboxyfluorescein succinimidyl ester
COX-2	cyclooxygenase-2
CTLA-4	Cytotoxic T lymphocyte-associated antigen 4
CuAAC	Copper(I)-catalysed azide-alkyne cycloaddition
DBCO	Dibenzocyclooctyne
DCs	Dendritic cells
DI	Deionised
DMEM	Dulbecco's Modified Eagle Medium
DMSO	Dimethyl sulfoxide
DPBS	Dulbecco’s phosphate-buffered saline
DSC	Differential scanning calorimetry
DTA	Diethylenetriamine
DTT	Dithiothreitol
EDC	1-ethyl-3-(3-dimethylaminopropyl)carbodiimide hydrochloride
EDC·HCl	N-(3-Dimethylaminopropyl)-N′-ethylcarbodiimide hydrochloride
EHD	Electrohydrodynamic
ELISA	Enzyme-linked immunosorbent assay

EMA	European Medicines Agency
FDA	Food and Drug Administration
FITC-BSA	Albumin–fluorescein isothiocyanate conjugate
FSC vs SSC	Forward versus side scatter
FTIR	Fourier-transform infrared spectroscopy
GFP	Green fluorescent protein
GM-CSF	Granulocyte macrophage-colony stimulating factor
GMP	Good Manufacturing Practice
IFNs	Interferons
IFN-γ	Interferon-γ
IgG	Immunoglobulin G
IL	Interleukin
iNKT	Immunostimulant-invariant natural killer T-cell
MHC	Major histocompatibility complex
NGF	nerve growth factor
NHS	National Health Service
NHS	N-hydroxysuccinimide
NHS-FITC	NHS-fluorescein
NICE	National Institute for Health and Care Excellence
NMR	Nuclear Magnetic Resonance
OD	Optical density
OGP	osteogenic growth peptide
PAP	Prostatic acid phosphatase
PBA	Protein blocking agent
PBMCs	Peripheral-blood mononuclear cells
PBS	Phosphate-buffered saline
PCL	Polycaprolactone
PD-1	Programmed cell death protein-1
PD-L1	Programmed death-ligand 1

PDO	Polydioxanone
PEG	Polyethylene glycol
PFPA	Perfluorophenyl azide
PGA	Polyglycolic acid
PLA	Polylactic acid
PLGA	Poly(lactic-co-glycolic acid)
PLHMGA	Poly(D,L-lactic-co-hydroxymethyl glycolic acid)
PLLA	Poly L-lactic acid
PRP	Platelet-rich plasma
PVP	Polyvinylpyrrolidone
scFv	Single chain variable fragment
SD	Standard deviation
SDS	Sodium dodecyl sulfate
SDS-PAGE	Sodium dodecyl sulfate–polyacrylamide gel electrophoresis
SEM	Scanning electron microscopy
SPAAC	Strain-promoted azide-alkyne cycloaddition
SPR	Surface plasmon resonance
Tc cells	Cytotoxic T cells
TCR	T cell receptor
TEM	Transmission electron microscopy
TFE	2,2,2–trifluoroethanol
TGF	Transforming growth factor
Th cells	T helper cells
TILs	Tumour infiltrating lymphocytes
TNF-α	Tumour necrosis factor-α
Treg cells	T regulatory cells
VEGF	Vascular endothelial growth factor
XPS	X-ray photoelectron spectroscopy
XRD	X-ray diffraction

Chapter 1 – Introduction

1.1 Role of the immune system in cancer

Until recently, oncology research focused largely on treating cancer as a single, genetic disease[1]. In 2000, *Hallmarks of Cancer*[2], the widely cited publication by Hanahan and Weinberg that extensively reviewed the most important publications in the oncology field, summarised six features that describe a cell as cancerous. These included: (1) resisting cell death, (2) inducing angiogenesis, (3) enabling replicative immortality, (4) activating invasion and metastasis, (5) evading growth suppressors and (6) sustaining proliferative signalling. Oncology research has progressed immensely since the early 2000s. Scientists now regard cancer as a group of systemic diseases, rather than an individual genetic condition, and the research focus has moved towards recognising the interaction between cancer and the host, and in particular, the host's immune system.

In the decade since the original *Hallmarks of Cancer* publication, four emerging cancer features were identified. In 2011, a follow-up review by the same authors described the mechanisms of immune destruction evasion as the recurring characteristic of most cancers[3,4]. Tumours have armed themselves with intricate protective mechanisms to escape immunosurveillance. During their development, malignant cells release an array of soluble factors, such as immunosuppressive cytokines, prostaglandins or vascular endothelial growth factor (VEGF), which facilitate their growth and protect them from the immune system[3,4].

Another emerging feature described by Hanahan and Weinberg is the existence of tumour-promoting inflammation in the cancer milieu. The immune system seems to play a paradoxical role in neoplasia (i.e. abnormal tissue growth). Through the action of tumour infiltrating lymphocytes (TILs), the immune system can suppress tumour growth by destroying malignant cells or inhibiting their proliferation. Conversely, it can facilitate cancer growth by providing favourable conditions within the tumour microenvironment[5].

1.1.1. Lymphocytes

It is now becoming clear that cells of the immune system, in particular cytotoxic and regulatory T lymphocytes, are involved in allowing malignancies to persist. Lymphocytes constitute about 20% of the total blood leukocytes[6]. The two major populations of lymphocytes are divided into T and B lymphocytes based on the origin of differentiation. B lymphocytes (B cells) are produced in the bone marrow and differentiate into plasma cells that produce soluble antibodies against antigens.

T lymphocytes (T cells), generated in the thymus, are essential for cell-mediated immunity and provide antigen-specific effector and immune memory responses. They can be distinguished from other lymphocytes by the presence of the T cell receptor (TCR). The stimulation of TCR is crucial for T cell activation and provocation of an immune response. Within the T cell population are several subpopulations of lymphocytes with specific immunological functions, which can be identified by the cluster of differentiation (CD) markers on the cell surface (Table 1-1).

Table 1-1: Cluster of Differentiation (CD) markers on lymphocytes.

CD Marker	Lymphocyte population
CD3+	All T cells
CD4+	Helper/amplifier population
CD4+, CD45RA+, CD30+	Th2 helper cells
CD4+, CD45RO+, CD30+	Th1 amplifier cells
CD4+, CD25+, FOXP3	T regulatory (Treg) cells
CD4+CCR4+CCR6+	Th17 helper cells
CD8+	Cytotoxic T cell population
CD8+ CD28-	Tc1 cells
CD8+ CD28+	Tc2 cells

1.1.2. Overview of T cell activation

In order to proliferate, perform effector functions and produce cytokines, T cells require activation by direct contact with antigen presenting cells (APCs) such as dendritic cells, B cells and macrophages.

Dendritic cells (DCs) are particularly important in T cell stimulation. Upon activation, DCs migrate to the lymphoid tissues, where they attract T and B cells by secreting chemokines and maintain the viability of existing T cell populations[7]. A schematic of early T cell activation is presented in Figure 1-1.

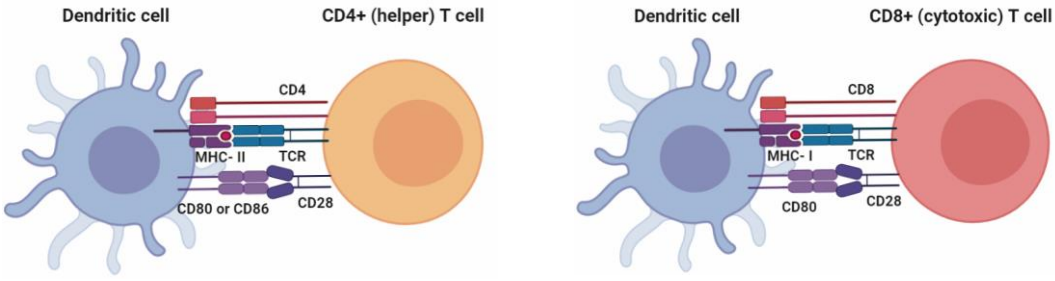

Figure 1-1: Overview of early T cell activation for CD4+ T cells (left panel) and CD8+ T cells (right panel). In Signal 1, the T cell encounters an antigen presenting region on a dendritic cell and binds the major histocompatibility complex (MHC) through TCR and CD4 or CD8. Signal 2, a co-stimulatory response, occurs through interactions with CD86 or CD80, achieving full activation and effector function in the T cell. This schematic was created with biorender.com.

Overall, T cell activation requires three signals. Signal 1 is facilitated by the interaction between the TCR, a multi-subunit transmembrane complex, and major histocompatibility complex (MHC) on the surface of the APC. Once the TCR binds to the antigen held in the MHC complex, the initial activation of T cells occurs. Accessory adhesion molecules, such as CD8 for MHC Class I and CD4 for MHC Class II are also expressed on the surface of T cells[8]. The interaction of naïve CD8+ T cells with the MHC Class I complex induces T cell proliferation and functional transformation into effector CD8+ T cells. Activation of CD4+ T (helper) cells, stimulated *via* MHC class II binding, prompts the synthesis of pro-inflammatory molecules (cytokines).

In Signal 2, co-stimulatory molecules such as CD28 and B7 (CD80, CD86) are essential for efficient TCR activation. CD28 is a co-stimulatory receptor present on 80% of CD4+ T cells and ~50% of CD8+ T cells[9]. The molecules B7-1 (CD80) and B7-2 (CD86) are expressed on many antigen-presenting cells and are the principal ligands for CD28. As an immunological synapse forms, CD28 is released from intracellular stores, where it enhances the initial weak signal from the TCR.

Both helper and cytotoxic T cells require secondary co-stimulatory signals to maintain an activated state. One response is regulated by an inhibitory molecule termed cytotoxic T lymphocyte-associated antigen 4 (CTLA-4)[10]. While B7-CD28 interaction triggers naïve T cell activation, CTLA-4 binding inhibits T cell proliferation and induces peripheral T cell tolerance.

CD8+ T cells rely on a CD28 response to a lesser extent and require additional stimulation from molecules such as CD70 and CD137 (also known as 4-1BB). Unlike CD28, CD137 ligands become expressed upon pathogen recognition, ensuring a cytotoxic T cell response only following interaction with a pathogen[11].

A third signal controls further cell programming, T cell survival and differentiation[12], and can be provided by distinct inflammatory cytokines. In CD8+ T cells, this stimulus can be provided by interleukin-12 (IL-12) or Type 1 interferons (IFNs), while CD4+ T cells respond to interleukin-1 (IL-1)[13]. Stimulation with all three signals triggers naïve T cell differentiation, increased proliferation, enhanced cytokine production (Figure 1-2) and the prevention of the activation of cellular death pathways[14,15].

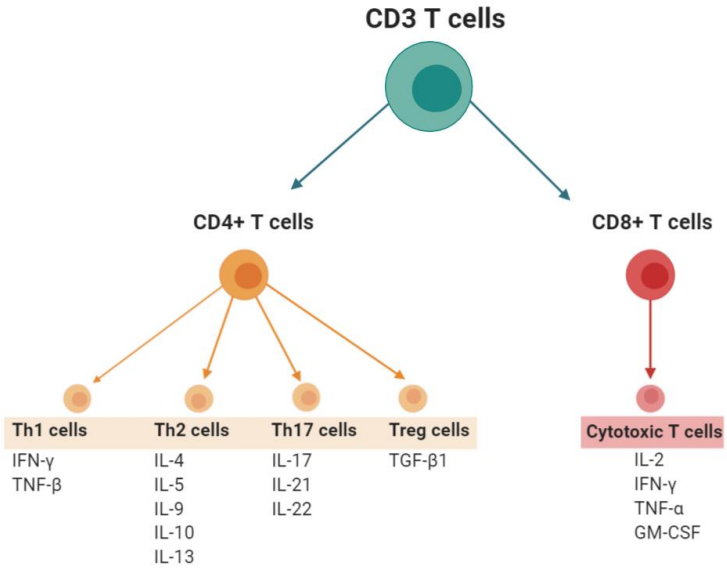

Figure 1-2: Schematic summarising the cytokines released by CD4+ and CD8+ T cell subsets. IFN – interferon, TNF- tumour necrosis factor, IL-interleukin, TGF- transforming growth factor GM-CSF- granulocyte macrophage-colony stimulating factor. This schematic was created with biorender.com.

Certain cancers are capable of paralysing infiltrating cytotoxic T cells by secreting immunosuppressive factors such as TGF-β or by recruiting immunosuppressive regulatory T cells[3,16,17]. An example of an immunosuppressive cytokine released by tumour cells is interleukin-10 (IL-10). It is a soluble factor predominantly secreted by regulatory T cells and is responsible for the inhibition of the CD4+ Th1 cell cytokine synthesis as well as the differentiation, maturation and function of DCs. The upregulation of IL-10 plays a dual role in cancer development as it both promotes

(by inhibiting the inflammatory T cell and macrophage responses) and inhibits (by inducing expansion of CD8+ T cells) tumour growth[18].

1.2 Cancer immunotherapy

The increasing understanding of cancer immunology has led to greater interest in targeting the immune system in oncology therapies. Immunotherapy is rapidly becoming a standard treatment modality in cancer, alongside surgery, radiotherapy and chemotherapy[19,20]. Cancer immunotherapy, or immuno-oncology, aims to improve the intrinsic ability of the body to generate effective immune responses against cancer. Many emerging cancer immunotherapies aim to promote tumour-specific T cell responses, and strongly rely on the mechanisms of T cell activation and regulation[21].

In 2013, *Science* selected cancer immunotherapy for the Breakthrough of the Year based on the recent developments in two particular areas – chimeric antigen receptor (CAR) engineering of T cells, and immune checkpoint inhibition[22]. Cancer immunotherapy is a fast-developing area of research, and currently can be broadly classified into two categories: checkpoint inhibitor monoclonal antibodies and cellular therapies. The latter include cancer vaccines, oncolytic virus therapies and adoptive cell transfers (Figure 1-3).

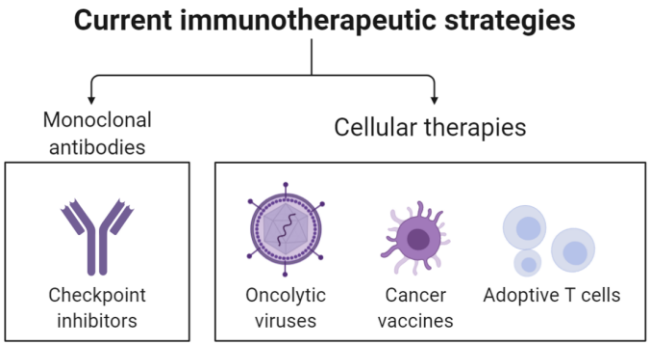

Figure 1-3: Summary of current immunotherapeutic strategies. This schematic was created with biorender.com.

1.2.1. Checkpoint inhibitors

T cell-mediated cellular responses are orchestrated by a balance of stimulatory and inhibitory proteins. The inhibitory molecules, often called checkpoint inhibitors, regulate function and activation of cytotoxic T cells in order to prevent autoimmunity[23]. Examples of checkpoint inhibitors relevant in oncology are CTLA-4 and programmed cell death protein 1 (PD-1). Blocking their expression can enhance immune-mediated tumour targeting by prolonging the action of activated T cells and reactivating cytotoxic T cells to target cancer[24]. Both CTLA-4 and PD-1 are present on the surface of activated T cells but upon interaction with their ligands, either on APCs (CTLA-4 binding to CD80/CD86) or tumour cells (PD-1 binding to PD-L1), they can elicit an antitumoural response (Figure 1-4)[25].

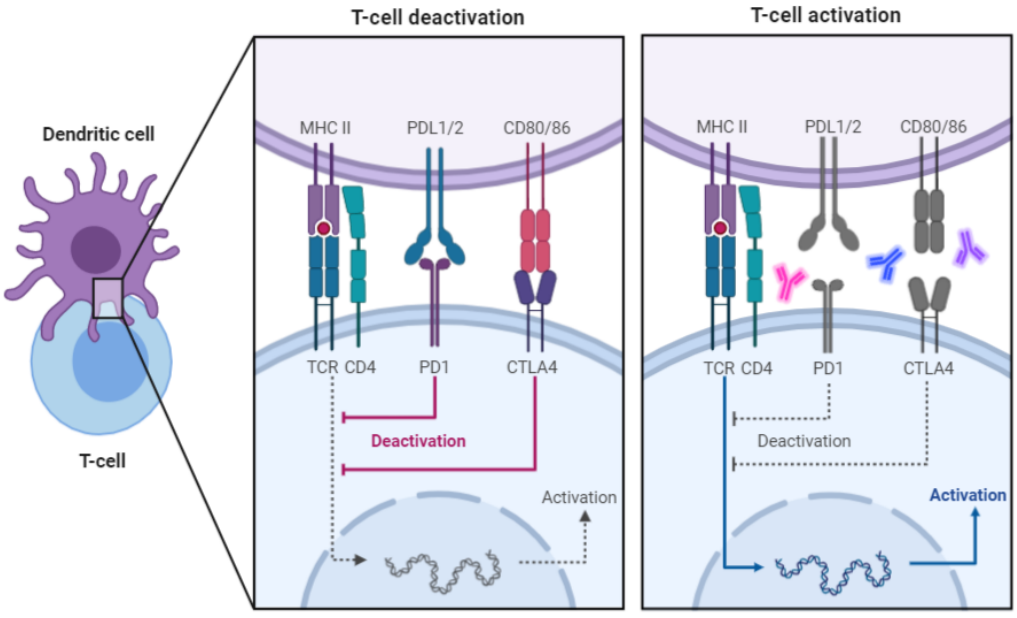

Figure 1-4: The role of CTLA-4 and PD-1 in T cell activation pathways. This schematic was created with biorender.com.

For this reason, monoclonal antibodies targeting immunoinhibitory interactions have been intensively explored in the past 20 years[23,24,26–29] and several checkpoint inhibitor treatments have been approved by the FDA (Table 1-2).

Table 1-2: FDA-approved list of checkpoint inhibitor therapies[30].

Name	Target	Indication
YERVOY (Ipilimumab)	Anti-CTLA-4	Melanoma, renal cell carcinoma
KEYTRUDA (Pembrolizumab)	Anti-PD-1	Melanoma, non-small-cell lung cancer, Hodgkin lymphoma, advanced gastric cancer, microsatellite instability-high cancer, head and neck cancer and advanced urothelial bladder cancer
OPDIVO (Nivolumab)	Anti-PD-1	Unresectable or metastatic melanoma, non-small cell lung cancer, metastatic small cell lung cancer, advanced renal cell carcinoma, Hodgkin lymphoma, head and neck squamous cell carcinoma, urothelial carcinoma, hepatocellular carcinoma
TECENTRIQ (Atezolizumab)	Anti-PD-L1	Metastatic non-small cell lung cancer, urothelial carcinoma, triple-negative breast cancer (in combination with paclitaxel)
BAVENCIO (Avelumab)	Anti-PD-L1	Metastatic Merkel cell carcinoma, urothelial carcinoma, renal cell carcinoma
IMFINZI (Durvalumab)	Anti-PD-L1	Unresectable stage III non-small cell lung cancer, urothelial carcinoma

1.2.1.1. CTLA-4

CTLA-4 is an inhibitory receptor responsible for downregulation of the initial T cell activation process that participates in physiological immune responses. Prior to T cell activation, CTLA-4 is an intracellular protein. Upon antigen-mediated engagement of the T cell receptor and a CD28 co-stimulatory signal, CTLA-4 migrates to the cell surface. There it competes with CD28 for binding to CD80 and CD86, thus inhibiting cytokine production, T cell activation and proliferation[31]. In the late 1990s and early 2000s, extensive research in the field revealed that blockage of the CTLA-4 pathway

could lead to tumour regression by preserving the antitumour activity of cytotoxic T cells[32,33].

This discovery led to the development of two monoclonal antibodies to CTLA-4, ipilimumab and tremelimumab, that entered clinical trials in 2000. Although capable of causing tumour regression, when administered systemically the treatments were associated with serious immune-mediated toxicities such as enterocolitis, inflammatory hepatitis and dermatitis[34]. Nevertheless, ipilimumab gained marketing authorisation in Europe and the United States as a first-line therapy for melanoma patients with metastatic disease based on phase III clinical trials showing improved patient survivability[35]. In 2011, Yervoy, the ipilimumab product currently owned by Bristol Myers Squibb, became the first checkpoint inhibitor treatment on the market.

1.2.1.2. PD-1 and PDL-1

Similarly to CTLA-4, PD-1 is largely expressed on the surface of activated immunosuppressing Treg cells and plays a pivotal role in T cell downregulation[23,36,37]. When a T cell recognises the antigen on the target cell, pro-inflammatory cytokines are produced, priming the inflammatory process. These cytokines cause PD-L1 expression in the tissue, which activates the PD-1 protein on the T cell. This leads to immune tolerance, where the immune system can no longer trigger the inflammatory response upon antigen-mediated activation. This pathway is particularly prominent in certain cancers, for example melanoma, where the tumour bypasses the immune system by overexpressing PD-L1[25].

Multiple studies have explored the use of monoclonal antibodies blocking PD-1 and PD-L1, since inhibition of the PD-1/PD-L1 pathway helps to maintain the function of effector T cells[23,25]. The first FDA and European Medicines Agency (EMA) authorisations of PD-1 monoclonal antibodies were pembrolizumab

and nivolumab, approved for the treatment of patients with refractory melanoma in 2014 and, in 2015, for patients with advanced non-small-cell lung carcinoma. The first anti–PD-L1 antibody approved was atezolizumab for urothelial cancers in 2016, followed by avelumab for Merkel cell carcinoma in 2017[28].

One of the largest obstacles facing checkpoint inhibitor monotherapies is the relatively low response rate in clinical trials. Response rate can be defined as the percentage of patients whose cancer decreases in size, or disappears, following treatment. To enhance the therapeutic efficacy, treatments are often explored in combination. For example, as a standalone therapy nivolumab achieved a 28% response rate in patients with melanoma[38]. This increased to 40% when combined with ipilimumab[39] and led to the approval of the combination treatment (ipilimumab and nivolumab) in 2018[26,40]. Recently, a dual checkpoint inhibition therapy developed by AstraZeneca (anti-PD-L1 durvalumab and anti-CTLA-4 tremelimumab) was granted orphan drug designation by the FDA for the treatment of hepatocellular carcinoma[41]. However, using combinations of immunomodulators leads to widespread systemic side effects due to nonspecific immune system activation[27,42,43].

Another major limitation of checkpoint inhibitory therapies is the time necessary for the immune system to become sufficiently activated to elicit an anti-tumour response. For patients with advanced cancers, only those who are predicted to survive for more than 6 months are expected to benefit from immune checkpoint inhibitor treatment[44].

1.2.2. Cellular therapies

Cell-based therapies aim to repair the mechanisms governing disease initiation and progression by stimulating or replacing cells. In the oncology context, T cell and dendritic cell therapies have been extensively explored. Cellular therapies hold great promise in regenerative oncology, but their clinical implementation is often hindered

by practical issues, such as production costs[45,46]. Nevertheless, several oncology cell therapies have gained FDA authorisation (Table 1-3) and are offered to patients at specialist treatment centres.

Table 1-3: FDA-approved oncology cell therapies[47].

Brand name	Generic name	Indication
IMLYGIC	Talimogene laherparepvec	Lesions in patients with melanoma recurrent after initial surgery
KYMRIAH	Tisagenlecleucel	Patients up to 25 years of age with B-cell precursor acute lymphoblastic leukemia that is refractory or in second or later relapse. Adult patients with relapsed or refractory large B-cell lymphoma after two or more lines of systemic therapy including diffuse large B-cell lymphoma (DLBCL) not otherwise specified, high grade B-cell lymphoma and DLBCL arising from follicular lymphoma.
PROVENGE	Sipuleucel-T	Asymptomatic or minimally symptomatic metastatic castrate resistant (hormone refractory) prostate cancer.
YESCARTA	Axicabtagene ciloleucel	Relapsed or refractory large B-cell lymphoma after two or more lines of systemic therapy.

1.2.2.1. Cancer vaccines

Theoretically, a therapeutic cancer vaccine would stimulate specific immune responses towards tumours without impacting healthy tissues. This immunomodulation could lead not only to the lysis of the existing tumour, but also prevent recurrent disease and metastasis through a systemic immunological memory[48].

To develop a successful cancer vaccine, several factors need to be considered. Firstly, an immunogenic tumour antigen that can be subsequently taken up and processed by mature APCs (primarily DCs) needs to be presented. In addition, to achieve full therapeutic efficacy the vaccine would require a favourable immune microenvironment within the tumour, with the presence of co-stimulatory signals and

the absence of inhibitory cues that will facilitate the proliferation and activation of Th1 and CD8+ T cells[49].

Dendritic cell vaccines are by far the most commonly researched class of cell-based cancer immunisations[50]. DCs are incredibly important in the cancer vaccination field due to their capacity to capture, process and present antigens to T cells[51]. A good example of a DC-based cancer vaccine is sipuleucel-T (Provenge), which consists of peripheral-blood mononuclear cells (PBMCs), including DCs, that have been activated *ex vivo* with a recombinant fusion protein containing prostatic acid phosphatase (PAP) fused to granulocyte-macrophage colony-stimulating factor (GM-CSF)[52]. PAP acts as a prostate antigen, while GM-CSF is a known T cell stimulator[53].

In 2014, Provenge gained marketing authorisation in the UK for the treatment of advanced prostate cancer. However, with the estimated cost being £47,132.68 per patient, the National Institute for Health and Care Excellence (NICE) did not recommend Provenge as a viable treatment option on the National Health Service (NHS)[54]. Consequently, the marketing authorisation was withdrawn by the European Medicines Agency (EMA) in 2015, following a request from the manufacturer, Dendreon UK Ltd. The product remains available in the US for the treatment of asymptomatic or minimally symptomatic metastatic castrate-resistant prostate cancer, but its clinical translation remains impeded by the manufacturing complexities and high costs[30].

1.2.2.2. Oncolytic virus therapies

Oncolytic viruses, which are viruses that specifically target cancer cells, are a relatively novel drug class with only one clinically registered example. Their antitumour effect relies on a dual mechanism. Firstly, oncolytic viruses are capable of selectively replicating within cancer cells, lysing them. Secondly, by releasing viral particles, the local infection within the tumour is amplified. This stimulates

the immune system, recruiting immune cells towards the cancer site[55,56]. Additionally, oncolytic viruses can be armed with T cell co-stimulatory molecules to favour intratumoural immune cell recruitment and activation[57,58].

In 2015, Imlygic (talimogene laherparepvec) became the first oncolytic immunotherapy approved by the FDA and EMA for 'the treatment of adults with melanoma that cannot be removed by surgery and that has spread either to the surrounding area or to other areas of the body'[59]. The preferred route of administration is a direct injection into the melanoma lesions. Imlygic is derived from a herpes simplex virus-1 (a common cold sore virus) that has been genetically modified to preferentially replicate within cancer cells by exploiting disrupted oncogenic and antiviral signalling pathways[60]. It is also capable of producing the immune-stimulating cytokine GM-CSF. The exact mechanism of action is not well understood, but recent research in the field has provided evidence for tumour-specific immunity being induced after the treatment with oncolytic viruses[60].

As of 2020, clinicaltrials.gov reports over 50 ongoing trials with 'oncolytic virus' as a keyword, testing their efficacy in a variety of tumours, including pancreatic cancer, glioblastoma or colorectal carcinoma[61]. It should be noted, however, that these trials usually explore a combination of checkpoint inhibitor and viral therapy, and the past decade has seen multiple failures of oncolytic viral monotherapies in phase III trials due to lack of clinical efficacy[62]. Paradoxically, the immune system often prevents the oncolytic virus therapy from reaching the desired efficacy levels. The initial host response to the virus frequently results in its rapid clearance, preventing viral replication and infection of a tumour cell at the level necessary for the initiation of an effective vaccination response[33,63].

Although oncolytic virus therapy has a relatively safe toxicity profile, extreme caution should be taken to prevent accidental viral contamination of the environment when

delivering the therapy in a healthcare setting[63]. Use is also limited to cancers accessible *via* intratumoural injection[63].

1.2.2.3. Adoptive cell therapies

Adoptive T cell therapy (ACT) involves harvesting cancer-specific lymphocytes from the patient, expanding and modifying them *ex vivo*, and re-infusing the cell product back into the bloodstream (Figure 1-5). While the cell product is processed *ex vivo*, the patient undergoes 'preparative lymphodepletion' to temporarily deactivate the regulatory T cells that mediate peripheral tolerance[64]. This improves the persistence and antitumour efficacy of infused lymphocytes and is often accomplished using chemotherapy alone or adjunct to total-body irradiation[65].

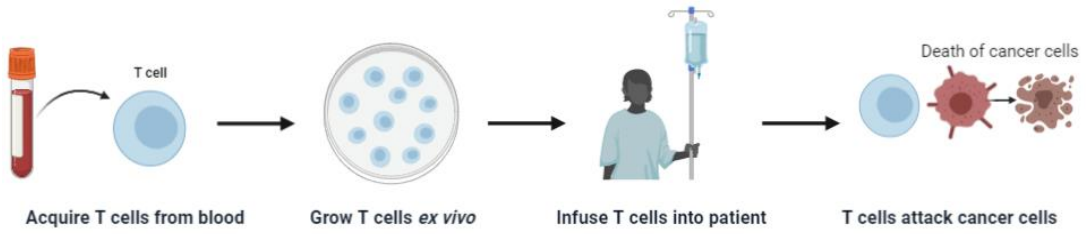

Figure 1-5: An overview of the adoptive T cell therapy procedure. This schematic was created with biorender.com.

After realising the potential of ACT, researchers worked towards amplifying antitumoural responses by modifying T cell receptors. Currently, research focuses on two genetic modifications: constructing T cells to express transgenic T cell receptors (TCRs) or chimeric antigen receptors (CARs). While TCRs require binding to MHC, CARs are modified with a single chain variable fragment (scFv), an antibody fragment which can target extracellular biomarkers on a cancerous cell without the need for MHC interaction[66,67]. CAR-T cell therapy research has progressed significantly further than the TCR approach, and two products have been recently approved by the FDA – Yescarta and Kymriah. However, global access to CAR-T cell

therapy remains hindered by high costs and the complexity of the manufacturing process, which is technically demanding and requires specialised centres[68].

1.3 Biomaterials in immunotherapy

While cancer immunotherapy is unquestionably a ground-breaking approach, it remains largely ineffective in the majority of cancer patients. It is estimated that with many tumours only ~15% of patients respond to immunomodulatory therapies[69]. Tumours are remarkably effective at overcoming immune barriers and building tolerance to immunotherapeutics, for example by modifying the signalling pathways and reducing the expression of genes responsible for T cell-mediated elimination of cancerous cells[70]. Breaking the local tumour immune tolerance without causing systemic toxicities or immune-related adverse events (such as colitis, myocarditis, pneumonitis or autoinflammatory processes) remains challenging, significantly delaying regulatory approval.

Selective activation of T cells in the local milieu of the tumour is conceptually interesting but challenging in terms of delivering a local stimulus capable of activating the T cell population for an appropriate duration of time without causing further toxicity. Using targeted implantable or injectable biomaterials could be a way of overcoming this issue[71].

The field of biomaterials has grown significantly in the past decade with the increasing importance of regenerative medicine and tissue engineering. The science of biomaterials combines medicine, chemistry, biology, physics and engineering, and recent years have seen considerable interest in biomaterial-assisted immunomodulation and cancer immunotherapy[72–78].

1.3.1. Biomaterial-assisted checkpoint inhibitor delivery

Although immunomodulatory antibodies are, in some patients, capable of inducing profound antitumour responses, their systemic delivery is often associated with cytokine release syndrome and abnormal liver function[79]. This off-site toxicity can be reduced by delivering checkpoint inhibitors in a localised and controlled fashion.

In one study, Rahimian et al.[80] focused on sustained delivery of anti-CTLA-4 and anti-CD40 encapsulated in polymer microparticles. The microspheres, prepared by a double emulsion method, were injected in mice near the site of the tumour and degraded completely within 60 days, releasing the two antibodies over 30 days. The initial burst release was minimal (1%) in microparticles containing a high percentage of the polymer. In an *in vivo* study, the antibodies encapsulated in microparticles showed lower local toxicity at the site of injection than the control (incomplete Freund's adjuvant), while the anti-tumour efficacy was comparable. To prepare the microparticles, the authors used a hydrophilic poly(D,L-lactic-co-hydroxymethyl glycolic acid) (PLHMGA), which is a derivative of the commonly used pharmaceutical polymer poly(lactic-co-glycolic acid) (PLGA). Upon degradation, PLHMGA showed lower acidification of the local environment than PLGA, therefore protecting the sensitive antibody cargo.

In 2017, Wang, Ye and Gu[81] designed biodegradable microneedle patches for localised delivery of anti-PD-1 in melanoma. The checkpoint inhibitor was encapsulated in nanoparticles and transported from the surface of microneedles through the epidermis to the interstitial fluid, delivering the cargo to the tumour site. Although promising for early-stage melanomas, the antibody-loaded microneedle patch has relatively low penetration depth (200 μm), and thus little application in deep tissue tumours[82].

Li et al.[83] described the localised delivery of anti-PD-1 and celecoxib from alginate hydrogels. Celecoxib, a cyclooxygenase-2 (COX-2) inhibitor, was expected to oppose the pro-inflammatory effects activated by PD-1 pathway blockade. The hydrogel delivery allowed for the administration of a lower antibody dose, minimising the potential toxicity, as well as maintaining a high level of anti-PD-1 in the local tumour regions for over 2 weeks. The combined therapy (anti-PD-1 and celecoxib) gave improved local and systemic anti-tumour immunity, showing increased numbers of CD4+ and CD8+ effector T cells in the tumours and surrounding draining lymph nodes.

1.3.2. Biomaterial-based cancer vaccines

The major limitation of cell-based cancer vaccine therapies is the need for *in vitro* processing to extract, grow and expand cells prior to transplantation. Implantable biomaterials have great potential in overcoming this issue by providing a physical structure to attract and support DCs *in situ*[30]. The Mooney laboratory was among the first to exploit the increasing understanding of immunology to design biomaterials that can potentiate specific immune cell functions. One of their early inventions was a macroporous PLGA matrix designed to deliver GM-CSF and cancer antigens, causing recruitment and programming of DCs *in vivo*[84]. When implanted subcutaneously in a melanoma mouse model, the implants showed increased cellular infiltration, suggesting that the matrix could also serve as a carrier for recruited DCs, and therefore act as a vaccine. The same group later established through *in vivo* studies in mice that there is preferential DC proliferation in macroporous scaffolds as opposed to microporous systems, and exploited this knowledge in their subsequent designs[85]. In contrast to the traditional bolus vaccination, the PLGA biomaterial-based vaccine can accumulate and present the antigens and stimulatory signals to DCs over at least

2 weeks[84]. The controlled release of GM-CSF allowed for continuous DC recruitment and programming.

The next step in PLGA scaffold development included immobilization of melanoma tumour lysates into the PLGA matrices to stimulate programmed DCs with tumour antigens. This putative cancer vaccine was tested in a B16-F10 (melanoma) mouse model and showed delayed tumour formation as well as prolonged survival in scaffold-treated animals. More recently, the Mooney lab explored the use of a PLGA cancer vaccine with checkpoint inhibitors for a combined antitumoural effect[86]. While the co-administration of the vaccine with anti-CTLA-4 led to the depletion of Tregs in the tumour microenvironment, combining the immunisation with anti-PD-1 antibodies did not bring therapeutic benefits. These tumour lysate-loaded PLGA matrices are currently tested in Phase 1 clinical trials, in which they are implanted surgically subcutaneously on the patient's arm, leg or torso by cutting into the skin and sliding the scaffold into the pocket formed[87].

Although the biomaterials described above have potential in improving DC vaccines, they require a possibly invasive surgical procedure for implantation, which could present a logistical challenge. In 2015, the Mooney lab offered a potential solution to this issue by designing injectable mesoporous silica rods that self-assemble into macroporous structures *in vivo*, and are capable of hosting immune cells[88]. In addition, they release embedded stimulatory molecules, such as GM-CSF, and tumour antigens. In animal studies, the silica rod-based scaffolds increased the proliferation of cytotoxic T cells and extended survival in a lymphoma mouse model.

Apart from scaffold-based delivery systems, several studies explored the feasibility of incorporating nanoparticles into a vaccine to enhance the localised delivery of therapeutic agents into organs and tissues. Platforms such a liposomes and PLGA nanoparticles have been used to deliver peptides and nucleic-acid based vaccines[89–91].

A major disadvantage of this approach is the longevity of therapeutic response. Due to their small size, nanoparticles are easily internalised by APCs in the tissue, leading to the loss of activity[58]. From a clinical point of view, this would require repeated vaccinations to achieve sufficient anti-tumoural response. While scaffold-based vaccines require a potentially invasive implantation procedure, they remain active at the cancer site for longer, providing an amplified anti-tumoural activity[58].

1.3.3. Biomaterials for adoptive cell therapy

While adoptive T cell therapy is a promising new strategy in the fight against some cancers, several hurdles are yet to be overcome before it becomes a viable and widely used treatment option. Firstly, the generation of DCs or T cells needed to produce a cell therapy product for an individual patient requires a large amount of blood product to be collected and processed, which increases the lead time and expense of this treatment. In oncology patients, lymphodepletive chemotherapy often has a negative effect on the DC count and quality[92,93]. Certain tumours have the ability to alter the immune response of the host by inducing the expression of co-stimulatory molecules to direct differentiation into regulatory T cells, therefore reducing cytotoxic T cell production[94]. Adoptively transferred T cells may not survive the transplant and could quickly die after injection into patients. To overcome this, scientists have been looking into maintaining cell survival or directly expanding T cells *in vivo* using biomaterial technologies[95].

1.3.3.1. Biomaterial-based implants for adoptive cell transfers

The Stephan lab has focused on enhancing CAR-T cell therapies with a range of biomaterials[96–98]. One of their most notable achievements has been the development of biopolymer implants for delivery of tumour-reactive T cells directly into the tumour[96]. These biopolymer scaffolds act as a cell depot, and upon polymer

degradation the cells are released directly into the tumour milieu. The scaffolds were loaded with porous silica microparticles, encapsulating the interleukin 15 superagonist to induce T cell proliferation and activation within the scaffold. By doing this, there is no need for *ex vivo* T cell expansion in adoptive cell therapy, which could simplify the procedure.

The same group used a mouse ovarian cancer to model advanced stage unresectable tumours. Following implantation of a scaffold, six out of ten mice were completely healed (i.e. tumours were eradicated), while the remaining four showed substantial tumour regression with a prolonged survival rate (on average 27 days). Due to their localised action, these scaffolds are not capable of treating widespread metastasised tumours but offer a relatively safe treatment of unresectable or incompletely resected cancerous tissue.

In 2010, Stephan et al.[97] designed a method for enriching adoptively transferred T cell products by conjugating cytokine-loaded lipid nanoparticles to the cell surface. Since T cells possess high levels of reduced thiol groups on their surface, the authors were able to covalently conjugate maleimide-modified nanoparticles *via* maleimide-thiol chemistry. The resultant constructs then released immuno-stimulating cytokines, namely interleukin 15 (IL-15) and interleukin 21 (IL-21), promoting *in vivo* T cell expansion and effector function in a mouse model. In a follow-up publication[99], antibody- and cytokine-decorated immunoliposomes effectively induced expansion of adoptively-transferred T cells, while minimising the systemic toxicity associated with cytokine treatments.

In another study[98], the Stephan group designed a tumour-targeted liposome delivering immunomodulatory drugs (an immunostimulant-invariant natural killer T-cell (iNKT) agonist and a selective inhibitor of the p110δ PI3K kinase) for pre-conditioning of the tumour microenvironment before CAR-T cell infusion. These liposomes were

capable of blocking immunosuppressive cells within the tumour microenvironment while activating and expanding cytotoxic T cells. In a mouse breast cancer model, infusing CAR-T cells after liposome-mediated preconditioning led to doubled overall survival rates as compared to traditional CAR-T cell therapy. Recently, the Stephan group developed CAR-T cell loaded micropatterned nickel titanium (nitinol) self-expandable stents. Although the implant showed promising results in animal studies, it is a non-biodegradable alloy stent which would have to be eventually removed, subjecting the patient to another invasive procedure[100].

1.3.3.2. Artificial antigen presenting cells

Many publications have explored the feasibility of *in vivo* T cell activation by delivering soluble MHC proteins[101–103]. However, it has been found that large quantities of MHC molecules per T cell were required to achieve an adequate cellular response in *in vitro* models. In nature, even a small number of MHC protein molecules on the APC surface can be sufficient to induce a potent response in T cells.

This observation was translated into the development of artificial antigen presenting cells (aAPCs) where MHC-peptides or T cell activating proteins are covalently conjugated to a physical substrate such as a latex bead or tissue culture plastic to induce a cellular response. The invention of acellular aAPCs has allowed for more flexibility in oncology cell therapy manufacturing processes. aAPCs have provided tools for efficient *ex vivo* activation and expansion of cells for adoptive T cell therapies bypassing the need for DC extraction from patient's blood[104].

Numerous non-biodegradable aAPCs for T cell activation *ex vivo* have been examined in the past, for example carbon nanotube-polymer composites[105] or iron-oxide nanoparticles[106]. Although these platforms can induce T cell responses *ex vivo*, they are unsuitable for *in vivo* administration as they are not biodegradable. Magnetic non-biodegradable aAPCs require *ex vivo* processing with a robust separation protocol

to remove them from cells without disrupting their integrity. This multi-step processing could potentially introduce contamination to the blood product. From a practical point of view, these processes usually occur at multiple manufacturing sites, take several weeks and are very costly[107]. T cells harvested from *ex vivo* expansion are deprived of their activating stimuli, hence the quality of the engineered blood product declines rapidly with storage time[108]. These key issues could be potentially solved by developing a biodegradable, biocompatible material capable of expanding T cell directly at the tumour site, *in vivo*, without a need for *ex vivo* manipulations[74]. Conceptually, this would resemble the scaffold-based DC cancer vaccine delivery described above (see Section 1.3.2, page 17). Further information on the development of biodegradable aAPCs is provided in Chapter 4 of this thesis (Section 4.1, page 121).

1.3.4. Clinical translation

Although the field of immuno-oncology is rapidly developing, the challenges of its therapeutic delivery remain largely unexplored due to large costs and processing constraints. Admittedly, the last ten years have seen major progress in immunomodulatory biomaterial development, but these have had relatively little impact on patient outcomes so far[30,109]. Side effects of checkpoint inhibitors, much like in chemotherapy, remain a major limitation for widespread clinical implementation. It is therefore anticipated that biomaterials allowing more controlled and localised delivery of these agents may be of great importance[30]. Equally, the manufacturability issues associated with cell-based therapies may be addressed by employing scaffold-based delivery platforms capable of activating immune cells directly *in vivo*[30,109].

1.4 Electrohydrodynamic processes

The electrohydrodynamic (EHD) technique is a material fabrication method in which a polymer solution is dispersed into a fine jet under the influence of an electric field. This results in the formation of fibres (electrospinning) or particles (electrospraying). EHD is a low-cost, time-effective and versatile technique that has been used to process a wide range of pharmaceutically relevant materials, such as suspensions of cells, bacteria or polymers[110]. For the purpose of this thesis, the discussion will centre on the processing of polymers and protein/polymer mixtures. Polymer-based fibres and particles loaded with therapeutic agents ranging from small molecules[111] to monoclonal antibodies[112] have both achieved sustained and localised drug release in preclinical models.

Electrospinning and electrospraying are sister technologies and use the same basic experimental apparatus, presented in Figure 1-6.

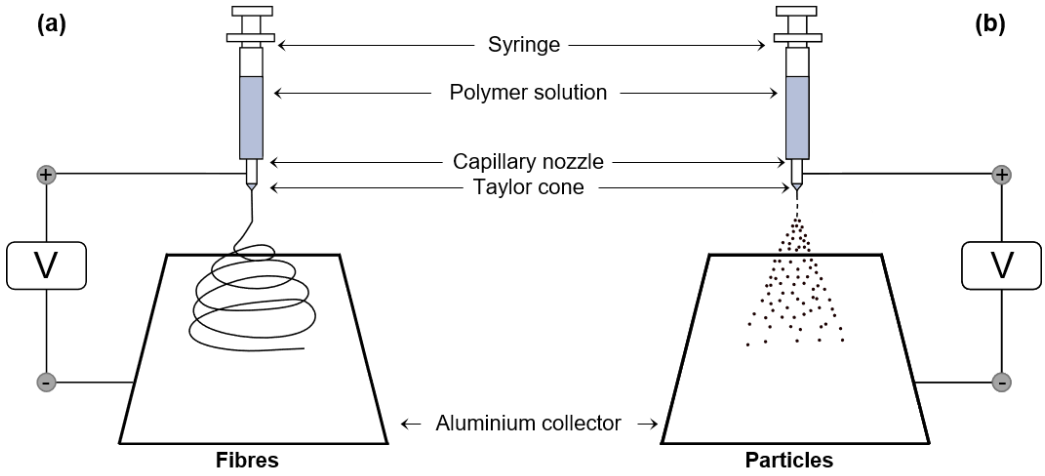

Figure 1-6: A schematic of standard EHD apparatus and the process of (a) electrospinning and (b) electrospraying. V – high voltage.

The main components of the EHD apparatus include a high-voltage power supply, a precision syringe pump, a syringe loaded with a polymer solution and fitted

with a conductive metal needle (the spinneret) and a collector. To maintain an electric field, the power supply is connected to both the spinneret and the collector[113].

The polymer solution is extruded through the charged spinneret, with the syringe pump ensuring a controlled flow rate. Without the application of electric charge, the polymer solution exits the needle forming a spherical droplet owing to the surface tension forces (Figure 1-7a)[113]. When subjected to high voltage during extrusion through a metal needle, the liquid surface becomes charged, causing the spherical droplet to be retained at the capillary tip (Figure 1-7b). With sufficient voltage applied, the meniscus deforms into a conical structure, which is often referred to as the Taylor cone (Figure 1-7c). [114].

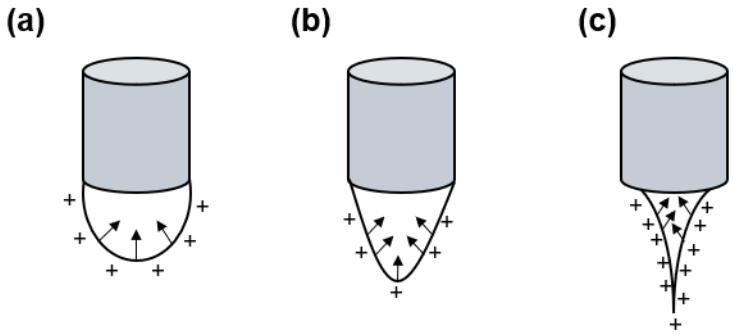

Figure 1-7: An illustration of the development of the Taylor cone jet when a polymer solution is extruded through a metal spinneret under the influence of electrical field. Without electrical field the shape of liquid droplet is spherical due to surface tension (a). High voltage results in a charge accumulation on the liquid surface causing deformation of fluid meniscus (b). Taylor cone is developed when sufficient voltage is applied (c).

In electrospinning, a polymer jet is emitted at the tip of the Taylor cone, which stretches and reduces in diameter as it travels towards the collector. The solvent present in the polymer solution evaporates as the jet is drawn and accelerates towards the collector, therefore producing a solid fibrous product[113]. In electrospraying, the Taylor cone breaks into droplets rather than forming a continuous jet, resulting in the formation of solid particles which are usually spherical in shape[113].

In mono-axial electrospinning, the spinneret is a single metal needle, resulting in the formation of monolithic fibres from a single working solution. Modified EHD set-ups include electrospinning through co-axial or side-by-side nozzles to produce bifunctional biomaterials. In co-axial EHD processing, the spinneret is composed of two nested concentric needles, which allows for simultaneous dispensing of two working solutions: the core solution pumped through the inner needle and the shell solution flowing through the outer needle. Use of side-by-side nozzles in EHD processing allows for the formation of so-called Janus structures, where the opposing sides of the material exhibit different surface structure[115].

1.4.1. Parameters affecting EHD processing

As described above, electrospinning and electrospraying rely on the same basic EHD apparatus. To achieve either fibre or particle formation, the processing parameters need to be adapted accordingly. Although the assembly of the EHD apparatus and product collection is relatively simple, the optimisation of experimental parameters necessary for the fabrication of uniform and reproducible scaffold or particle requires extensive and detailed experimentation. Critical variables can be broadly classified into solution properties and processing parameters.

1.4.1.1. Solution properties

An extremely important characteristic to consider is the viscosity of the EHD solution, which reflects the level of polymer chain entanglement in the liquid. At low viscosity, the polymer molecular entanglement will be insufficient for electrospinning to occur and a polymer jet to be generated. The solution viscosity is largely dependent on the concentration of the polymer in the solution and its molecular weight, with higher values of both usually leading to increased viscosity. For electrospinning to happen, the polymer solution should be viscous enough to form a Taylor cone without clogging

the nozzle. If electrospraying is the desired EHD process, the solution should be less viscous, leading to the atomisation of the polymer jet and subsequent production of particles. It is, therefore, possible to alternate between electrospraying and electrospinning by changing the molecular weight and concentration of the polymer used[113].

1.4.1.1.1. Choice of polymer

Several aspects need to be considered when choosing the polymer for the electrospinning/spraying solution. Probably the most important consideration is the intended application of the product. The polymer degradation half-life and by-products, biocompatibility, and solubility will heavily influence the potential applications of the product. For example, for fast-release applications, a polymer with a relatively rapid dissolution/degradation rate and high solubility in aqueous solvents (such as polyvinylpyrrolidone (PVP)) would be preferred[113]. In contrast, when designing a long-term surgical implant, a hydrophobic polymer with slow degradation rates would be more suitable. In some cases, polymers with special characteristics such as thermo- or pH-sensitivity are of interest, aiding targeted delivery to the action site[116].

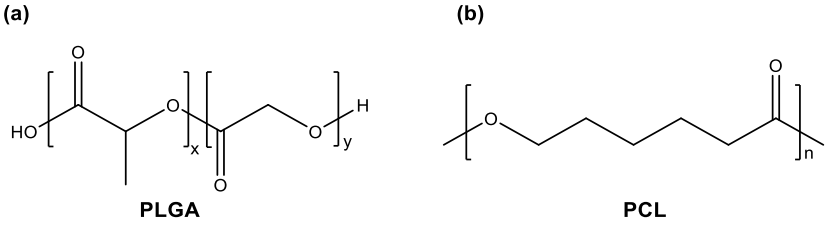

Figure 1-8: Chemical structures of (a) PLGA and (b) PCL.

One of the most commonly used pharmaceutical polymers in EHD is poly(lactic co-glycolic) acid (PLGA) (Figure 1-8a). PLGA is a synthetic copolymer formed of polylactic (PLA) and polyglycolic acids (PGA). PLA can be rendered completely amorphous (poly D-lactic acid; PDLA) or highly crystalline (poly L-lactic acid;

PLLA) due to disordered polymer chains[117]. On the other hand, the lack of methyl side groups makes PGA highly crystalline[117]. By altering the molar ratio of the monomers, PLGA can be rendered either amorphous or crystalline[118]. PLGA degrades by hydrolysis of its ester linkages *via* bulk erosion in aqueous environments. The rate of degradation can be controlled, for example by adjusting the molecular weight of the polymer or the molar ratio of the monomer components. As an example, PLGA copolymers with a higher content of lactic acid will degrade more slowly due to the presence of hydrophobic methyl groups[119].

Another medically important polymer is poly(ε-caprolactone) (PCL; Figure 1-8b), which is an aliphatic polyester composed of hexanoate repeat units. It is a semi-crystalline polymer widely used in the manufacturing of surgical sutures, drug delivery systems and tissue engineering scaffolds, and biodegrades through hydrolysis over a time period ranging from several months to years, depending on the molecular weight[111,120].

Biomaterials manufactured from PLGA and PCL follow a similar triphasic breakdown profile. In the hydration step, water penetrates into the amorphous region of the material, thus disrupting the van der Waals forces. Subsequently, the polymer chain starts to degrade either by end-chain or random-chain scission and the cleavage of covalent bonds. This leads to a decrease in the molecular weight[121]. The degradation process is then autocatalysed by carboxylic end groups and the particle structure is severely disrupted by the breakdown of backbone covalent bonds. The resulting metabolite monomers incorporate into the Krebs cycle and can be safely eliminated from the body[122,123].

1.4.1.1.2. Choice of solvent

Solvent choice can greatly impact the processability of the working solution. The solvent used in EHD should be volatile enough to achieve complete evaporation during the journey between the spinneret and the collector.

Interestingly, using a solvent with lower solubility for the polymer may increase the likelihood of nanofibre formation by changing the value of the so-called critical concentration[124]. A critical minimum concentration (c_e) is achieved when the number of molecular chain entanglements is sufficient to overcome surface tension in the EHD process, preventing the jet in electrospinning from breaking up. At concentrations below c_e the charged polymer solution will form droplets (electrospraying), while concentrations above c_e will form fibres (electrospinning). The value of c_e is dependent on several properties, for example molecular chain length, polymer structure and the solvent used to dissolve the polymer. Solvent volatility is critical for successful EHD process optimisation and has a significant effect on fibre morphology and diameter[113]. A solvent should be volatile enough to allow the fibres or particles to dry completely before reaching the grounded collector. However, if volatility is too high, the resulting fibres or particles may show defects such as wrinkled or porous surface morphologies.

1.4.1.2. Process parameters

In EHD fabrication, process parameters include applied voltage, flow rate, internal diameter of the spinneret used, collection substrate and the spinneret-to-collector distance, as well as environmental features, such as temperature and humidity.

1.4.1.3. Applied voltage

Electrical potential, or voltage, is an important parameter for every EHD experiment. The applied voltage should be high enough to overcome the surface tension

of the polymer solution and allow a stable Taylor cone to form. Increasing the voltage can also result in the alteration of the morphology of the produced material, for example by moving from the fabrication of particles (electrospraying) through elongated particles or bead-on-string fibres to uniform fibres (electrospinning)[125] or by decreasing diameter size of the produced fibre[126].

1.4.1.4. Flow rate

The rate at which polymer solution is ejected through the spinneret to feed the Taylor cone needs to be optimised on a case-by-case basis. In general, a low flow rate is preferable as it enable the formation of a more stable Taylor cone and facilitates efficient solvent evaporation. Conversely, at flow rates below the optimum, the polymer jet may become discontinuous as not enough polymer solution is passing through the spinneret in a given unit of time[113], therefore leading to the formation of defected particles or fibres.

1.4.1.5. Collector distance

The distance between the tip of the spinneret and the collecting substrate will affect the electric field strength. This can be increased by reducing the collector distance. However, a shorter collection distance can negatively influence the solvent evaporation process, leading to incomplete evaporation and the formation of fused or deformed fibres and particles. The collector distance is particularly important when using solvents with low volatility, and must be sufficiently large to allow the complete evaporation of the solvent in the polymer jet before it hits the collecting substrate. It should be noted, though, that with increasing distance the processing yield tends to drop as weaker electric field means that particles/fibres may not land on the collector and deposit elsewhere instead. [113]

1.4.1.6. Environmental parameters

Temperature and humidity have a major effect on the solution viscosity, surface tension and conductivity, as well as solvent evaporation rates. The stability of the Taylor cone and the resulting polymer jet is often influenced by the movement of air. Environmental chambers are often used to ensure reproducibility and protect the experiment from the changes to temperature, humidity and air flow[113].

1.4.2. Protein delivery using EHD

Protein-loaded biomaterials have long generated considerable interest due to the growing importance of immunotherapy and tissue engineering in modern medicine[127,128]. The complex and fragile structures of many therapeutic proteins require advanced delivery methods and careful optimisation of formulation and manufacturing conditions[129]. Quite often the protein integrity is compromised by the route of administration, leading to denaturation, aggregation or misfolding. For example, the loss of fragile tertiary structures of proteins, defined by non-covalent interactions, may result in loss of biological activity.

For now, parenteral administration of proteins remains the gold standard, as other delivery routes are limited or not yet clinically feasible. The field of pharmaceutical technology has long sought possible solutions to protein formulation challenges, leading to the development of multiple inorganic, lipid or polymer-based formulations. Some examples of biomaterial technologies used to encapsulate proteins include solvent evaporation and extraction, coacervation or spray-drying[130].

EHD technology could offer a simple route to the fabrication of protein-loaded biocompatible scaffolds and particles that can be easily implanted or injected at the desired site of action. Although relatively unexplored in the oncology field (further discussed in Chapter 6), the EHD technology could be potentially applied

for the delivery of therapeutic antibodies in cancer therapy, for example for localised release of checkpoint inhibitors or delivery of T cell activating cues on the surface of artificial antigen presenting cells. Multiple approaches have been proposed for the incorporation of therapeutic proteins within electrospun and electrosprayed materials, including monoaxial and co-axial electrospinning.

Both approaches rely on the same basic EHD apparatus (presented in Figure 1-6) but differ in the spinneret used. For monoaxial electrospinning a uniaxial needle is used, while co-axial setup requires a concentric nozzle formed from two needles nested within one another. A schematic showing the differences in the design of these spinnerets, as well as in the resulting electrospun/sprayed product, is presented in Figure 1-9.

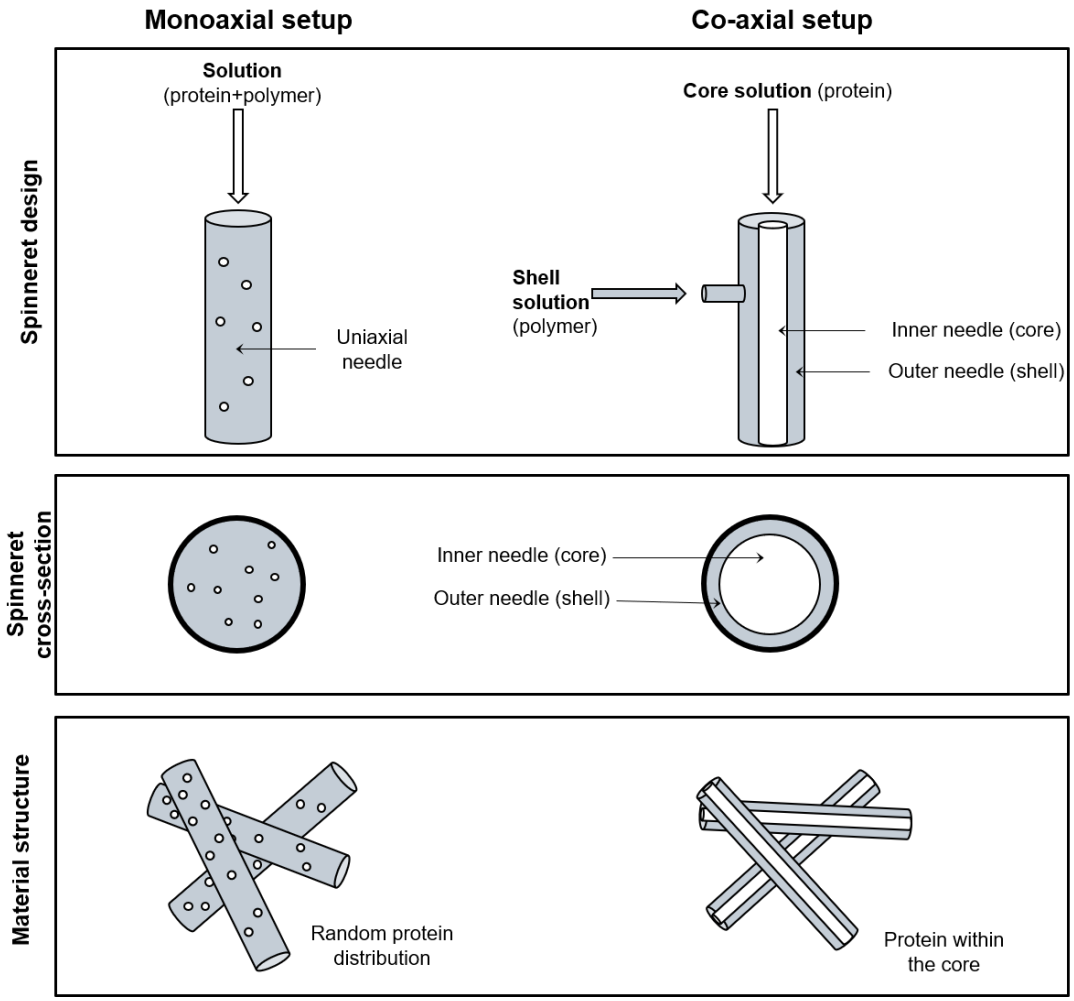

Figure 1-9: The differences in monoaxial and co-axial spinneret design and the resultant material produced. Grey shading represents polymer solution, while white represents the protein solution being processed.

1.4.2.1. Monoaxial EHD

Unarguably the simplest EHD process used in protein drug delivery is blend processing, where the active substance of choice is dissolved or dispersed in a polymer carrier (usually a volatile solvent)[131]. Upon application of a high voltage, monolithic materials are yielded with the drug uniformly dispersed on the molecular level within the fibre or particle. However, a prolonged exposure to the organic solvent typically required for EHD may cause misfolding or aggregation of labile biomolecules like

proteins, leading to loss of activity For this reason, blend electrospinning is rarely used for encapsulation of therapeutic proteins[132].

A controlled and sustained protein delivery can be achieved using emulsion EHD, where a core-shell structure is formed by electrospraying/spinning of a water-in-oil emulsion formed from an aqueous phase (protein) and an organic phase (polymer)[133]. When subjected to electric charge, the organic phase (typically containing a volatile solvent) rapidly evaporates. This causes the migration of the aqueous phase (with protein) to the centre of the jet, forming core-shell structures[134] with favourable localisation of proteins within the centre of the fibres/particles, minimising the risk of the initial burst release of therapeutic cargo.

In 2017, Frizzell et al.[116] developed enzyme-loaded electrospun fibres for peroral delivery using surfactant-assisted emulsion electrospinning. Horseradish peroxidase and alkaline phosphatase were blended with a pH-sensitive polymer (Eudragit L100) in the presence of the surfactant Tween® 20. Eudragit L100 is an anionic co-polymer of methacrylic acid and methyl methacrylate that is only soluble at pH above 6. The nanofibres fabricated from Eudragit L100 showed pH-dependent enzyme release patterns, with ~5% release at pH 2 and almost 100% at pH 7. Use of Eudragit L100 ensured dissolution of the fibres only occurred in neutral and basic pH conditions, ensuring protected transit of the enzymes through the stomach and preventing acid-medicated protein degradation. The authors found that the bioactivity of the protein was best preserved by decreasing the aqueous phase content in the emulsion.

Furtmann et al.[135] presented a method for the production of PVA-coated PLGA nanoparticles encapsulating subunit antigens (cytomegalovirus peptides) for the targeted stimulation of antigen-specific CD8+ T cells. The particles were prepared by blending peptides with PLGA dissolved in TFE and dimethyl sulfoxide. When tested

against a soluble peptide, the electrosprayed particles enhanced proliferation and promoted TNF-α and IFN-γ production.

Although the relative simplicity of emulsion electrospinning is attractive from the manufacturability point of view, the protein-polymer blend composition must be carefully optimized to ensure there is no loss of bioactivity resulting from accidental exposure of the biomolecule to the organic solvent. A non-ionic surfactant is often incorporated in the formulation to decrease the contact between protein and organic solvents by forming reverse micelles (emulsions), therefore avoiding denaturation or aggregation[136].

1.4.2.2. Coaxial EHD

In coaxial EHD, the core solution is pumped through the inner needle and the shell solution flows through the outer needle. As both solutions are physically separated until the formation of the fibre or the particle, protein exposure to organic solvents is limited and therefore accidental degradation can be minimised. The resulting fibre or particle usually holds the protein in the core with a hydrophobic polymeric shell allowing for the gradual release of the cargo at the site of action. A notable example of antibody encapsulation within electrospun fibres using this approach has been recently published by Angkawinitwong et al.[112], and is described in more detail in Chapter 6 (page 208).

1.4.2.3. Choice of EHD process

The selection of protein incorporation method will largely depend on the therapeutic application, the desired release profile and the structure of the protein being processed. The advantages and disadvantage of the processes described above are summarised in Table 1-4.

Table 1-4: Summary of the advantages and disadvantages of blend, emulsion, and coaxial EHD processing with regard to protein delivery systems[131,137,138]

EHD Method	Advantages	Disadvantages
Monoaxial	· Simplicity · Protein dissolution within an appropriate solvent and separation from the organic conditions required to dissolve the carrier polymer · Core-shell structures are obtained without the use of complex coaxial spinnerets	· Direct contact with organic solvents may cause protein denaturation and loss of function · Lack of control over the distribution of the therapeutic agent within the fibres or particles · Unsuitable for polymer solutions with low surface tension · Use of ultrasonication or absence of surfactants during the emulsification process may compromise emulsion stability, protein structure, and bioactivity
Coaxial	· Precise control over the location of the drug within the core or shell of the fibres or particles · High protein loading capacity · Creation of more complex systems and multiphasic release profiles	· More complex and expensive setup

1.5 Surface functionalisation

In certain applications, surface presentation of therapeutic molecules is essential for adequate biological performance, for example in biomaterial-based cancer vaccines (see Section 1.3.2, page 17), artificial antigen presenting cells design (see Section 1.3.3.2, page 21), or wound healing[139]. In such cases, loading of protein cargo into the interior of a particle or fibre would not be suitable. Instead, bioactive molecules can be immobilised on the surface of electrospun or electrosprayed materials.

The ability to safely coat a polymer surface with a protein without the loss of its functional activity is often critical in the successful targeted delivery of biomolecules. Broadly speaking, proteins can be deposited on the surface by physical adsorption (e.g. by dip-coating or spray-coating) or by chemical methods, such as bioconjugation. Bioconjugation often involves the reaction of two molecules, one of which is usually a biomolecule, and a crosslinking agent that enables the formation of covalent bonding

between those two entities. A schematic summarising surface functionalisation approaches discussed in this section is presented in Figure 1-10.

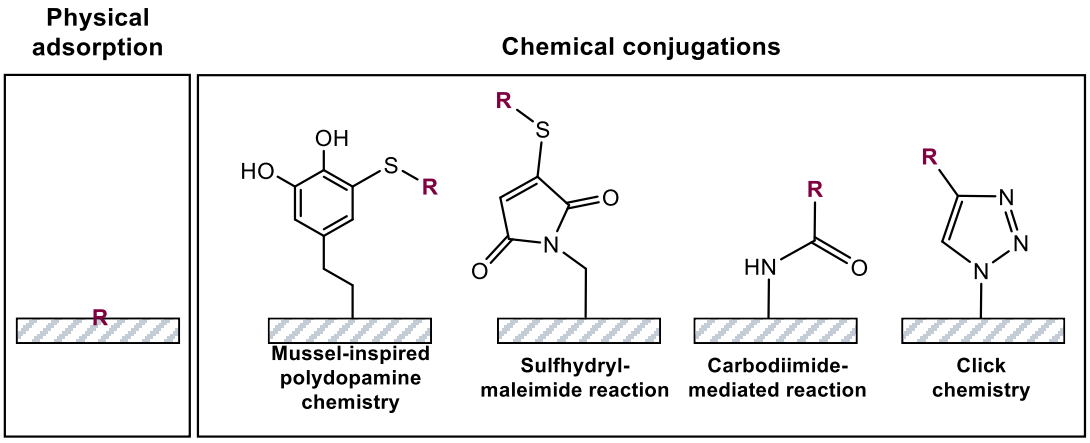

Figure 1-10: Schematic showing functionalisation approaches for attachment of proteins to polymeric surfaces. R – protein.

1.5.1. Physical adsorption

Physical adsorption is often used to deposit proteins on polymer surfaces. The 3D-structure of intertwined electrospun fibres provides a large surface area for protein adsorption, making it an attractive material for surface protein delivery. This approach does not require multi-step treatments in harsh conditions but relies solely on relatively weak electrostatic, van der Waals and hydrophobic interactions[140].

Norde and Hayes described the mechanism of protein adsorption to solid surfaces (Figure 1-11). Broadly speaking, a protein in its native state confirmation travels towards the surface by diffusion and convection (being therefore influenced by the electrostatic potential of the solid surface). This process may involve perturbations of the protein structure Upon attachment, the protein molecule undergoes further rearrangements in secondary and tertiary structures through hydrophobic interactions with the surface. Desorption and diffusion back into the solution can occur, but are less probable for unfolded proteins due to the presence of a higher number of binding points after unfolding.[141,142]

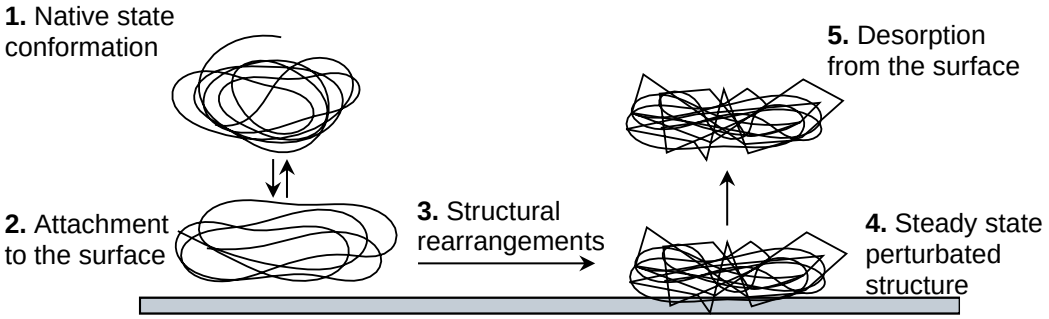

Figure 1-11: Schematic explaining the mechanism of protein adsorption to solid surfaces. Adapted from Norde and Hayes[141].

A clear advantage of the adsorption approach is that it does not require any modifications to the protein or the substrate. It is possible to achieve enhanced protein adsorption to polymer surfaces by optimising experimental properties, such as the pH and ionic strength of the protein solution or the duration and temperature of incubation[143,144]. For example, at the isoelectric point, proteins possess no net charge, so the electrostatic repulsion between adsorbed molecules is minimal[145]. Previous literature suggests that at the isoelectric point proteins are highly stable, causing reduced spreading at the interface and less steric hindrance[21], and thereby favouring adsorption. Therefore, enhanced protein adsorption can be achieved by adjusting the protein solution pH to a value near its isoelectric point[145].

Physical adsorption is heavily used in the functionalisation of gold nanoparticles with therapeutic proteins, with examples including human follicle-stimulating hormone and chorionic gonadotropin antibodies for use in biosensors[146]. The relatively rapid release of adsorbed bioactive agents caused by their weak interactions with the surface is desired for certain applications where instant biological action at the delivery site is needed, for instance in antimicrobial applications[147]. For example, Xia and Lv[148] described the dual delivery of growth factors for peripheral nerve regeneration using PLA nanofibres. In this study, recombinant human nerve growth factor (NGF) was first loaded into the core of the

fibre *via* emulsion electrospinning. The fibres were then surface-functionalised with VEGF by physical adsorption. The resulting dual VEGF-NGF PLA nanofibres were extensively evaluated *in vivo*, and the walking ability of nerve-injured rats was visibly enhanced after treatment with the dual-release scaffolds as compared to controls (autograft, plain fibre, and fibre bearing either NGF or VEGF). Moreover, *in vitro* studies showed preferential nerve differentiation of neural crest stem cells following incubation with the dual-delivery nanofibres. Enzyme-linked immunosorbent assay (ELISA) results confirmed that physically adsorbed VEGF was released much faster than NGF loaded in the core of the fibre. However, the authors did not discuss the stability or activity profile of the released proteins.

Grafahrend et al.[149] developed electrospun polymer fibres coated with adhesion-promoting peptides (e.g. a fibronectin fragment (GRGDS) or a collagen IV fragment). The functionalised scaffolds showed enhanced keratinocyte attachment, indicating this approach may be suitable for tissue engineering purposes. In another study, PCL fibres were dip-coated with platelet-rich plasma (PRP) and freeze-dried. Immobilisation of PRP enhanced hydrophilicity and mesenchymal stem cell attachment and proliferation on the PCL surface, without inducing differentiation to a particular linage[150].

The physical adsorption approach, however, may not be suitable if prolonged protein release at the action site is desired. Another potential disadvantage is the effect of hydrophobic interactions on the protein, which may result in a change to the 3D conformation and lead to irreversible denaturation by aggregation[151]. The lack of site-specific binding to the surface in adsorption may also result in an unfavourable orientation of the protein on the surface, therefore losing the protein functionality[152].

1.5.2. Chemical conjugation

Covalent chemical conjugation of bioactive molecules onto the surface of polymeric biomaterials is generally preferred over physical adsorption in regenerative medicine applications. The covalent bonding ensures effective immobilization of molecules on the fibre or particle surface over an extended period of time, whereas physically adsorbed macromolecules can easily desorb from the surface (as illustrated, for example, in the Xia and Lv[148] article). However, the bioconjugation method should be carefully selected to prevent partial or full loss of activity of the biomolecule following chemical manipulation[153].

1.5.2.1. Mussel-inspired polydopamine chemistry

Owing to its simplicity and versatility, polydopamine chemistry has lately emerged as a promising tool in surface modification of polymeric materials. Often referred to as mussel-inspired functionalisation[154,155], this approach relies on the unique ability of polydopamine to self-polymerize on polymeric surfaces *via* oxidation in a weak alkaline environment[156]. In recent years, there has been considerable interest in the use of this method for peptide and protein surface modification of hydrophobic nanofibres. Cheng et al.[157] reported successful modification of PLGA fibrous scaffolds with various biomolecules using the mussel-inspired approach. When tested with human dermal fibroblasts, nanofibres functionalised with a polymer (polyethylene glycol; PEG), cell adhesive peptide (RGD) and basic fibroblast growth factor (bFGF) showed a positive effect on cell repulsion, adhesion and proliferation, respectively.

In a 2019 study, Liu et al.[158] explored polydopamine-assisted conjugation of osteogenic growth peptide (OGP) to PLA nanofibres. Surface-functionalised nanofibres showed improved human mesenchymal stem cell adhesion and proliferation *in vitro*, owing to increased hydrophilicity and a rougher topology. In an *in vivo* bone formation model, OGP-coated fibres achieved superior results than

unmodified fibres, which the authors attributed to osteogenic effects of OGP. More recently, Chen and colleagues[139] used polydopamine chemistry to immobilize an enzyme (bromelain) on the surface of PCL fibre patches. Similarly to the previous studies, the modification led to increased cellular adhesion and proliferation, attributed to a reduction in material hydrophobicity. An *in vivo* model demonstrated reduced inflammation and improved healing rates in rats treated with bromelain-functionalised fibres, revealing the polydopamine chemistry approach to be suitable for effective protein surface immobilization.

1.5.2.2. Sulfhydryl-reactive crosslinker chemistry

The maleimide-sulfhydryl reaction has been largely described in the context of bioconjugation of proteins containing free thiol groups onto the surface of nanoparticles. The double bond of maleimides can undergo an alkylation reaction with sulfhydryl groups at pH between 6.5 to 7.5, forming stable thioether bonds[159]. In alkaline conditions, the reaction efficiency decreases due to cross-reactivity with primary amines and an increased rate of hydrolysis of the maleimide group[159] (Scheme 1-1).

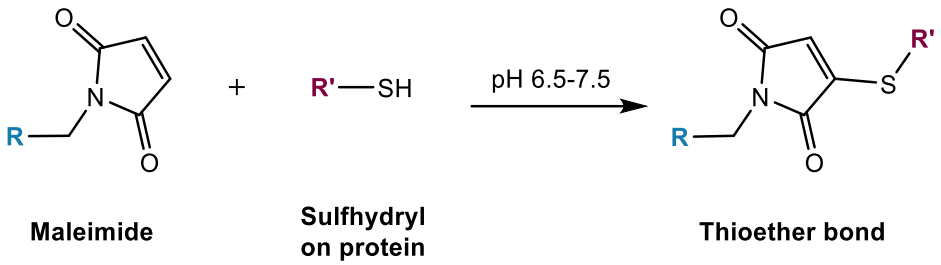

Scheme 1-1: Maleimide reaction scheme for chemical conjugation to a sulfhydryl.

Martínez-Jothar[160] used maleimide-modified PLGA-PEG to manufacture thiol-reactive nanoparticles for conjugation of the peptide cRGDfK. The authors identified the reaction parameters needed to achieve maximum conjugation of biomolecules, highlighting the importance of precise reagent stoichiometry in cost-effective

preparation of protein-targeted using this route. Another example applying this approach involves conjugation of anti-CD44 antibody to the surface of maleimide-modified microparticles prepared by electrospraying a blend of PLGA, maleimide-PEG-NH_2 and cisplatin[161]. The inclusion of anti-CD44 on the surface led to an enhanced cytotoxic effect against ovarian cancer cell lines.

1.5.2.3. Carbodiimide crosslinker chemistry

Bioconjugation *via* carbodiimide crosslinker chemistry has been a popular tool in chemical modification of biomaterials. This functionalisation approach is highly attractive as it can occur in an aqueous environment at physiological pH. Carbodiimides (e.g. EDC (1-ethyl-3-(3-dimethylaminopropyl)carbodiimide hydrochloride)) are zero-length crosslinkers used to form amides from carboxylic acids and amines in mild conditions[162]. EDC and its by-products are water-soluble, making the reaction products easily purifiable by dialysis or gel filtration[163]. However, EDC and its intermediates are hydrolytically labile, potentially leading to inactivation[164]. This can be overcome to some extent by the incorporation of N-hydroxysuccinimide (NHS). This results in the formation of a reactive ester of the carboxylic acid (NHS ester) that undergoes an acylation reaction with an amine to form an amide (Scheme 1-2). NHS esters are generally more stable intermediates in aqueous media at neutral pH than the corresponding EDC intermediates, therefore increasing the yield of subsequent protein conjugation[165].

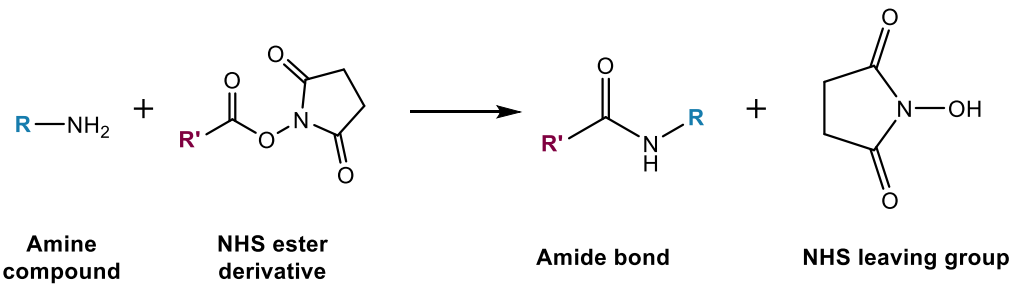

Scheme 1-2: The reaction between amine compounds and NHS esters.

NHS esters undergo rapid hydrolysis under physiological pH conditions. Typically, the half-life of NHS derivatives decreases with increasing pH[162,166]. The rate of hydrolysis can be minimised by maintaining a high concentration of protein in the reaction medium[167].

EDC/NHS chemistry has been widely applied in the surface modification of electrospun materials. Using this approach, Li et al.[168] immobilised collagen on the surface of poly(methyl methacrylate) nanofibres for use in neural stem cell culture model. The collagen-modified nanofibres promoted cell attachment, proliferation and viability compared to unmodified controls. More recently, Guex and colleagues[169] evaluated VEGF-functionalised PCL fibres in primary and immortalised HUVEC cells. Although the growth factor was successfully immobilised on the nanofibre surface, in cell culture the VEGF-treated fibres performed similarly to the untreated fibre controls. These unfavourable results may suggest the loss of VEGF functionality, possibly due to the non-selective nature of the EDC/NHS reaction. The authors showed that VEGF retained its biological integrity to some extent and was able to complex with an anti-VEGF antibody. However, protein functionality was confirmed with fluorescence and not quantified: thus, it is possible that the retention of structural integrity was only partial and insufficient for triggering biological responses *in vitro*.

Sadeghi et al.[170] combined the partial hydrolysis approach and EDC/NHS chemistry to functionalise PLGA scaffolds with collagen for skin substitutes (Scheme 1-3). Similarly to the VEGF-PCL study[169], the PLGA-collagen fibres did not achieve superior biological performance, but rather maintained the cell adhesion and viability at levels comparable to non-functionalised controls.

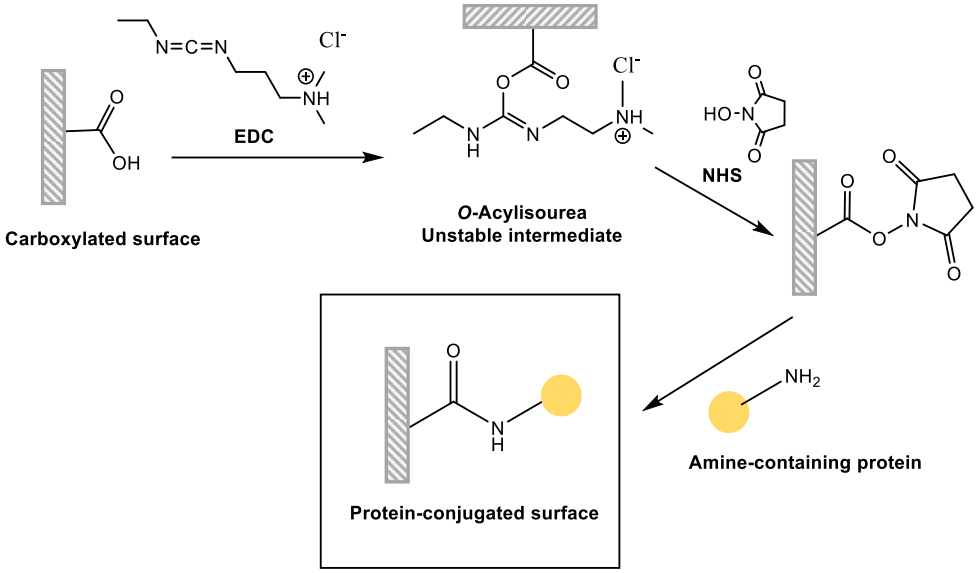

Scheme 1-3: The chemical reaction scheme for EDC/NHS-assisted coupling of a protein ligand to a carboxylated surface.

Schaub et al.[171] explored the effect of surface modification on neurite extension. In this study, PLA fibres were pretreated with oxygen plasma and modified with EDC/NHS to conjugate diethylenetriamine (DTA, for amine functionalization), 2-(2-aminoethoxy)ethanol (AEO, for alcohol functionalization), or GRGDS (cell adhesion peptide) to the surface. X-ray photoelectron spectroscopy showed a decrease in nitrogen signal after washing, suggesting that the active agents were removed from the surface during washing steps and indicating that covalent conjugation was unsuccessful. Although GRGDS remained on the surface of the fibre, the performance of the conjugated fibres was inferior to the unmodified fibre control. The above case studies suggest that EDC/NHS chemistry may not always be a suitable approach for surface modification in biological applications.

In another study, aminolysis was combined with N,N′-disuccinimidylcarbonate to immobilize biomolecules on the surface of PCL scaffolds (Scheme 1-4)[172]. N,N′-disuccinimidylcarbonate is an active carbonate comprised of two NHS moieties. Partial aminolysis of the PCL using a diamine is followed by activation of free amino

groups on the scaffold surface with N,N′-disuccinimidylcarbonate to give an activate carbamate. Upon reaction of the carbamate with a primary amine, the NHS group is cleaved and a functionalised urea is formed. The resulting peptide-functionalised aminolysed PCL scaffolds showed adequate biocompatibility and increased cellular attachment and proliferation in tested cell lines.

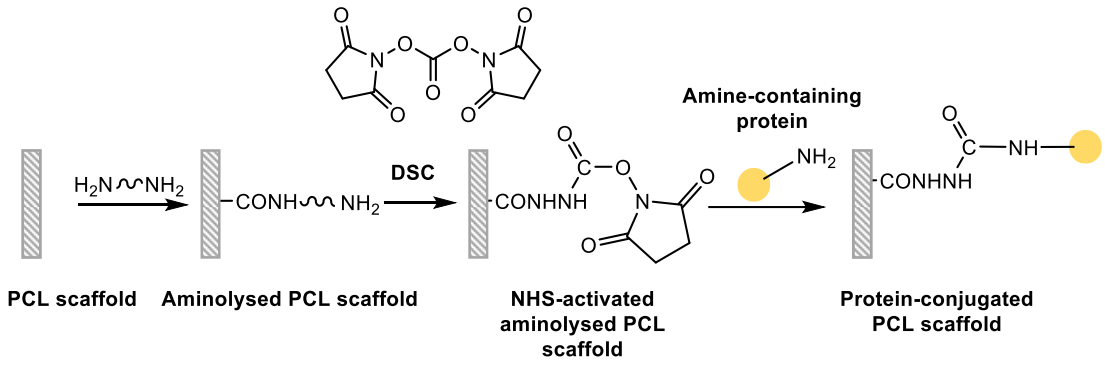

Scheme 1-4: Immobilisation of biomolecules on PCL scaffolds using aminolysis-assisted N,N′-disuccinimidylcarbonate chemistry[172].

A major disadvantage of carbodiimide-mediated NHS ester reactions is the lack of site-specificity and control over protein orientation on the surface of the substrate, which can lead to the loss of biological activity of the conjugated macromolecules[173].

1.5.2.4. Click chemistry

Click chemistry is an overarching term covering a relatively new family of chemical reactions and coined by Karl Barry Sharpless in 2001[174]. The reactions in this group are modular in nature and achieve high yields, producing non-toxic by-products that can be easily removed without the use of chromatographic methods[175]. Click chemistry requires mild reaction conditions and readily available starting materials. The reaction products are stable in physiological conditions and easily purifiable by simple methods such as crystallisation or distillation[176]. Initially developed as a drug discovery tool, click chemistry has created new methods for fields such

as polymer therapeutics, gold and magnetic nanoparticle production, or bioconjugation[177].

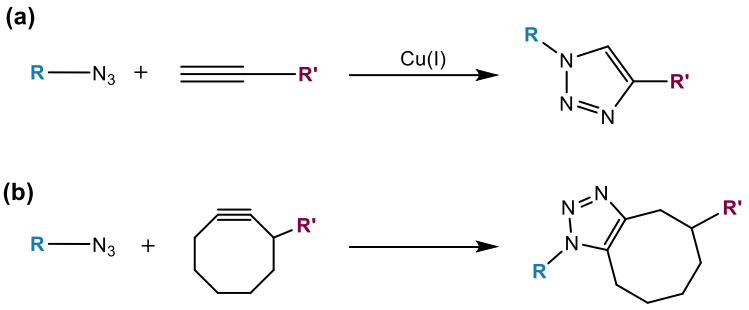

Scheme 1-5: Two exemplar click reactions. (a) Cu-catalysed azide-alkyne cycloaddition and (b) strain-promoted azide-alkyne cycloaddition (SPAAC).

Copper(I)-catalysed azide-alkyne cycloaddition (CuAAC) is one of the most common click reactions explored (Scheme 1-5a). CuAAC is a highly chemoselective reaction occurring at physiological temperature and pH in the presence of a copper catalyst. Due to its orthogonal nature, it has been widely used for the site-selective conjugation of targeting peptides[178,179] and antibodies[180] to the surface of nanoparticles for applications in medical imaging.

Functionalisation of solid polymeric biomaterials with azide or alkyne groups to facilitate 'click' reactivity has now been attempted. One study explored site-selective functionalisation of electrosprayed PLGA Janus particles with acetylene groups, which were then reacted with azido-PEG-amine in the presence of Cu^{2+} ions to undergo Huisgen 1,3-dipolar cycloaddition.[181] A similar study was conducted by Chen et al.[182], who functionalised silica Janus microparticles with 1-bromopropane plasma. These were further reacted with sodium azide *via* SN_2 nucleophilic exchange to achieve azide functionalisation. The particles were then reacted with fluorescently-labelled alkyne compounds in the presence of a copper catalyst.

It became clear, however, that the copper catalyst damages the structure of conjugated biomolecules[183,184]. Moreover, Cu(I) is known to be cytotoxic even at very

low concentrations and therefore may not be suitable for use in drug delivery materials[185,186]. Recently, a Cu-free strain-promoted azide-alkyne cycloaddition (SPAAC) has emerged as a more suitable biorthogonal alternative (Scheme 1-5b). Unlike CuAAC, SPAAC relies solely on the strain within the alkyne ring, enhancing biocompatibility and simplifying reaction conditions[187]. The formation of rigid bonds ensures no interaction between linked molecules, which should prevent possible aggregation of proteins in the final product. Moreover, such bonds are also stable in the mildly reducing aqueous biological environment[175].

Although the concept of SPAAC is theoretically promising in protein-biomaterial bioconjugation, it remains relatively unexplored in the current literature. The applications of SPAAC in surface functionalisation of polymeric materials are discussed in more detail in Chapter 5 (Section 5.1, page 165).

1.6 Project aims

The field of immuno-oncology is fast-developing, but there is still a strong need for robust drug delivery systems to simplify manufacturing protocols, amplify their therapeutic efficacy and minimise immune-associated side-effects. This project therefore explores the feasibility of assisting adoptive T cell therapies and checkpoint inhibitor monoclonal antibody delivery with novel biomaterials. It is hypothesised that protein-decorated biomaterials can be used to enhance the efficacy of immune-oncology

Firstly, functionalisation of implantable electrospun polymeric scaffolds with pharmaceutically relevant proteins will be explored. To achieve this, a relatively unexplored method of perfluorophenyl azide surface functionalisation will be evaluated and tested in *in vitro* studies.

Thereafter, the antibody functionalisation of electrosprayed PCL particles will be attempted in order to design artificial antigen presenting cells, exhibiting T cell stimulating cues (anti-CD3) on the surface to potentiate T cell activation in PBMC-derived human cells. Two methods of surface functionalisation will be explored – perfluorophenyl azide chemistry and strain-promoted azide-alkyne cycloaddition.

Finally, the fabrication of ipilimumab-loaded scaffolds using coaxial electrospinning will be explored, and their *in vitro* functional performance assayed.

Chapter 2 - Materials and methods

2.1. Materials

2.1.1. Chemicals

Chemicals and materials used in experiments for this project are listed by chapter in Table 2-1, Table 2-2, Table 2-3 and Table 2-4.

Table 2-1: List of chemicals and materials used for experiments in Chapter 3.

Chemicals	**Cat No.**	**Supplier**
2-propanol	190764	Sigma-Aldrich
2,2,2–trifluoroethanol (99.8%, TFE)	75898	(UK)
Albumin–fluorescein isothiocyanate conjugate (FITC-BSA)	A9771	
Catalase from bovine liver	C9322-5G	
Chloroform-d (for NMR)	151823	
Dichloromethane	270997	
Dimethyl sulfoxide (DMSO) (cell culture reagent)	D4540	
Dimethyl sulfoxide-d_6 (for NMR)	151874	
Ethyl acetate	319902	
Hydrochloric acid	320331	
Hydrogen peroxide solution	H1009	
Magnesium sulfate	M7506	
Methanol	34860	
Methyl pentafluorobenzoate	AC10247660	
N-(3-Dimethylaminopropyl)-N′-ethylcarbodiimide hydrochloride (EDC·HCl)	E7750-5G	
N-Hydroxysuccinimide (NHS)	130672	
Phosphate-buffered saline (PBS) tablets	003002	

Poly(-ε-caprolactone) (PCL) (80 kDa)	440744	
Potassium hydroxide	221473	
Potassium periodate	210056	
Purpald®	162892	
Sodium azide	8223350100	
Sodium chloride	S9888	
Sodium hydroxide	221465	
Sodium phosphate dibasic heptahydrate	S9390	
Sodium phosphate monobasic monohydrate	S9638	
Tetrahydrofuran	401757	
Toluene	179418	
N-(6-Aminohexyl)rhodamine 6G-amide bis(trifluoroacetate)	SC-301226	Santa Cruz Biotechnology (UK)
N-Succinimidyl 4-Azido-2,3,5,6-tetrafluorobenzoate	SC-208056	
0.4% Trypan Blue Solution	15250061	ThermoFisher Scientific (UK)
Dulbecco's Modified Eagle Medium, high glucose, GlutaMAX™ Supplement, HEPES (DMEM)	32430100	
Gibco® Dulbecco's phosphate-buffered saline (DPBS), no calcium, no magnesium	14190250	
Gibco® heat inactivated, Fetal Bovine Serum	10082139	
Gibco® Penicillin-Streptomycin	15140122	
Pierce™ Bovine Serum Albumin Standard, 2 mg/mL	23210	
PrestoBlue™ Cell Viability Reagent	A13261	
RPMI 1640 Medium, GlutaMAX™ Supplement	61870044	
Bradford Ultra™	EP119216	Expedeon (UK)
Ultra-LEAF™ Purified anti-human CD3 Antibody (anti-CD3)	300465	BioLegend (UK)
Ultra-LEAF™ Purified anti-human CD28 Antibody (anti-CD28)	302943	
Human IL-2 DuoSet ELISA	DY202	R&D systems (UK)

Table 2-2: List of chemicals and materials used for experiments in Chapter 4.

Chemicals	Cat No.	Supplier
2,2,2–trifluoroethanol (99.8%, TFE)	75898	Sigma-Aldrich (UK)
Albumin–fluorescein isothiocyanate conjugate (FITC-BSA)	A9771	
Dimethyl sulfoxide (DMSO) (cell culture reagent)	D4540	
EDTA (BioReagent)	E6758	
Methanol	34860	
Phosphate-buffered saline (PBS) tablets	003002	
Poly(-ε-caprolactone) (PCL) (45 kDa)	704105	
N-(6-Aminohexyl)rhodamine 6G-amide bis(trifluoroacetate)	SC-301226	Santa Cruz Biotechnology (UK)
0.4% Trypan Blue Solution	15250061	ThermoFisher Scientific (UK)
Gibco® Dulbecco's phosphate-buffered saline (DPBS), no calcium, no magnesium	14190250	
Gibco® heat inactivated, Fetal Bovine Serum	10082139	
Gibco® Penicillin-Streptomycin	15140122	
LIVE/DEAD™ Fixable Violet Dead Cell Stain Kit, for 405 nm excitation	L34955	
NanoOrange™ Protein Quantitation Kit	N6666	
OneComp eBeads™ Compensation Beads	01-1111-42	
Pierce™ 16% Formaldehyde (w/v), methanol free	28906	
Pierce™ Bovine Serum Albumin Standard, 2 mg/mL	23210	
PrestoBlue™ Cell Viability Reagent	A13261	
RPMI 1640 Medium, GlutaMAX™ Supplement	61870044	
UltraPure™ DNase/RNase-Free Distilled Water	10977035	
Bradford Ultra™	EP119216	Expedeon (UK)
APC anti-human CD4 Antibody	300514	BioLegend (UK)
CFSE Cell Division Tracker Kit	423801	
ELISA MAX™ Deluxe Set Human IFN-γ	430104	
ELISA MAX™ Deluxe Set Human TNF-a	4302045	
FITC anti-human CD3 Antibody	317306	
Human IL-2 DuoSet ELISA	DY202	
Lymphopure™	426202	
PE anti-human CD8 Antibody	344706	

PE/Cyanine7 anti-human CD3 Antibody	317334	
Ultra-LEAF™ Purified anti-human CD28 Antibody (anti-CD28)	302943	
Ultra-LEAF™ Purified anti-human CD3 Antibody (anti-CD3)	300465	
CD4 Antibody, anti-human, PerCP	130-113-217	Miltenyi
MACSQuant running Buffer	130-092-747	Biotec (UK)
EasySep™ Human CD3 Positive Selection Kit II	17851	Stemcell Technology (UK)
Honeywell Fluka™ Sulfuric acid solution, 1M	15644920	Fisher Scientific (UK)

Table 2-3: List of chemicals and materials used for experiments in Chapter 5.

Chemicals	**Cat No.**	**Supplier**
PCL-N_3 (~45 kDa)	N/A	Prepared by Dr Aram Saeed (University of East Anglia, UK)
Chloroform	32211-1L-M	Sigma-Aldrich (UK)
DMSO		
1,4-Dithiothreitol	10197777001	
2,2,2–trifluoroethanol (TFE)	75898	
Click-iT™ Alexa Fluor™ 488 sDIBO Alkyne	C20020	
LIVE/DEAD™ Fixable Violet Dead Cell Stain Kit, for 405 nm excitation	L34955	
NuPAGE® LDS sample buffer	NP0007	ThermoFisher Scientific (UK)
NuPAGE® MOPS running buffer	NP0001	
EDTA (BioReagent)	E6758	
Dimethyl sulfoxide (DMSO) (cell culture reagent)	D4540	
Phosphate-buffered saline (PBS) tablets	003002	
Gibco® Dulbecco's phosphate-buffered saline DPBS), no calcium, no magnesium	14190250	

Gibco® heat inactivated, Foetal Bovine Serum	10082139	
Gibco® Penicillin-Streptomycin	15140122	
Goat anti-Mouse IgG (H+L), Superclonal™ Recombinant Secondary Antibody, Alexa Fluor 488	A28175	
0.4% Trypan Blue Solution	15250061	
Novex sharp pre-stained standard marker	LC5800	
Ultra-LEAF™ Purified anti-human CD3 Antibody (anti-CD3)	300465	BioLegend (UK)
Ultra-LEAF™ Purified anti-human CD28 Antibody (anti-CD28)	302943	
CFSE Cell Division Tracker Kit	423801	
Human IL-2 DuoSet ELISA	DY202	
ELISA MAX™ Deluxe Set Human TNF-a	4302045	
ELISA MAX™ Deluxe Set Human IFN-γ	430104	
PE/Cyanine7 anti-human CD3 Antibody	317334	
PE anti-human CD8 Antibody	344706	
APC anti-human CD4 Antibody	300514	
FITC anti-human CD3 Antibody	317306	
Lymphopure™	426202	
CD4 Antibody, anti-human, PerCP	130-113-217	Miltenyi Biotec (UK)
MACSQuant running Buffer	130-092-747	
EasySep ™ Human CD3 Positive Selection Kit II	17851	Stemcell Technology (UK)
Honeywell Fluka™ Sulfuric acid solution, 1M	15644920	Fisher Scientific (UK)

Table 2-4: List of chemicals and materials used for experiments in Chapter 6.

Chemicals	**Cat No.**	**Supplier**
Yervoy® (ipilimumab 5 mg/mL, 50 mL)	N/A	Clinical leftover
2,2,2–trifluoroethanol (TFE)	75898	Sigma-Aldrich (UK)
Dimethyl sulfoxide (DMSO) (ACS reagent)	472301	
InstantBlue™	ISB1L	
MicroBCA™ Protein Assay Kit	23235	
NHS-Fluorescein (5/6-carboxyfluorescein succinimmidyl ester), mixed isomer (NHS- FITC)	46409	

Novex sharp pre-stained standard marker	LC5800
NuPAGE® LDS sample buffer	NP0007
NuPAGE® MOPS running buffer	NP0001
Phosphate-buffered saline (PBS) tablets	003002
Poly(-ε-caprolactone)(PCL) (80 kDa)	440744
Sodium azide (ReagentPlus®)	S2002
Sodium dodecyl sulfate (SDS) (ACS reagent)	436143
Sodium hydroxide	221465
Trizma® base	T1503
Trizma® hydrochloride (reagent grade)	T3253
TWEEN® 80	P1754

2.1.2. Cell lines

A human T cell line (Jurkat E6.1; TIB-152™) and colorectal adenocarcinoma cell line Caco-2 (HTB-37) were purchased from ATCC®.

2.1.3. Biological samples

Human leukocyte cones from anonymous donors were acquired from the NHS Blood and Transplant Service (BTS). Ethical approval for these products to be used in research work was obtained from donors by BTS, and all experiments were conducted in accordance with the requirements of the Human Tissue Act.

2.2 Methods

2.2.1. Monoaxial electrospinning

Full details of the processing parameters, including polymer properties (molecular weight, viscoelasticity), applied voltage, polymer solution flow rate and collecting distance, are described in each chapter. These solutions were carefully loaded into 5 mL disposable plastic syringes (Terumo, UK), ensuring no air bubble formation. The syringe was then mounted on a 78-9100C syringe pump (Cole Parmer,

UK). A stainless-steel dispensing needle (20G for electrospinning, 21G for electrospraying; Nordson EFD, UK) was attached to the tip of the syringe. The positive electrode of HCP 35-35000 high voltage DC power supply (FuG Elektronik, Germany) was then clamped to the spinneret. The grounded electrode was connected to a 14.7 cm × 20 cm metal plate collector covered with aluminium foil. The polymer solution was ejected from the syringe at a constant rate at ambient conditions (25 ± 2 °C and relative humidity 35 ± 10%).

2.2.2. Morphological characterization

2.2.2.1. Scanning electron microscopy (SEM)

A sample of approximately 0.5 cm × 0.5 cm was cut from each fibre formulation. For particle samples, approximately 1 mg of powder was used. The samples were mounted onto aluminium stubs (TAAB Laboratories, UK) with carbon-coated adhesive tabs and sputter-coated with 20 nm gold for 5 minutes (Q150R coater, Quorum, UK) in an argon atmosphere and analysed with a cerium hexaboride thermionic filament scanning electron microscope (Phenom Pro, Thermo, Netherlands) connected to a secondary electron detector. The size of the fibres/particles produced using EHD process was calculated using ImageJ software version 1.52a (National Institutes of Health, USA) with a minimum sample size of 100, from three SEM images. The size distribution curves were prepared using Prism software version 8.4.2 (GraphPad, USA).

2.2.2.2. Digital microscopy

Transmitted light and green fluorescent protein (GFP) microscope images were obtained from an EVOS XL Cell Imaging System digital inverted microscope (ThermoFisher Scientific, UK).

2.2.3. Physicochemical characterisation

2.2.3.1. Fourier transform infrared spectroscopy (FTIR)

FTIR spectra of samples (approximately 0.2 cm × 0.2 cm for fibres or 5 mg for powders) were obtained using a Spectrum 100 spectrometer (Perkin Elmer, USA). The spectral data were analysed with the Spectragryph v1.2.10 software (Dr. Friedrich Menges, Germany) or Prism software version 8.4.2 (GraphPad, USA). Data were collected over the wavenumber range from 650-4000 cm^{-1}, with resolution 1 cm^{-1} and 4 scans obtained per sample.

2.2.3.2. X-ray photoelectron spectroscopy (XPS)

X-ray photoelectron spectroscopy (XPS) of samples (approximately 0.2 cm × 0.2 cm for fibres or 5 mg for powders) was performed using a Thermo Scientific K-alpha spectrometer (ThermoFisher Scientific, UK) equipped with a 180° hemispherical analyser, an aluminium K-alpha micro-focused monochromator (1486.68eV) with a 100W power source, and measurements performed in constant analyser energy (CAE) mode. Pass energy was set to 50-200 eV, base pressure in the analysis chamber below 2×10^{-8} Pa, energy step size 0.1 eV and total scan numbers of 15 and 30 were used for survey and high-resolution scans respectively. Peaks areas were quantified and corrected for atomic sensitivity from high-resolution elemental surface spectra using C1s, O1s, N1s, and F1s using Thermo Avantage v.5 software (ThermoFisher Scientific, UK) or CasaXPS version 2.3.16 (Casa Software Ltd, UK). Prism software version 8.4.2 (GraphPad, USA) was used to plot survey spectra.

2.2.3.3. Differential scanning calorimetry (DSC)

Analysis was conducted using a Q2000 DSC (TA Instruments, UK). A small amount of sample was placed inside a non-hermetically sealed aluminium pan (T130425, TA Instruments, Germany). DSC analysis was carried out from 0 ºC - 300 ºC

at a temperature ramp of 10 ºC/min, unless stated otherwise. Oxygen-free nitrogen gas at a purge rate of 50 mL/min was supplied to the furnace throughout the experiment. To calculate the degree of crystallinity, the measured values of enthalpy were divided by the melting enthalpy of 100% crystalline PCL (139.5 J g^{-1})[188]. Data analysis was carried out using the TA Universal Analysis software version 4.5 (TA Instruments, USA). Prism software version 8.4.2 (GraphPad, USA) was used to plot thermograms.

2.2.3.4. X-ray diffraction (XRD)

X-ray diffraction (XRD) patterns of the samples and reference materials were obtained using a Miniflex 600 (Rigaku) diffractometer supplied with Cu-Kα radiation (λ= 1.5418 Å). A glass sample holder was used. The patterns were recorded in the 2Θ range of 3 - 60º at a speed of 0.5º min^{-1}. The generator voltage was set at 40 kV and the current at 15 mA. Data were analysed using the X'Pert Data Viewer software package (PANAlytical, Netherlands) and visualised using Prism software version 8.4.2 (GraphPad, USA).

2.2.4. Microplate reader

A SpectraMax M2e microplate reader (Molecular Devices, UK) was used to read absorbance and fluorescence in microplate based-assays. The instrument was equipped with dual monochromators and a high-power Xenon flashlamp. The reader was controlled by the SoftMax Pro software, version 6.3 (Molecular Devices, UK).

2.2.5. Protein characterisation

2.2.5.1. Sodium dodecyl sulfate–polyacrylamide gel electrophoresis (SDS-PAGE)

SDS-PAGE analyses were performed to characterise the size and estimate the purity of protein samples in Chapters 5 and 6. Briefly, a NuPAGE® Novex® 4-12% Bis-Tris Precast gel cassette (Life Technologies, UK) was washed with deionised water. The plastic comb was removed from the cassette and the sample wells were rinsed with DI water. The gel was then loaded and locked in an XCell SureLock™ Mini-Cell (Life Technologies, UK) filled with 1X NuPAGE® MOPS running buffer (ca. 800 mL). Aliquot samples (20.0 μL) were mixed with NuPAGE® LDS sample buffer (4X) (6 μL; Life Technologies, UK) and loaded into the sample wells (20.0 μL/well). SDS-PAGE was performed for 45 min at 200 V and 120 mA, under ambient conditions. Afterwards, the gel cassette was removed from the running chamber and rinsed with deionised (DI) water. The cassette was disassembled, and the gel was immersed in InstantBlue® Coomassie Protein Stain (ca. 20.0 mL; Abcam, UK). Following incubation at room temperature for 1 h, the gel was destained in DI water for 2 h before imaging with a digital scanner.

2.2.6. Protein concentration assays

2.2.6.1. Absorbance at 280 nm

Antibody working solutions in Chapters 5 and 6 were quantified using the Protein A280 application module (NanoDrop UV-Vis spectrophotometer, Thermo Scientific, UK). Sample protein concentrations were calculated using the mass extinction coefficient of 13.7 at 280 nm for a 10 mg/ml IgG solution.

2.2.6.2. Bradford Ultra assay

In perfluorophenyl azide-containing samples (Chapters 3 and 4), proteins were quantified using a Bradford ULTRA™ kit, which is a Coomasie-binding protein quantification assay. The assay was performed in accordance with the manufacturer's microplate protocol for lower protein concentration range (1-25 µg/mL). Briefly, 150 µL of sample and 150 µL of Bradford ULTRA™ reagent were added to a 96 well plate and the plate was mixed thoroughly on a plate shaker at 100 rpm for 30 s. The absorbance was read at 595 nm using the SpectraMax M2e microplate reader (Molecular Devices, UK). The absorbance of the blank was subtracted from the reading of the standards or unknown samples. A standard curve was prepared for each measured protein. Each condition was measured in triplicate.

2.2.6.3. MicroBCA assay

Proteins were quantified using MicroBCA™ protein assay kit (ThermoFisher Scientific, UK), which is a bicinchoninic acid-based protein quantification assay. The assay was performed in accordance with the manufacturer's protocol for microplate format (linear working range of 2-40 µg/mL). Briefly, the working reagent (WR) was prepared by mixing MicroBCA reagent A (MA) 50 parts: MicroBCA reagent B (MB) 48 parts: MicroBCA reagent C (MC) 2 parts. The WR (100 µL/well) was added to protein solutions (100 µL/well) in a 96 well plate, and the plate mixed thoroughly on a plate shaker at 100 rpm for 30 s. The plate was then incubated at 37 °C for 2 h. The plate was allowed to cool down to room temperature (5 min) before reading the absorbance at 562 nm using the SpectraMax M2e microplate reader (Molecular Devices, UK). A standard curve was prepared for each measured protein. The absorbance of the blank was subtracted from the reading of the standards or unknown samples. Each condition was measured in triplicate.

2.2.6.4. NanoOrange® assay

Samples containing low concentrations of protein (below 10 µg/mL) were quantified using a NanoOrange® Protein Quantitation Kit (ThermoFisher Scientific, UK), which allows for accurate detection of proteins in solution at concentrations between 10 ng/mL and 10 µg/mL. The manufacturer's protocol was adjusted for microplate format. Briefly, the concentrated Component B (NanoOrange® protein quantitation diluent) was diluted 1:10 v/v in distilled water. Component A (NanoOrange® protein quantitation reagent) was diluted 1:500 v/v with the working concentration (1X) of component B to make the NanoOrange® working solution. Samples and standards (100 µL) were firstly pipetted onto a black flat-bottomed 96-well plate (Corning, UK). Then, 100 µL of NanoOrange® working solution was added into each well. The plate was covered with a heat-resistant plate seal, wrapped in aluminium foil, briefly mixed on a plate-shaker and incubated for 10 minutes at 95°C to denature the protein. Afterwards, the plate was allowed to cool down to room temperature (ca. 20 min) and 180 µL of denatured solution was pipetted into a fresh black flat-bottomed 96-well plate. The fluorescence (excitation 485 nm, emission cut-off 570 nm, and emission 590 nm, 20 flashes per read) was read using SpectraMax M2e microplate reader (Molecular Devices, UK). A standard curve was prepared for each measured protein. The fluorescence of the blank was subtracted from the reading of the standards or unknown samples. Each condition was measured in triplicate.

2.2.7. Cytokine production assays

Cytokine production in T cell activation assays was quantified using commercially available sandwich enzyme-linked immunosorbent assay (ELISA) kits according to the manufacturer's protocol. A summary of the ELISA assays used in this thesis is given in Table 2-5.

Table 2-5: Summary of ELISA assays used in chapter 3,4 and 5.

Target cytokine	Product name	Manufacturer
IL-2	Human IL-2 DuoSet ELISA	R&D Systems, UK
TNF-α	ELISA MAX™ Deluxe Set Human TNF-a	BioLegend, UK
IFN-γ	ELISA MAX™ Deluxe Set Human IFN-γ	BioLegend, UK

The experimental method was identical for all kits used. A high protein-binding 96-well plate (Nunc MaxiSorp™ flat-bottomed microplates, ThermoFisher Scientific, UK) was loaded with 100 µl of capture antibody solution per well and incubated overnight. On the following day, the capture antibody solution was discarded, and the plates were thoroughly washed four times with washing buffer (PBS supplemented with 0.05% Tween 20). Non-specific binding was blocked by adding block buffer (1% BSA w/v in PBS) and incubating at room temperature for 1 hour. Each plate was then washed four times as described above.

Subsequently, freshly prepared cytokine standards and cytokine-containing cell supernatants were diluted with assay diluent (to 100 µl) and pipetted into the microplates, following by an incubation at room temperature for 2 hours and washing. A solution of biotin-labelled detection antibody was then added to each well, incubated at room temperature and washed. After washing away the unbound biotinylated antibodies, horseradish peroxidase-conjugated streptavidin was pipetted into the wells and incubate at room temperature. The plate was then once again washed and a colorimetric substrate solution (100 µL) was added. The reaction was stopped by adding 2N sulfuric acid (100 µL) and the absorbance at 405 nm measured using a SpectraMax M2e microplate reader (Molecular Devices, UK) with a wavelength correction at 540 nm. The absorbance reading of the blank was subtracted from the reading of standards/unknown samples. The standard curve and interpolation of values was performed using GraphPad Prism 8.4.2 (GraphPad, USA) software.

2.2.8. Cell culture

2.2.8.1. Cell viability testing using Trypan Blue exclusion approach

Cell viability and density in cell culture maintenance was performed using the Trypan Blue exclusion approach. The dye exclusion test is based upon the concept that viable cells do not take up impermeable dyes (like Trypan Blue), but dead cells are permeable and will appear blue when observed under the microscope. Cell suspension (30 µl) mixed with 0.4% Trypan Blue solution (30 µL; Gibco™, UK) was prepared and 10 µL was loaded into a haemocytometer. The number of all cells and blue-stained cells were counted under a microscope. The total cell count (cells/mL) and percentage of viable cells was calculated using the equations below (Equations (2.1), (2.2), (2.3)).

$$Total\ cell\ count\ \left(\frac{cells}{mL}\right) = \frac{number\ of\ counted\ cells\ \times dilution\ factor\ \times 10^4}{number\ of\ counted\ squares} \quad (2.1)$$

$$Total\ viable\ cell\ count\ \left(\frac{cells}{mL}\right) = \frac{number\ of\ counted\ live\ cells\ \times dilution\ factor\ \times 10^4}{number\ of\ counted\ squares} \quad (2.2)$$

$$Viability\ (\%) = \frac{total\ viable\ cell\ count}{total\ cell\ count} \times 100 \quad (2.3)$$

2.2.8.2. Cell viability testing using PrestoBlue™ Cell viability reagent

Cell viability in multi-well plate experiments was measured using PrestoBlue™ Cell viability reagent (ThermoScientific, UK) according to the manufacturer's protocol. Briefly, following experimental treatments, the multi-well plate was centrifuged at 1200 rpm for 5 minutes to pellet the cells and the supernatant was removed for further testing (e.g. ELISA as described in Section 2.2.7, page 59). Then, the pelleted cells were resuspended in culture medium and the cell viability reagent was added directly to cells in culture medium at a 1:10 v/v ratio. For example, in the 96-well plate format the volume of cells + culture medium was 90 µL for 10 µL of the cell viability reagent. The plate was then incubated for 3 hours at 37 °C under a 5% CO_2 atmosphere, protected from direct light. The results were recorded using fluorescence optical

densities (excitation wavelength of 560 nm and emission of 590 nm) measured on SpectraMax M2e plate reader. The value of blank (culture medium, no cells) was subtracted from experimental values and the cell viability was expressed as a percentage where untreated cells or the negative control were taken to have 100% viability.

2.2.8.3. Jurkat E6.1

The human T cell line (Jurkat E6.1) was used in T cell activation assays. The cell culture was maintained in suspension at 37 °C under a 5% CO_2 atmosphere in RPMI-1640 medium containing L-glutamine (Sigma-Aldrich, UK), supplemented with 10% v/v heat-inactivated foetal bovine serum (FBS; Gibco™, UK) and 1% v/v penicillin-streptomycin solution (Gibco™, UK). The culture was maintained between 1×10^5 and 1×10^6 viable cells/mL by addition or replacement (by centrifugation and subsequent resuspension) of fresh medium every 2 to 3 days. The cell suspension was cultured in Corning® T-75 flasks (ThermoFisher, UK) kept upright.

2.2.8.4. Caco-2

The adherent epithelial cell line Caco-2 was used in Chapter 3 to determine the cytotoxicity of functionalised fibres. The cell culture was maintained at 37 °C, under 5% CO_2, in Dulbecco's modified Eagle medium (DMEM; Gibco™, UK) supplemented with penicillin-streptomycin solution (1% v/v) and 20% v/v heat-inactivated foetal bovine serum (Gibco™, UK). The culture was maintained between 8×10^4 and 1×10^5 viable cells/mL, with media renewal twice per week. The cells were subcultured upon reaching 80% confluency in Corning® T-75 flasks (ThermoFisher, UK) according to standard cell culture protocols. Briefly, culture medium was removed and discarded and the cell layer was rinsed with 0.25% (w/v) trypsin-0.53 mM EDTA solution (Gibco™, UK). Afterwards, 3 mL of trypsin-0.53 mM EDTA solution was added and the flask was incubated at 37 °C, under 5% CO_2

until the cell layer was dispersed when observed under a microscope. Once the cells appeared detached, 7 mL of pre-warmed complete DMEM was added, and the cells were aspirated by gentle pipetting. The cell suspension was centrifuged, and the resultant supernatant was discarded. The cells were then resuspended in pre-warmed complete DMEM and appropriate aliquots (around 1×10^4 viable cells/cm^2) were placed in a new culture vessel.

2.2.8.5. Isolation of mononuclear cells from leukocyte cones

Isolation of mononuclear cells from human leukocyte cones was performed in a biosafety cabinet under sterile conditions. Heparinised blood from leukocyte cones (ca. 10-15 mL) was diluted with an equal volume of Dulbecco's PBS (DPBS) buffer without calcium and magnesium in a sterile 50 mL centrifuge tube. A cold Lymphopure™ (Biolegend, UK) buffer was carefully layered dropwise under the diluted blood mixture using a sterile plastic Pasteur pipette until a transparent and clear layer was formed under the blood. No mixing of blood and Lymphopure™ was allowed to occur.

The tube was then centrifuged at 2000 rpm for 30 minutes at 22°C without braking. After centrifugation, peripheral blood mononuclear cells (PBMCs) form a defined cell layer (buffy coat) at the plasma: Lymphopure™ interface, which can be carefully collected using a sterile plastic Pasteur pipette without disturbing the other fractions. The harvested buffy coat was then diluted to 50 mL with cold DPBS buffer supplemented with 2% foetal bovine serum (PBA buffer) and centrifuged at 1800 rpm at 4 °C for 15 minutes. The cell pellet was then washed with cold PBA buffer and centrifuged at 1500 rpm at 4 °C for 10 minutes, followed by another wash in cold PBA containing 5 mM EDTA (PBA-EDTA) and centrifugation at 1200 rpm at 4 °C for 5 minutes. Finally, the isolated PBMCs were resuspended in cold PBA-EDTA and their viability was determined using the Trypan Blue exclusion approach.

2.2.8.6. Cryopreservation of isolated PBMCs

The isolated PBMCs (section 2.2.8.5) were frozen for future use in liquid nitrogen. All reagents and freezing container (Mr Frosty™, Sigma-Aldrich, UK) were kept chilled during the cryopreservation procedure. Briefly, PBMCs were resuspended in a dropwise manner in a freezing medium (10% DMSO in complete RPMI-1640 medium; 1×10^8 of PBMCs per 1 mL of medium) and transferred to 2 mL cryovials (Sigma-Aldrich, UK). The cryovials were then placed in a freezing container filled with isopropyl alcohol and stored at -80 °C overnight. Afterwards, the frozen cryovials were transferred to the vapour phase of a liquid nitrogen storage vessel.

2.2.8.7. CD3 T cells

CD3 T cells were generated *in vitro* using EasySep™ Human CD3 Positive Selection Kit II (STEMCELL, UK) from PBMCs. Briefly, a vial containing 1×10^8 PBMCs in 1 mL of freezing medium (10% DMSO in complete RPMI-1640 medium) was thawed and the contents were transferred to a 5 mL polystyrene round-bottom tube (Miltenyi, UK). Then, 100 µL of selection cocktail was added, and the contents of the tube were gently mixed and incubated for 3 minutes at room temperature. RapidSpheres™ were vortexed for 30 seconds and 60 µL was added to the tube. After brief mixing and three-minute incubation, the contents were topped up with PBA-EDTA and the uncapped tube was placed into a magnet (EasySep™, STEMCELL, UK) and incubated for 3 minutes. Afterwards, the magnet was inverted and the supernatant was poured off from the tube. The tube was then removed from the magnet and the contents were washed with ice cold PBA-EDTA. The washing step was repeated three times. Afterwards, the cells were resuspended in complete RPMI-1640 medium.

2.2.8.8. Carboxyfluorescein succinimidyl ester (CFSE) staining

Isolated CD3+ T cells were stained with CFSE to track proliferation using a CFSE Cell Division Tracker Kit (BioLegend, UK). A stock solution of CFSE dye was prepared by reconstituting one vial of CFSE dye in 36 µL of DMSO to give 5 mM solution. A 5 µM working solution was prepared by diluting 1 µL of stock solution in 1 mL PBS for every 1 mL of cell suspension. CD3+ T cells prepared in Section 2.2.8.7 were centrifuged and resuspended at 2×10^7 cells/mL in the CFSE working solution. The cells were then incubated for 20 minutes at 37 °C under a 5% CO_2 atmosphere. The staining was quenched by adding 5 times the original staining volume of complete RPMI-1640. Subsequently, the cells were pelleted and resuspended in pre-warmed complete RPMI-1640 for *in vitro* experiments.

2.2.9. Flow cytometry

Flow cytometry analyses were performed using a MACSQuant® Analyzer 10 (Miltenyi Biotec, UK) equipped with three lasers (40 mW diode 405 nm, 30 mW diode pumped solid state 488 nm, 20 mW diode 638 nm), and 10 optical emission channels. Compensation beads (OneComp eBeads™, ThermoFisher, UK) were used to compensate for spectral overlap in multicolour panels. The instrument was controlled with the MACSQuantify™ software version 2.6 (Miltenyi Biotec). Pre-cooled MACS® Chill 96 Racks (Miltenyi Biotec) were used with a microplate to cool cell samples during flow cytometry experiments. Data were analysed using the FlowJo software version 10.6.2 (FlowJo, USA) or FCS Express software version 7.04 (USA).

2.2.10. Statistical analysis

All quantitative data are presented as mean ± standard deviation (SD), and have been calculated and statistically analysed using the Prism software version 8.4.2 (GraphPad, USA). An unpaired two tailed t-test was used for two group comparison.

Analysis of variance was performed using one-way or two-way repeated measures ANOVA, with Tukey's post hoc test. Statistical significance is denoted on figures as: ns (*p-value* >0.05), * (*p-value* ≤0.05) ** (*p-value* ≤0.01), *** (*p-value* ≤0.001), **** (*p-value* ≤0.001).

Chapter 3 - Perfluorophenyl azide functionalisation of electrospun polycaprolactone fibres

3.1 Introduction

Surface functionalisation of polymeric biomaterials is frequently explored for applications in regenerative medicine and tissue engineering[154,189–191]. Modification of a material, for example by increasing the hydrophilicity of the surface, is often associated with better biological performance by promoting cell attachment[192–194] and stem cell differentiation[195–198]. Equally, the presentation of therapeutic proteins on the surface, rather than in the core of a biomaterial, is preferred for some applications, such as presentation of antigens for T cell activation[105] or wound healing[139].

Several bioconjugation methods suitable for the surface functionalisation of electrospun materials have been described in the introductory chapter of this thesis (see Section 1.5, page 35). Another approach, relatively unexplored in the literature, involves surface functionalisation using photo-assisted perfluorophenyl azide (PFPA) chemistry. The concept of protein photografting using aryl azide crosslinkers has now been researched for over 20 years. In 1995 Pritchard, Morgan and Cooper[199] reported successful site-specific attachment of antibodies to SiO_2 using an analogue of streptavidin containing a photoactivatable functional group. This compound, photobiotin, had a terminal aryl azide group capable of forming a reactive aryl nitrene

group upon exposure to light[200]. Further heterobifunctional linkers made of photoreactive phenyl azides and amine-binding NHS groups were developed[201–203] and showed enhanced protein conjugation to hydrocarbon containing surfaces. The photochemical C-H insertion of an NHS functionalised azide was successfully used to graft proteins such as albumin[204], insulin[205] or growth factors[189] to various polymer surfaces.

3.1.1. Surface functionalisation *via* PFPA chemistry

Perfluorophenyl azides can be easily modified with functional groups to enable the direct conjugation of bioactive molecules[206], for example carbohydrates[207–209] or proteins[210]. In a study of carbohydrate conjugation to surface plasmon resonance (SPR) interfaces, Maalouli et al.[211] found the efficiency of a PFPA functionalisation approach comparable to the popular Cu(I)-catalysed 'click' chemistry. Theoretically, since the nitrene-driven C-H insertion is non-specific, PFPA functionalisation can be applied to any molecule possessing a hydrocarbon chain. This makes the method highly attractive for modification of pharmaceutically relevant biodegradable polymers, such as polycaprolactone, PLGA or polydioxanone (PDO)[212].

3.1.2. Principles of nitrene chemistry

The photoinitiated C-H insertion reactions observed in aryl azide-assisted conjugations are a result of a reactive nitrene intermediate being formed upon UV irradiation of the precursor azide group. Upon photochemical or thermal activation, azides decompose to give singlet nitrene, releasing N_2 as a by-product[213] (Scheme 3-1). Nitrenes are highly reactive, and therefore can lead to rearrangements in the parent molecule, provoking a chain of non-specific reactions[214]. To overcome this,

aryl azides are used. Resonance stabilisation within the aromatic ring suppresses molecular rearrangements during photochemical C-H insertion reactions[215].

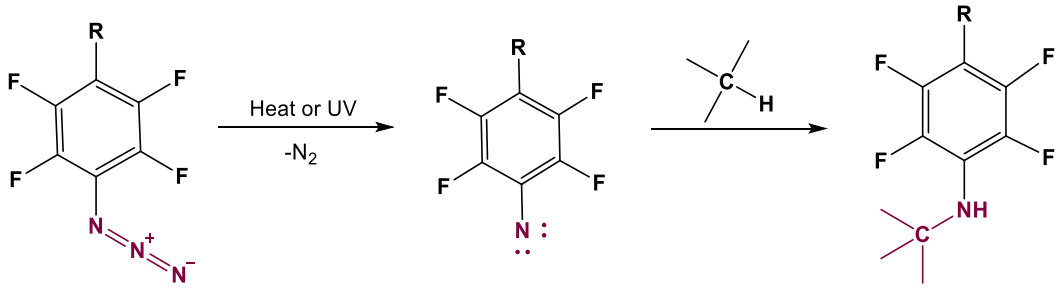

Scheme 3-1: Insertion reaction of singlet perfluorophenylnitrene generated from photolysis or thermolysis of PFPAs[216].

Such phenyl azides are often further substituted with fluorine to give perfluorophenyl azides (PFPAs). The highly inductive electron-withdrawing effect of the aryl fluorine substituents ortho to the azido group prolongs the lifetime of the single phenyl nitrene[217,218]. This leads to increased reactivity of the nitrogen species by a combined steric effect and high electronegativity of the fluorine atom[219]. Functionalised PFPAs can act as heterobifunctional coupling agents by the combined action of two reactive centres – a chemoselective functional group and the light-activatable azido group[220].

3.1.3. Protein conjugation *via* PFPA chemistry

The development of perfluorophenyl azide functionalised with a N-hydroxysuccinimide ester (PFPA-NHS) was first reported in 1994 by Mingdi Yan[210] and has widened the array of PFPA functionalisation applications. The NHS group is capable of undergoing reaction with primary amine-containing molecules, therefore enabling protein conjugation. By adding the NHS group to the PFPA structure, any amine-containing molecule can in principle be covalently conjugated to a hydrocarbon-containing molecule *via* a stable covalent bond. To support this hypothesis, Yan et al. successfully attempted immobilization of horseradish peroxidase on a spin-coated polymer film using PFPA-NHS. [210]

Recently, Luetzow et al. reported an effective method of PDO fibre surface modification using photo-assisted C-H insertion chemistry[221]. An electrospun nanofibre mesh was successfully functionalised with an amine-containing rhodamine dye that acted as a model for a covalent protein conjugation reaction. The functionalisation was performed in two steps – firstly, a NHS functionalised heterobifunctional linker (PFPA with an NHS end group; PFPA-NHS), was grafted *via* UV-assisted C-H insertion into the hydrocarbon chain of PDO. Subsequently, the NHS group was allowed to react under aqueous conditions with an amine groups of the dye, resulting in surface functionalisation.

3.1.4. Aims of this chapter

Although preliminary studies have shown effective conjugation of model molecules to hydrocarbon-based surfaces using PFPA-NHS[210,221], little is known about the *in vitro* performance of such composites. This chapter therefore aimed to explore the feasibility of conjugating pharmaceutically relevant proteins to electrospun PCL nanofibres using PFPA-NHS chemistry. An extensive physicochemical characterisation of the modified fibres was performed, together with an investigation of conjugation efficiency and screening for biological activity in cell culture models. Finally, the PFPA functionalisation approach was used to prepare antibody-decorated scaffolds for *in vitro* T cell activation.

3.2 Materials and methods

3.2.1. Synthesis of PFPA-NHS

The three-step synthesis of PFPA-NHS was performed in the dark according to a previously published synthetic procedure (Scheme 3-2)[221].

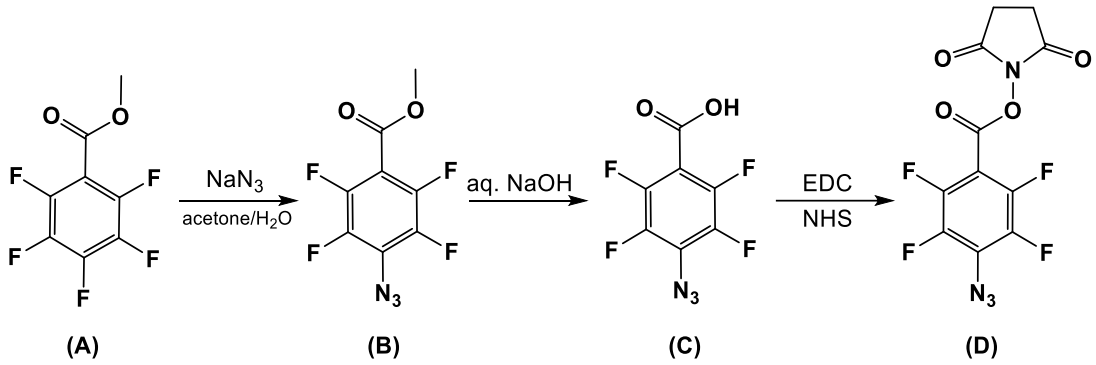

Scheme 3-2: Synthesis of N-succinimidyl 4-azidotetrafluorobenzoate (PFPA-NHS).

3.2.1.1. Synthesis of methyl 4-azidotetrafluorobenzoate (B)

Methyl pentafluorobenzoate (A) (10 mL, 15.3 g, 68 mmol) was dissolved in a 2:1 v/v mixture of acetone (100 mL) and deionized water (50 mL). Sodium azide (5.75 g, 88.5 mmol) was added and the reaction mixture was stirred and heated under reflux for 5 hours. Afterwards, the reaction mixture was allowed to cool down to room temperature, diluted with water (200 mL) and extracted with ethyl acetate (4 × 100 mL). The extract was washed with brine (2 × 100 mL) and the organic phase was dried with magnesium sulfate. Ethyl acetate was removed under reduced pressure by rotoevaporation to produce a yellowish solid (13.30 g, 87%). ^{1}H NMR (500 MHz, $CDCl_3$): δ = 3.97 (s, 3 H, OCH_3) ppm. ^{13}C NMR (500 MHz, $CDCl_3$): δ = 160.0 (s, CO_2CH_3), 146.6-139.5 (qm, C-F), 123.5 (tt, CN_3), 107.8 (t, CCO_2CH_3), 53.4 (q, OCH_3) ppm.

3.2.1.2. Synthesis of 4-azidotetrafluorobenzoic acid (C)

Methyl 4-azidotetrafluorobenzoate (13.30 g, 56.6 mmol) (B) was dissolved in methanol (75 mL) and aqueous sodium hydroxide (5M, 10 mL) was added. After 5 hours of stirring more methanol (35 mL) and aqueous sodium hydroxide (5M, 2 mL) were added. After 24 hours, the reaction mixture was diluted with water (15 mL) and acidified with aqueous 1M hydrochloric acid in a dropwise manner under constant stirring until the solution reached pH=1. The reaction mixture was then diluted with water (100 mL) and extracted with dichloromethane (4 × 100 mL). The extract was washed with brine (2 × 100 mL) and the organic phase was dried with magnesium sulfate. The solvent was removed under reduced pressure by rotoevaporation to produce a yellowish solid (C) (10.37 g, 78%). ^{13}C NMR (500 MHz, DMSO-d_6): δ = 164.3 (s, CO_2H), 146.6-139.5 (qm, C-F), 122.7 (s, CN_3), 108.4 (s, CCO_2H) ppm.

3.2.1.3. Synthesis of PFPA-NHS (D)

A mixture of (C) (3.2 g, 13.6 mmol), EDC·HCl (3.1 g, 16.2 mmol) and NHS (1.85 g, 16.1 mmol) was dissolved in dichloromethane (70 mL) and allowed to react at 35°C for 24 hours under constant stirring. Additional EDC·HCl (1.62 g, 8.6 mmol) was added to the reaction mixture and stirring continued for a further 24 hours. The reaction mixture was diluted with water (60 mL) and extracted with dichloromethane (3 × 100 mL). The extract was washed with brine (2 × 100 mL) and the organic phase was dried with magnesium sulfate. The solvent was removed under reduced pressure by rotoevaporation to produce a beige solid. The obtained product was purified by precipitation into ice-cold 2-propanol to produce PFPA-NHS (D) as a white solid (2.65 g, 83%). ^{1}H NMR (500 MHz, $CDCl_3$): δ = 2.90 (s, 4 H, $COCH_2$) ppm. ^{13}C NMR (500 MHz, $CDCl_3$): δ = 168.4 (s, $COCH_2$), 155.3 (t, CO_2N), 146.6-139.5 (qm, C-F), 126.5 (s, CN_3), 102.1 (t, CCO_2N), 25.8 (t, CH_2) ppm. IR: ν = 2995, 2955 (C─ H), 2120 (N_3),

1775, 1735, 1705,1640 (C═O), 1480 (C═C), 1410, 1360, 1250, 1205, 1135, 1065, 990 cm^{-1}.

3.2.2. Functionalisation of polycaprolactone with PFPA-NHS

Functionalisation of commercially available PCL (Mw ~80 kDa) with PFPA-NHS in solution was attempted. PFPA-NHS and PCL were dissolved in toluene at varying ratios (1:9, 5:5, 9:1 w/w) to give a solution with 10% w/v total solute concentration. The solutions were transferred to a quartz round bottom flask and stirred using a magnetic bar under UV light (8-watt, 50 Hz, 10 cm, 254 nm) for 2.5 hours. Afterwards, the reaction mixture was purified by precipitating the product in cold methanol (3 × 10 mL). The residual solvent was removed under reduced pressure by rotoevaporation to produce a white solid.

3.2.3. Nuclear magnetic resonance (NMR)

Solution-state ^{1}H NMR and ^{13}C NMR were performed using a Bruker Avance 500 MHz spectrometer equipped with a helium-cooled multinuclear cryoprobe. A Bruker Avance Neo 700 instrument equipped with a helium-cooled multinuclear cryoprobe was used to acquire ^{19}F NMR spectra. The Larmor frequency was 500.13 MHz for ^{1}H NMR, 125.76 MHz for ^{13}C NMR and 658.780 MHz for ^{19}F NMR. The results were analysed with the TopSpin 4.0.5 software.

3.2.4. Preparation of electrospun polycaprolactone fibres

Fabrication of electrospun fibres was performed using the equipment described in Section 2.2.1 (page 53). PCL fibres were prepared by electrospinning a solution of 12 % w/v PCL (Mw ~80 kDa) in 2,2,2-trifluoroethanol (TFE). The solution was carefully loaded into 5 mL disposable syringes and dispensed through a 21G stainless steel needle connected to a high-voltage direct-current power supply (15 kV)

at a flow rate of 1.8 mL/h. The fibres were collected on aluminium foil placed on top of a 14.7 cm × 20 cm metal plate collector connected to the grounded electrode. The distance from the needle to the collector was 16 cm. The experiments were conducted at 25 ± 2 °C and relative humidity 35 ± 10%.

3.2.5. Functionalisation of PCL fibres

A solution of PFPA-NHS (20 mg/mL in methanol, 10 μL) was pipetted onto the surface of a square cut from a PCL fibre mat (0.5 cm × 0.5 cm) and subsequently dried under reduced pressure (in a desiccator) to remove solvent. Afterwards, the fibre mats were placed under a UV lamp (8-watt, 254 nm, 50 Hz) and irradiated from a distance of 10 cm. The length of exposure needed to achieve functionalisation was experimentally determined by monitoring the reaction using FTIR (see Section 2.2.3.1, page 55). Control samples of untreated and PFPA-treated but non-irradiated fibres were included in experiments. Following functionalisation, the scaffolds were briefly immersed in methanol to remove unbound PFPA-NHS and dried under reduced pressure. The fibres were washed twice with sterile PBS before incubation with proteins.

3.2.6. Physicochemical characterisation of fibres

The morphology and physicochemical properties of the fibre surface were evaluated with SEM, FTIR and XPS as described in Section 2.2.3 (page 55).

3.2.7. Conjugation of fluorescently-labelled model molecules

N-(6-aminohexyl)rhodamine 6G-amide bis(trifluoroacetate) (termed "rhodamine-amine") was dissolved in methanol (5 mg/mL). Albumin–fluorescein isothiocyanate conjugate (termed 'FITC-albumin') was diluted with PBS (20 μg/mL). A small piece of a PFPA-functionalized electrospun PCL fibre mat (0.5 cm × 0.5 cm) was immersed

in the dye solution of either rhodamine-amine or FITC-albumin overnight at room temperature. After thorough washing with PBS to remove the unbound dye, the fibres were dried and viewed under an inverted fluorescence microscope as described in Section 2.2.2.2 (page 54).

3.2.8. Preliminary albumin attachment study

Functionalised fibres cut to 1 × 1 cm pieces were placed in a 12-well plate. Each well was then filled with 1 mL of BSA solution (40 µg/mL in PBS). The fibres were incubated in the protein solution for 1, 3, 6, 8, 11 and 24 hours. At each time point, the fibre mat was taken out of the well and washed with PBS. The protein concentration in the incubation and washing solutions was measured using a Bradford Ultra protein assay as detailed in Section 2.2.6.2 (page 58). The amount of protein was calculated by multiplying concentration by the initial BSA solution volume (1 mL).

The percentage protein attachment was calculated using the equation below (3.1).

$$\%\ attachment = \frac{amount_0 - amount_x}{amount_0} \times 100\% \qquad (3.1)$$

where $amount_0$ corresponds to the amount of protein at 0 hours (i.e. incubation solution; ~ 40 µg) and $amount_x$ is the amount of protein present at x hours.

3.2.9. Cytotoxicity to Caco-2 cells

The colorectal adenocarcinoma cell line Caco-2 (ATCC® HTB-37) was used to test the cytotoxicity of the functionalised fibres. Cells were maintained as described in Section 2.2.8.4, page 62. For cytotoxicity studies, 150 µL of cells at 5×10^4 cells/mL were seeded in a flat-bottom 96-well plate (Costar, UK) and incubated for 24 hours. Functionalised fibres cut to 0.5 × 0.5 cm pieces were pre-sterilised by brief immersion in methanol, then thoroughly washed in sterile PBS under aseptic conditions and introduced to the wells containing adhered cells using sterile tweezers. The plate

was incubated for one or three days to measure cell viability. At the end of the incubation period, the fibres were removed, and cell viability was quantified using the PrestoBlue™ Cell Viability reagent (Sigma-Aldrich, UK) as described in Section 2.2.8.2 (page 61). Each experiment was performed three times on separate days, with three replicate wells per experiment.

3.2.10. Characterisation and biological performance of sonicated fibres

3.2.10.1. Washing step

Following PFPA-functionalisation as described in Section 3.2.5 (page 74), the fibres were treated with two brief sonication steps. In step one, the scaffolds (cut to 0.5 × 0.5 cm pieces) were placed in a glass vial with 15 mL of methanol and sonicated in an ultrasonic bath for one minute. In step two, the same procedure was followed, except methanol was replaced with sterile PBS. Subsequently, the fibres were gently removed with tweezers and blotted with tissue paper to remove excess PBS from the surface.

3.2.10.2. Model protein surface attachment study

Three model proteins were tested in a surface attachment study – BSA, infliximab and catalase. PFPA-functionalised and sonicated fibres cut to 0.5 × 0.5 cm pieces were placed in a flat-bottomed 96-well plate and 200 µL of a 25 µg/mL protein solution in PBS was added. The plate was then tightly sealed and placed on a plate shaker set to 500 rpm. After 24 hours at room temperature, the incubation solutions were collected and the fibres washed twice with PBS. The protein concentrations of the incubation and washing solutions were measured using the Bradford Ultra protein assay and the total protein loading was calculated using the formula described previously (Section 3.3.4, page 75).

3.2.10.3. Physical characterisation of sonicated fibres

Fibres were characterised using DSC, FTIR and XRD as described in Section 2.2.3 (page 55).

3.2.10.4. Catalase activity assay

The retention of catalase activity following grafting onto the fibre surface was assessed using an assay based on the previously published protocol[222]. Briefly, catalase-functionalised fibres were prepared as outlined in Section 3.2.10.2 (page 76) and placed at the bottom of a 96-well plate. The positive control included a freshly prepared catalase solution (25 µg/mL). For the negative control, the same catalase solution was heated at 95°C for 10 min to denature the enzyme.

To each well, 100 µL of assay buffer (100 mM sodium phosphate buffer, pH 7.0), 30 µL of methanol and 20 µL of sample buffer (25 mM sodium phosphate buffer, 1 mM EDTA, 0.1% BSA w/v, pH 7.5) were added. The reaction was initiated by quickly adding 20 µL of H_2O_2 (35.28 mM) to all wells. Afterwards, the plate was covered and incubated for 20 minutes on a plate shaker (100 rpm) at room temperature. Next, 30 µL of 10 M KOH solution was added to terminate the reaction, followed by 30 µL of Purpald® solution (25 mg of Purpald® in 4 mL 480 mM HCl). The plate was once again covered and incubated for 10 minutes on a plate shaker (100 rpm) at room temperature. To stop the assay, 10 µL of KIO_4 (75 mg of KIO_4 in 4 mL 470 mM KOH) was added to each well and the plate was incubated for another 5 minutes on a plate shaker (100 rpm) at room temperature. Afterwards, the fibres were removed from the wells and 100 µL of reaction mixture was transferred onto a clean 96-well plate to read absorbance at 540 nm using a SpectraMax M2e microplate reader (Molecular Devices, UK). Each formulation was tested in triplicate. The results are presented as optical density (OD) at 540 nm.

3.2.10.5. Catalase release assay

PFPA-functionalised and sonicated fibres cut to 2 × 2 cm pieces were placed in a flat-bottomed 12-well plate and 1 mL of 1 mg/mL catalase in PBS was added. The plate was then tightly sealed and incubated for 24 hours at room temperature under constant shaking (100 rpm). Afterwards, the fibres were removed from the wells using tweezers, washed with PBS (2 × 1 mL) and placed in glass vials containing 5 mL of PBS at 37°C under constant shaking (100 rpm). At pre-determined timepoints, 0.5 mL of supernatant was removed and replenished with fresh PBS. The protein concentrations of the incubation and washing solutions were measured using the Bradford Ultra protein assay and the total amount of protein attached to the fibre was calculated by depletion using Equation (3.1) (page 75). Cumulative release of catalase was then calculated using the formula below (3.2).

$$Cumulative\ release\ (\%) = \frac{C_x \times V_t + \sum C_{x-1} \times V_a}{Protein\ loading} \times 100\% \qquad (3.2)$$

where C_x is the protein concentration in release supernatant at time x, V_t is the total volume of release media (5 mL), V_a is the sampling volume (0.5 mL) and the $Protein\ loading$ is the total amount of protein attached to the fibre.

3.2.10.6. Contact angle measurements

The hydrophobicity of surface-functionalised fibres was measured using a goniometer (FTA 1000USA). A water droplet (15 µL) was dispensed from a Gilmont micrometer syringe (Cole-Parmer Instrument Co. Ltd, UK) fitted to a 20-gauge blunt needle onto the fibre surface. The liquid droplet was allowed to stabilize on the fibre surface and photographed to allow for calculation of the contact angle using FTA 1000 software. Each sample was measured in triplicate, and the results are presented as mean ± standard deviation (n=3).

3.2.11. *In vitro* T cell activation

An *in vitro* T cell activation assay was optimized to achieve a reliable protocol for quantification of IL-2 release upon T cell receptor activation in anti-CD3 stimulated Jurkat E6.1 cells. The Jurkat E6.1 cell culture method is provided in Section 2.2.8.2, page 61.

Pieces (0.5 × 0.5 cm) of PFPA-treated fibre mats were incubated with 50 µL of 5, 10 or 20 µg/mL human anti-CD3 antibody solutions (clone: OKT3, Biolegend, UK) in sterile PBS. Incubation was performed overnight at room temperature on a plate shaker (500 rpm), and with the plates protected from light.

Following incubation, the fibres were washed once in sterile PBS under aseptic conditions and transferred to the bottom of a standard flat-bottomed 96-well plate (Corning, UK) using sterilised tweezers.

Jurkat cells were resuspended at 2.5 x 10^5 cells/mL and 200 µL of the cell suspension was transferred to each well. For the positive control, a plate-bound anti-CD3 antibody solution at the same concentration and volume (50 µL) as the fibre incubation solution was used. Wells with no antibody stimulation were used as a negative control. For a co-stimulatory response, soluble anti-CD28 was added to the cell suspension (10 µL of 10 µg/mL solution in PBS) according to published protocols[223]. The plate was then placed in a humidified 37ºC, 5% CO_2 incubator under constant shaking (500 rpm) for four days.

Afterwards, the fibres were carefully removed from each well using sterile tweezers and the plate was centrifuged at 1200 rpm for 5 minutes to allow the suspended cells to sediment at the bottom. The supernatant was collected for human IL-2 DuoSet ELISA (R&D Systems, UK; for experimental details see Section 2.2.7, page 59), while the viability of the cells following the four-day incubation was measured using the

PrestoBlue™ Cell Viability Reagent (Sigma-Aldrich, UK) as previously described (see Section 2.2.8.2, page 61). Each experiment was performed three times on separate days, with three replicate wells per experiment.

3.3 Results and discussion

3.3.1. PFPA-NHS synthesis

The three-step synthesis of PFPA-NHS was performed following a known synthetic route[221]. Briefly, methyl pentafluorobenzoate underwent nucleophilic aromatic substitution when reacted with sodium azide to yield methyl 4-azido-2,3,5,6-tetrafluorobenzoate. In the next step, the methyl ester group was hydrolysed under basic conditions to give 4-azido-2,3,5,6-tetrafluorobenzoic acid. Finally, the carbodiimide-assisted (EDC·HCl) coupling of the NHS group to the carboxylic acid yielded N-succinimidyl 4-Azido-2,3,5,6-tetrafluorobenzoate.

The structure of the purified compound was confirmed using C^{13} NMR (Figure 3-1) and FTIR (Figure 3-2). Both NMR and FTIR spectra are consistent with previously published data on PFPA-NHS[210,221] and confirm the successful synthesis of this compound. In ^{13}C NMR (Figure 3-1), four multiplets between 148 and 138 ppm correspond to aromatic carbons substituted with fluorine[221]. The azide group can be observed as a singlet at 126.5 ppm, while the peaks at 168.4, 155.3, 126.5 and 102.1 ppm match the chemical structure of the NHS group.

In FTIR (Figure 3-2), C─H stretching vibrations were observed between 3000 and 2850 cm^{-1}. The prominent signal at 2125 cm^{-1} corresponds to the azide moiety, while the carbonyl vibrational bands between 1775 and 1640 cm^{-1} are characteristic for the NHS group. The CH_2 bending modes between 1470-1360 cm^{-1}, CH_2 asymmetric stretching at 2942 and symmetric stretching at 2862 cm^{-1} as well as the bands at 1160 and 1290 assigned to C─C and C═O stretching are all characteristic for the PFPA structure[224].

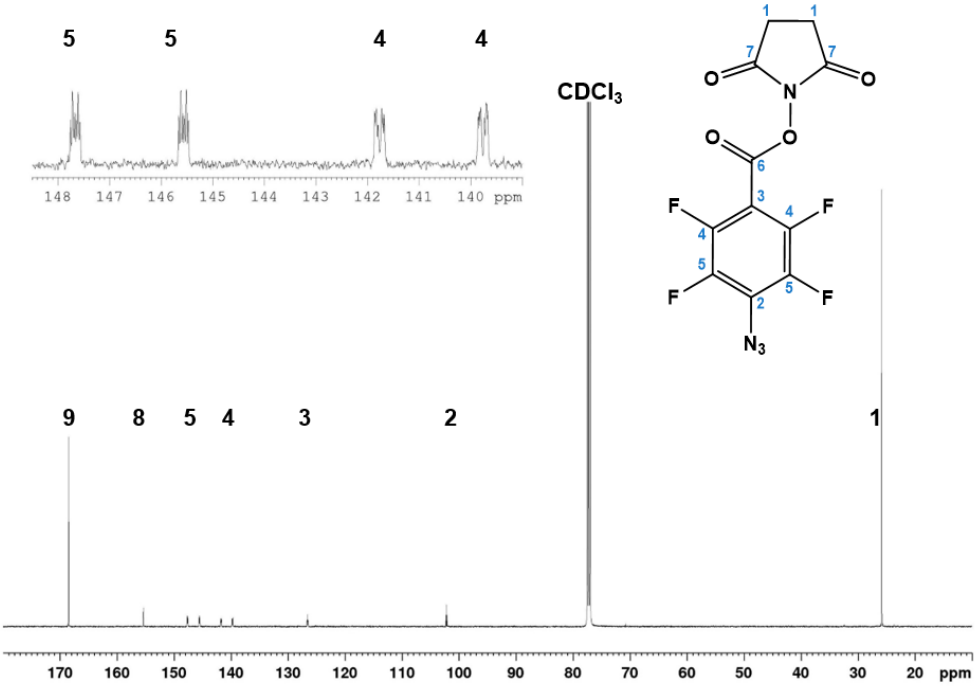

Figure 3-1: Representative ^{13}C NMR (500 MHz, $CDCl_3$) spectrum of PFPA-NHS. δ = 168.4 (s, $COCH_2$), 155.3 (t, CO_2N), 147.7-139.6 (qm, CF), 126.5 (s, CN_3), 102.1 (t, CCO_2N), 25.8 (t, CH_2) ppm.

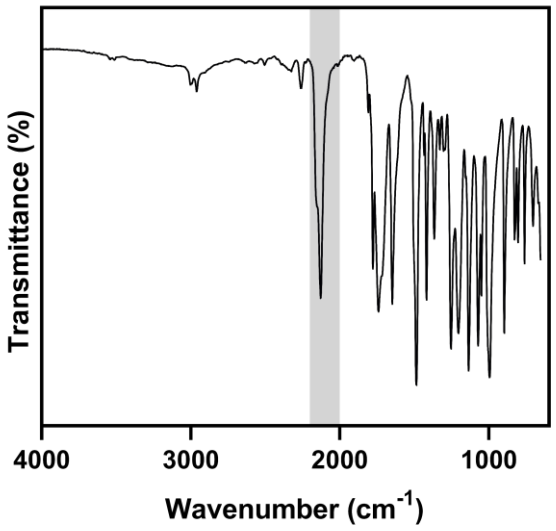

Figure 3-2: Representative FTIR spectrum of synthesised PFPA-NHS. The grey shading highlights the signal at 2127 cm^{-1} corresponding to the azide peak.

3.3.2. Coupling of PFPA-NHS to PCL in solution

Many examples of perfluorophenyl azide functionalisation on solid polymeric surfaces have been reported[220]. However, not many attempts[225] have been made to conjugate PFPA directly onto a polymer in solution, providing a precursor which could be then purified and used for further material fabrication. Using such 'off-the-shelf' functionalised polymer could potentially simplify the preparation of protein-decorated electrospun fibres, as it would not require the post-processing step of surface functionalisation. As the reaction takes place in solution, the products can in theory be easily isolated and purified to remove unconjugated PFPA-NHS. Therefore, this experiment aimed to attempt the modification of PCL (Mw 80 kDa) with PFPA-NHS *via* photo-mediated C-H insertion in an organic solvent.

It has been previously described that functionalised perfluorophenyl azides undergo effective C-H insertion reaction when subjected to UV irradiation in hydrocarbon solvents such as toluene and cyclohexane[217]; however, reactions in the latter resulted in lower yield (28%) as compared to the former (52%)[213]. Solvents that possess many methylene groups (CH_2), such as cyclohexane, may undergo C-H insertion reaction, therefore interfering with the C-H insertion on the polymer backbone and reducing the efficiency of the reaction. Although benzene would be an ideal solvent for this reaction due to the lack of methylene groups, it was not used here because of its toxicity profile[226]. Toluene, a CH_3 mono-substituted benzene derivative, was selected instead.

Scheme 3-3 shows the proposed synthesis of PCL-PFPA. Briefly, PCL and PFPA-NHS were dissolved in toluene at varying ratios (1:9, 5:5, 9:1 w/w). The reaction mixture, placed in a quartz round bottomed flask, was subjected to prolonged UV irradiation to induce photolysis of the azide moiety on PFPA-NHS and the formation of highly reactive nitrene species capable of C-H insertion into the hydrocarbon backbone of PCL.

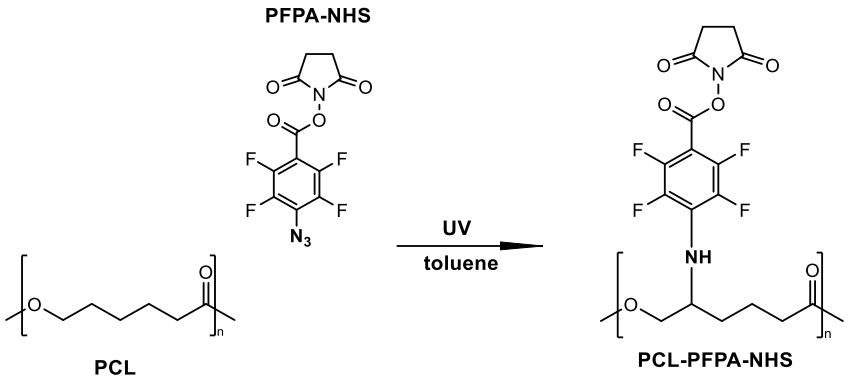

Scheme 3-3: The proposed synthesis of polycaprolactone-PFPA functionalisation in solution.

Following 2.5 hours of UV irradiation, the reaction mixtures containing a larger proportion of perfluorophenyl azide changed colour from pale straw to dark yellow (Figure 3-3). This could indicate chemical rearrangements in the PFPA structure and the formation of a new compound. The final purification in cold methanol yielded a white reaction product.

Figure 3-3: Digital photograph of the PCL-PFPA reaction products before purification. Three ratios of PCL to PFPA were tested: 9:1 w/w (left), 5:5 w/w (middle) and 1:9 w/w (right).

The ^{13}C NMR, ^{19}F NMR and ^{1}H NMR spectra of the reaction products and starting materials (PFPA-NHS and PCL) were acquired to investigate the structural changes following reaction in toluene. As expected, in ^{13}C NMR (Figure 3-4a) the PCL carbon peaks can be observed in all reaction products. Since the PCL chain has a significantly higher molecular weight, it is expected to largely overwhelm the signals from the smaller PFPA molecules. However, a prominent peak at 168 ppm corresponding to the $COCH_2$ on PFPA-NHS can be seen in samples containing higher ratios of PFPA to PCL (9:1 and 5:5 w/w).

The disappearance of the PFPA CN_3 signal at 126.5 ppm in all PCL-PFPA samples could suggest the successful photolysis of the azide group following extended UV exposure, indicating the formation of nitrene species and possible insertion of PFPA into the PCL structure. Although C-F groups were undetectable for PCL-PFPA mixtures at all ratios in ^{13}C NMR, the peaks visible in ^{19}F NMR spectra (Figure 3-4b) confirm their presence. It is possible that the intensity of the C-F peaks was below the detectable level for ^{13}C NMR. The ^{1}H NMR spectra (Figure 3-4c) show a prominent peak at 2.9 ppm corresponding to the NHS moiety in all PCL-PFPA samples, decreasing in intensity with a decreasing PFPA to PCL ratio.

Although the results presented in Figure 3-4 may suggest successful functionalisation of PCL with PFPA-NHS, the experimental protocol requires further optimisation to address key issues. Firstly, a solvent incapable of undergoing C-H insertion (for example carbon tetrachloride) may increase the reaction yield. Moreover, the current reaction protocol requires large quantities of PFPA to be used in the synthesis, which would significantly increase production time. For these reasons, the approach of the PCL-PFPA-NHS functionalisation in solution was not explored further in this project.

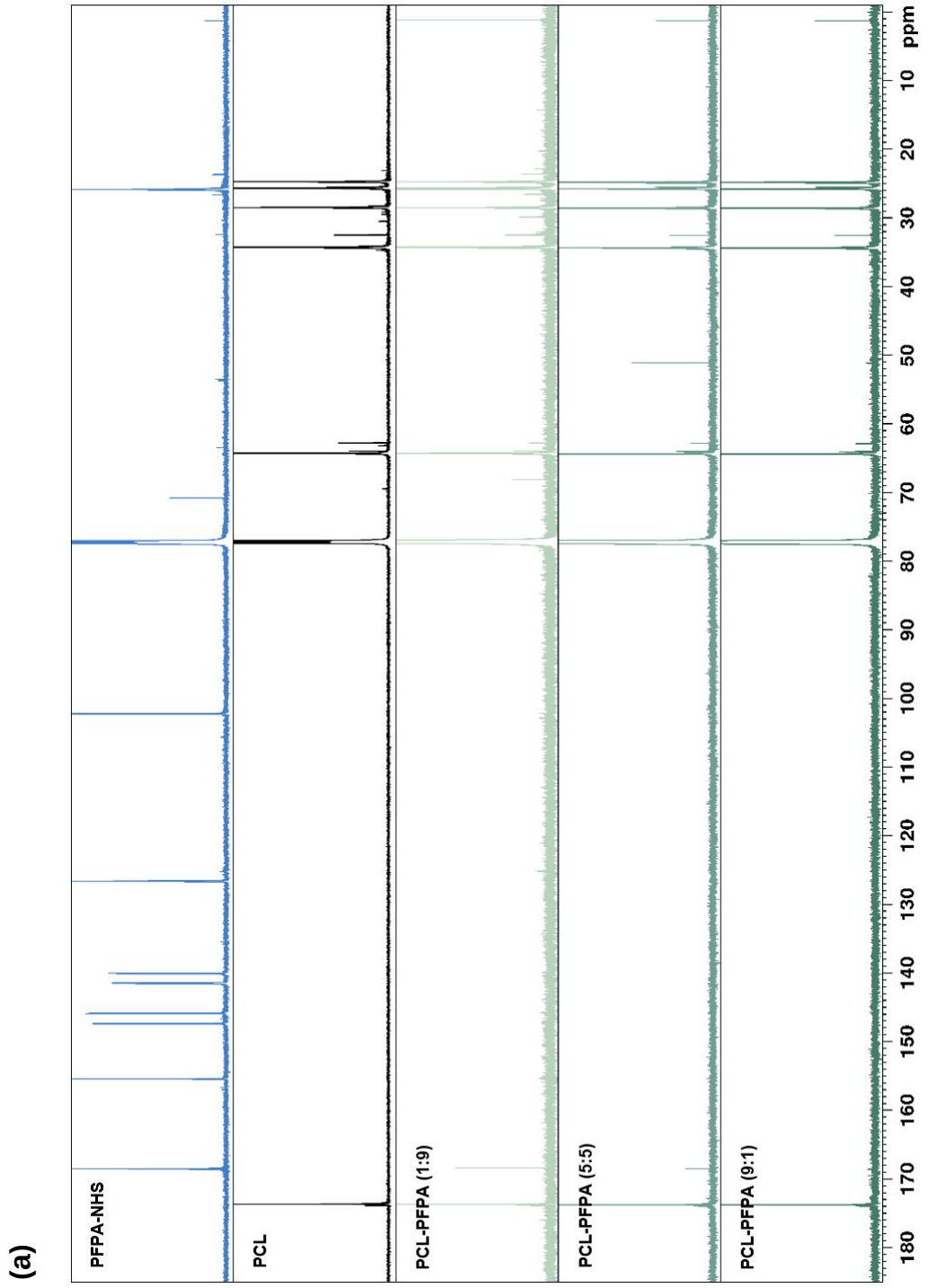
(a)
PFPA-NHS
PCL
PCL-PFPA (1:9)
PCL-PFPA (5:5)
PCL-PFPA (9:1)
ppm
180
170
160
150
140
130
120
110
100
90
80
70
60
50
40
30
20
10

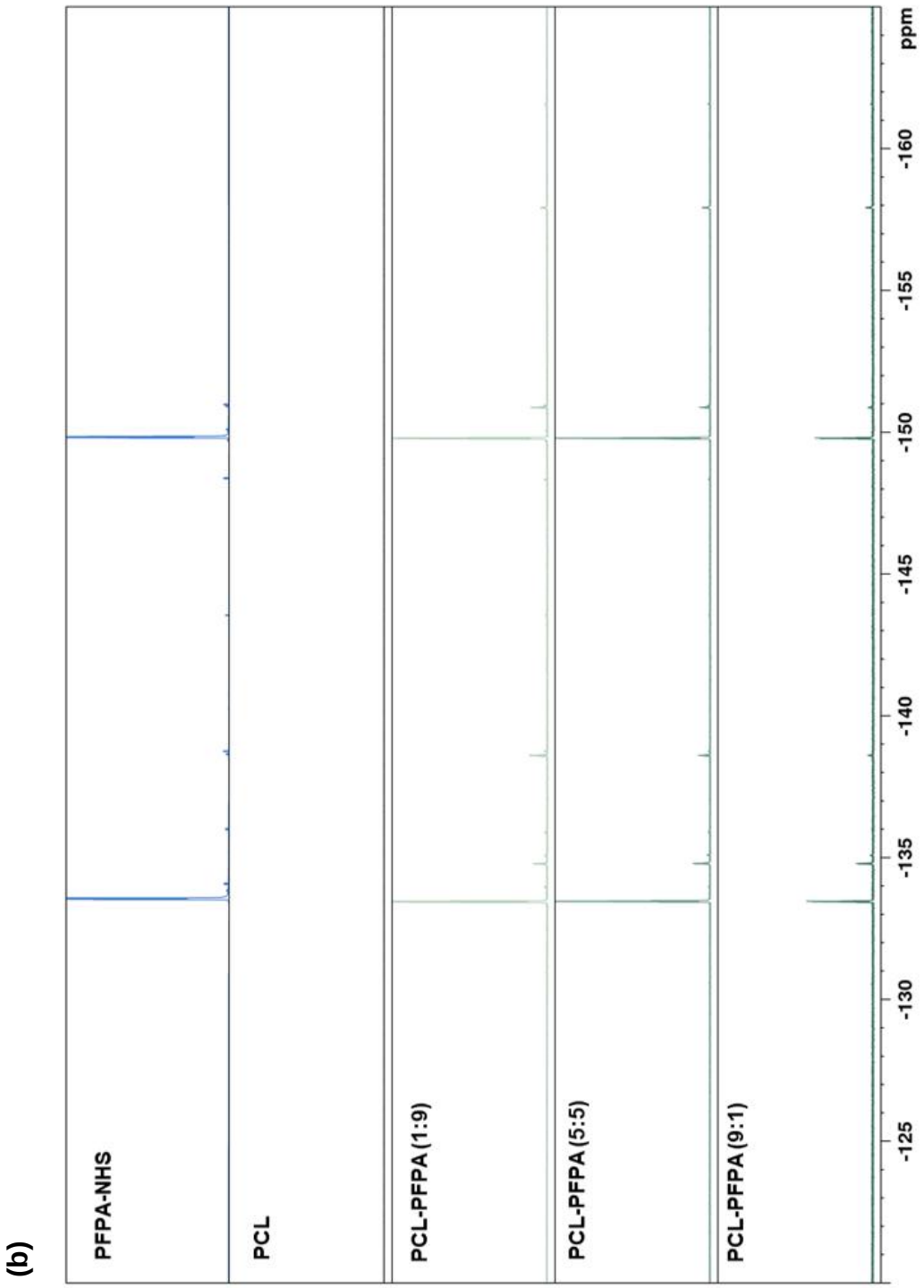
(b)
PFPA-NHS
PCL
PCL-PFPA (1:9)
PCL-PFPA (5:5)
PCL-PFPA (9:1)
-125
-130
-135
-140
-145
-150
-155
-160
ppm

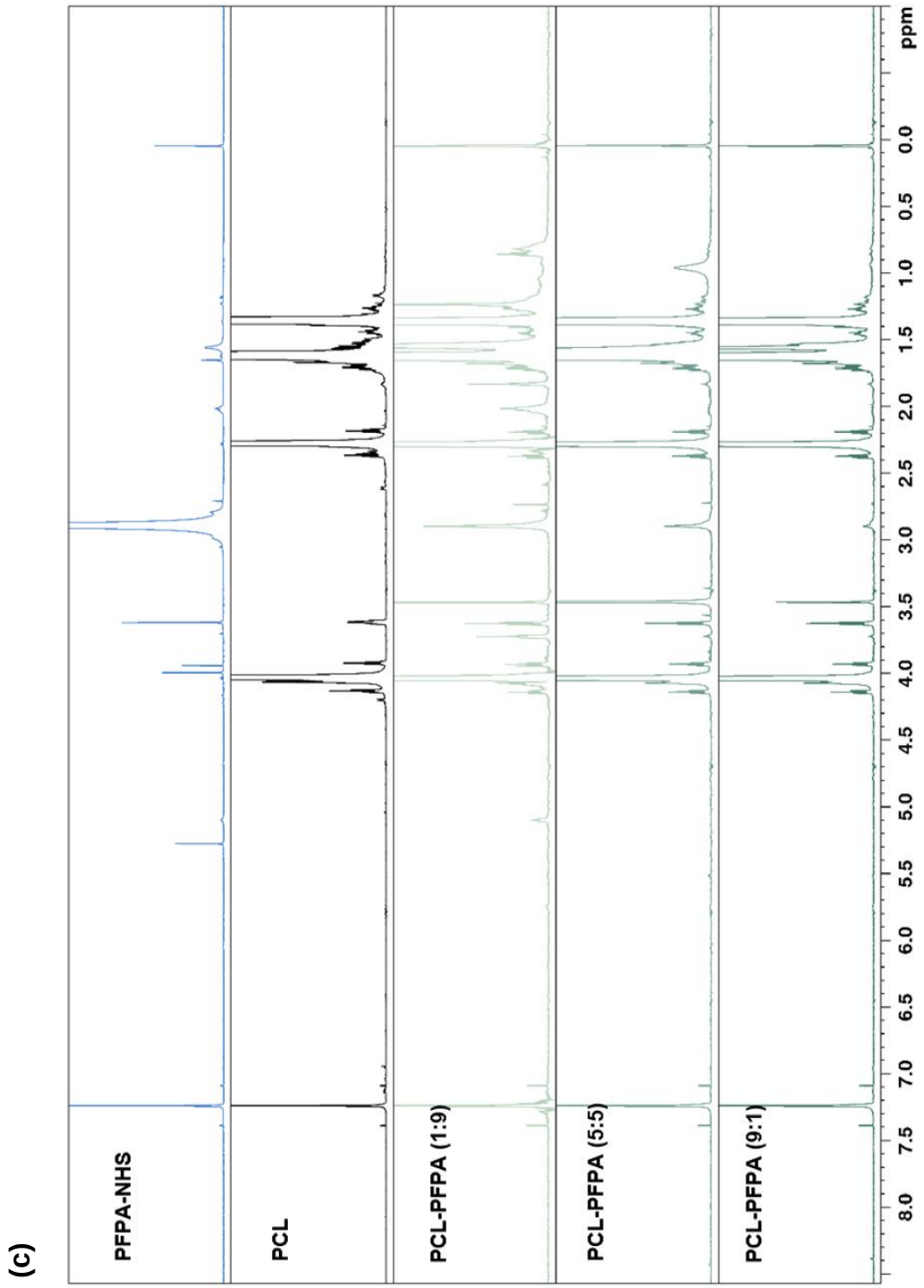

Figure 3-4: ^{13}C NMR (panel a), ^{19}F NMR (panel b) and ^{1}H NMR (panel c) stacked spectra of PCL-PFPA synthesised in solution using different mass ratios of PCL and PFPA. The spectra of starting materials (PFPA-NHS, PCL) are shown for reference. $CDCl_3$ was used as a solvent in all acquired spectra.

3.3.3. PFPA-NHS functionalisation of electrospun fibres

The next step was to explore the post-fabrication functionalisation of electrospun PCL fibres using PFPA-NHS to enable safe conjugation of pharmaceutically relevant proteins to the surface (Scheme 3-4). In this approach, plain PCL fibres are first produced and post-functionalised with PFPA-NHS by immersion in methanolic solution of the compound, followed by photoactivation under UV lamp. The PFPA-NHS functionalised fibres can then undergo reaction with any amine-containing compounds (such as proteins) *via* the NHS moiety.

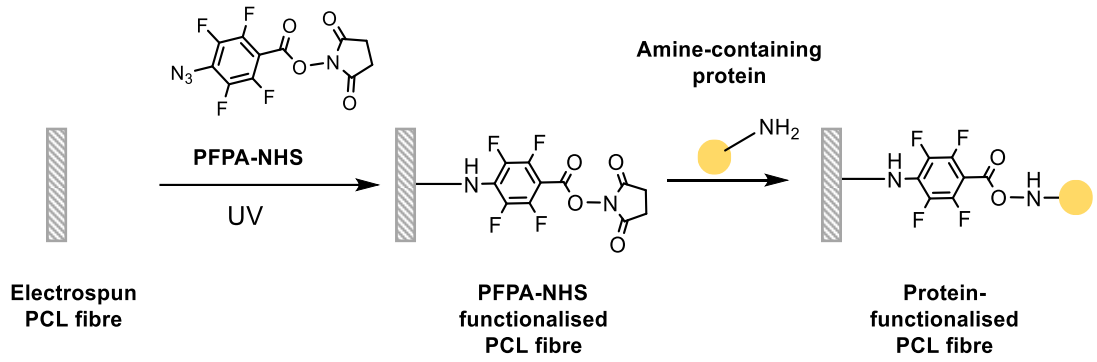

Scheme 3-4: A schematic of PCL fibre functionalisation using PFPA-NHS followed by protein conjugation.

Such implantable protein-decorated fibres have a wide array of applications in tissue engineering, regenerative medicine and drug delivery[153]. PCL was chosen for this study due to its long-term degradation profile, making it an attractive polymer for an implantable fibre (see Section 1.4.1.1.1, page 26 for further information on PCL). Moreover, PCL is not soluble in methanol or ethanol and can be safely functionalised with a methanolic PFPA-NHS solution and pre-sterilised in EtOH for biological applications.

3.3.3.1. PCL fibre fabrication

The PCL fibres were prepared using the monoaxial electrospinning technique described in Section 1.4.2.1 (page 32). The successful formation of electrospun patches largely depends on the polymer and solvent selected for the fibre fabrication. For this application, 2,2,2-trifluoroethanol (TFE) was chosen as the solvent due to its well-described applications in nanofibre fabrication[112,190,227]. A solution of 12% w/v PCL (Mw ~ 80 kDa) in TFE was previously found to have appropriate viscosity for the electrospinning process and thus chosen for use here[228]. Scanning electron microscopy images of the scaffolds produced (Figure 3-5a and b) revealed successful fabrication of smooth, cylindrical fibres with no bead-on-string structures, suggesting appropriate optimisation of electrospinning conditions. The mean fibre size, calculated from particle size distribution curve, was found to be 709 nm ± 366 (Figure 3-5c). This formulation was therefore selected for further surface functionalisation with PFPA-NHS.

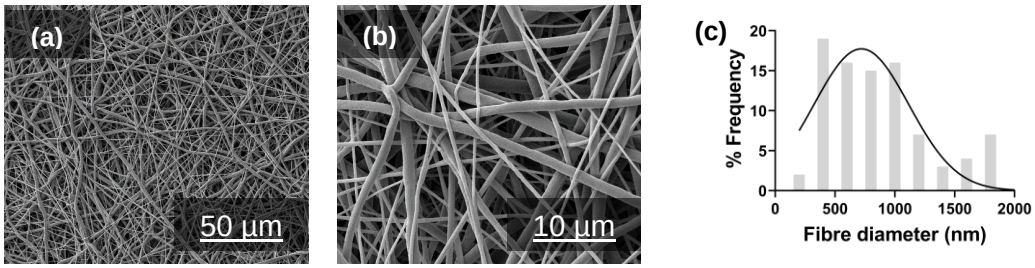

Figure 3-5: Scanning electron micrographs at two magnifications (a) 2000X; (b) 10 000X and size distribution (c) of electrospun PCL fibres.

3.3.3.2. Fibre morphology following PFPA-NHS functionalisation

Physicochemical characterisation was performed to obtain information on the chemical composition of the modified PCL surface. The initial optimisation of PFPA conjugation reaction conditions was performed by monitoring the disappearance of the azide peak in the FTIR spectra (Figure 3-6).

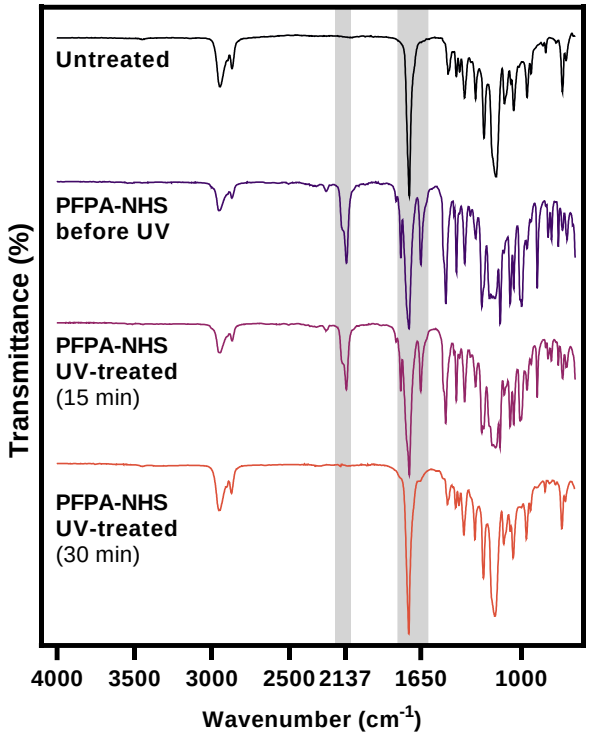

Figure 3-6: Representative FTIR spectra of untreated fibres and PFPA-treated fibres both before UV treatment and after 15 or 30 minutes of UV treatment. The grey shadowing at 2127 cm^{-1} corresponds to the azide peak, while the shadowing at 1650 cm^{-1} highlights the amide carbonyl bond. Complete disappearance of the azide peak after 30 minutes of UV-radiation was observed. Similar results were obtained from three independent experiments and the results of one representative experiment are shown.

Completion of PFPA photolysis was monitored for 30 minutes with spectra acquired at 0, 15 and 30 minutes of UV-treatment on each side of the mat. The FTIR spectrum of the untreated fibres is identical to that of raw PCL[111]. An asymmetric stretching vibration of the azide group at 2127 cm^{-1} and multiple carbonyl stretches of the NHS moiety between 1650 and 1775 cm^{-1} were observed in PFPA-treated fibres before UV treatment. Following 15 minutes of UV radiation, the intensity of the azide peak decreased, suggesting successful initiation of PFPA photolysis but that the reaction was not complete. After 30 minutes of UV radiation the reaction appeared to be complete as evidenced by the disappearance of the azide peak. The carbonyl stretch at 1650 cm^{-1}, attributed to the coupled NHS group, was retained throughout UV treatment, although its intensity was markedly reduced after 30 minutes.

Therefore, it was concluded that a 30-minute UV treatment on each side of the mat (1 hour in total) is necessary for the completion of a photochemical reaction on the fibres, and further testing was performed using fibres prepared under these conditions.

The effect of the functionalisation step on fibre morphology was then investigated with SEM as presented in Figure 3-7.

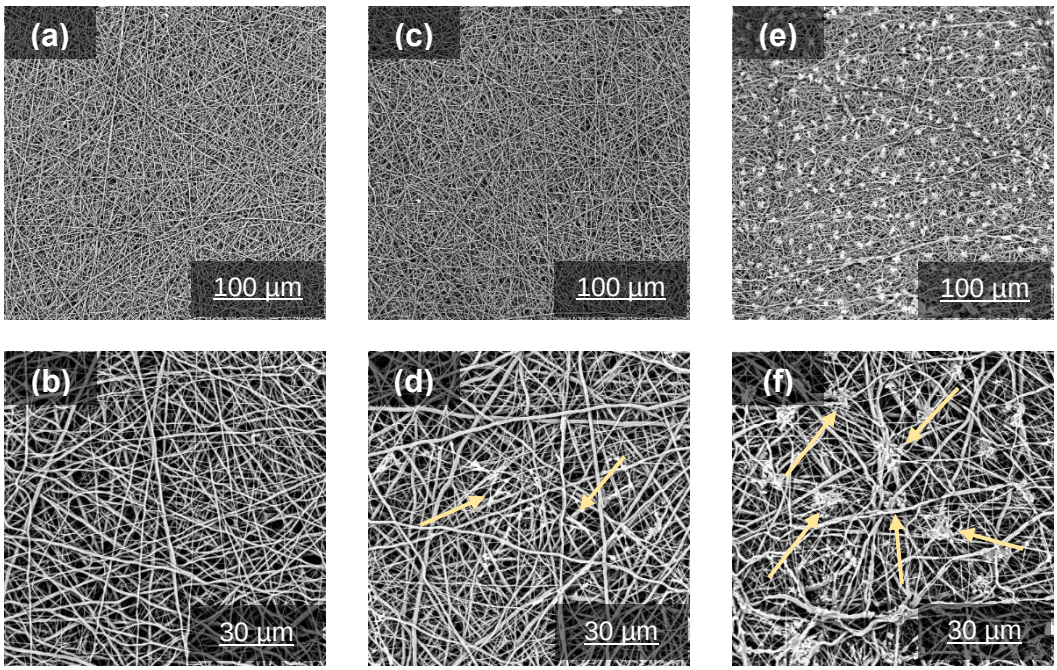

Figure 3-7: Scanning electron micrographs of functionalised electrospun fibres at 500X (panels a, c, e) and 2250X magnification (panels b, d, f). Untreated (a, b) and PFPA-NHS-functionalised fibres before (c, d) and after a 30-minute UV treatment (e, f) are presented. Yellow arrows highlight morphological changes. All the scaffolds were dipped in methanol and dried under reduced pressure before SEM analysis. Similar results were obtained from three independent experiments and the results of one representative experiment are shown.

Figure 3-7a and b show the morphology of untreated fibres, with uniform cylindrical fibres present before surface manipulation. Dipping in methanol clearly does not affect the fibre morphology. Following incubation in PFPA-NHS solution (Figure 3-7c and d), the fibres are slightly more irregular in shape and white deposits are visible in the higher magnification images, as highlighted by yellow arrows. PFPA-and UV-treated fibres (Figure 3-7e and f) are visibly bundled and intertwined, with white clusters distributed evenly across the surface of the fibre. The white residue coating the fibres

could be a precipitate of PFPA-NHS. The fibre patters are markedly less regular after UV treatment, suggesting that the UV treatment negatively impacted the morphology of electrospun scaffolds.

As PFPA-NHS functionalisation on the surface of electrospun materials has been tried only once before[221] with PDO patches, little is known about its impact on the fibre morphology. The authors of the previous study did not include electron micrographs of the PDO nanofibres after the PFPA functionalisation[221]. However, the confocal microscope images they presented do show a rather distorted structure as compared to the SEM of PDO fibres before functionalisation. A similar observation was made here for PFPA-treated PCL fibres. The degree of surface morphology change will strongly depend on the polymer used to fabricate the fibre and the PFPA solvent. For example, PLGA fibres could not be used for this approach as the polymer is soluble in the same solvents as PFPA. Therefore, any post-fabrication functionalisation steps would destroy the integrity of the nanofibre structure. Overall, it appears that the fibre mat remains intact after PFPA treatment, but the effect of the distorted surface on biological performance needs to be explored in further experiments.

X-ray photoelectron spectroscopy (XPS) was used to further characterise the chemistry of the fibre surface. This sensitive method enables detection and quantification of chemical elements on a solid surface up to 10 nm depth[229]. In addition, XPS provides information on the chemical states of the observed atoms[230]. Since PFPA-NHS contains fluorine and nitrogen in its structure, these elements were chosen as diagnostic markers to corroborate successful surface functionalisation. Representative XPS survey spectra are presented in Figure 3-8.

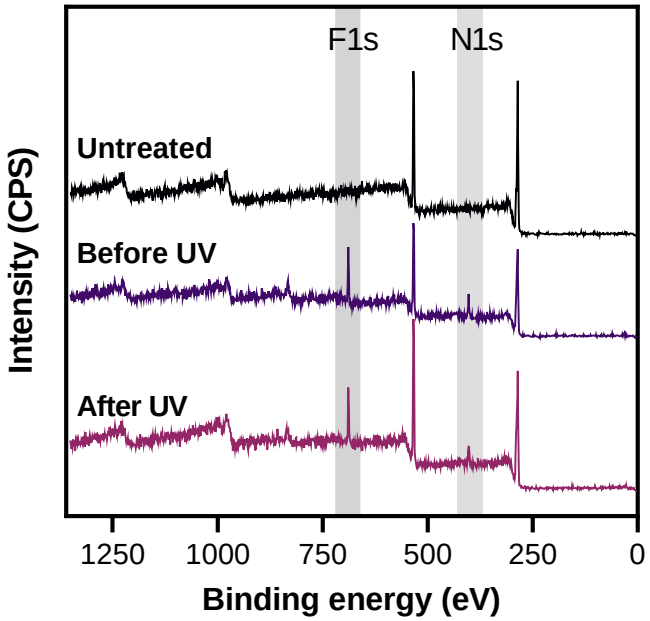

Figure 3-8: Representative XPS survey spectra measured for untreated (black) and PFPA-treated fibres before (dark purple) and after UV treatment (light purple). The fluorine 1s (~ 690 eV) and nitrogen 1s (~ 450 eV) peaks are shaded in grey. Similar results were obtained from three independent experiments and the results of one representative experiment are shown.

For untreated samples, the survey spectra identified elements corresponding to the PCL structure (carbon and oxygen)[111], while in PFPA-treated samples additional fluorine and nitrogen signals were detected. The XPS survey analysis allowed for the quantification of surface elements, and the results are given in Table 3-1.

Table 3-1: Elemental composition of the fibre surface. Data are shown as mean ± standard deviation (n=3).

Sample	Surface C (at%)	Surface O (at%)	Surface N (at%)	Surface F (at%)
Untreated	76.4 ± 0.7	23.6 ± 0.7	0	0
Before UV	64.7 ± 2.8	20.6 ± 0.3	6.4 ± 1.6	7.8 ± 1.0
After UV	58.7 ± 1.0	22.4 ± 0.2	5.9 ± 0.4	13.0 ± 1.1

The elemental surface compositions display increased nitrogen and fluorine content in the functionalised fibres, indicating the successful deposition of PFPA on the fibre surface. As expected, untreated PCL fibres contained no surface nitrogen or fluorine, while for the PFPA-functionalised fibres before and after UV treatment both elements

could be detected. The percentage of nitrogen decreases after UV treatment, which indicates that photolysis of the azide group occurred. However, the percentage of nitrogen and fluorine present on the surface is relatively low compared to carbon and oxygen. This can be attributed to the polycaprolactone structure that dominates in the XPS analysis. Similar observations were made in other studies where PFPA was conjugated to a polymer surface[221,231,232]. Next, high resolution C1s XPS spectra were acquired to investigate the chemical state of carbons present on the surface (Figure 3-9).

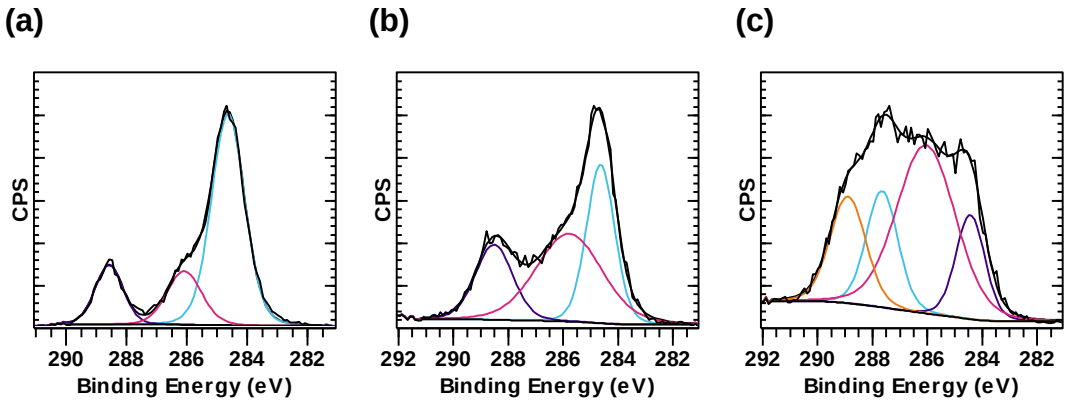

Figure 3-9: High resolution C1s XPS spectra for (a) untreated and PFPA-treated fibres before (b) and after (c) UV treatment. Similar results were obtained from three independent experiments and the results of one representative experiment are shown.

The C 1s high-resolution XPS spectra (Figure 3-9) show the changes in carbon environment following photografting onto the PCL surface. In untreated (Figure 3-9a) and PFPA-treated fibres before UV treatment (Figure 3-9b), peaks at 284.5 (C─H), 286.2 (C─O─C) and 288.5 eV (O═C─O) are characteristic of the PCL backbone. The peak detected for UV-treated samples (Figure 3-9c) was fitted into four components: 284.4 (C─H), 286.1 (C═C─N and C─O), 287.6 (C═C─F) and 288.8 eV (O═C─O)[231], confirming the structural change of the fibre.

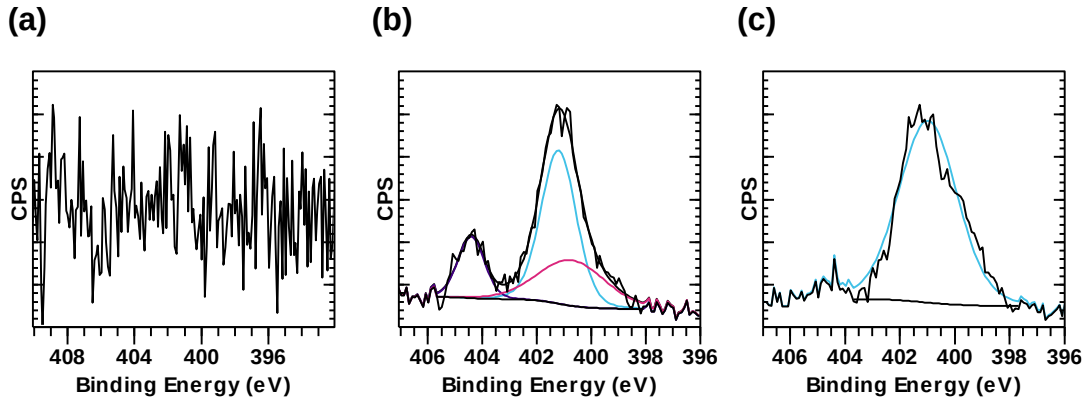

Figure 3-10: High resolution N1s XPS spectra for (a) untreated and PFPA-treated fibres before (b) and after (c) UV treatment. Similar results were obtained from three independent experiments and the results of one representative experiment are shown.

High-resolution N1s XPS spectra (Figure 3-10) confirmed the covalent immobilisation of PFPA on the PCL fibre. No nitrogen signal was detected in untreated fibres (Figure 3-10a). In PFPA-treated samples before UV irradiation (Figure 3-10b), a prominent peak at 404.5 eV can be assigned to the azide moiety[231]. After UV treatment (Figure 3-10c), the peak at 404.5 eV disappears. This peak corresponds to the N^+ in the azide group of PFPA, which decomposes upon photoactivation. The amine/amide species are visible at 401.5 eV[231] as highlighted by the blue line and are visible in both before and after UV treatment samples . The results agree with the extensive XPS analysis of nitrogen species present in perfluorophenyl azide-functionalised surfaces performed by Zorn et al.[231]

Overall, physicochemical characterisation confirmed the successful deposition of PFPA on the surface of electrospun fibres. Following UV treatment, chemical changes observed in FTIR (disappearance of the azide peak, formation of carbonyl bonds) and XPS spectra (lack of peak at 404.5 eV corresponding to N_3 moiety, changes to the chemical state of carbon) give strong evidence for the covalent conjugation of PFPA to the surface of the PCL scaffold.

3.3.4. Model protein conjugation

The functionality of the NHS ester group after immobilisation on the polymer fibre surface was explored using fluorescently-labelled model molecules. Fluorescence imaging offers visual proof of biomolecule conjugation to the PFPA-modified fibre. Moreover, it can also provide information on the spatial distribution of the coupled dye on the surface.

The NHS-assisted amine coupling was simulated using amine-modified rhodamine (rhodamine-amine) and FITC-albumin. Figure 3-11 presents the fluorescence images acquired after treating the fibres with these model compounds.

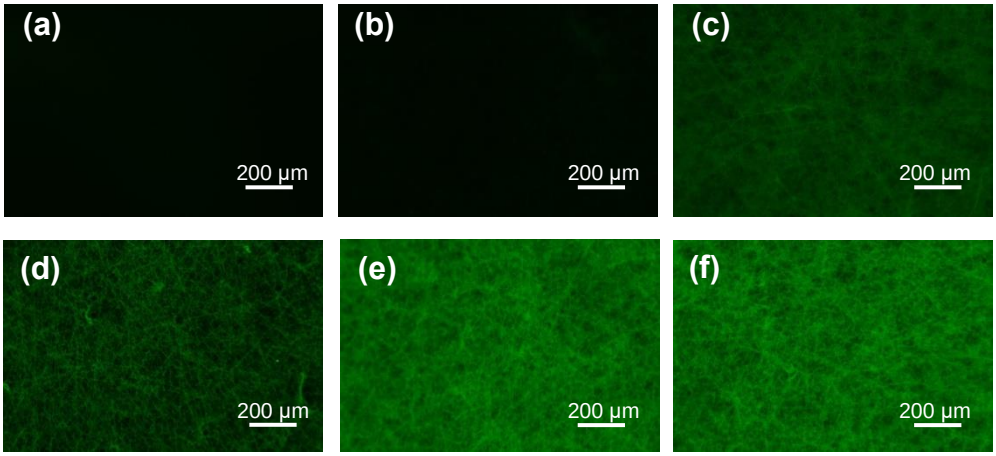

Figure 3-11: Conjugation of fluorescently-labelled model molecules to untreated electrospun fibres (a,d) and PFPA-treated fibres before UV (b,e) and after UV irradiation (c,f). Top row (a,b,c) shows the micrographs of rhodamine-amine treated samples, while bottom row (d,e,f) presents fibres incubated with FITC-albumin. Similar results were obtained from three independent experiments and the results of one representative experiment are shown.

Rhodamine-amine has been previously used to confirm the functionality of the PFPA-NHS moiety following grafting on the electrospun PDO fibre[221]. Following overnight incubation in a solution of rhodamine-amine dye, untreated (Figure 3-11a) and PFPA-treated fibres before UV exposure (Figure 3-11b) showed no fluorescence, while the micrograph of the UV-irradiated sample (Figure 3-11c) revealed a homogenous distribution of the dye. On the other hand, FITC-albumin treated samples showed

some level of fluorescence, with relatively lower intensity observed in blank fibres (Figure 3-11d) than in PFPA samples before and after UV treatment (Figure 3-11e and f, respectively). This could be due to non-specific adsorption of albumin to the surface. The fluorescence intensity of the PFPA-treated sample before and after UV treatment was comparable, suggesting that both formulations were loaded with similar levels of FITC-BSA.

Compared to rhodamine-amine, FITC-BSA-functionalised fibres showed increased fluorescence intensity, possibly due to higher number of amine groups: there are lysine residuess in the BSA structure which are capable of undergoing conjugation.[233] Overall, fluorescence imaging confirmed the functionality of the NHS moiety after photografting onto the PCL surface.

To quantify the effect of PFPA-NHS functionalisation on the protein binding efficiency, a 24-hour albumin attachment study was next carried out (Figure 3-12). The percentage of bovine serum albumin conjugation to the PCL fibres was calculated indirectly by depletion.

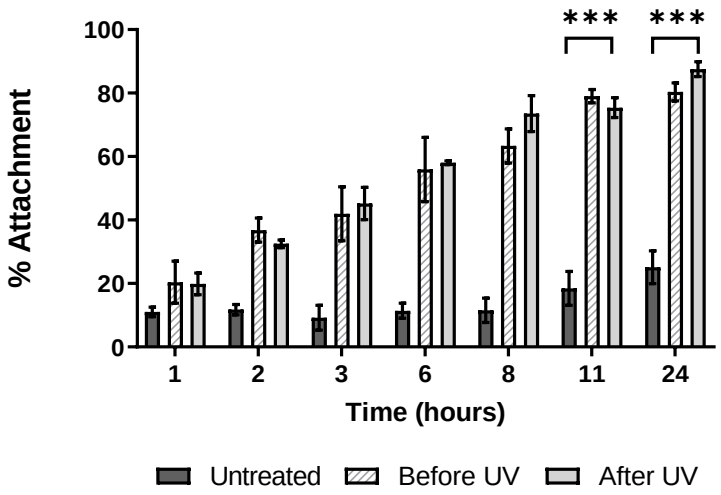

Figure 3-12: Percentage of bovine serum albumin attachment to electrospun PCL fibres as a function of time. Data are shown as mean ± S.D. and are representative of two independent experiments performed on separate days, with three replicate wells per experiment. *Repeated measures one-way ANOVA with post hoc Tukey's test. The asterisks (***) denote p ≤ 0.001.*

At all measured time points the BSA percentage attachment was higher for PFPA-treated samples compared to the untreated control. In PFPA-treated fibres, the conjugation efficiency increased gradually with time, reaching around 80% at 11 hours. At this time point, the efficiency of protein attachment was significantly higher ($p < 0.001$) in surface-treated fibres than in plain PCL scaffolds. Although the mean percentage attachment was slightly, but insignificantly ($p > 0.05$), higher after 24 hours of incubation, the 11-hour time point was selected as more experimentally practical for further fibre testing. This way the fibres can be fabricated, functionalised with PFPA-NHS and incubated in protein solution on day 1, allowing further *in vitro* testing to be performed on the following morning.

There was no significant difference in BSA uptake by the functionalised fibres before and after UV irradiation, suggesting that the photografting of PFPA-NHS was not necessary for successful protein attachment to the polymeric surface. The results of the protein conjugation study (Figure 3-12) are consistent with the fluorescence imaging (Figure 3-11) described above, where the PFPA-NHS samples without UV treatment show a significant level of fluorescence intensity upon treatment with FITC-BSA. It can be assumed that a certain amount of PFPA-NHS strongly adsorbs to the PCL fibre and the NHS moieties remain active on the surface, allowing efficient conjugation of proteins even without covalent attachment. It is possible that the washing method applied, dipping in methanol solution, may not be sufficient to remove unconjugated, surface adsorbed, PFPA-NHS from the fibre surface.

Another interesting difference between the PFPA-treated formulations was discovered after an 11-hour incubation in BSA solution. Figure 3-13 shows digital photographs of PCL patches before (a,c,e) and after (b,d,f) albumin conjugation to the surface. A significant change in fibre colour was observed in the PFPA-treated samples.

Figure 3-13: Digital photograph of electrospun fibres before and after incubation in BSA solution. Top row shows PCL patches before incubation (a,b,c), while the bottom row images were captured after 11 hours in BSA solution (d,e,f). Left – PFPA-untreated, UV-treated fibres (a,d), middle – PFPA-NHS before UV (b,e), right – PFPA-NHS after UV (c,f).

The untreated PCL patches remained uncoloured following UV treatment (Figure 3-13a and d), while initially white PFPA-functionalised patches before UV irradiation (Figure 3-13b) turned dark pink upon incubation with BSA (Figure 3-13e). Fibres treated with UV light became yellowish in appearance before incubation (Figure 3-13c). The darkening of the surface may be caused by the increased oxidation of the irradiated samples, suggesting the possibility of photocatalysed PCL degradation[234]. However, this effect was not observed in UV-treated plain PCL fibres (Figure 3-13a), and therefore the change in colour is most probably caused by a change in chemical structure following photografting of PFPA-NHS, as was observed earlier following PCL-PFPA functionalisation in solution (Figure 3-3). The yellow hue darkened following prolonged contact with the aqueous BSA solution (Figure 3-13f). Although the explanation for the colour changes observed in PFPA-treated fibres is unclear, it indicates a chemical change occurring on the surface.

3.3.5. Cytotoxicity of PFPA functionalisation

To assess the cytotoxicity of PFPA-functionalised fibres, a model human epithelial cell line (Caco-2) was employed. Cell viability was measured following incubation with fibres for one or three days. The results are presented in Figure 3-14.

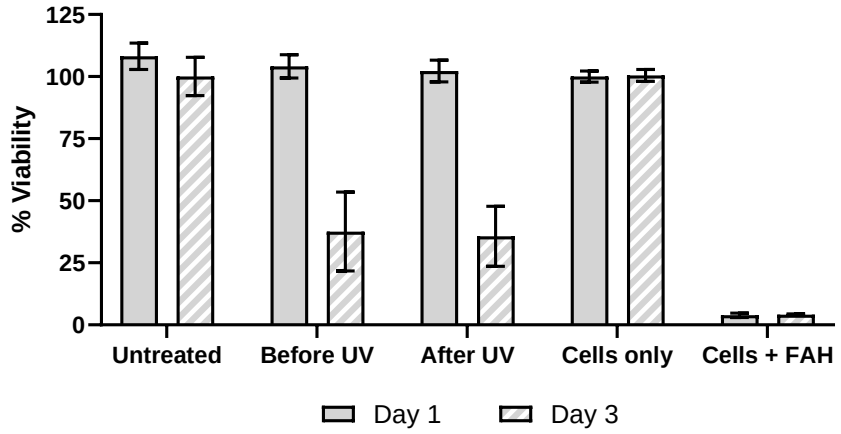

Figure 3-14: Viability of Caco-2 cells following incubation with PFPA-functionalised fibres for one (grey) and three (dashed) days. 'Untreated' corresponds to untreated (no PFPA) PCL fibres. Cells only are the negative control. Cells+FAH denotes the positive control (cells treated with formaldehyde). Data are shown as mean ± S.D. and are representative of three independent experiments performed on separate days, with triplicate wells per each condition tested.

Caco-2 cells retained their viability at around 100% after one day of incubation with the test formulations. However, PFPA-treated fibres, both before and after UV irradiation, showed cytotoxic properties at day three of incubation, where viability decreased from ~100% to ~30%. This could suggest that the washing method of briefly dipping the functionalised fibres in methanol to remove unreacted PFPA-NHS may not be sufficient, resulting in a possibly toxic azide compound leaching out to the cell culture medium with longer incubation times.

To test this hypothesis, a more vigorous washing method comprising a two-step sonication process in an ultrasonic bath was employed. In step 1, unreacted PFPA-NHS was removed *via* one-minute sonication in methanol. This step also pre-sterilises the fibres for cell culture use. In step 2, the functionalised scaffolds were washed in sterile PBS to remove organic solvent that could be potentially dangerous for the integrity of the protein that will subsequently be attached to the surface. The results of cell viability experiments using the new washing protocol are given in Figure 3-15.

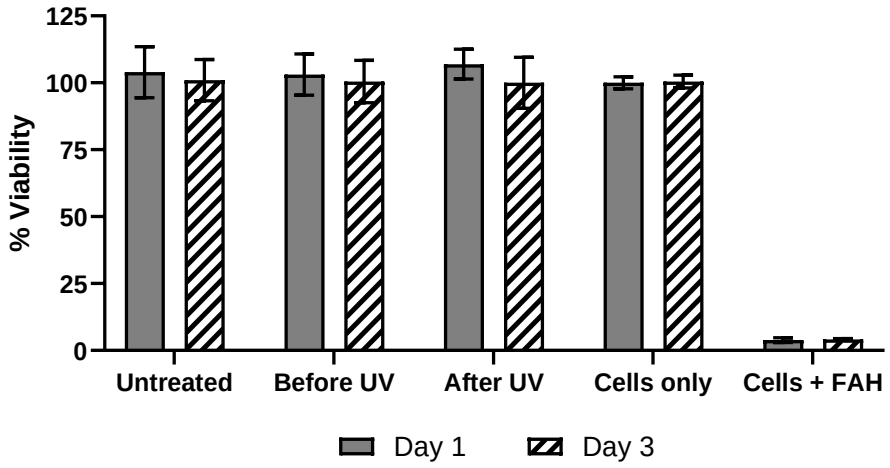

Figure 3-15: Viability of Caco-2 cells following incubation with sonicated PFPA-functionalised fibres for one (grey) and three (dashed) days. 'Untreated' corresponds to untreated (no PFPA) PCL fibres. Cells only are the negative control. Cells+FAH denotes the positive control (cells treated with formaldehyde). Data are shown as mean ± S.D. and are representative of three independent experiments performed on separate days, with triplicate wells per each condition tested.

A brief sonication in methanol has a positive effect on cell survival, possibly due to the efficient removal of unbound PFPA-NHS from the surface of the fibre. Moreover, high-energy washing steps such as sonication could potentially improve the penetration of methanol deeper into the nanofibre mesh, therefore aiding better sterilisation before *in vitro* experiments. Based on these results, the sonication washing step was deemed crucial for the effective performance of functionalised fibres in a biological environment and was introduced to the functionalisation method in subsequent experiments. The effect of this change to the functionalisation protocol on the performance and physicochemical properties and performance of the fibres is explored in the following section.

3.3.6. Protein attachment to sonicated fibres

The attachment of BSA on PFPA-functionalised fibres without the sonication step was previously investigated in a preliminary study (Figure 3-12). The experiment presented in Figure 3-16 reflects the effect of the washing method on the surface

attachment of three model proteins. Functionalised fibres before and after a sonication washing step were incubated for 11 hours in a solution of BSA, infliximab or catalase. The model antibody infliximab is a monoclonal antibody against the proinflammatory cytokine TNF-α, and is used to treat autoimmune conditions such as Crohn's disease or rheumatoid arthiritis[235]. Recently, infliximab has emerged as a potential treatment for immune checkpoint inhibitor-related colitis[236–238]. Catalase is an enzyme with a pivotal role in the protection of cells against the toxic effects of hydrogen peroxide. The well-established catalase activity assays can be used to confirm the integrity of protein following attachment to the PCL surface[239,240]. Albumin was picked to allow direct comparison with the preliminary protein attachment studies (Figure 3-12).

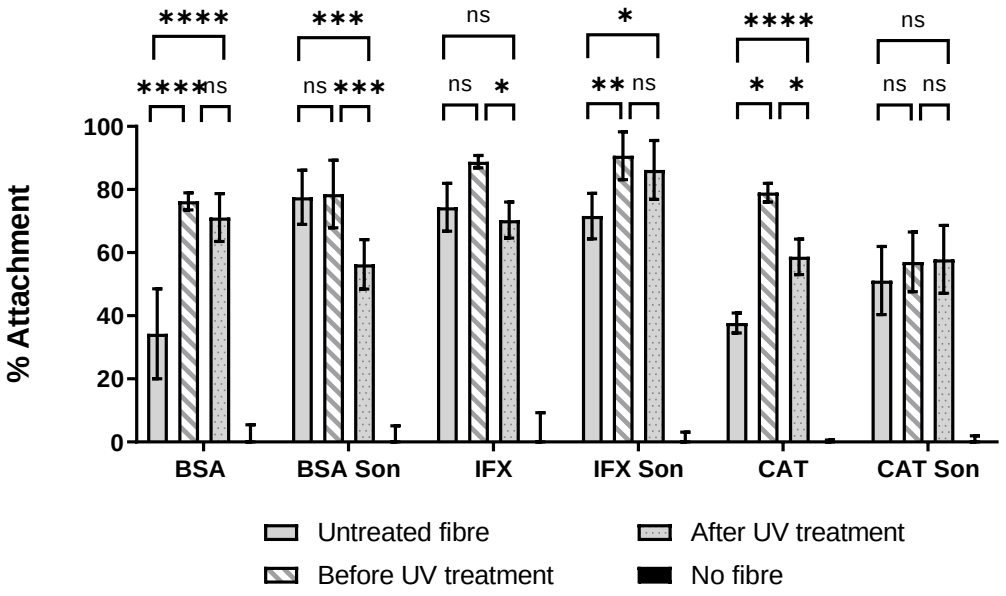

Figure 3-16: Attachment of model proteins (BSA – bovine serum albumin, IFX – infliximab, CAT – catalase) to unwashed and sonicated (Son) PFPA-functionalised fibres following overnight incubation. Data are shown as mean ± S.D. and are representative of two independent experiments performed on separate days, with triplicate wells per each condition tested. *Repeated measures one-way ANOVA with post hoc Tukey's test; statistical significance: ns (p-value >0.05), * (p-value < 0.05), ** (p-value ≤0.01), *** (p ≤ 0.001) **** (p-value ≤0.0001).*

All tested conditions achieved at least 30% attachment following overnight incubation in a protein solution. For non-sonicated samples, the amount of BSA and catalase associated with untreated fibres was considerably lower than with the PFPA-treated fibres. The samples before UV treatment performed better than UV-irradiated ones.

Interestingly, a one-minute sonication in methanol generally resulted in enhanced protein attachment in PFPA-untreated fibres incubated with BSA and catalase. The percentage protein loading on sonicated blank PCL fibres was therefore comparable to those of PFPA-functionalised patches. PFPA-functionalised fibres before UV treatment performed slightly better than those after UV exposure. The observed difference in the percentage of protein loaded onto PCL was insignificant, suggesting that PFPA functionalisation may not be needed to achieve an effective surface coating of PCL fibres pre-treated with a brief sonication in methanol and PBS.

In this study, infliximab achieved a high percentage adsorption on the untreated, dip-washed PCL fibre, contrary to the results obtained for BSA or catalase. This result agrees with existing literature, as antibodies are more hydrophobic than enzymes or BSA[241] and will adsorb more easily to the hydrophobic surface of the untreated PCL fibre. Previous studies showed that the efficacy of protein adsorption largely depends on the hydrophobicity/hydrophilicity of the proteins as well as the polymer substrates. Absolom et al.[241] investigated the attachment of four model proteins (fibrinogen, IgG, human serum albumin and bovine serum albumin) to four types of small particles (SiO_2, polytetrafluoroethylene, polyvinyl chloride and Nylon 66). Increased protein hydrophobicity was associated with improved surface adsorption, regardless of the surface hydrophobicity. Similarly, poor wettability of the substrate has been linked to elevated surface protein adsorption[242].

The introduction of fluorine[243] or fluoro-substituted benzene rings[244] onto the surface has been previously associated with increased surface hydrophobicity. Similarly,

Li et al.[232] reported decreased hydrophilicity of a polyurethane film following functionalisation with PFPA-NHS. This could explain the enhanced protein adsorption in the PFPA-treated fibres.

Although the attachment of model proteins was achieved in both untreated and PFPA-functionalised fibres, it is expected that PFPA functionalisation results in a covalent conjugation of proteins to the fibre (rather than surface adsorption on the untreated fibres). This could potentially prevent rapid detachment of proteins upon exposure to physiological fluids, therefore prolonging the therapeutic efficacy of the scaffold at the implantation site. This hypothesis is further explored in Section 3.3.9 (page 111).

3.3.7. Changes to surface hydrophobicity post-sonication

Given the above observations, the next step was to investigate changes to surface hydrophobicity before and after sonication as well as PFPA-NHS functionalisation. It is possible that sonication in methanolic solution could cause modification of the PCL surface with hydroxyl groups of the alcohol, therefore rendering the scaffold more hydrophilic. To test this hypothesis, goniometer measurements were performed on the surface of the functionalised fibres. The curvature angle of a water droplet upon contact with the fibres was calculated and is presented in Figure 3-17.

(a)

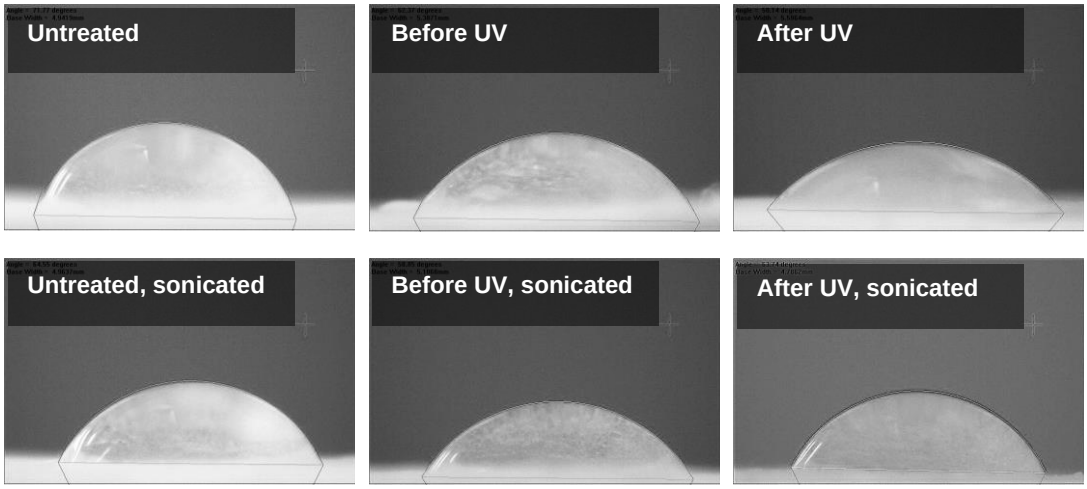

(b)

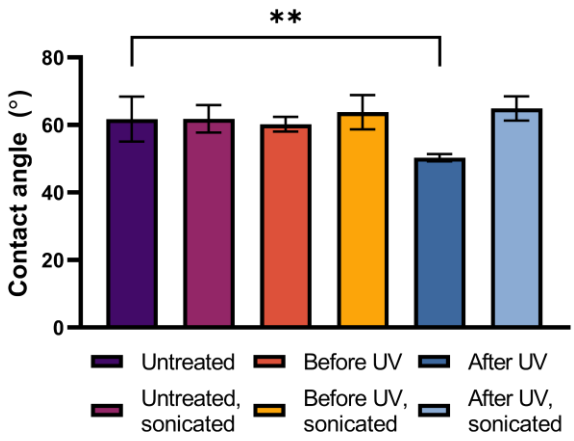

Figure 3-17: Contact angle measurements performed on untreated and PFPA-treated fibres before and after UV exposure and sonication treatment. Panel (a) shows the examples of water droplet contact angle photographs used to derive the contact angle measurements presented as mean ± SD (n=3) in panel (b). No statistical significance was observed between untreated fibre controls and the various treatments, apart from with PFPA- and UV-treated fibres before sonication. *Repeated measures one-way ANOVA with post hoc Tukey's test; statistical significance: ** (p-value ≤0.01)*. Similar results were obtained from three independent experiments and the results of one representative experiment are shown.

It appears that sonication of PCL fibres did not bring significant changes to the fibre hydrophobicity. A similar trend was observed for PFPA-treated fibres before UV exposure, where samples before and after sonication had contact angles comparable to those of untreated fibre controls. The only statistically significant difference was observed between the untreated control and PFPA-treated fibres after UV

treatment, where surface functionalisation led to a decreased water droplet contact angle, suggesting increased hydrophilicity of the surface. This observation once again contrasts the hypothesis that the introduction of fluorine would lead to enhanced surface hydrophobicity. Nevertheless, the sonication washing resulted in an increased contact angle, bringing the value near to that of the untreated control. Further assessment of physicochemical properties of the functionalised fibres before and after sonication may be required to explain the differences in these formulations.

3.3.8. Morphology and physicochemical properties of sonicated fibres

Sonication in an organic solvent (methanol), although brief (1 min), could potentially affect the morphology of the electrospun fibres. To explore this, SEM was performed, and the results are presented in Figure 3-18.

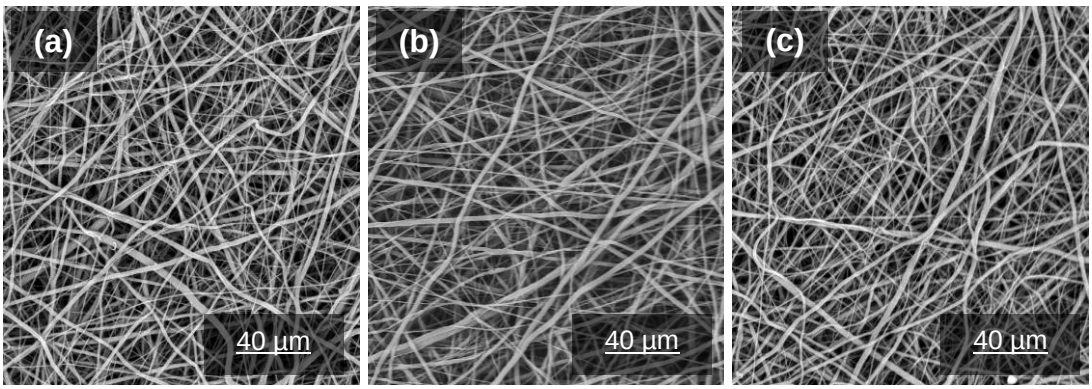

Figure 3-18: Post-sonication scanning electron micrographs of untreated (a) and PFPA-treated fibres before (b) and after UV exposure (c).

Compared to non-sonicated, dip-washed fibres (Figure 3-7, page 90), the morphology of the untreated fibres (Figure 3-18a) is somewhat distorted after sonication, which could suggest that the sonication step introduced changes to the fibre morphology. The clusters observed in PFPA-treated samples in Figure 3-7b and c are no longer observed

post-sonication (Figure 3-18b and c), indicating that the introduction of the washing step was necessary for the removal of excess PFPA-NHS from the fibre surface.

The sonicated and non-sonicated fibres were then investigated with FTIR, DSC and XRD to probe for any physicochemical changes that could have led to increased protein adsorption post-sonication and changes to the morphology. Figure 3-19 summarises the finding of these experiments.

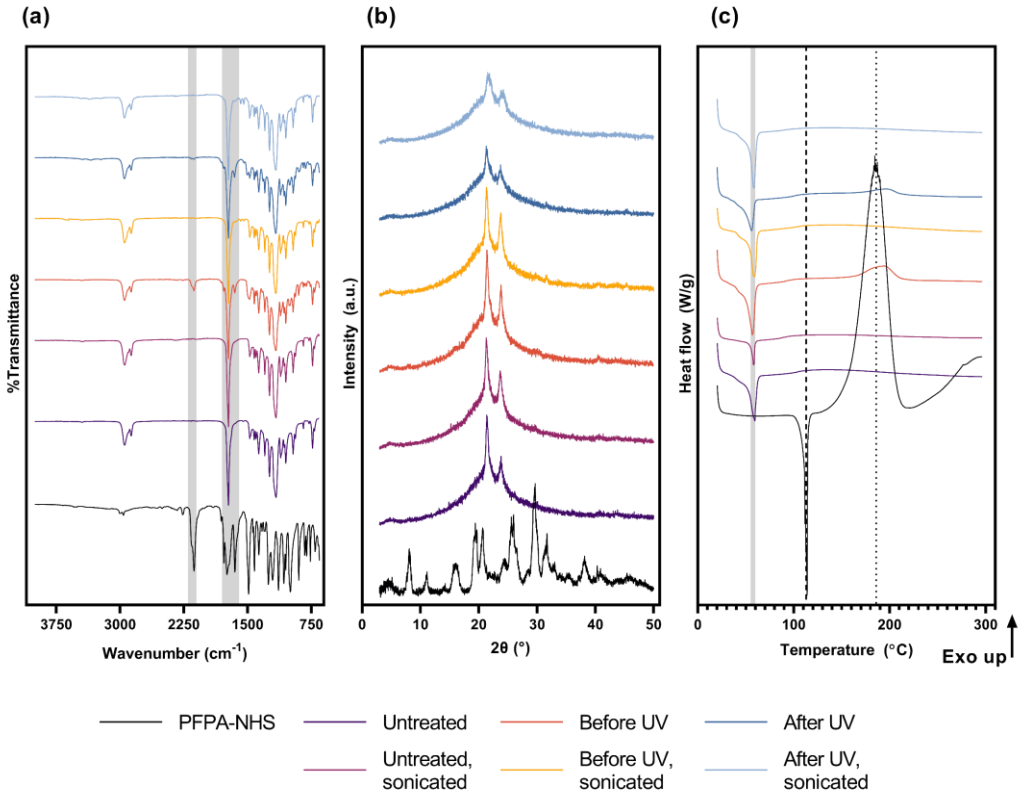

Figure 3-19: Summary of physical characterisation of sonicated electrospun fibres, showing FTIR (a), XRD (b) and DSC (c) data collected for untreated and PFPA-treated fibres before and after UV exposure and sonication treatment. In FTIR, grey shading denotes the areas of interest – azide and carbonyl peaks. In DSC, the greyed area corresponds to the melting peak of PCL (~57 °C), the dashed line signifies the melting peak of PFPA-NHS (113 °C), and the dotted line shows a possible PFPA-NHS degradation peak at 186 °C. Similar results were obtained from all three independent experiments and the results of one representative experiment are shown.

In FTIR (Figure 3-19a), no differences were observed for untreated PCL fibres before and after sonication. The effective washing of the scaffold was confirmed with the

PFPA-treated scaffold before UV irradiation. The disappearance of the azide peak at 2100 cm^{-1} and lack of carbonyl stretches of the NHS group at 1650 cm^{-1} confirm that the unbound compound was removed from the surface by sonication washing. In the UV-exposed PFPA-treated fibres, the carbonyl bond at 1650 cm^{-1} was retained following washing, confirming a strong covalent attachment to the surface. The intensity, however, was lower than in dip-washed scaffolds, suggesting that a significant amount of unbound PFPA-NHS was successfully removed.

XRD measures the crystallinity of the sample. The sharp Bragg reflections present in Figure 3-19b for PFPA-NHS (black line) confirm the crystalline nature of the compound. On the other hand, this signal is not present in any of the fibre formulations tested, as would be expected given the PFPA-NHS will be molecularly dispersed across the polymer surface. PCL itself has two broad Bragg reflections, consistent with the literature and its nature as a semi-crystalline polymer[111]. After UV functionalisation, the C-H insertion reaction occurring between PCL and PFPA-NHS is expected to disrupt the crystal domains, therefore reducing overall crystallinity. Moreover, the reduced intensity of the peaks after sonication suggests a low reduction in the extent of crystallinity.

The DSC data (Figure 3-19c) revealed the melting point for PCL-based nanofibres to be ~ 57 °C, which agrees with existing literature[111,245]. The melt of PFPA-NHS is not observed in the fibrous formulations, hence the DSC results are consistent with the XRD spectra (Figure 3-19b). The fibres before and after UV treatment but no sonication show a small exothermic peak at ~186 °C, which can be attributed to degradation of PFPA-NHS. This peak, however, disappears after the sonication

washing step. The DSC analysis allowed for the calculation of the degree of PCL crystallinity (X_c) by integration of the melting events at 57 °C (Figure 3-20).

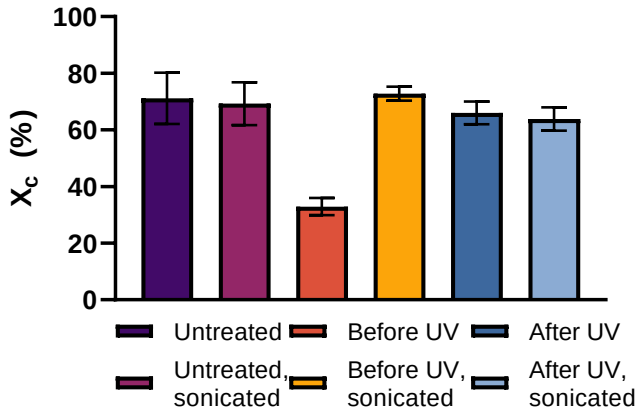

Figure 3-20: The effect of fibre sonication on the degree of PCL crystallinity as calculated from the DSC data for untreated and PFPA-treated fibres before and after UV treatment. Data are shown as mean ± S.D. and are representative of three independent experiments (n=3).

With the sonication treatment, no changes in X_c were observed for untreated and UV-irradiated PFPA-treated fibres. Interestingly, the degree of crystallinity increased from ~30% to ~70% for non-UV exposed PFPA-functionalised scaffolds after the sonication step. Previous studies have found that UV-irradiated PCL showed a significant increase in the degree of crystallinity following exposure to UV light[246]. However, the photolytic effect is decreased in PCL of higher molecular weights (60 kDa and over) owing to an increased level of crystallisation of the polymer. In this study, no changes in the degree of crystallinity were observed for the UV-treated samples, which could indicate that the scaffold retains its structural integrity following PFPA-NHS photografting.

Overall, the exploration of changes to physicochemical properties following the introduction of the sonication washing step did not bring conclusive results. The reason for increased protein adsorption to the sonicated fibres compared to non-sonicated controls (Figure 3-16, page 103) remains unclear. However, thanks

to the improved cytotoxicity profile following sonication, PFPA-functionalised fibres show promise for use in biomedical applications.

3.3.9. Catalase activity and release profile

Although protein-loaded electrospun fibres are generally well characterised from the physicochemical perspective, the published studies often lack conclusive protein stability or bioactivity data[247,248], even though proteins are often mixed with organic solvents during the fabrication process[138]. In the PFPA-NHS functionalisation approach, the fibres are only exposed to organic solvents in the initial PFPA-NHS functionalisation step before proteins are introduced on the surface. This can potentially protect the structure of a protein from accidental damage during the functionalisation procedure.

To test this hypothesis, the activity of a model enzyme, catalase, was measured following attachment to the fibre surface. As previously mentioned, catalase is responsible for the decomposition of hydrogen peroxide to water and oxygen. The catalase activity assay is well-characterised in the literature[222,239,240,249].

Here, a modified protocol was developed to test the activity of catalase directly on the surface of the fibre, rather than from release study supernatants. The results are presented in Figure 3-21.

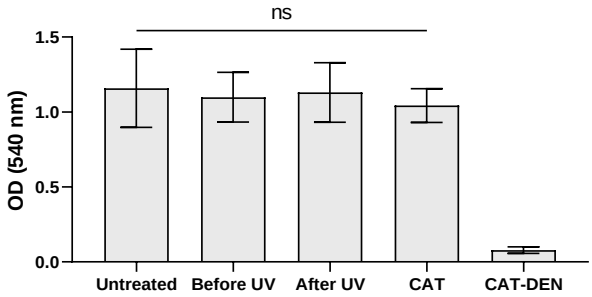

Figure 3-21: Catalase activity for sonicated untreated and PFPA-treated fibres before and after UV exposure. A freshly prepared catalase solution (CAT) and denatured catalase (CAT-DEN) were used as positive and negative controls, respectively. The data are presented as mean ± S.D. (n=3). *Repeated measures one-way ANOVA with post hoc Tukey's test; statistical significance was not observed (ns).*

The results of the catalase assay showed no differences in the enzyme activity following attachment to the fibre surface. The optical density values were similar for the freshly prepared solution containing an amount of catalase comparable to this attached to the fibre surface, while the negative control – catalase heated to 95°C – showed markedly reduced optical density (OD), suggesting the loss of enzymatic activity following denaturation at high temperature. Therefore, it can be concluded that the PFPA-NHS functionalisation does not negatively impact the biological activity of a protein being conjugated.

The final step in the fibre characterisation was to investigate the release of catalase from the fibres. Since after sonication the extent of protein attachment to the untreated PCL fibres was comparable to the PFPA-treated ones (Figure 3-16), it is possible that simple physical adsorption to the surface may be enough to safely attach proteins to the electrospun fibres. However, it is anticipated that the reaction with the NHS group of the PFPA-treated fibres should prolong the presentation of ligands on the surface due to the covalent bond being formed. To investigate this, the release of catalase following incubation in PBS over six days was measured and is presented in Figure 3-22.

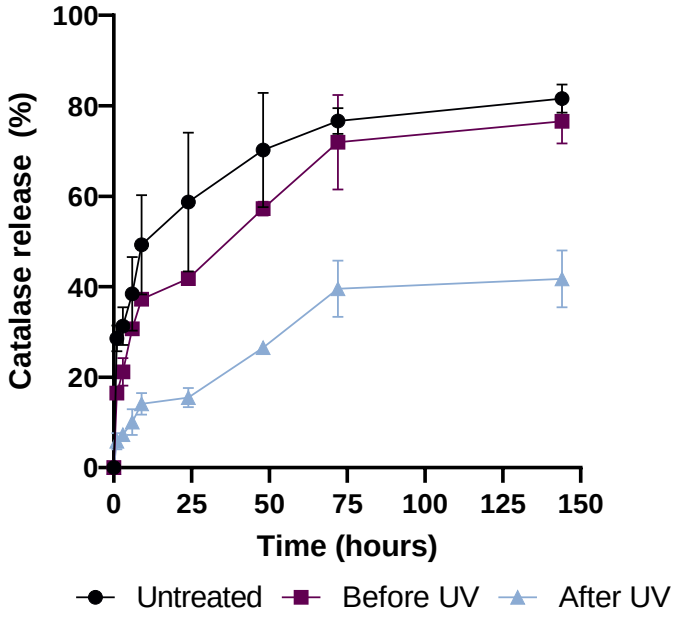

Figure 3-22: Catalase release profile over six days following incubation with untreated and PFPA-treated fibres before and after UV exposure. Data are shown as mean ± S.D. (n=3).

The release profiles confirm that PFPA-NHS functionalisation prolongs the presentation of catalase on the electrospun fibres. Within the first 24 hours, untreated and PFPA-treated fibres before UV exposure exhibited rapid release of catalase (60% and 40%, respectively). PFPA-treated fibres after UV exposure did not follow this trend, with less than 20% of the protein loading being released after one day. After six days, the cumulative release reached 40% for photo-exposed PFPA-treated fibres, while both untreated and PFPA-treated fibres before UV exposure showed 70%. It became evident that weak forces of physical adsorption were unable to retain catalase on the fibre surface in aqueous media under constant shaking. The data presented above clearly support the idea of using photo-activated PFPA-NHS on the surface of PCL fibres for prolonged presentation of proteins on the polymeric surface.

3.3.10. *In vitro* activation of Jurkat cells using anti-CD3-decorated fibres

The delivery of anti-CD3 on a surface of biomaterials for *in vivo* T cell activation has been heavily explored [73,74,95,250–252]. Biopolymer implants for enhancing adoptive T cell therapy have been attracting considerable interest in the growing field of cancer immunotherapy[96]. Therefore, the PFPA-NHS functionalisation of electrospun fibres was explored for this application by conjugating T cell activating anti-CD3 to the surface of PCL scaffolds. Due to the ease of manufacture and controllable size and thickness of the electrospun patch, such material could be easily implanted near a tumour resection site and act as an artificial lymph node by attracting T cells to the area. The covalent conjugation provided by the PFPA-NHS functionalisation will prolong the presentation of antigens on the surface.

The percentage of protein attachment to the PCL fibres was previously established using model proteins (Figure 3-16). The effect of varying protein concentration on the percentage attachment was established using the target therapeutic anti-CD3 (OKT3). The untreated and PFPA-treated fibres following sonication washing were incubated in a solution of 5, 10 and 20 µg/mL OKT3 in PBS overnight. The percentage attachment was calculated and is given in Figure 3-23.

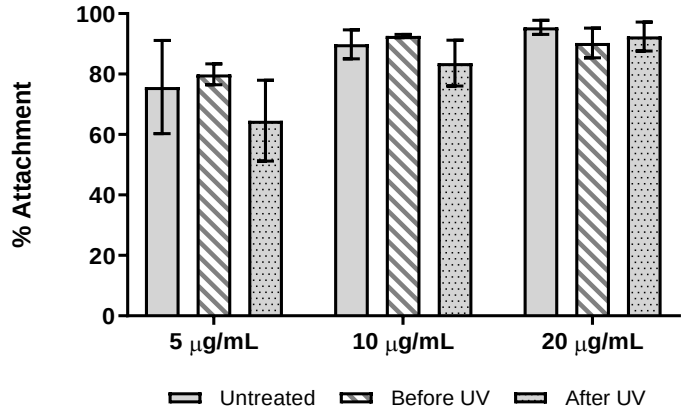

Figure 3-23: Percentage of OKT3 attachment to electrospun fibres after overnight incubation. Data are shown as mean ± S.D. and are representative of three independent experiments performed on separate days, with two replicates per experiment.

Overall, all three formulations achieved over 60% attachment in the 5 µg/mL treatment group and 80% in 10 µg/mL and 20 µg/mL. At lower antibody concentration (5 µg/mL), the calculated percentage attachment was more variable with higher standard deviations. This could be due to the antibody concentration values reaching the limit of detection for the protein assay used for this study (10 ng/mL for NanoOrange®). However, the conjugation of OKT3 to the PCL fibres appeared to be highly efficient for 10 µg/mL and 20 µg/mL dosing groups, with no significant differences observed between the two conditions.

The biological performance of antibody-decorated fibres was assessed in an *in vitro* T cell activation model, where the functionalised scaffolds were incubated in a culture of Jurkat cells for four days. Untreated and PFPA-functionalised PCL fibres were incubated with varying concentrations of anti-CD3 (5, 10, 20 µg/mL) to investigate the dose-response effect on T cell activation. A standard method of stimulating cells with tissue culture plastic plate-bound antibody was used as a positive control[253,254]. The cytokine IL-2 was chosen as an effective marker of late T cell activation[255] and its concentration in the cell culture supernatant was quantified using ELISA. Cell

viability following the four-day treatment with fibres was also measured to investigate the potential cytotoxicity of the modified scaffolds.

Figure 3-24 shows the percentage viability of Jurkat cells following incubation with anti-CD3-functionalised fibre formulations at three antibody concentrations. Unstimulated Jurkat cells were used as the baseline for viability calculations.

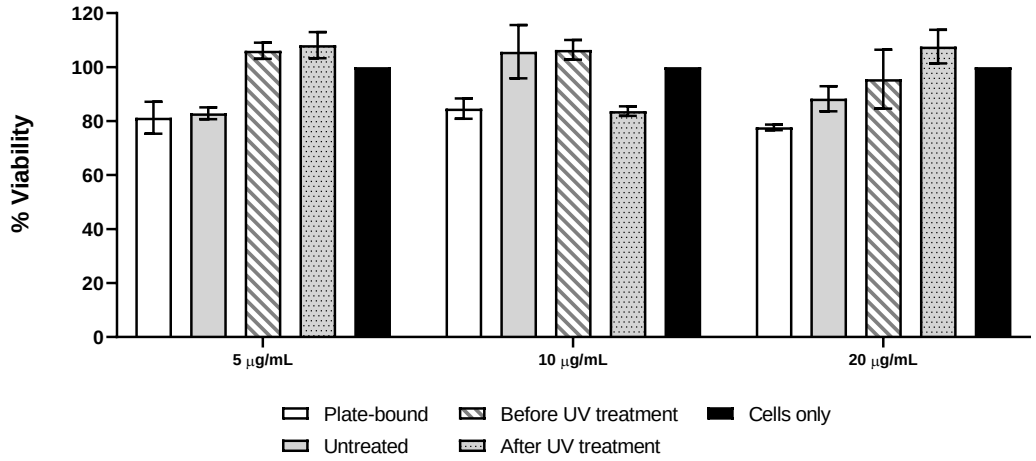

Figure 3-24: Percentage of viable Jurkat cells following a four-day incubation with fibre formulations functionalised with varying concentrations of OKT3 (5 µg/mL, 10 µg/mL, 20 µg/mL). Plate-bound antibody (white) was used as a positive control. All fibre samples were sonicated post-PFPA treatment. Cells only without antibody stimulation (black) acted as the baseline viability (100%). Untreated (grey) and PFPA-treated fibres before (dashed) and after UV treatment (dotted) were tested. Data are shown as mean ± S.D. and are representative of two independent experiments performed on separate days (n=6).

Cell viability remained between 80 and 110%, suggesting adequate biocompatibility of the formulations tested. Generally, Jurkat cells stimulated with plate-bound antibody showed lower viability (~ 80% for all tested Ab concentrations). This indirect cytotoxicity evaluation revealed that neither the neat nor modified PCL scaffolds released any substances at levels harmful to Jurkat cells. Wells treated with PFPA-functionalised fibres before UV treatment at 5 µg/mL and 10 µg/mL of antibody generally achieved slightly higher cell viability than the baseline, which could be an indicator of cell proliferation.

Figure 3-25 depicts the IL-2 concentrations detected in the supernatant of Jurkat cell culture following treatment with the antibody-coated fibres.

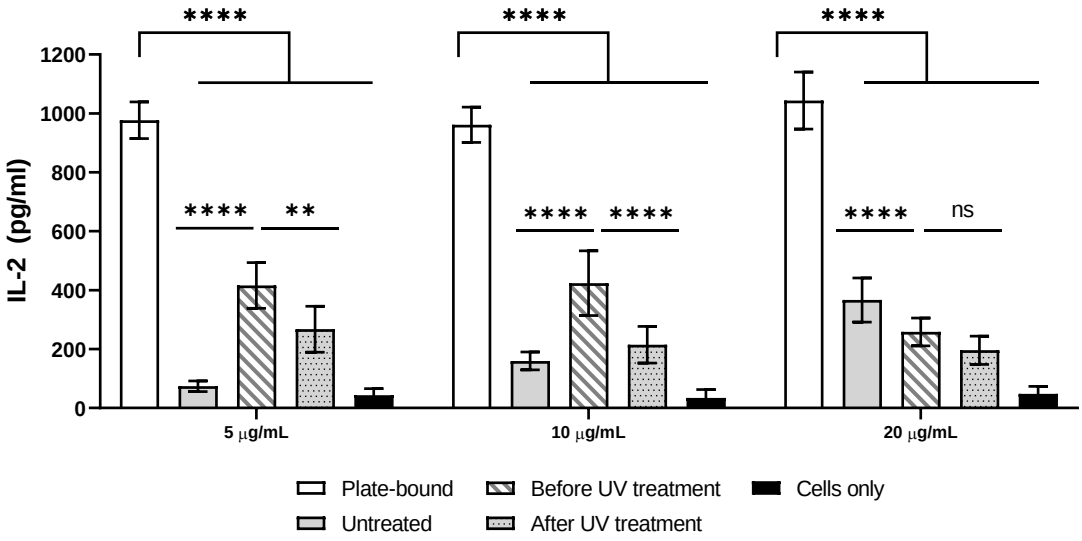

Figure 3-25: IL-2 production in Jurkat T cells following four-day incubation with fibre formulations functionalised with varying concentrations of OKT3 (5 µg/mL, 10 µg/mL, 20 µg/mL). Plate-bound antibody (white) was used as a positive control. Cells only without antibody stimulation (black) acted as the negative control. Untreated (grey) and PFPA-treated fibres before (dashed) and after UV treatment (dotted) were tested. All fibre samples were sonicated post-PFPA treatment. Data are shown as mean ± S.D. and are representative of two independent experiments performed on two separate days, with three replicate wells per tested condition. *Repeated measures two-way ANOVA with post hoc Tukey's test; statistical significance: ns (p-value >0.05), ** (p-value ≤0.01), **** (p-value ≤0.001).*

Stimulation with functionalised fibres achieved a relatively low level of T cell activation as measured by IL-2 release. At all tested antibody concentrations, IL-2 production was the highest in Jurkat cells stimulated with a plate-bound antibody. Large standard deviations observed for cells treated with PFPA-functionalised fibres may suggest uneven antibody conjugation to the surface or uneven cell interactions with the surface. For untreated PCL scaffolds, a dose-response relationship was observed, where more IL-2 was released in samples incubated with higher concentrations of antibody. Interestingly, PFPA-treated fibres before UV treatment performed significantly better than UV-treated formulations for 5 µg/mL ($p \leq 0.01$)

and 10 µg/mL ($p \leq 0.001$), possibly due to the rapid release of physically adsorbed antibody form the fibre surface. In the 20 µg/mL dosing group, the difference between these formulations was insignificant. Similarly, the untreated fibre achieved significantly lower IL-2 stimulation than PFPA-treated non-UV exposed fibres for the same dosing groups ($p \leq 0.001$ for 5 µg/mL and 10 µg/mL).

The *in vitro* study suggest that this antibody delivery method did not achieve sufficient level of T cell activation. One explanation for lack of biological activity is that the conjugated antibody molecules are buried deep into the nanofibre mesh, therefore reducing the possibility for contact with T cells. Potentially, this could be overcome by introducing a spacer molecule, such as PEG, that would bring the antibodies back to the surface of the fibre. It is possible, however, that the buried antibodies may eventually be released through hydrolysis of the fibre mat.

Using antibody-decorated fibres, rather than particles, could potentially result in better retention of the biomaterial at the tumour resection site, and therefore prolonged T cell activation *in vivo*. However, past studies have reported that T cell stimulation is most effective with biomaterials that resemble the natural size and shape of lymphocytes, i.e. spherical or slightly elongated structures of around 10 µm in size[12,256]. The pore size of PCL nanofibres may be too small for T cells to enter into the scaffold, leading to a limited interaction with the antibodies. Therefore, the biological efficacy of electrospun patches could be enhanced by scission of long fibre strands into shorter, needle-shaped structures using ultrasonication[257] or mortar grinding[258]. Breaking down dense PCL fibres into loosened, micro-scale needles would not only enable more effective interaction with T cells but also increase the functionalisation surface area and enhance wettability. Another approach would be to produce spherical microparticles by electrospraying by altering the solution parameters used in the EHD process.

3.4 Conclusions

The findings of this study indicate the feasibility of electrospun PCL fibre functionalisation with perfluorophenyl azides. A thorough surface analysis using SEM, XPS and FTIR successfully confirmed covalent modifications of the scaffold by PFPA and encouraged further investigation into potential applications of this approach. Protein conjugation using perfluorophenyl azide with an NHS moiety was extensively explored using fluorescence staining and attachment studies, confirming the retention of amine coupling capability following photografting of PFPA-NHS to the PCL surface.

The importance of the washing method used to remove unreacted PFPA was highlighted in Caco-2 viability studies, where unbound PFPA-NHS leaching out of electrospun fibres appeared to be toxic to cells. A brief sonication in methanol and PBS seemed to resolve this issue. Protein attachment studies showed that antibodies can be easily deposited on the surface of PCL fibres with or without pre-functionalisation with NHS moieties. In case of enzyme or albumin attachment, PFPA-treated samples showed increased surface attachment over the untreated controls. Catalase retained its enzymatic activity following attachment to the fibres *via* PFPA-NHS and released in a sustained manner over the period of 6 days. On the other hand, physically adsorbed showed much faster release, highlighting the importance of covalent conjugation *via* PFPA-NHS to the surface. The PFPA-NHS functionalisation approach could be of great potential in applications where a prolonged presentation of protein on the surface is required, for example in the design of growth factor-decorated implantable scaffolds in bone and cartilage tissue engineering[259,260].

In vitro T cell activation experiments highlighted the potential of surface functionalisation *via* physical adsorption. Following incubation with anti-CD3, the untreated fibres showed a dose-dependent performance *in vitro*. However, antibody-

decorated fibres did not stimulate T cell activation as potently as the positive control. Although not effective in short-term *in vitro* experiments, the UV-treated fibres could show potential *in vivo* where a prolonged retention of the scaffold at the tumour resection site is required. It is anticipated that overall cellular stimulation could be improved by using electrosprayed particles, rather than electrospun scaffolds, to mimic the size and shape of T cells. This will be explored in Chapter 4.

Chapter 4 - Antibody-functionalised electrosprayed microparticles for T cell activation.

4.1 Introduction

Nature has long provided inspiration in pharmaceutical development. With an increasing understanding of immunological processes governing conditions such as cancer[2,3], scientists are now more able to translate some of these processes into effective therapeutic strategies. Research has shown that activated T cells are capable of infiltrating tumours, recognizing and killing cancerous cells[73]. This unique property of the immune system has been widely explored and multiple cell-based immunotherapies have now been approved and indicated for a variety of solid and liquid tumours[20]. The on-going effort to harness the immune response to treat cancer is particularly evident in recent advancements in chimeric antibody receptor T cell (CAR-T cell) therapy, a type of adoptive T cell therapy. In this approach, cancer-specific cytotoxic lymphocytes are harvested from the patient, expanded and modified *ex vivo* and subsequently re-infused back into the bloodstream.

Two recently FDA-approved lymphoma treatments are now on the market (Kymriah[261] and Yeskarta[262]) and over 700 clinical trials are currently in the pipeline*.

A promising tool in the delivery of adoptive immunotherapy entails direct *in vivo* T cell activation using biomimetic particulate systems acting as artificial antigen presenting cells (aAPCs)[14,263,264]. The concept of aAPCs has been previously described in the introductory chapter of this thesis (see Section 1.3.3.2, page 21).

The pioneering work of Jonathan Schneck and subsequent developments by the Green and Fahmy groups have led to the emergence of a new generation of aAPCs[106,256,265–268]. These novel particulate-based aAPCs were created using biodegradable polymers, allowing for efficient local immuno-stimulation *in vivo*. As they are fabricated from biodegradable materials, they can be safely implanted, or injected, into living organisms, eliminating the need for strenuous *ex vivo* processing that is currently required in adoptive T cell therapy protocols.

Surface-functionalised particles for triggering T cell responses have been extensively explored as biodegradable aAPCs. Such particles should mimic biological APCs by resembling their size and spherical shape as well as presenting stimulatory cues on the surface[77,255,256,269,270]. These essential aAPC design parameters are described below.

4.1.1. Choice of ligand and bioconjugation method

Broadly speaking, aAPCs are created by coupling T cell activating cues to a biocompatible substrate. The major advantage of synthetic aAPCs is the control over ligand choice and density on the surface. As previously discussed (Section 1.1.2,

* The number of clinical trials published on www.clinicaltrials.gov with 'CAR-T cell' keyword in the title is 769 on 12/05/20. Available from [334].

page 3), effective T cell stimulation depends on the provision of two signals, 1 and 2. Signal 1 is usually provided by an agonistic CD3 antibody or a recombinant antigen-loaded MHC protein, while co-stimulatory signal 2 is often recreated by an agonistic anti-CD28[255,265,270] or anti-41BB[271]. Another approach is to use a mixture of multiple signal proteins. For example, Rudolf et al.[272] explored the co-delivery of CD28 and 41BB antibodies, achieving a three-to fivefold preferential expansion of CD8+ T cells than with anti-CD28 or anti-41BB alone.

Artificial APCs are sometimes explored for sustained delivery of signal 3 cues. Steenblock et al.[273] developed PLGA particles for *in-situ* release of IL-2, which showed preferential activation of CD8+ T cells. Based on these findings, the group then designed TGF-β and IL-2-loaded nanoparticles for targeted stimulation of CD4+ T cells.

With time, biodegradable aAPCs have become even more elaborate. In 2019 Zhang et al.[274] described the design of PLGA microparticles bearing 11 immunostimulatory molecules – five encapsulated in the core and six surface-conjugated using polyethylenimine modification and EDC/NHS chemistry. The encapsulated proteins (IL-2, IL-15, CCL-21, anti-CTLA-4 and anti-PD1) showed a burst release in the first two days (62.3%- 71.0%), followed by more sustained release over 28 days, reaching approximately 81.0 to 88.3% cumulative release.

4.1.2. Particle size

Particle size of aAPCs plays a pivotal role in the potency of immune modulation. Lymphocyte research by the Mescher lab has largely directed the design of modern aAPCs[12,13,275,276]. In 1992, the group demonstrated a clear correlation between particle size and effective T cell stimulation[12]. The biological response declined rapidly for latex microbeads of sizes lower than 4 μm, and this could not be compensated for by increasing the amount of smaller particles used in the experiment. The clear

conclusion from this study was that a successful cytotoxic T cell response is highly dependent on the size of the particle on which stimulatory cues are being delivered, with preference given to micro-scale materials.

Based on these findings, micro-scale platforms resembling biological T cells have become hugely popular in aAPC design. Microparticles (1-10 μm) of sizes comparable to T cells and DCs in diameter (5-7 μm[277] and 10-15 μm[278], respectively) have been widely explored[76,266,279]. In 2008, Steenblock and Fahmy proposed a concept of using antibody-functionalised biodegradable PLGA micro- and nanoparticles as an *ex vivo* T cell expansion platform. CD3 and CD28 antibodies were biotinylated and immobilised onto avidin-PLGA at a 1:1 (w/w) ratio, and the effect of particle size on aAPC efficacy was explored. The results of this study showed that micro-sized aAPCs induced a 3-fold higher response in CD8+ T cell IL-2 release than nano-sized aAPCs functionalised with the same protein dose[255].

More recently, there has been some dispute over the use of nano-sized particles in aAPC design. Based on the findings in cancer vaccine research[280], where OVA-coated polystyrene nanoparticles induced a significantly higher immune response than their micro-sized equivalent, the authors concluded that nano-APCs may be linked to a more favoured *in vivo* biodistribution. Due to their smaller size, nanoparticles are capable of draining to the lymph nodes, which are the natural site of T cell-APC interaction[264]. With the fast-developing landscape of biodegradable aAPC design research, more research into the effect of particle size and morphology is anticipated, but currently injectable micro-sized particles that could act as a tissue-localised depot remain the gold standard in aAPC design.

4.1.3. Aims of this chapter

The previous chapter described the potential for the simple and efficient presentation of proteins on the surface of polymer-based biomaterials using perfluorophenyl azide

chemistry. Although the target OKT3 antibody was successfully deposited on PCL fibres, they did not achieve adequate *in vitro* cellular response in a T cell activation model.

Based on the literature reviewed in Section 4.1.2 (page 123), it is anticipated that delivering anti-CD3 on the surface of spherical microparticles would achieve a more potent biological response due to the biomimetic nature of the substrate size and morphology.

Therefore, this chapter aims to employ the previously described PFPA-NHS chemistry for the conjugation of OKT3 to the surface of electrosprayed PCL particles, with the ultimate goal of achieving targeted T cell activation when the particles are injected intratumorally.

Several variations of the electrospraying methodology will be investigated to produce separated particles in the range of 1-10 μm in diameter. The particles will be thoroughly characterised to investigate the effect of PFPA-NHS functionalisation on surface morphology and composition. Following preliminary studies with model proteins (albumin, rhodamine-amine, FITC-albumin), anti-CD3-functionalised PCL microparticles will be tested in *in vitro* T cell activation models created using a cell line and T cells derived from human blood.

4.2 Experimental details

4.2.1. PCL microparticle fabrication using EHDA

4.2.1.1. Standard uniaxial electrospraying

The principles of EHDA are described elsewhere in this thesis (see Section 1.4, page 23). PCL microparticles of ca. 10 µm were prepared by electrospraying a solution of 10 % w/v polycaprolactone (Mw~ 45 kDa, Sigma-Aldrich, UK) in 2,2,2-trifluoroethanol (99.8%, ThermoFisher, UK). The solution was dispensed through a 21G stainless needle (inner diameter 0.51 mm, Nordson EFD, UK) connected to a high-voltage direct-current power supply (HCP 35-35000, FuG Elektronik, Germany) at a voltage set at 15 kV. A syringe pump (789100C, Cole Parmer, UK) was used to control the solution flow rate (1.0 mL/h). The particles were collected on aluminium foil placed on a grounded plate collector (14.7 × 20 cm). The distance from the needle to the collector was 16 cm. Temperature was at approximately 25 ± 2 °C and relative humidity was 35 ± 10%. The resultant particles (named PCL-TD) were carefully scraped from the foil with a scalpel held perpendicularly (90 º) to the aluminium plate and stored in air-tight glass vials at room temperature.

4.2.1.2. Electrospraying into liquid nitrogen

The same procedure as in Section 4.2.1.1 was employed, except that the particles were collected into liquid nitrogen. Liquid nitrogen was placed in a stainless-steel bowl, which was hemispheroidal with an inner diameter of 14 cm. The bowl was filled with liquid nitrogen to 2 cm below the top. The distance from the needle to the surface of the liquid nitrogen was kept at 16 cm. Once the liquid nitrogen had entirely evaporated, two methods were used to dry the particles: by freeze-drying (VirTis Company Inc., Gardiner, UK) overnight at -40 °C (termed PCL-LN-FD) or storing the

frozen particles in an oven (PF 30, Carbolite, UK) overnight at 45 °C (termed PCL-LN-OV). The product was then stored in air-tight glass vials at room temperature.

4.2.1.3. Electrospraying assisted by pressurised gas

These materials were a kind gift from Bioinicia S.L. (Spain). These were obtained by the so-called electrospraying assisted by pressurised gas technique using the Fluidnatek™ LE500 Capsultek™ pilot system. The system comprises an injection unit, a drying chamber, and a cyclonic collector[281]. The experiments were performed at controlled ambient conditions, 25 °C and 30% relative humidity. PCL (Mw ~ 14000 kDa; Sigma Aldrich, UK) was dissolved in acetone (Labkem, Spain, Ph. Eur. 99.5%) at a concentration of 15 % w/w. The solution was pumped at 1 mL/min into an injector supplied with an assisted air pressure of 10 L/min and a variable electric voltage. Particles of PCL-PG-1 were prepared at 5 kV and particles of PCL-PG-2 were manufactured at 2 kV and stored in airtight glass vials at room temperature.

4.2.2. Perflurophenyl azide functionalisation

PFPA-NHS was synthesised as described in Section 3.2 (page 71). PFPA functionalisation was performed by allowing the microparticles to react with PFPA-NHS at a final concentration of 50 mg/mL of particles in the functionalisation solution, with the latter comprising 20 mg/mL PFPA-NHS in methanol. The particles were then immediately dried under reduced pressure. Afterwards, the particles were transferred to quartz cuvettes, sealed with parafilm and attached to a plate-shaker with a 0.3 cm circular orbit (Microplate Mixer, SciQuip, UK) set to 200 rpm. The formulation was then exposed to UV radiation (8-watt, 254 nm, 50 Hz at a distance of 10 cm) for 20 minutes. After that, the particles were briefly mixed with a spatula and treated with UV for another 20 minutes. Subsequently, the particles were moved to centrifuge tubes and washed once with 1 mL of methanol and twice with 1 mL of PBS,

by centrifuging and resuspending in fresh solution, to remove unbound PFPA-NHS and to ensure sterility for *in-vitro* experiments. Blank PCL particles (no PFPA solution, no UV radiation) and a set of non-UV treated samples (treated with PFPA solution, no UV radiation) were prepared as controls.

4.2.3. Morphological and physicochemical characterisation

Particles pre- and post-functionalisation were characterised using SEM, FTIR and XPS as described in Section 2.2.3 (page 55).

4.2.4. Conjugation of fluorescently-labelled model biomolecules

The conjugation of biomolecules to particles was simulated using two amine-bearing model molecules - rhodamine-amine (Santa Cruz Biotechnology, UK) and FITC-albumin (Sigma-Aldrich, UK). PCL particles were incubated either in 20 μg/mL rhodamine-amine or FITC-albumin in PBS (5 mg of particles in each Eppendorf tube, immersed in 100 μL of FITC-albumin solution or 100 μL of rhodamine-amine solution). After 24 hours of incubation at room temperature under constant shaking and light exclusion, the particles were washed with 2 mL of PBS four times by centrifuging and resuspending in fresh solution, and imaged with fluorescence microscopy (EVOS XL Cell Imaging System digital inverted microscope, ThermoFisher Scientific, UK).

4.2.5. Protein attachment study

The protein attachment was tested indirectly. Five sets of samples were prepared, corresponding to five time points. In each set, 0.5 mL of a 20 μg/mL solution of bovine serum albumin (BSA, ThermoFisher Scientific, UK) was added to 20 mg of surface-functionalised PCL particles. Afterwards, the particles were incubated in Eppendorf

tubes at room temperature under constant shaking (500 rpm) on a plate shaker. Subsequently, after an appropriate incubation period, the individual set corresponding to each time point (1, 2, 3, 6 or 24 hours) was removed from the plate shaker and centrifuged. The supernatants were collected, and the protein content of the supernatants quantified using the Bradford Ultra protein assay (see Section 2.2.6.2, page 58). The percentage attachment was calculated as outlined in Section 3.2.8 (page 75). Each experiment was performed three times on separate days, with three replicate wells per treatment.

4.2.6. Preparation of anti-CD3-functionalised microparticles

Two methods of PCL microparticle functionalisation were explored. Anti-CD3 IgG (clone OKT3, BioLegend, UK) was immobilised on the particle surface either by physical adsorption or *via* PFPA-NHS functionalisation (as described in Section 4.2.2). The optimal length of the functionalisation reaction and the amount of antibody used for conjugations was established experimentally (as described in Section 4.2.6.1, page 129 and Section 4.2.6.2, page 130, respectively).

4.2.6.1. Anti-CD3 loading quantification

Anti-CD3 attachment onto the particles was determined by depletion, similarly to the study described in Section 4.2.5, page 128. Microparticles (5 μg) were incubated at ambient temperature under gentle agitation with a 10 μg/mL (1 mL) solution of OKT3. The concentration of protein supernatant was determined after particle separation using the NanoOrange® protein assay as described in Section 2.2.6.4 (page 59), and compared to the protein concentration prior to particle incubation. Measurements were taken at 1, 2, 3, and 6 hours post-incubation. The optimal particle functionalisation reaction time was established based on the results of this experiment.

4.2.6.2. *In-vitro* T cell activation using Jurkat cells

An *in vitro* assay was optimized to achieve a reliable protocol for quantification of IL-2 release upon T cell receptor activation in anti-CD3 stimulated Jurkat E6.1 cells in a 96-well plate format. The antibody-functionalised particles were resuspended in cell culture medium at varying concentrations (~50-700 µg/well) or antibody doses (0-10 µg/well) and 50 µL of the suspension was pipetted onto the bottom of a standard flat-bottomed 96-well plate (Corning, UK). The desired concentration of particle suspension was established experimentally. The cells were resuspended at 2.5×10^5 cells/mL and 150 µL of the cell suspension was transferred to each well. The total volume in each well was 200 µL (150 µL cell suspension and 50 µL particle suspension). For the positive control, a plate-bound antibody solution at the same OKT3 concentration as in the microparticle suspensions was used. Wells with no antibody stimulation were used as a negative control. For control wells, the 50 µL particle suspension was replaced with 50 µL of pre-warmed cell culture media to maintain the same cell density per well.

For a co-stimulatory response, 10 µL of 10 µg/mL soluble anti-CD28 in PBS was added to the cells[223]. The plate was then placed in a humidified 37 ºC 5% CO_2 incubator under constant shaking (500 rpm) on a plate-shaker with a 0.3 cm circular orbit (Microplate Mixer, SciQuip UK) for four days. Afterwards, the plate was centrifuged at 1200 rpm for five minutes to allow the suspended cells and microparticles to sediment at the bottom. The supernatant was collected for Human IL-2 DuoSet ELISA analysis (R&D Systems, UK; for experimental details see Section 2.2.7, page 59), while the viability of the cells was measured using the PrestoBlue™ Cell Viability Reagent (Sigma-Aldrich, UK) as previously described in Section 2.2.8.2 (page 61).

4.2.7. Visualisation of antibody conjugation using fluorescence microscopy

PCL microparticles (5 mg) were functionalised as described in Section 4.2.2 and then were subsequently incubated for one hour at room temperature with constant gentle shaking (200 rpm on a plate-shaker with a 0.3 cm circular orbit (Microplate Mixer, SciQuip, UK)) in a 5 µg/mL solution of FITC-conjugated anti-human CD3 antibody (clone OKT3, BioLegend, UK). Afterwards, the particles were thoroughly washed with PBS (3×1 mL) and observed with fluorescence microscopy (EVOS XL Cell Imaging System digital inverted microscope, ThermoFisher Scientific, UK).

4.2.8. *In-vitro* T cell activation using CD3 positive T cells isolated from peripheral blood mononuclear cells.

In vitro T cell activation was performed on CD3+ T cells isolated from peripheral blood mononuclear cells obtained from three healthy donors, with three replicate wells per treatment tested.

CD3 positive T cells were isolated as described in Section 2.2.8.5 (page 63). The antibody-functionalised particles were resuspended in cell culture media (5 mg/mL) and 50 µL of this suspension was pipetted onto the bottom of a standard flat-bottomed 96-well plate (Corning, UK). The cells were resuspended in complete RPMI at 2.5×10^5 cells/mL and 150 µL of the cell suspension was transferred to each well. The total volume in each well was 200 µL (150 µL cell suspension and 50 µL particle suspension). For the positive control, an antibody solution at the same concentration as was present in the microparticle incubation solution was pipetted directly into the well and incubated for 1 hour at room temperature (plate-bound antibody control). Wells with no antibody stimulation were used as a negative control. For control wells,

50 µL of particle suspension was replaced with 50 µL of pre-warmed cell culture media.

For a co-stimulatory response, 10 µL of 10 µg/mL soluble anti-CD28 in PBS was added to the cells. The plate was then placed in a humidified 37 ºC 5% CO_2 incubator under constant shaking (500 rpm) for four days.

4.2.8.1. Determination of T cell proliferation using flow cytometry

Immunofluorescent staining was performed to examine the expression of T cell surface markers by flow cytometry. Following a four-day incubation of particles with PBMC-derived T cells (see Section 4.3.7), the 96-well culture plate was centrifuged at 4 °C and 1200 rpm for 5 min. The resultant supernatant was collected and stored at -20 °C for cytokine production analysis (see Section 4.2.8.2, page 133).

The cells were resuspended in 200 µL of ice-cold PBS (without Ca/Mg^{2+}) and pipetted into a 96-well V-bottomed plate (Sigma-Aldrich, UK). The cells were then washed once in 200 µL of ice-cold PBS and resuspended in 30 µL of LIVE/DEAD™ Fixable Violet Dead Cell Stain (1:1000 v/v dilution in PBS, ThermoFisher, UK). The cells were mixed by gentle pipetting up and down and incubated with shaking on ice, while protected from light, for 20 minutes. Following incubation, the cells were washed in 200 µL of ice-cold PBS (without Ca/Mg^{2+}) and 25 µL of antibody cocktail (1 µL of anti CD3-PE/Cy7, 1 µL of CD4-PerCP in 23 µL of PBA (2% v/v FBS in PBS)) was added. The plate was again incubated on ice with shaking, and protected from light, for 30 minutes. Following staining, the cells were washed once in 200 µL of ice-cold PBA and fixed with 2% formaldehyde solution (80 µL per well, incubated for 10 minutes, shaking, at room temperature). The fixing solution was neutralised with 120 µL of ice-cold PBA and the plate was centrifuged at 4 °C and 1200 rpm for 5 min, and washed with another 200 µL of ice-cold PBA. Following resuspension in 200 µL of

ice-cold PBA, the cells were ready for flow cytometry analysis. A summary of immunofluorescence staining used in proliferation panels is provided in Table 4-1.

Table 4-1: Summary of fluorochromes and markers used in the flow cytometry proliferation panel.

Fluorochrome	Marker
PE/Cy7	CD3
PerCP	CD4
CellTrace CFSE (488)	Proliferation
Violet (405)	Live/Dead

Flow cytometry analyses were performed using a MACSQuant® Analyzer 10 (Miltenyi Biotec, UK) as previously described (Section 2.2.9, page 65). The results were analysed using FCS Express version 7.04. The proliferation index was calculated using the software's built-in proliferation analysis tool, which uses the following formula (Equation (4.1)).[282]

$$Proliferation\ index = \sum_{i=0}^{P-1} \frac{N_i}{2^i} \tag{4.1}$$

where P is the total number of peaks found and N is the number of cells in a generation.

4.2.8.2. Cytokine production assays

The cell culture supernatant collected prior to flow cytometry analysis (see section 4.2.8.1, page 132) was used for the determination of cytokine release following a 4-day incubation of CD3+ T cells with particle formulations. The production of IFN-γ, TNF-α and IL-2 were quantified using commercially available ELISA kits as described in Section 2.2.7, page 59).

4.3 Results and discussion

This chapter discusses the fabrication, functionalisation, characterisation and the *in vitro* biological performance of electrosprayed microspheres surface-functionalised with anti-CD3 *via* PFPA chemistry. The work presented below builds on the findings discussed in the previous chapter (see Chapter 3, page 67), where PFPA-NHS was used to conjugate model proteins to the surface of electrospun fibres.

Electrospraying is a relatively simple and fast technique for the fabrication of micro- and nanosized spheres. The intricacies of the process optimisation have been previously described in the introductory chapter of this thesis (see Section 1.4, page 25). Scheme 4-1 summarises the concept of anti-CD3 decorated PCL particles that will be explored in the *in vitro* T cell activation models discussed in this chapter.

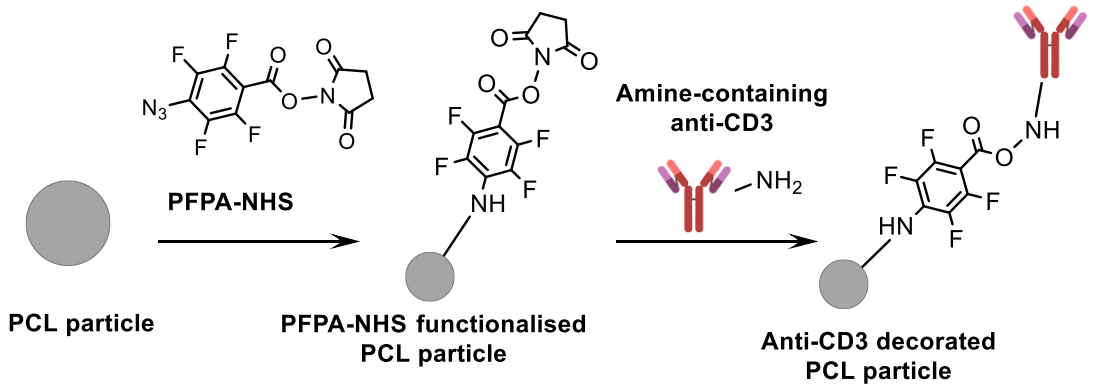

Scheme 4-1: Surface functionalisation of electrosprayed microparticles with anti-CD3 using perfluorophenyl azide chemistry.

4.3.1. Morphology of electrosprayed microparticles

The effect of PFPA-NHS treatment on the surface morphology and the average diameter of PCL microparticles prepared *via* a standard top-down electrospraying method was investigated using SEM (Figure 4-1).

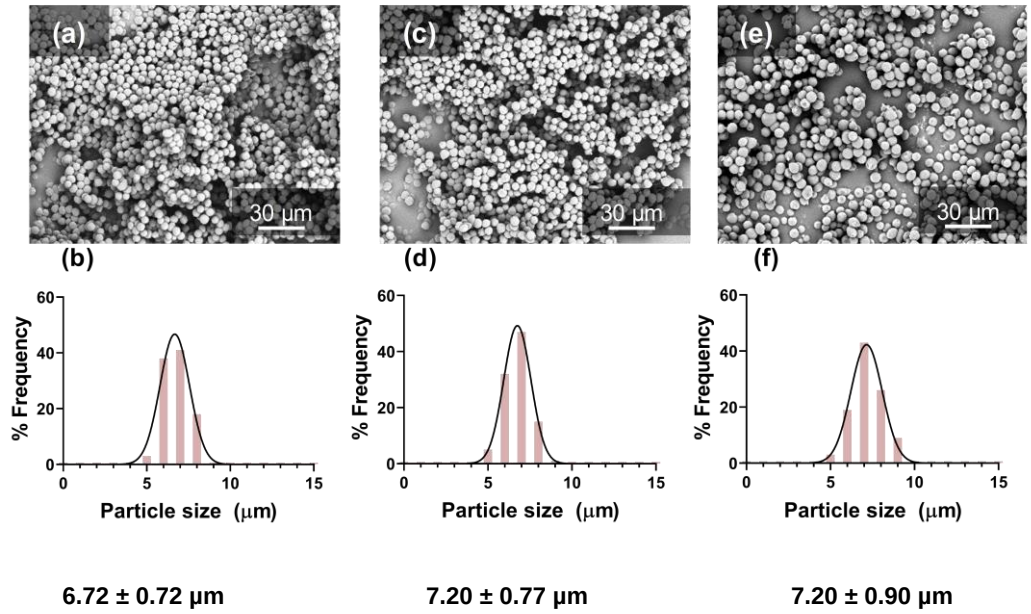

Figure 4-1: Morphology and size of electrosprayed polycaprolactone particles (PCL-TD) following PFPA-NHS functionalisation. Scanning electron micrographs and particle size distribution with mean and standard deviation of untreated (a, b) and PFPA-treated particles before (c, d) and after UV exposure (e, f). Similar results were obtained from all three independent experiments and the results of one representative experiment are shown.

Scanning electron micrographs revealed the microsphere morphology to be the same before and after functionalisation with PFPA-NHS (Figure 4-1a, c, e). In all tested conditions the particles remained smooth and spherical, suggesting that electrosprayed microparticles are capable of withstanding exposure to methanol and PBS as well as centrifugation washing step applied during functionalisation.

It should be noted, however, that a significant level of particle aggregation was observed in all tested conditions, which could potentially have a negative effect on the efficiency of surface functionalisation in PFPA-NHS-treated samples. The possible solutions to particle aggregation will be discussed later in this chapter (see Section 4.3.5, page 147).

A unimodal size distribution with an average particle diameter of ~7 µm was consistently observed for all particles (Figure 4-1 b, d, f). This lies within the preferred particle size range for T cell activation purposes (1-10 µm) as previously discussed

(Section 4.1.2, page 123)[266,283]. Overall, the PFPA-NHS functionalisation did not affect the morphology and size of the electrosprayed microparticles. As a simple and tunable microparticle production method, electrospraying appears to be an appropriate method for the production of polymeric microparticles for this application.

4.3.2. Physical characterisation

Figure 4-2 shows representative spectra of PFPA-functionalised microparticles before and after UV-light treatment.

The effect of particle washing and sterilisation method (by immersing in methanol, followed by subsequent centrifugation and resuspension two times in sterile PBS) was also investigated. The spectrum of the untreated particles before and after the wash are identical, suggesting that the repeated washing cycle in methanol and PBS does not affect the chemical composition of the polymer.

In unwashed PFPA-treated particles before UV treatment the prominent azide peak at 2134 cm^{-1} (arising from an asymmetric stretching vibration) and carbonyl stretches of the NHS moiety between 1650 and 1775 cm^{-1} can be observed. These features cannot be seen after the washing step, which means that the unbound PFPA-NHS was successfully removed from the surface of the particle.

After UV treatment, the azide peak significantly decreased in intensity, confirming the photolysis of the PFPA. However, a small peak remains at 2134 cm^{-1}, which could be evidence of the unreacted compound still present on the surface. Following washing in methanol and PBS, the azide peak is removed. Interestingly, the carbonyl stretches at 1650 and 1775 cm^{-1} also disappear. The results observed above may indicate that the photo-initiated C-H insertion reaction did not occur. This could suggest that either PFPA-NHS was not covalently conjugated to the surface or that the amount of PFPA-NHS bound to the surface was below the detection limit of FTIR.

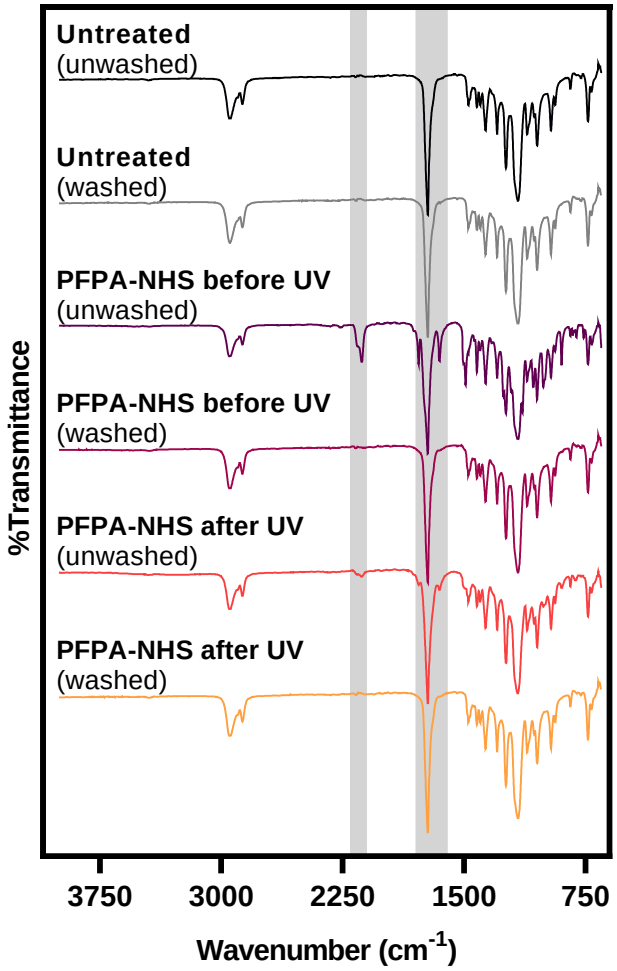

Figure 4-2: Representative FTIR spectra of PFPA-NHS functionalised PCL-TD microparticles. Untreated particle control is included, as well as PFPA-treated particles before and after UV exposure. The grey shading denotes the areas of interest – azide (~2134 cm^{-1}) and carbonyl (~1650 cm^{-1}) peaks. PFPA-NHS functionalisation is visible in microparticles before the methanol washing step. Afterwards, the carbonyl stretches of the NHS bond are no longer visible. Similar results were obtained from all three independent experiments and the results of one representative experiment are shown.

To test the latter, the surface of the microparticles was investigated with a more sensitive technique. Similarly to the PFPA-treated electrospun fibres described before (see Section 3.2.6 of chapter 3, page 74) the functionalised microparticles were analysed with XPS to assess the chemical composition of the particle surface. The results of the elemental survey analysis are presented in Figure 4-3.

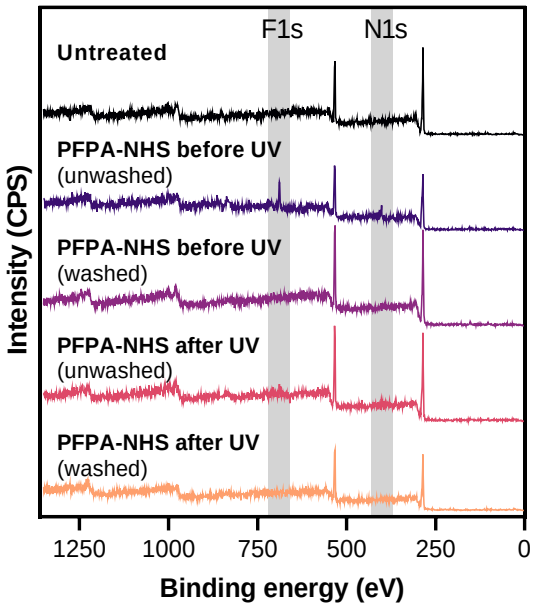

Figure 4-3: Representative XPS survey spectra measured for untreated and PFPA-treated PCL-TD particles before and after UV exposure. The effect of a post-functionalisation washing step on the retention of fluorine and nitrogen on the surface is explored. The fluorine (~ 690 eV) and nitrogen (~ 450 eV) peaks are shaded in grey. Similar results were obtained from all three independent experiments and the results of one representative experiment are shown.

The highlighted fluorine and nitrogen peaks were used as markers of PFPA functionalisation. As predicted, untreated particles show no N1s or F1s peaks. It can be seen that a significant level of fluorine and nitrogen is detected in unwashed PFPA-treated particles before UV treatment, but these elements are no longer present after the washing cycle. Similarly, while a small fluorine peak can be seen in PFPA- and UV-treated samples, it vanishes following the washing step.

To gain a better understanding of surface composition, the elements were quantified based on the survey spectra, and the results are presented in Table 4-2.

Table 4-2: Elemental surface composition of functionalised particles before and after the washing step. Data are shown as mean ± SD (n=3).

	Surface C (at%)	**Surface O (at%)**	**Surface F (at%)**	**Surface N (at%)**
Untreated	78.32 ± 0.56	21.68 ± 0.57	**0.00**	**0.00**
PFPA-NHS before UV (unwashed)	68.33 ± 0.17	20.20 ± 0.71	**7.36 ± 0.82**	**4.12 ± 1.35**
PFPA-NHS before UV (washed)	76.39 ± 0.95	23.28 ± 0.77	**0.17 ± 0.06**	**0.16 ± 0.02**
PFPA-NHS after UV (unwashed)	74.86 ± 0.43	23.87 ± 0.03	**0.43 ± 0.10**	**0.84 ± 0.23**
PFPA-NHS after UV (washed)	75.34 ± 0.95	24.66 ± 0.90	**0.00**	**0.00**

The results of XPS analysis on the surface of PFPA-functionalised microparticles match those previously described for electrospun fibres (see Section 3.2.6, page 74). Elevated nitrogen and fluorine contents in PFPA-treated samples confirm the presence of the compound on the PCL surface, although in unwashed PFPA- and UV-treated samples it is relatively low. The decrease in nitrogen content visible in PFPA-NHS treated samples before (4.12 ± 1.35%) and after UV treatment (0.84 ± 0.23%) could be partially attributed to the breakdown of the N_3 group upon photo-triggered C-H insertion reaction, releasing N_2 as a by-product. This, however, does not explain the significant drop in surface fluorine content (from 7.36 ± 0.82 % to 0.43 ± 0.10 %).

In both PFPA-treated formulations, the washing cycle removes the majority of F and N from the surface, suggesting that PFPA-NHS was not covalently conjugated to the surface or that the washing step was too aggressive. Surprisingly, some surface fluorine (0.17 ± 0.06 %) and nitrogen (0.16 ± 0.02 %) remains bound to the PFPA-treated particles without UV treatment. This could mean that there is some level of strong surface adsorption of PFPA-NHS to the PCL particle surface.

Although the results obtained in FTIR and XPS are rather unfavourable, it is hypothesised that the level of functionalisation could be below the detection limit of these analytical techniques. A further investigation into the protein conjugation

capability was performed to assess the functional performance of the PFPA-NHS particles.

4.3.3. Model protein conjugation

Fluorescence staining was performed to model protein conjugation using two model molecules, an amine-bearing small molecule (rhodamine-amine) and albumin (FITC-BSA), similarly to the model protein conjugation study discussed for PFPA-functionalised electrospun fibres in Chapter 3 (see Section 3.2.7, page 74). After thorough washing, the particles were imaged with a fluorescence microscope as depicted in Figure 4-4.

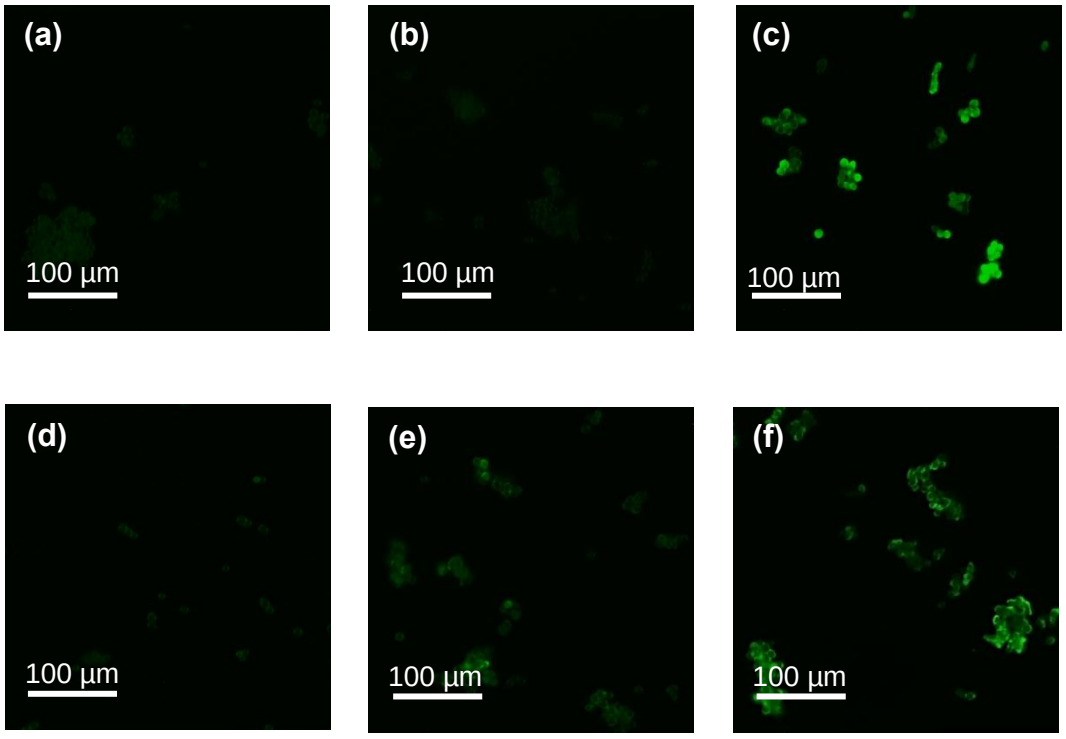

Figure 4-4: Conjugation of fluorescently-labelled model molecules to untreated (a,d,) and PFPA-treated microparticles before UV (b,e) and after UV irradiation (c,f). All samples were washed following functionalisation. Top row (a,b,c) shows the micrographs of rhodamine-amine treated samples, while bottom row (d,e,f) presents microparticles incubated with FITC-albumin. Similar results were obtained from all three independent experiments and the results of one representative experiment are shown.

The results presented in Figure 4-4 agree with the similar experiment carried out on the electrospun fibres (see Figure 3-11, page 97). For rhodamine-amine samples, untreated (Figure 4-4a) and PFPA-treated particles without UV exposure (Figure 4-4b) showed no fluorescence in the GFP channel, while the UV-irradiated PFPA-treated sample (Figure 4-4c) appeared bright green under the microscope.

Although no fluorescence was observed in untreated particles incubated with FITC-BSA (Figure 4-4d), some signal was detected in PFPA-treated microspheres. Samples without UV treatment (Figure 4-4e) were less fluorescent than after photoactivation (Figure 4-4f).

For both fluorescent dyes, UV-irradiated PFPA-treated particles showed the highest intensity. Similarly to the fibre functionalisation, the enhanced protein adsorption in PFPA-treated fibre before UV treatment could be attributed to the presence of fluorine atoms on the surface. Fluorination of polymers can increase their hydrophobicity, therefore favouring protein adsorption[243]. Although the extent of surface fluorination is quite small, it may be enough to promote protein adsorption, as observed above. This effect, however, is not observed with small molecules such as rhodamine-amine and therefore no fluorescence signal can be observed.

Protein surface attachment was additionally quantified by monitoring the percentage attachment of a model protein (BSA) to the particles (Figure 4-5) over 24 hours.

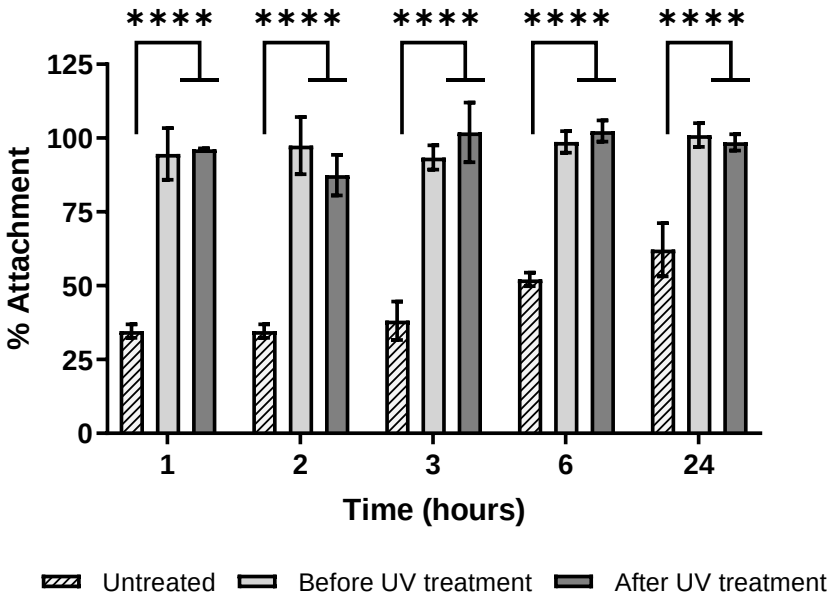

Figure 4-5: Percentage of bovine serum albumin attachment to electrosprayed PCL particles as a function of time. Data are shown as mean ± S.D. and are representative of three independent experiments performed on three separate days (n=3). *Repeated measures one-way ANOVA with post hoc Tukey's test; Statistical significance: **** ($p \leq 0.0001$).*

At all measured time points, PFPA-treated particles performed significantly ($p \leq 0.0001$) better than the blank PCL microspheres, with over 90% protein attachment after just one hour of reaction. As each sample was incubated with 10 µg of protein, this would correspond to ~9 µg of BSA being bound to the surface. For the untreated particles, protein adsorption to the surface appears to be following a trend where percentage attachment increases at longer incubation times (6 and 24 hours). There was no significant difference between PFPA-functionalised samples before and after UV treatment.

Even though the physicochemical characterisation showed considerably low PFPA-NHS deposition on the PCL particles (as shown in Figure 4-2 and Figure 4-3), the surface functionalisation undoubtedly promoted protein conjugation to these particles. Although the percentage attachment was comparable for PFPA-treated samples before- and after UV treatment, it is expected that UV-initiated C-H insertion reaction

will result in covalent binding of the protein to the surface. It is therefore likely that UV treatment will decrease the rate of protein elution from the surface (as discussed in Chapter 3, Figure 3-22). The results presented above encouraged further testing with a target therapeutic molecule.

4.3.4. *In vitro* T cell activation in Jurkat cells with microparticles prepared *via* standard electrospraying.

As the primary aim of this chapter was to develop artificial antigen-presenting cells, anti-CD3 conjugation was attempted on the surface of electrosprayed particles to try to recreate TCR signal 1-delivering aAPCs.

The initial optimisation experiment involved monitoring the antibody attachment over time (6 hours), to determine the optimal functionalisation reaction time. Each formulation was incubated in 1 mL of 10 µg/mL OKT3 antibody in PBS. Therefore, 100% conjugation would mean that 10 µg of OKT3 was attached to the surface. The results are presented in Figure 4-6.

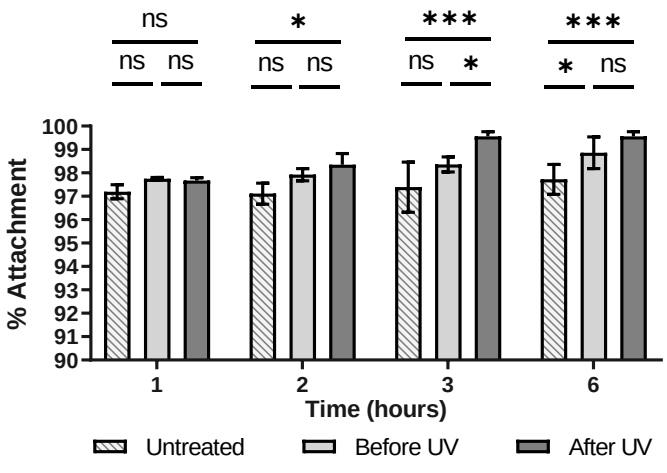

Figure 4-6: Percentage of OKT3 attachment to the electrosprayed particles as a function of time. Data are shown as mean ± S.D. and are representative of three independent experiments performed on separate days (n=3). *Repeated measures one-way ANOVA with post hoc Tukey's test; Statistical significance: ns (p-value > 0.05), * (p-value ≤ 0.05), *** (p-value ≤ 0.001).*

All formulations led to over 96% of the soluble protein being taken up onto the particle surface within the first hour. PFPA-NHS treated particles achieved slightly higher attachment percentages at all measured time points compared to the particles prepared by adsorbing the antibody to the surface. At longer incubation times (3 and 6 hours), the difference in percentage attachment between untreated and UV-irradiated PFPA-treated became significant ($p \leq 0.001$). In general, the difference in attachment was insignificant between PFPA-treated fibres before and after UV treatment, apart from the difference observed at 3-hour time point ($p \leq 0.05$).

The results presented here are consistent with the protein conjugation experiment conducted for PFPA-NHS functionalised electrospun fibres discussed in Chapter 3 (see Figure 3-16, page 103), where in the untreated PCL fibre control the attachment of a model antibody, infliximab, was much higher than that of BSA. Here, the attachment of OKT3 within the first hour of incubation was already at 96% for untreated PCL particles, while the BSA attachment presented in Figure 4-5 (page 142) reached 25%. A possible explanation for this effect could be the relatively high hydrophobicity of antibodies as compared to albumin, which would result in a favoured adsorption to hydrophobic surfaces as observed in Figure 4-6.

Since the protein loading was over 96% in the first hour post-incubation, this reaction time was chosen for further experiments. Although no statistical significance was observed between PFPA-NHS-treated samples and untreated controls, the catalase release profile evaluated for the electrospun fibres suggests that PFPA-treated materials may retain the protein at the surface for a longer period of time. A shorter period of incubation will decrease the exposure of the NHS moiety to an aqueous buffer, therefore reducing the risk of its hydrolysis and possibility of degradation[162]. Moreover, since the PFPA-NHS reaction is carried out at room temperature, longer incubation times could negatively impact the stability of the antibody being attached to the surface.

4.3.4.1. Optimisation of particle and antibody dose

Once the attachment of OKT3 was successfully confirmed in the protein loading study, the follow-up experiment aimed to identify the optimal amount of antibody and particles needed to elicit a response in Jurkat cells. In this study, a varying amount of antibody-functionalised particles was added to each well: 125 µg (Figure 4-7a and b), 250 µg (Figure 4-7 c and d), 500 µg (Figure 4-7e and f), 750 µg (Figure 4-7g and h). Additionally, the effect of antibody amount added to each particulate formulation was tested: 0, 0.5, 1, 5 and 10 µg. This way, both the effect of particle dosage and antibody dosage could be isolated. The viability and IL-2 concentration were tested as presented in Figure 4-7.

For UV-treated samples, this experiment further clarified the cytotoxicity at higher antibody (Figure 4-7a) and particle (Figure 4-7c, e, g) dosages. Moreover, the UV-treated systems had only minimal biological efficacy (in terms of IL-2 production) at lower dosages (125 and 250 µg/well; Figure 4-7b and d, respectively) as compared to the two other treatments. Due to the 100% cell death in the 500 and 750 µg/well testing groups, the UV-treated formulation was excluded from the IL-2 release quantification presented in Figure 4-7f and h. This formulation was therefore excluded from further immunological testing as it was deemed unsuitable for *in vivo* application. The reasons for the observed cytotoxicity remain unknown.

The highest release of IL-2 was achieved in the 250 µg/well dosing group (Figure 4-7d). In particular, cells treated with 0.5 µg of antibody retained viability at ~ 75% (Figure 4-7c) and performed significantly better ($p \leq 0.0001$) than the plate-bound antibody control. Therefore, the dose of 0.5 µg of antibody on 250 µg particles per well was selected for further testing in T cells isolated from peripheral blood mononuclear cells.

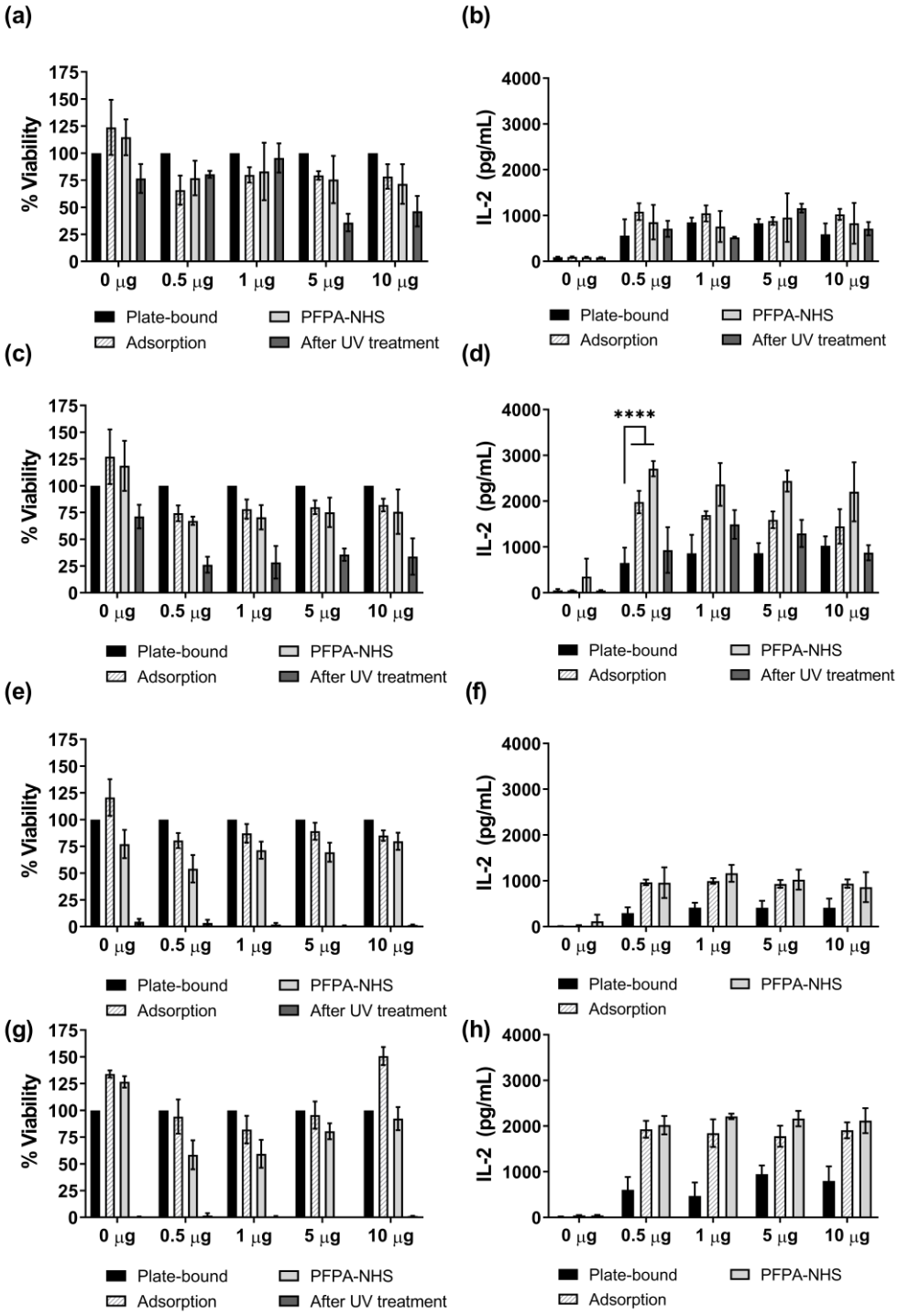

Figure 4-7: Summary of cell viability (panels a,c,e,g) and IL-2 concentration (panels b,d,f,h) in Jurkat cells following treatment with particle. Panels a and b, c and d, e and f, g and h correspond to treatment with the following doses of particles: 125 µg/well, 250 µg/well, 500 µg/well and 750 µg/well, respectively. Data are shown as mean ± S.D. and are representative of two independent experiments performed on separate days, with three replicate wells per condition. *Repeated measures two-way ANOVA with post hoc Tukey's test; Statistical significance: **** (p-value ≤ 0.0001).*

4.3.5. Particle separation

The efficiency of the surface PFPA-NHS functionalisation approach requires an even surface coating on the individual particles. A major drawback of microparticles prepared *via* electrospraying is their tendency to aggregate (see Figure 4-1). Several approaches have been described to minimise particle aggregation, for example by changing the collection vessel from aluminium foil to a water bath[284]. However, particles prepared from hydrophobic polymers, such as PCL, collected on a surface of an aqueous solution often form a film that cannot be easily broken down to individual particles[284,285]. Although collection into ethanolic solution has been previously reported[286], this approach may not be suitable for this application, as a prolonged treatment with alcohols may alter the surface chemistry of the polymer particle[287].

Three electrospraying fabrication set-ups were explored in an attempt to achieve complete separation of the generated microspheres. These included: standard top-down electrospraying, electrospraying into liquid nitrogen and electrospraying assisted by pressurized gas (EAPG). Figure 4-8 presents the morphology and size distribution of the microparticles obtained as a result.

The microparticles produced with a standard top-down electrospraying setup (PCL-TD) are depicted in Figure 4-8a, and experimental details are discussed above (see Section 1.4, p. 23 and Section 4.3, p.134). The resulting microparticles exhibited a unimodal size distribution (Figure 4-8b) with a mean size of 7.21± 0.91 μm.

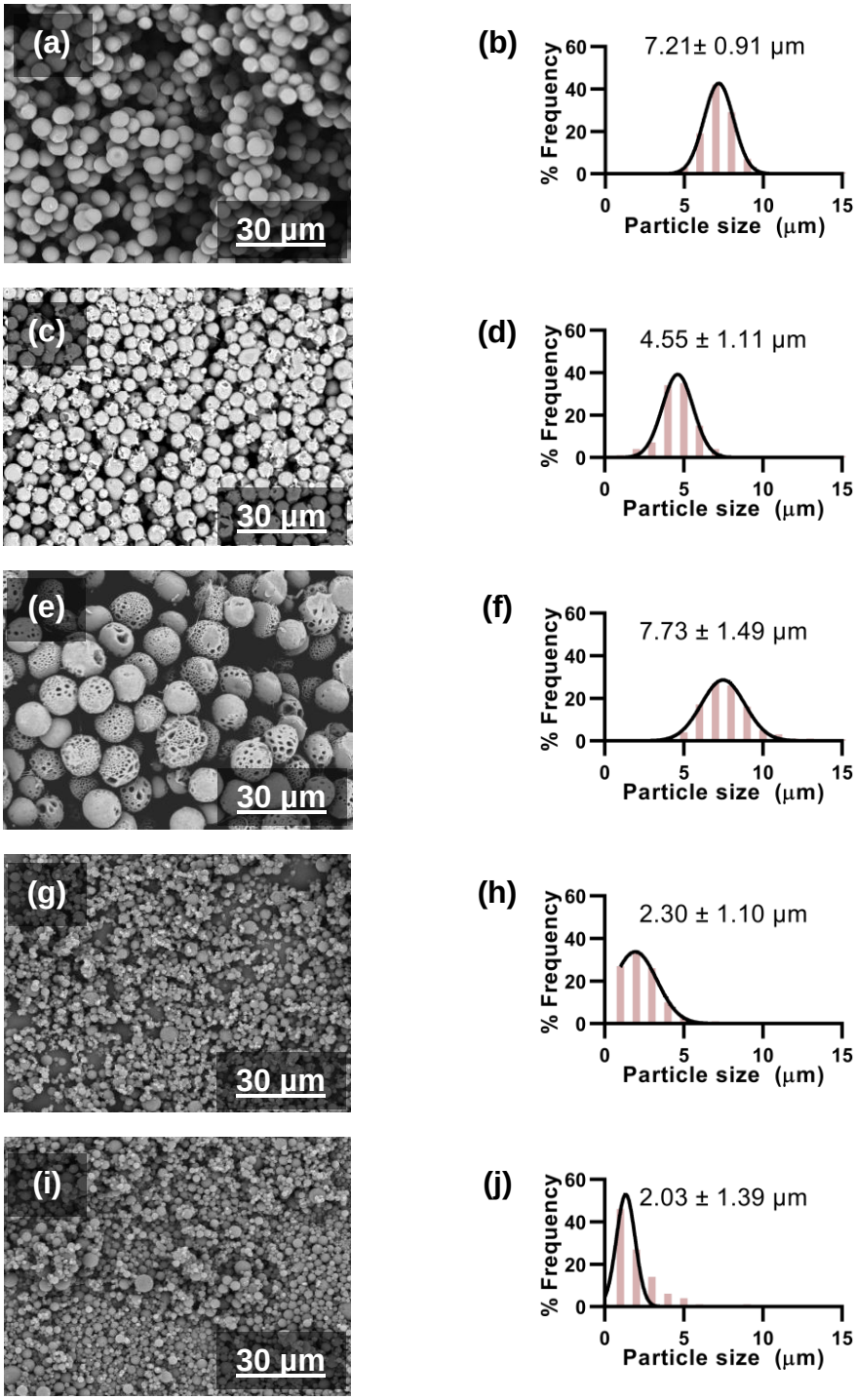

Figure 4-8: Scanning electron microscopy and particle size distribution curves (N=100, mean ± SD) of electrosprayed PCL particles. Following fabrication methods were tested: top-down electrospraying (PCL-TD; panels a, b), electrospraying into liquid nitrogen followed by drying in an oven at 45 °C (PCL-LN-OV; c, d) or freeze-drying at - 40 °C (PCL-LN-FD; e, f), electrospraying assisted by pressurized gas (PCL-PG-1 (g and h) and PCL-PG-2 (i and j)). Similar results were obtained for three independent experiments.

The second method involved electrospraying into liquid nitrogen[288]. In this approach, a polymer solution is ejected *via* a charged needle into a dewar containing liquid nitrogen placed on a grounded aluminium plate to maintain the electric field. Once the polymer droplets come into contact with liquid nitrogen, any residual solvent becomes trapped inside the particles, which subsequently sediment at the bottom of the container. The residual solvent is then removed from the frozen particles *via* drying in an oven (PCL-LN-OV; Figure 4-8c and Figure 4-8d) or freeze-drying (PCL-LN-FD; Figure 4-8e and Figure 4-8f).

As shown in Figure 4-8c, the particles obtained using liquid nitrogen-assisted electrospraying showed better separation than in conventional electrospraying (Figure 4-8a), with only minimal defects in the spherical shape. Particle size distribution remained unimodal with a decrease in mean particle size, where a drop from 7.21 ± 0.91 µm (Figure 4-8b) to 4.55 ± 1.11 µm (Figure 4-8d) was observed.

On the contrary, Figure 4-8e reveals a change in the morphology of particles subjected to freeze-drying following electrospinning into liquid nitrogen. While the particle size (Figure 4-8f) was comparable to the reference PCL-TD (Figure 4-8b), the morphology was significantly altered. During the freeze-drying process, the removal of any residual frozen solvent *via* sublimation leads to a characteristic porous structure[289], which is not observed when the solvent is removed in mild conditions such as oven-drying. This morphology could be beneficial for the PFPA-NHS functionalisation efficiency due to increased surface area. Conversely, it could lead to increased particle brittleness and higher chance of breakdown upon post-treatments such as immersion in the functionalisation solvent (PFPA-NHS in methanol) or subsequent washing steps *via* centrifugation.

A major drawback of the electrospraying into liquid nitrogen presented in PCL-LN-OV and PCL-LN-FD was a low product yield, estimated to be around 5%.

For comparison, PCL-TD yields around 90%. This could potentially be improved with further apparatus optimisation, as the low yield is hypothesised to be due to the distortion of electric field by the collection vessel. The dewar is made of stainless steel and so is well grounded under the electric field. On the other hand, liquid nitrogen would not hold charge as well as stainless steel does. It is likely that electrosprayed droplets are attracted to the dewar, therefore depositing not into the liquid nitrogen, but on the outer sides of the container. Potentially, using an alternative collection vessel and focusing the electric field by enclosing the dispensing needle in a copper ring[290] could increase the product yield. However, as the electrospraying process optimisation was not the primary aim of this study, no further attempts were made to increase the efficiency of this method.

Electrospraying assisted by pressurized gas (EAPG) is a novel technology developed by Bioinicia S.L. where a compressed air-assisted pneumatic injector nebulizes the polymer solution within a high electric field. The solvent is then evaporated in an evaporation chamber under ambient conditions, allowing the collection of microparticles as a free-flowing powder[291]. This high-throughput approach facilitates industrial-scale manufacture of electrosprayed particles and has been tested in the production of omega-3[281] and docosahexaenoic acid-enriched fish oil[291] microcapsules.

EAPG technology resulted in the production of separated particles (PCL-PG-1 and PCL-PG-2; Figure 4-8g and i, respectively). However, the particles were much smaller in diameter than the batch manufactured in house on standard electrospinning apparatus. The average particle size of around 2 µm (Figure 4-8h and j, respectively) is approximately 3-4 times lower than of microspheres fabricated *via* a standard top-down electrospraying technique. As the *in vitro* T cell activation experiments were optimised with much larger microparticles prone to aggregation, the cellular responses

observed for PCL-PG-1 and PCL-PG-2 may be significantly different than those in PCL-TD.

Formulations PCL-TD, PCL-PG-1 and PCL-PG-2 were selected for further testing due to their ease of fabrication and high production yields[291]. The particles are morphologically uniform, lying in the preferable size range of 1-10 μm[76,266,279]. The effect of particle size and aggregation differences will be investigated in biological models.

4.3.6. Anti-CD3 attachment on electrosprayed microparticles

OKT3 antibody attachment over time was previously established using microparticles prepared by standard electrospraying (PCL-TD), and the results are shown in Figure 4-6. To visualise anti-CD3 surface functionalisation of PCL-PG-1 and PCL-PG-2, the particles were incubated in a solution of FITC-OKT3 for one hour, based on the antibody attachment experiment presented in Figure 4-6, where over 96% OKT3 attachment was achieved within the first hour of incubation with the microparticles.

Figure 4-9 shows the fluorescence micrographs of PCL-PG-1 (a, b), PCL-PG-2 (c, d) and PCL-TD (e, f) following incubation with OKT3-FITC. Both antibody attachment approaches achieved a similar level of fluorescence, suggesting efficient antibody distribution on the surface of particles both with the PFPA-NHS and adsorption approaches. This method of antibody conjugation detection, however, was not sensitive enough to differentiate between the two attachment approaches.

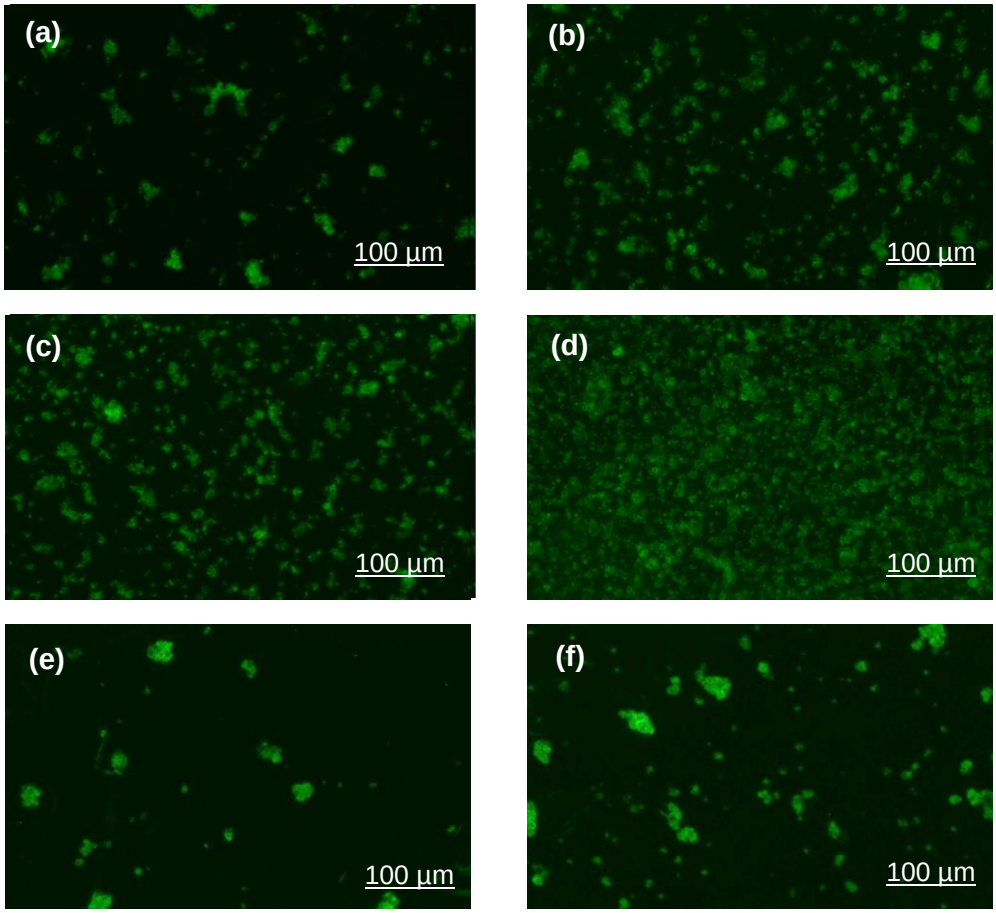

Figure 4-9: Fluorescence microscopy images obtained after reacting microparticles with OKT3-FITC. The following formulations were tested: PCL-PG-1 with (a) and without PFPA-NHS treatment (b), PCL-PG-2 with (c) and without PFPA-NHS treatment (d), with (e) and without PFPA-NHS treatment (f). Similar results were obtained from all three independent experiments and the results of one representative experiment are shown.

4.3.7. *In vitro* PBMC-derived T cell activation assay

Previous experiments in Jurkat cells have shown significant activation of T cells by antibody-decorated particles, as measured by IL-2 release. However, a study by Bartelt et al.[292] explored the differences between continuous cell lines and peripheral blood-derived T cells. In this comparison, Jurkat E6.1 cells showed exaggerated IL-2 responses upon CD3/CD28 stimulation, but did not produce other activation markers such as TNF-α or IFN-γ. For the purpose of this thesis, the Jurkat T cell line was used for initial optimisation experiments on PCL-TD microparticles due to the lower costs

of cell culture maintenance and the lack of donor to donor variation. Following preliminary studies, the lead formulations were then tested in PBMC-derived T cells.

4.3.7.1. CD3+ T cell viability following particle treatment

The viability of CD3+ T cells derived from human PBMCs following incubation with particle formulations was established before setting up further immunological tests. Percentage viability was calculated using T cells stimulated with a plate-bound antibody as the baseline (100%).

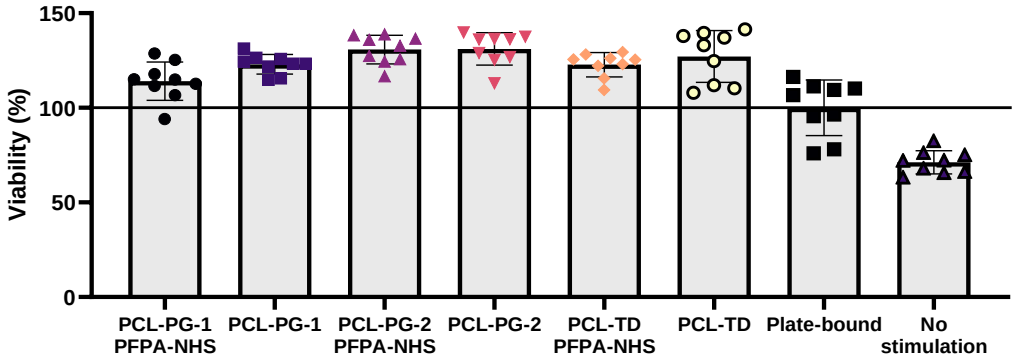

Figure 4-10: Viability of CD3+ T cells stimulated with antibody-coated microparticles. Formulations tested were: PCL-PG-1, PCL-PG-2 and PCL-TD with (PFPA-NHS) and without PFPA-NHS functionalisation. 'Plate-bound' denotes cells stimulated with a plate-bound antibody. 'No stimulation' denotes cells only. Data are shown as mean ± S.D. and are representative of independent experiments performed on PBMCs isolated from three donors (one experiment per donor, three replicates per experiment).

As seen in Figure 4-10, cell viability was above 100% in cells incubated with particulate formulations, with means ranging from 100 to 150%. Percentage viability above 100% could be an indicator of increased T cell proliferation in these samples. The PrestoBlue® cell viability assay is based on the reduction of resazurin to resorufin in the redox environment of metabolically active cells[293]. With increasing numbers of proliferated and viable cells, more resorufin is formed, leading to higher fluorescence output.

4.3.7.2. Production of T cell activation markers in CD3+ T cells

Once the viability of the tested T cells was confirmed, further immunological testing was performed by measuring the levels of cytokines released into the cell culture. The characteristic feature of CD4+ T cells is the generation of large amount of IFN-γ and TNF-α[294]. Similarly, CD8+ T cells release IL-2, IFN-γ and TNF-α upon activation[294]. Measuring the levels of these three T cell activation markers will allow an accurate estimation of the primary T cell stimulation in the *in vitro* model. The results for IFN-γ (Figure 4-11), TNF-α (Figure 4-12) and IL-2 (Figure 4-13) production are presented as the mean supernatant cytokine concentration pooled from cells derived from three donors.

The release of the pro-inflammatory cytokine IFN-γ is readily observed in Th1 CD4+ T cells and CD8+ T cells (Figure 1-2, page 3), and is responsible for activation of effector cells such as macrophages and neutrophils as well as regulation of CD4+ Th cell differentiation. Thanks to their role in the cell activation pathways, IFN-γ is commonly used as a late-stage T cell activation marker[15,267,295–297]. The production of IFN-γ in particle-stimulated CD3+ T cells is given in Figure 4-11.

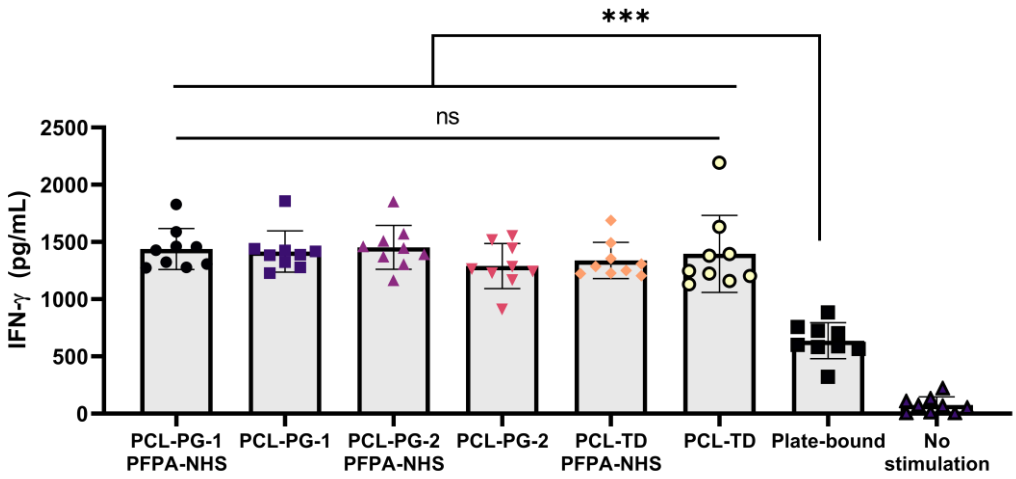

Figure 4-11: Production of IFN-γ in CD3+ T cells stimulated with antibody-coated microparticles. Formulations tested were: PCL-PG-1, PCL-PG-2 and PCL-TD with (PFPA-NHS) and without PFPA-NHS functionalisation. 'Plate-bound' denotes cells stimulated with a plate-bound antibody. 'No stimulation' denotes cells only. Data are shown as mean ± S.D. and are representative of independent experiments performed on PBMCs isolated from three donors (one experiment per donor, three replicates per experiment). *Repeated measures one-way ANOVA with post hoc Tukey's test; Statistical significance: ns (p-value >0.05), *** (p-value ≤0.001).*

The production of IFN-γ was significantly enhanced ($p \leq 0.001$) in the cells incubated with surface-functionalised microparticles as compared to the antibody delivered on tissue culture plastic. No significant variation between formulations was observed. The mean IFN-γ concentration in all particle-treated wells (~1400 pg/mL) was double that of plate-bound antibody controls (~ 650 pg/mL). In cells with no anti-CD3 treatment IFN-γ production was minimal (~75 pg/mL). The results presented above could suggest an efficient activation of both CD4+ and CD8+ T cell populations in particle-treated samples, although does not show any differentiation between the formulations tested.

The next cytokine tested was TNF-α, a pro-inflammatory cytokine released by a variety of immune cells. It is responsible for the activation and proliferation of T cells, natural killer (NK) cells, B cells, macrophages and dendritic cells. However, although its presence is necessary for effective immunosurveillance, high

levels of TNF-α may induce pathogenic effects[298]. When dysregulated, TNF-α has been associated with a wide variety of cancers[299]. Although it is not a specific T cell activation marker, it provides information on the induction of pro-inflammatory responses following therapeutic treatment. Figure 4-12 presents a summary of TNF-α production in T cells following incubation with microparticles.

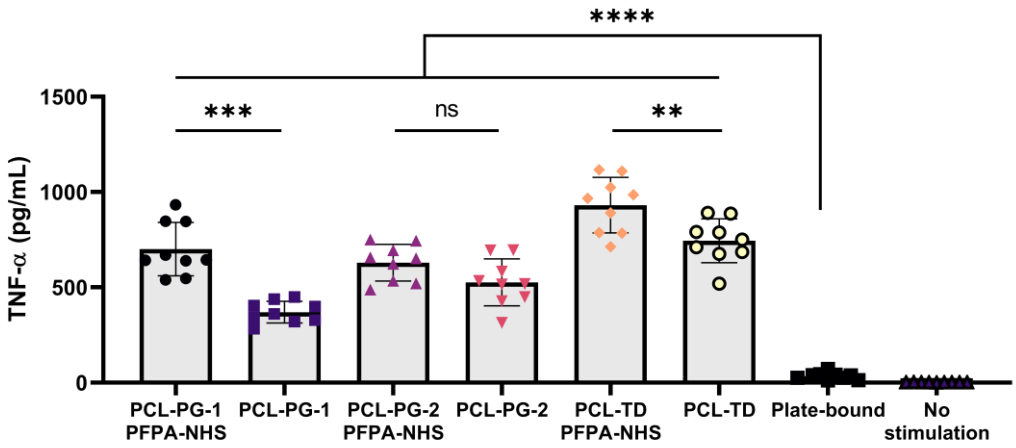

Figure 4-12: Production of TNF-α in CD3+ T cells stimulated with antibody-coated microparticles. Formulations tested were: PCL-PG-1, PCL-PG-2 and PCL-TD with (PFPA-NHS) and without PFPA-NHS functionalisation. 'Plate-bound' denotes cells stimulated with a plate-bound antibody. 'No stimulation' denotes cells only. Data are shown as mean ± S.D. and are representative of independent experiments performed on PBMCs isolated from three donors (one experiment per donor, three replicates per experiment). *Repeated measures one-way ANOVA with post hoc Tukey's test; Statistical significance: ns (p-value >0.05), ** (p-value ≤0.01), *** (p-value ≤0.001), **** (p-value ≤0.0001).*

The quantification of TNF-α release revealed some differences between the formulations. In agreement with the IFN-γ data (Figure 4-11), all treatments resulted in significantly higher cytokine production than the positive control ($p \leq 0.0001$) and no TNF-α release was measured in unstimulated cells (negative control). Interestingly, some differences were observed between PFPA-NHS-functionalised and untreated particles. For PFPA-NHS treated formulations prepared from EAPG particles (PCL-PG-1+PFPA-NHS), TNF-α release was significantly higher ($p \leq 0.001$) than in particles functionalised *via* physical adsorption (PCL-PG-1). Although no significance was observed with PCL-PG-2+PFPA-NHS and PCL-PG-1, the mean TNF-α concentration was still higher in PFPA-treated samples (629 ± 92 pg/mL) than

in untreated particles (PCL-PG-2; 526 ± 123 pg/mL). The same trend was observed in larger particles with (PCL-TD+PFPA-NHS) and without functionalisation (PCL-TD) ($p \leq 0.01$).

Although increased TNF-α production could be an indicator of successful T cell activation, the results should be interpreted with caution as it is not a cytokine specific to T cell populations, and overstimulating with TNF-α may result in pathological responses *in vivo*, as discussed above. IL-2 is much more established in immunological protocols as an indicator of early T cell activation, specifically in CD8+ cytotoxic T cell populations, which are of paramount importance in cancer immunotherapy treatments[300]. Figure 4-13 summarises the release of IL-2 observed in CD3+ T cell treated with particles.

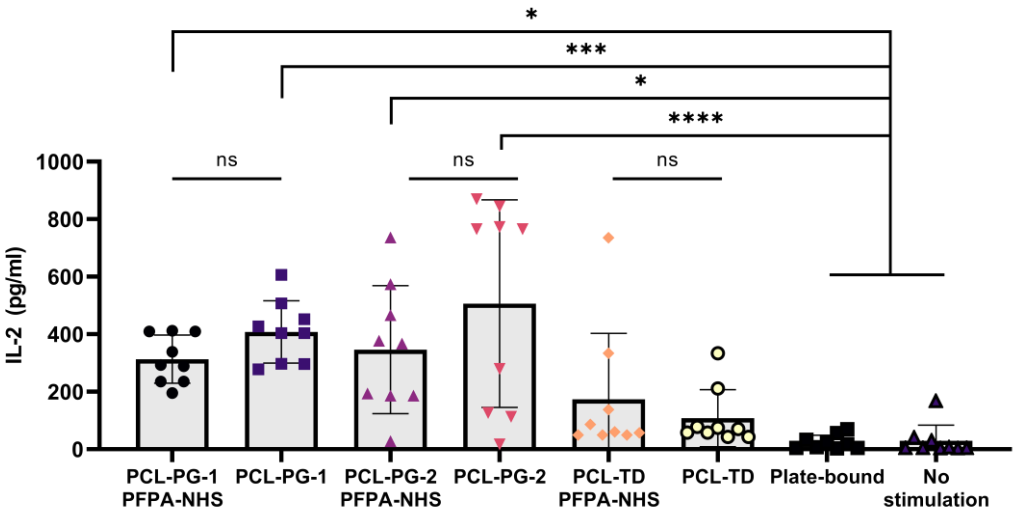

Figure 4-13: Production of IL-2 in CD3+ T cells stimulated with antibody-coated microparticles. Formulations tested were: PCL-PG-1, PCL-PG-2 and PCL-TD with (PFPA-NHS) and without PFPA-NHS functionalisation. 'Plate-bound' denotes cells stimulated with a plate-bound antibody. 'No stimulation' denotes cells only. Data are shown as mean ± S.D. and are representative of independent experiments performed on PBMCs isolated from three donors (one experiment per donor, three replicates per experiment). *Repeated measures one-way ANOVA with post hoc Tukey's test; Statistical significance: ns (p-value >0.05), ** (p-value ≤0.01), *** (p-value ≤0.001), **** (p-value ≤0.0001).*

Overall, large donor-to-donor variability was observed, with some donors showing extremely low IL-2 production. The extent of IL-2 release was significantly lower than

in the Jurkat cells (Figure 4-7). This is consistent with previously published studies[292] where IL-2 secretion was reduced in primary cells than in Jurkat cells. Nevertheless, plate-bound antibody and unstimulated cells led to negligible levels of IL-2 release compared to any of the particle treatments. All tested formulations showed significantly higher IL-2 production. Interestingly, the formulations without PFPA-NHS functionalisation (PCL-PG-1 and PCL-PG-2) performed significantly better than those treated with PFPA-NHS (PCL-PG-1+PFPA-NHS and PCL-PG-2+PFPA-NHS) when compared with the plate-bound antibody control. No significance was observed between pairs of formulations prepared from the same microparticles with and without functionalisation (e.g. PCL-PG-1 and PCL-PG-1+PFPA-NHS). An effect of particle separation was clearly visible, with smaller and separated particles (PCL-PG-1 and PCL-PG-2 with and without PFPA-NHS) showing higher IL-2 production than larger and aggregated ones (PCL-TD and PCL-TD+PFPA-NHS).

4.3.7.3. Proliferation assessment

A further understanding of the T cell behaviour following stimulation with the surface-functionalised microparticles was gained from flow cytometry-based assessment of cell proliferation. The carboxyfluorescein succinimidyl ester (CFSE) proliferation assay is a tool commonly used in immunological studies[301,302]. Staining of T cells with this vital dye allows for live monitoring of proliferating cells by dye dilution. Live cells are covalently labelled with a bright and stable dye visible in the green fluorescence protein (GFP) channel. With every generation produced, the dye concentration should in theory halve. Hence, when subjected to flow cytometry analysis, every generation of cells should appear as a different peak on a CFSE channel histogram. An example of the visualisation of CFSE-stained T cells with fluorescence microscopy is presented in Figure 4-14. An overlay micrograph of brightfield and GFP microscopy is shown, with bright green spherical T cells and dark green particle outlines present.

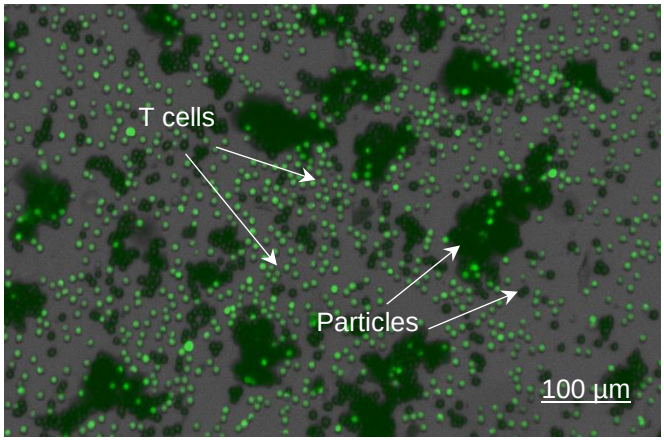

Figure 4-14: An exemplar micrograph of CFSE-labelled T cells incubated with unlabelled microparticles. Bright green spherical dots correspond to CFSE-labelled T cells, while dark green clusters show PCL-TD microparticles, as indicated by arrows.

As the microparticles used as aAPCs are supposed to resemble the size and shape of T cells, it is particularly difficult to differentiate between them in cellular assays. Due to the nature of the experiment, with a high density of both cells and microspheres present in each well, the flow cytometry study was particularly challenging to optimise and analyse. An example of a gating strategy is shown in Figure 4-15.

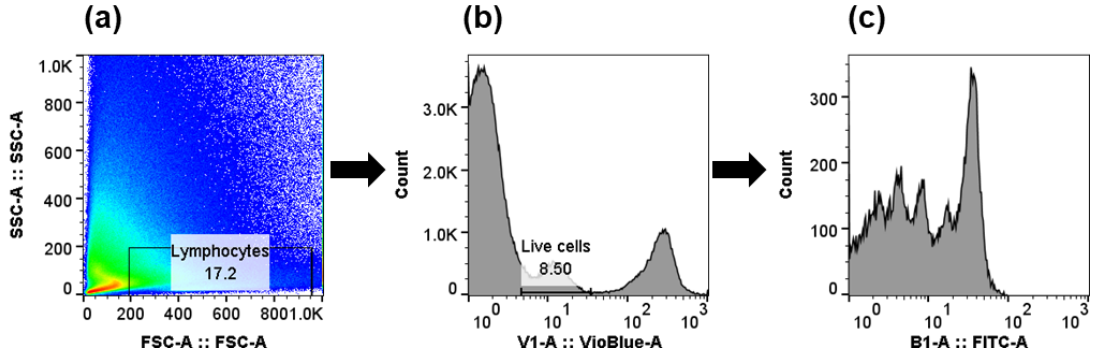

Figure 4-15: Example of gating strategy in flow cytometry analysis. In this exemplar gating, cells were first gated for lymphocytes (SSC-A vs. FSC-A) (panel a). The lymphocyte gate is further analysed for their uptake of the Live/Dead Violet stain to determine live versus dead cells and exclude unstained microparticles (panel b). The gated population can be then analysed for proliferation using the CFSE stain (panel c).

FSC vs SSC gating is commonly used to identify cells of interest based on size and granularity. In this study, the particles present in the samples introduced a significant level of noise in forward versus side scatter (FSC vs SSC) plots. Lymphocytes, with

an average size of 10 µm, would normally appear in the bottom right region of the plot[303]. To remove some of the noise created by the microparticles, the first step was to gate the region of interest (lymphocytes) as presented in Figure 4-15a.

A live/dead stain was then used to differentiate between viable and dead cells as well as non-cellular material, such as particles. The reactive dye used here can permeate the compromised membranes of necrotic cells and react with free amines both in the interior and on the cell surface, resulting in intense fluorescent staining. As the membranes of viable cells are not permeable, only the cell surface can react with the dye, resulting in a relatively dim staining. A live/dead channel histogram (Figure 4-15b) can therefore be used to gate the live cell population, removing both intensively stained dead cells and unstained particles. Once the cells of interest were successfully gated, the CFSE histograms (Figure 4-15c) could be used to analyse the proliferation behaviour following microparticle treatments (Figure 4-16).

The CFSE histograms presented above confirm the successful formation of T cell generations in particle-treated samples. The dashed line denotes the parent generation of unstimulated T cells. Subsequent generations can be observed as distinct peaks with decreasing dye intensity (i.e. to the left of the parent peak on the x-axis).

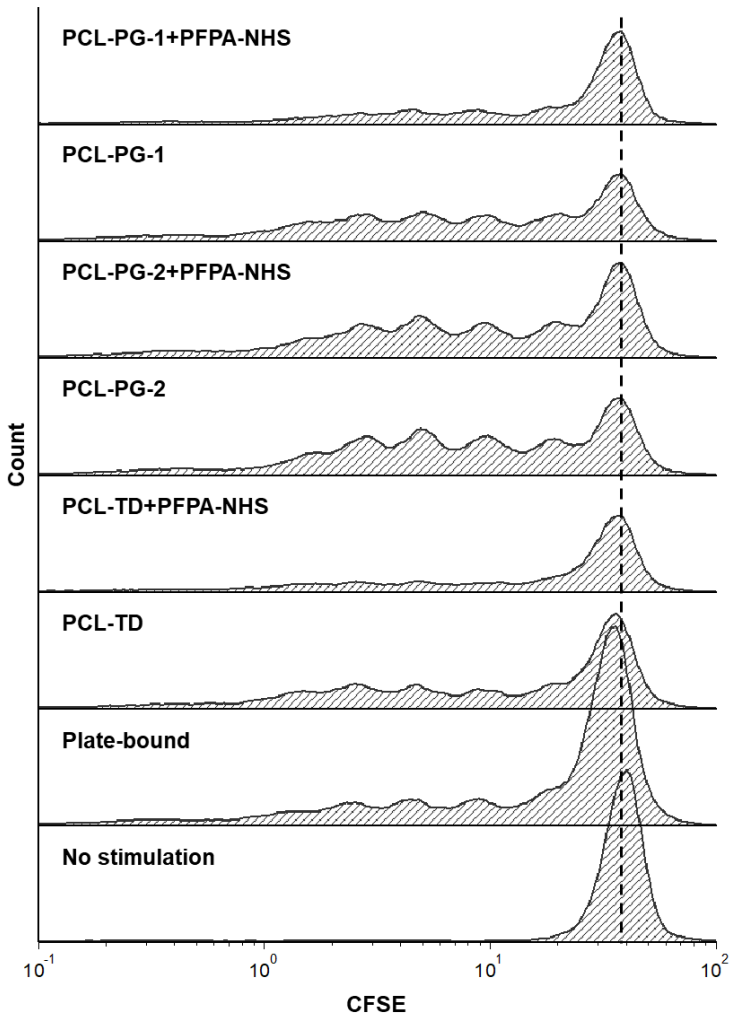

Figure 4-16: Proliferation of CD3+ T cells stimulated with functionalised particles, observed by monitoring CFSE dye dilution after 4 days of culture. The data shown are gated on the viable CD3+ T cells (see Figure 4.15). The unstimulated parent generation is denoted with a dashed line. Data are shown as mean ± S.D. and are representative of independent experiments performed on PBMCs isolated from three donors (one experiment per donor, three replicates per experiment).

In unstimulated cells, only the parent peak is observed, showing the requirement for antibody stimulation in the proliferation of T cells. Although the histograms allow for the estimation of the number of T cell generations formed (by counting the peaks), it is more accurate to calculate the proliferation index (i.e. mean number of divisions of responding cells[304]) using the built-in flow cytometry software tools. This is provided in Figure 4-17.

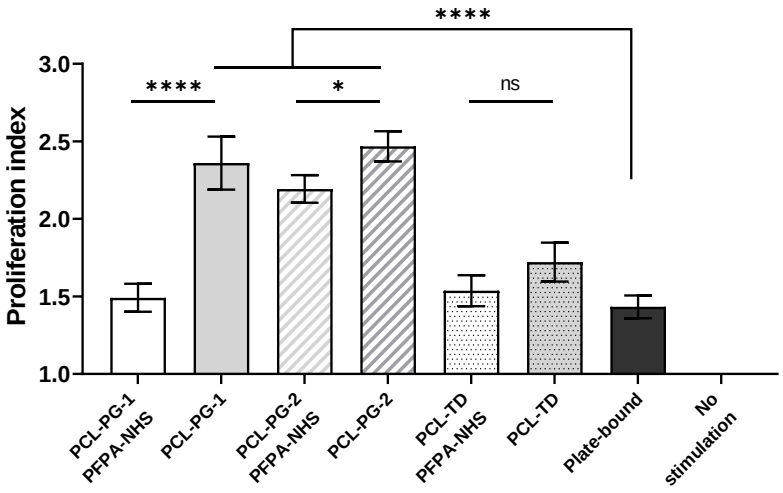

Figure 4-17: Proliferation index calculated by modelling of cell proliferation in CD3+ T cells. Data are shown as mean ± S.D. and are representative of independent experiments performed on PBMCs isolated from three donors (one experiment per donor, three replicates per experiment). *Repeated measures one-way ANOVA with post hoc Tukey's test; statistical significance: ns (p-value >0.05), * (p-value <0.05), **** (p-value ≤0.001).*

The results of proliferation index calculations clearly show the enhanced proliferative effect achieved with all microparticle formulations. No proliferation was observed in unstimulated cells. Compared to the plate-bound antibody control, formulations PCL-PG-1, PCL-PG-2+PFPA-NHS and PCL-PG-2 showed significantly higher ($p \leq 0.001$) proliferation. Moreover, for all three microparticle types tested, formulations without PFPA-NHS performed better than those functionalised with the compound. Altogether, the results of the proliferation testing encourage the use of antibody-functionalised microparticles for the stimulation of CD3+ T cells.

4.3.7.4. Summary of T cell activation characterisation

The activation of PBMC-derived CD3+ T cells was characterised by measuring the production of three cytokines (IFN-γ, TNF-α and IL-2) and the investigation of cellular proliferation using CFSE dye. Taken together, the results show benefits of delivering antibodies on the surface of electrosprayed microparticles in immune system stimulation. For all tested markers, the particle-treated cells showed enhanced stimulation of CD3 positive T cells.

It should be noted, however, that the PFPA-NHS functionalisation may not be necessary to achieve efficient T cell stimulation. Although IFN-γ and TNF-α results did not clearly differentiate between formulations, the IL-2 and proliferation index data suggest that the deposition of the antibody on the microparticle by physical adsorption may be sufficient to trigger cellular responses.

Another important parameter tested in T cell activation studies was the effect of particle size on the efficiency of the designed aAPCs. Here, IL-2 production and proliferation index clearly demonstrate the superiority of smaller and more separated microparticles prepared *via* electrospraying assisted with pressurised gas (PCL-PG-1 and PCL-PG-2) compared to larger and more aggregated microspheres prepared using standard top-down electrospraying (PCL-TD-1). This agrees with previous literature, where biomaterials of 1-10 μm are generally preferred for T cell activation (see Section 4.1.2, page 123). Although the individual particle size of PCL-TD-1 is ~ 7 μm, this formulation should be considered as a cluster of multiple particles. On the other hand, PCL-PG-1 and PCL-PG-2 particles are separated and therefore can be more efficiently coated with the target OKT3 antibody, allowing for an easier access for individual particles to interact with T cells.

4.4 Conclusions and future work

The experiments presented in this chapter focused on the development of anti-CD3-functionalised polymeric microparticles mimicking biological T cells in size and shape. PCL particles in the desired size range (1-10 μm) were first prepared using standard top-down electrospraying. The surface conjugation of model proteins was then attempted, with albumin attaching more readily to PFPA-NHS-functionalised particles than untreated ones. This effect was not observed in the anti-CD3 attachment studies, where both untreated and PFPA-NHS particles performed similarly. The anti-CD3-decorated particles were then used in Jurkat T cell line activation studies, and the

optimal antibody and particle dosage were established experimentally by monitoring cell viability and IL-2 production.

Next, the problem of particle aggregation in electrospraying was addressed, and several solutions to the problem offered. These included collecting particles into liquid nitrogen and electrospraying assisted with pressurised gas. The latter was selected due to higher yields, and further immunological testing was conducted to investigate the effect of particle size and surface functionalisation on T cell activation.

In human PBMC-derived CD3+ T cell studies, the screening of three activation markers and proliferation showed superior results when the antibody was delivered on the surface of spherical electrosprayed particles, as opposed to the tissue culture plastic flat substrate. No cytotoxicity to CD3+ T cells was observed. Smaller and more separated particles generally performed better than larger and aggregated ones (as shown in enhanced T cell cytokine production and proliferation), and there is some evidence suggesting that attaching anti-CD3 by physical adsorption, without the PFPA-NHS linker, may be sufficient to provoke cellular responses.

Anti-CD3 stimulation is a simple way to deliver signal 1 of T cell activation, butit does not provide the antigen specificity that a biological APC offers. More targeted T cell stimulation could be provided by using MHC class I (for CD8+ T cells) or MHC class II (for CD4+ T cells) molecules, such as anti-CD28. The versatility of the surface protein delivery platform developed in this chapter should allow future studies involving conjugation of other stimulatory cues, moving beyond anti-CD3 delivery.

Although PFPA-NHS appeared not to be necessary for the attachment of anti-CD3 to the particle surface, this could be due to the relatively higher hydrophobicity of antibodies as compared to other biomolecules. It is therefore possible that the PFPA-NHS chemistry may still be beneficial for the surface presentation of other, less hydrophobic proteins that may not adsorb readily to hydrophobic polymeric surfaces.

Chapter 5 – Surface functionalisation of PCL particles using strain-promoted azide-alkyne cycloaddition.

5.1. Introduction

The attachment of proteins to surfaces using NHS esters is often criticised for its lack of site-specific selectivity or control over the number of proteins conjugated[173]. Moreover, the NHS-bearing compounds are susceptible to hydrolysis in aqueous conditions, leading to reduced immobilisation yield[220].

Bioorthogonal reactions with paired functional groups could be a way of solving this site-selectivity challenge. For example, strain-promoted azide-alkyne cycloaddition (SPAAC) between an azide-bearing substrate and strained alkyne-modified protein could prevent non-selective conjugation that commonly occurs in carbodiimide-based reactions. SPAAC belongs to the family of cycloaddition reactions (known as click reactions), the concept of which has been described in the introductory chapter of this thesis (see Section 1.5.2.4, page 44).

5.1.1. Modification of proteins to enable SPAAC reactions

A way of enabling SPAAC conjugation is to modify a protein of interest with a strained alkyne functional group. To achieve this, a dibenzocyclooctyne (DBCO) moiety can be used. DBCO compounds can undergo reaction with azide functionalised compounds without the need for a Cu(I) catalyst, resulting in a stable triazole linkage (as previously presented in Scheme 1-5, page 45). Numerous DBCO protein

modification agents are now commercially available, with some examples presented in Figure 5-1.

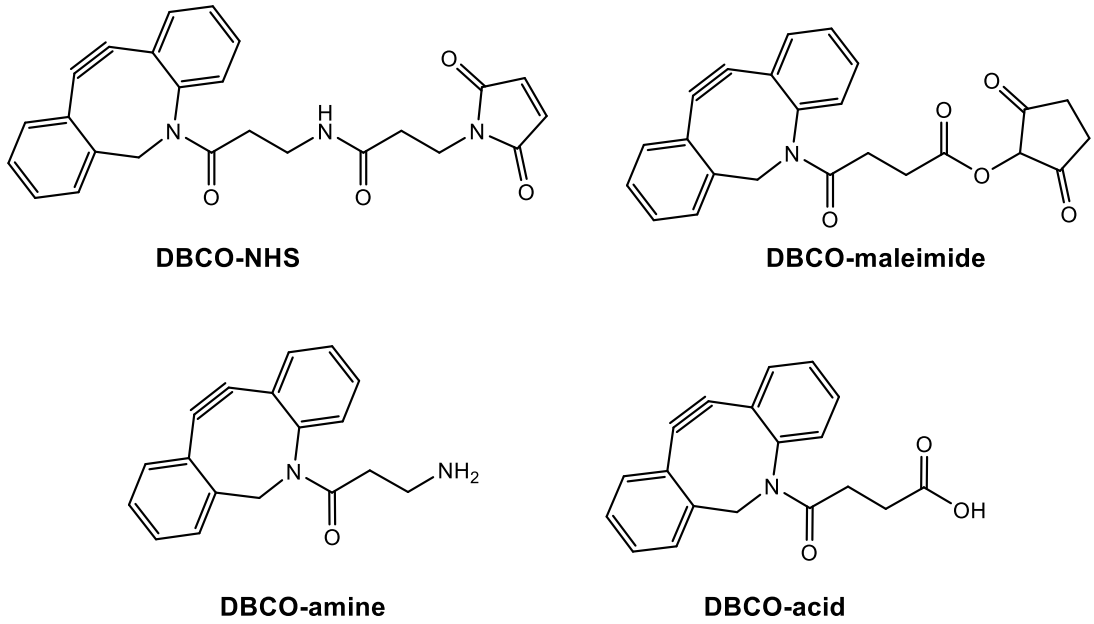

Figure 5-1: Chemical structures of commercially available DBCO-based crosslinking agents.

The DBCO reagents can be selected based on the desired site of conjugation. Further modification to the linker can be made by adding a PEG spacer arm to increase its solubility in water. An example of a site-specific DBCO reagent is bis-sulfone-PEG-DBCO (Figure 5-2), which comprises three structural entities: a substituted propenyl group (the conjugation moiety), a PEG linker and a DBCO moiety.

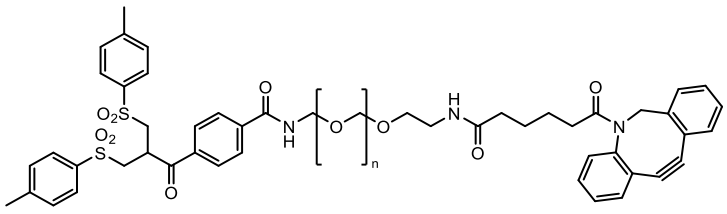

Figure 5-2: Chemical structure of bis-sulfone-PEG-DBCO.

Bis-sulfone-PEG-DBCO undergoes site-specific protein modification by disulfide rebridging conjugation. This approach benefits from the fact that most proteins (such as IgGs) have thiol groups as paired cysteines in disulfide bridges (Figure 5-3).

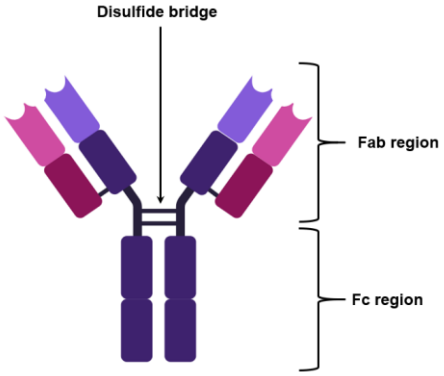

Figure 5-3: Schematic drawing showing the basic structure of IgG antibodies.

Partial reduction of the accessible IgG disulfides to cleave the sulfur-sulfur bond can be accomplished using dithiothreitol (DTT) (Scheme 5-1). Reduction is initiated when DTT forms a mixed disulfide followed by intramolecular disulfide cyclisation of DTT, which drives the reaction to completion. [305] To avoid re-oxidation of the IgG disulfide, the buffers used for conjugation should include EDTA (to exclude metal ions) and be purged with argon or nitrogen to exclude oxygen from the solution[306].

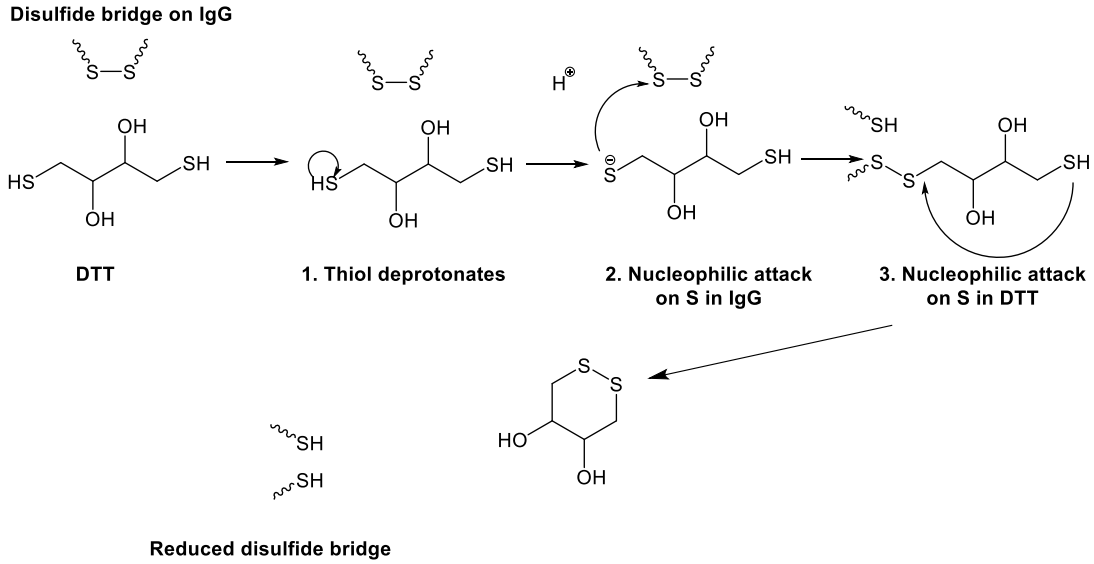

Scheme 5-1: Reaction mechanism of disulfide bridge reduction using dithiothreitol (DTT).

Once the disulfide bridge is reduced, the liberated cysteine thiols can undergo a series of addition-elimination reactions with a PEG bis-sulfone reagent (Scheme 5-2). The

bis-sulfone first undergoes elimination to give the corresponding unsaturated monosulfone adduct. Afterwards, the disulfide is re-bridged by bis-alkylation *via* a three-carbon bridge to which PEG and DBCO are covalently attached. Antibody PEGylation using bis-sulfone-PEG has been reported to cause no irreversible denaturation of the protein or disruption of the tertiary structure, as a result of which the protein retains its biological activity[306–309]. To date, there are no published examples of DBCO-antibody modification using bis-sulfone-PEG-DBCO.

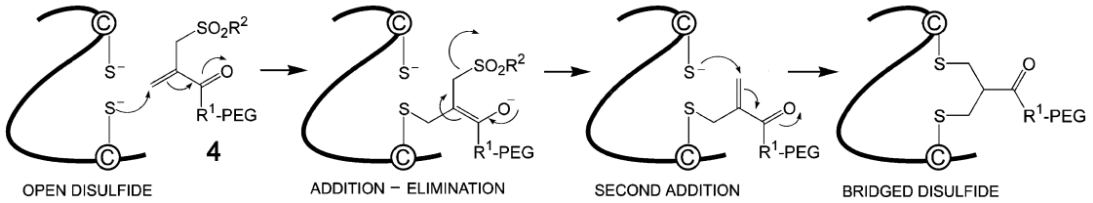

Scheme 5-2: Site-specific PEGylation of a reduced disulfide bond. The reduced disulfide bond exposes thiols that are capable of reacting with PEG monosulfone, followed by sulfinic acid elimination to create a double bond, which undergoes second thiol addition to re-bridge disulfides with the incorporated PEG-DBCO moiety. Adapted with permission from Balan et al.[309]

Although in theory a protein can be modified with either a strained alkyne or azide (with the counterpart bearing an azide or a strained alkyne moiety, respectively), it is noticeably more common to attach the DBCO group to the protein, and functionalise the polymer particle with an azide. However, an example of the opposite conjugation strategy was described by Jung and Yi, who used NHS-PEG_{12}-azide to modify anti-green fluorescent protein (GFP) antibody for conjugation to DBCO-functionalised chitosan-PEG microparticles.[310] The proposed modification does not offer site-specific conjugation of the antibody since it is based on the NHS-primary amine interaction. Nevertheless, the particle-conjugated antibodies retained their structural activity and showed long-term stability upon storage in aqueous conditions.

5.1.2. Azide-functionalisation of polymer materials

Another component necessary for the SPAAC reaction to occur is an azide-functionalised substrate to which a DBCO-modified protein can undergo reaction. Although SPAAC reactions are generally discussed in the context of reactions between two reagents in solution, there has been a considerable interest in using the SPACC reaction for surface functionalisation of solid polymer substrates. For example, Lallana et al.[311] reported the SPAAC conjugation of an anti-BSA rabbit IgG modified with PEG-DBCO compound to chitosan-PEG-N_3 nanoparticles, showing retention of binding ability using laser scanning confocal microscopy. The preparation of chitosan-PEG-N_3 nanoparticles required a three-step modification of chitosan by grafting an azide-terminated PEG carrying a carboxylic acid.

In a 2019 paper, Walden et al.[312] used the click chemistry approach for the conjugation of a model biomolecule, albumin, to the surface of polymer microparticles. In this study, human serum albumin was modified with dibenzylcyclooctyne−PEG_4−maleimide (DBCO−PEG-mal) by reaction with the free cysteine thiol in albumin. The modified biomolecule was then allowed to react with microspheres prepared from an azide-functionalised PCL (Figure 5-4), forming a particle-protein conjugate through a SPAAC reaction at physiological conditions (phosphate saline buffer, pH 7.4). Unfortunately a major limitation of this study is the lack of reported protein stability or cellular toxicity data.

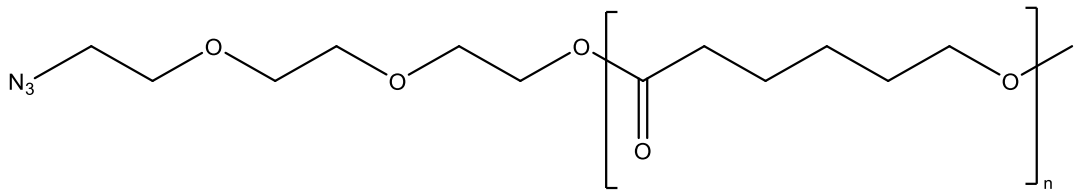

Figure 5-4: Chemical structure of azide-functionalised polycaprolactone (PCL-N_3)[312].

5.1.3. Aims of this chapter

Recent examples in the literature suggest that it is possible to conjugate therapeutically relevant proteins directly to the surface of a polymer substrate using SPAAC chemistry. This chapter therefore focuses on the attachment of an anti-CD3 antibody to the surface of PCL microparticles using strain-promoted azide-alkyne cycloaddition. For preliminary studies, azide-bearing PCL microparticles were prepared using standard top-down electrospraying. An anti-CD3 antibody (OKT3) was modified with a strained alkyne (DBCO) to facilitate the SPAAC reaction. The microparticles were allowed to react with the strained-alkyne anti-CD3, and the retention of protein functionality was tested in *in vitro* T cell activation studies using the Jurkat cell line. Finally, the ability of the PCL-N_3-DBCO-OKT3 conjugates to activate T cells was tested in human PBMC-derived CD3+ T cell activation studies.

5.2. Experimental details

5.2.1. Preparation of azide-functionalised microparticles

Azide-functionalised PCL (Mw~ 45 kDa) was a kind gift from Dr Aram Saeed, University of East Anglia. Azide-functionalised PCL particles of ca. 20 µm were prepared by electrospraying a solution of 10 % w/v PCL-N_3 (Mw~ 45 kDa) in either TFE, chloroform or mixtures of both (25/75 v/v; 50/50 v/v; 75/25 v/v) (ThermoFisher, UK). The solution was dispensed through a 21G stainless needle (inner diameter 0.51 mm, Nordson EFD) connected to a high-voltage direct-current power supply (HCP 35-35000, FuG Elektronik, Germany) at a voltage set at 10 kV. A syringe pump (789100C, Cole Parmer, UK) was used to control the solution flow rate (1.0 mL/h). The particles were collected on aluminium foil placed on a grounded plate collector (14.7 × 20 cm). The distance from the needle to the collector was 20 cm. Temperature was at approximately 25 ± 2 °C and relative humidity was 35 ± 10%. The resultant particles (named PCL-N_3) were carefully scraped from the foil with a scalpel held perpendicularly (90 º) to the aluminium plate and stored in air-tight glass vials at room temperature. The average diameter of the PCL-N_3 particles was calculated using SEM as described in Section 2.2.2.1, page 54.

5.2.2. Preparation of PCL and PCL-N_3 films

PCL and PCL-N_3 films were prepared by dipping 13 mm diameter, 0.16 mm thick D263 M borosilicate coverslip glasses (VWR, UK) in a solution of either 10% w/v PCL (Mw ~45 kDa, Sigma-Aldrich, UK) in $CHCl_3$ or PCL-N_3 (Mw~ 45 kDa) in $CHCl_3$ and letting the solvent evaporate overnight.

5.2.3. Characterisation of PCL-N_3 particles

The fabricated PCL-N_3 particles were characterised using SEM, FTIR and XPS as described in Sections 2.2.2 (page 54) and 2.2.3 (page 55).

5.2.4. Confirmation of azide group presence in PCL-N_3 particles

To confirm the presence of azide groups on the particle and film surfaces and their ability to undergo click reaction with strained alkynes, a fluorescently-labelled strained alkyne compound was used. A small amount of PCL-N_3 particles (1 mg) was mixed with Click-iT™ Alexa Fluor™ 488 sDIBO Alkyne (2 µL; 20 mM in DMSO; ThermoFisher, UK) and PBS (48 µL, pH 7.4). After 24 hours of incubation at room temperature under constant shaking and light exclusion, the particles were washed with 2 mL of PBS four times by centrifuging and resuspending in fresh solution and imaged with fluorescence microscopy (EVOS XL Cell Imaging System digital inverted microscope, ThermoFisher Scientific, UK).

5.2.5. Cytotoxicity of PCL-N_3 particles to Jurkat cells

The effect of azide-bearing particles on the viability of Jurkat cells was investigated in a 96-well plate format. The Jurkat E6.1 cell culture method is provided in Section 2.2.8.2, page 61. A varying amount of particles per well (125-500 µg) was tested, using non-functionalised PCL particles as a control (PCL-PG-1, prepared as described in Section 4.2.1.3, page 127).

Briefly, PCL-N_3 particles (5 mg) were thoroughly washed with sterile PBS (4 × 1 mL) by centrifuging and resuspending in fresh solution. Next, the particles were resuspended in 1 mL of pre-warmed cell media (5 mg/mL), and, a varying volume of particle suspension (25-100 µL) was pipetted onto the bottom of a standard flat-

bottomed 96-well plate. The volume of liquid in each well was adjusted to 100 µL by adding pre-warmed cell media. Afterwards, a suspension of Jurkat cells (100 µL, 6×10^5 cells/mL) was added to all wells to give a final number of 3×10^5 cells per well. The plate was placed in a humidified 37ºC 5% CO_2 incubator under constant shaking (500 rpm) and cell viability was measured after 2, 3 and 4 days using the PrestoBlue™ Cell Viability Reagent (Sigma-Aldrich, UK) as previously described (see Section 2.2.8.2, page 61). Each experiment was performed on three separate days, with three replicate wells per treatment.

5.2.6. DBCO-PEG-OKT3 conjugation

The modification of anti-CD3 (OKT3) antibody with a strained alkyne moiety (DBCO) was performed using a bis-alkylating labelling reagent (bis-sulfone-PEG-DBCO, prepared by Prof Steve Brocchini). Conjugation buffer (50 mM sodium phosphate, pH 7.4, 10 mM EDTA in ultrapure water, purged with argon) was freshly prepared prior to DBCO-PEG-OKT3 conjugation. 1,4-Dithiothreitol (DTT; 1 mg) was dissolved in the conjugation buffer (2 mL). A solution of OKT3 in PBS (1 mL, 1 mg/mL) was added to the reaction vessel containing DTT, mixed and incubated for 30 minutes at room temperature. Afterwards, the reaction mixture was eluted through a PD-10 desalting column (VWR International Ltd, UK) equilibrated with conjugation buffer (3 mL). Bis-sulfone-PEG-DBCO was dissolved in the conjugation buffer (5 mg/mL) and added to the eluted reaction mixture at various molar equivalents of bis-sulfone-PEG-DBCO to OKT3 (2, 4, 10, 20, 40). Following a 3-hour incubation at room temperature, unreacted bis-sulfone-PEG-DBCO, was removed using a Vivaspin 6® centrifugal concentrator (molecular weight cut-off 30 kDa; VWR International, UK). The conjugation reaction was monitored with SDS-PAGE (as described in Section 2.2.5.1, page 57). The concentration of the modified antibody was established using the Bradford assay (Section 2.2.6.2, page 58).

To test the retention of biological activity and potential cytotoxicity to Jurkat cells, the DBCO-modified OKT3 (DBCO-OKT3) was tested in an *in vitro* T cell activation experiment. The Jurkat E6.1 cell culture method is provided in Section 2.2.8.2, page 61. Briefly, 50 µL of either native OKT3 or DBCO-OKT3 (10 µg/mL in PBS), or PBS only (for unstimulated cells control) was pipetted onto a flat-bottomed 96-well plate (Corning, UK) and incubated for 2 hours at room temperature. After thorough washing of the wells to remove unbound antibody (3 × 400 µL PBS), a suspension of Jurkat cells (200 µL, 3×10^5 cells/mL) was added to all wells. The plate was then placed in a humidified 37ºC 5% CO_2 incubator for four days. The supernatant was collected for human IL-2 DuoSet ELISA (R&D Systems, UK; for experimental details see Section 2.2.7, page 59), while the viability of the cells following the four-day incubation was measured using the PrestoBlue™ Cell Viability Reagent (Sigma-Aldrich, UK) as previously described (see Section 2.2.8.2, page 61). Each experiment was performed three times on separate days, with three replicate wells per experiment.

5.2.7. SPAAC of DBCO-OKT3 to PCL-N_3 particles

PCL-N_3 microparticles (named PCL-N_3) were weighed into 2 mL Eppendorf tubes (9 mg) and pre-sterilised by washing once with methanol (1 mL) and twice with sterile PBS (2 × 1 mL) through centrifuging and resuspending in fresh solution. Particles with no azide functionality (named PCL) were used as a control. To each tube, 200 µL of sterile PBS and 18 µL of either native OKT3 (named OKT3; 1 mg/mL) or DBCO-modified OKT3 (named DBCO; 1 mg/mL) were added to give the following formulations: DBCO-PCL-N_3, DBCO-PCL, OKT3-PCL-N_3, OKT3-PCL. The particles were incubated for four hours under constant shaking (500 rpm) on a plate-shaker with a 0.3 cm circular orbit (Microplate Mixer, SciQuip, UK). Afterwards, the unbound antibody was removed by washing the particles twice with 1 mL PBS via centrifuging and resuspending in fresh solution.

5.2.7.1. Conjugation of a fluorescently-labelled secondary antibody

A small sample of antibody-functionalised particles (~ 1 mg) prepared as described in Section 5.2.7 was incubated with 100 µL of goat anti-mouse IgG Superclonal™ recombinant secondary antibody conjugated to Alexa Fluor 488 (2 µg/mL in PBS; ThermoFisher, UK). The suspended particles were incubated for 3 hours protected from light at room temperature and under constant shaking (500 rpm) on a plate-shaker with a 0.3 cm circular orbit (Microplate Mixer, SciQuip, UK). Afterwards, the particles were washed four times with sterile PBS (4 × 1 mL) by centrifuging and resuspending in fresh solution. After this, the particles were resuspended in 100 µL PBS and pipetted onto a glass microscope slide. After allowing PBS to evaporate overnight, the particles were imaged with fluorescence microscopy (EVOS XL Cell Imaging System digital inverted microscope, ThermoFisher Scientific, UK).

5.2.7.2. Preliminary *in vitro* T cell activation experiment

The antibody-functionalised particles prepared as described in Section 5.2.7 were resuspended in cell culture media to give a final concentration of 5 mg/mL and 50 µL of such suspension was pipetted onto the flat-bottomed 96-well plate. The cells were resuspended at 2.5×10^5 cells/mL and 150 µL of the cell suspension was transferred to each well. The total volume in each well was 200 µL (150 µL cell suspension and 50 µL particle suspension). For the positive control, a plate-bound antibody solution at the same concentration as in the microparticle suspensions was used. Wells with no antibody stimulation were used as a negative control. For control wells, the 50 µL particle suspension was replaced with 50 µL of pre-warmed cell culture media to maintain the same cell density per well.

For a co-stimulatory response, soluble anti-CD28 was added at 2 µg/mL of cell suspension. The plate was then placed in a humidified 37ºC 5% CO_2 incubator under constant shaking (500 rpm) on a plate-shaker with a 0.3 cm circular orbit (Microplate

Mixer, SciQuip, UK) for four days. Afterwards, the plate was centrifuged at 1200 rpm for five minutes to allow the suspended cells and microparticles to sediment at the bottom. The supernatant was collected for human IL-2 DuoSet ELISA (R&D Systems, UK; for experimental details see Section 2.2.7, page 59), while the viability of the cells following the four-day incubation was measured using the PrestoBlue™ Cell Viability Reagent (Sigma-Aldrich, UK) as previously described (see Section 2.2.8.2, page 61).

5.2.8. Performance of DBCO-PCL-N_3 particles in human PBMC-derived CD3+ T cell activation model

5.2.8.1. Preparation of antibody-functionalised particles

PCL-N_3 microparticles were weighed into 2 mL Eppendorf tubes (9 mg) and pre-sterilised by washing once with methanol (1 mL) and twice with sterile PBS (2 × 1 mL) through centrifuging and resuspending in fresh solution. To each tube 200 µL of sterile PBS and 18 µL of either native OKT3 (1 mg/mL) or DBCO-modified OKT3 (1 mg/mL) were added. The tubes were incubated on a plate-shaker set to 500 rpm for 4 or 24 hours at room temperature. The particles were washed once with sterile PBS (1 mL) in preparation for incubation with CD3+ T cells. A small amount of particles (~10 µg) was removed from each tube and stored for surface analysis using XPS as previously described (Section 2.2.3.2, page 55).

5.2.8.2. CD3+ T cell isolation and CFSE staining

In vitro T cell activation was performed on CD3+ T cells isolated from peripheral blood mononuclear cells obtained from three healthy donors, with three replicate wells per treatment tested. The assay was conducted in a flat-bottomed 48-well plate format (Corning, UK). CD3 positive T cells were isolated as described in Section 2.2.8.5 (page 63) and stained with the CFSE proliferation stain (Section 2.2.8.8, page 65). staining was confirmed with fluorescence microscopy (EVOS XL Cell Imaging

System digital inverted microscope, ThermoFisher Scientific, UK) prior to further experiments.

5.2.8.3. Incubation of particles with CD3+ T cells

The particles prepared in Section 5.2.8.1 were resuspended in complete RPMI-1640 (1.8 mL) and 150 µL of particle suspension was added to each well. For the positive control, an antibody solution at the same concentration as was present in the microparticle incubation solution was pipetted directly into the well (18 µg of antibody in 200 µL PBS) and incubated for 4 hours or 24 hours at room temperature (plate-bound antibody control). Wells with no antibody stimulation were used as a negative control. For control wells with no particles, the suspension was replaced with 150 µL of complete RPMI-1640.

Finally, 450 µL of CD3+ T cell suspension at 1×10^6 cells/mL was added. The total volume in each well was 600 µL (150 µL particle suspension/media and 450 µL cell suspension). For a co-stimulatory response, 30 µL of 10 µg/mL soluble anti-CD28 in PBS was added to the cells. The plate was then placed in a humidified 37 ºC 5% CO_2 incubator under constant shaking (500 rpm) for four days.

5.2.8.4. Immunofluorescence staining

Immunofluorescence staining was performed to examine the expression of T cell surface markers by flow cytometry. Following a four-day incubation of particles with PBMC-derived T cells (see Section 4.3.7), the 48-well culture plate was centrifuged at 4 °C and 1200 rpm for 5 min. The resultant supernatant was collected and stored at -20 °C for cytokine production analysis (see Section 4.2.8.2, page 133). The cells were resuspended in 200 µL of ice-cold PBS (without Ca/Mg^{2+}) and pipetted into a 96-well V-bottomed plate (Sigma-Aldrich, UK). The cells were then washed once in 200 µL of ice-cold PBS and resuspended in 30 µL of LIVE/DEAD™ Fixable Violet Dead

Cell Stain (1:1000 v/v dilution in PBS, ThermoFisher, UK). The cells were mixed by gentle pipetting up and down and incubated with shaking on ice, while protected from light for 20 minutes. Following incubation, the cells were washed in 200 µL of ice-cold PBS (without Ca/Mg^{2+}) and 25 µL of antibody cocktail (1 µL of anti CD3-PE/Cy7, 1 µL of CD4-APC, 1 µL of CD8-PE in 22 µL of PBA) was added. The plate was again incubated on ice with shaking, and protected from light, for 30 minutes.

Following staining, the cells were washed once in 200 µL of ice-cold PBA and fixed with 2% v/v formaldehyde in PBS solution (80 µL per well, incubated for 10 minutes, shaking, at room temperature). The fixing solution was neutralised with 120 µL of ice-cold PBA and the plate was centrifuged at 4 °C and 1200 rpm for 5 min, and washed with another 200 µL of ice-cold PBA. Following resuspension in 100 µL of ice-cold PBA, the cells were ready for flow cytometry analysis. The summary of immunofluorescence staining used in proliferation panels is summarised in the table below (Table 5-1).

Table 5-1: Summary of fluorochromes and markers used in the flow cytometry cell phenotyping and proliferation marker

Fluorochrome	Marker
PE/Cy7	CD3
PE	CD8
APC	CD4
CellTrace CFSE (488)	Proliferation
Violet (405)	Live/Dead

Flow cytometry analyses were performed using a CytoFLEX S cell analyser (Beckman Coulter, UK). The results were analysed using FCS Express version 7.04 (US). The proliferation index was calculated as previously described in Section 4.2.8.1 (page 132).

5.2.8.5. Cytokine production assays

The cell culture supernatant collected prior to the flow cytometry analysis (see Section 4.2.8.1, page 132) was used for the determination of cytokine release following the four-day incubation of CD3+ T cells with the particle formulations. The production of IFN-γ, TNF-α and IL-2 were quantified using commercially available ELISA kits as described in Section 2.2.7, page 59).

5.3 Results and discussion

Scheme 5-3 summarises the concept of the bioconjugation of anti-CD3 IgG to the surface of PCL microparticle *via* SPAAC reaction.

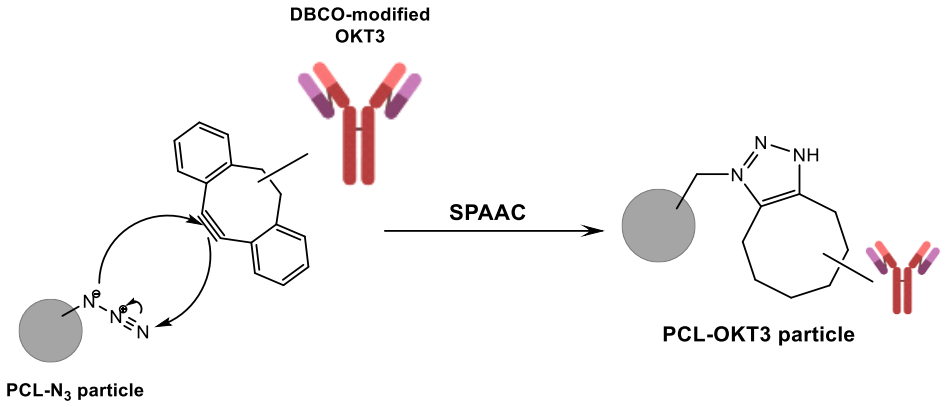

Scheme 5-3: A schematic of the DBCO-modified OKT3 antibody conjugation to azide-functionalised microparticles using strain-promoted azide-alkyne cycloaddition.

For SPAAC conjugation to occur, there is a need for azide modification of the particle and strained alkyne labelling of the antibody. The preparation of both will be discussed in this section.

5.3.1. Preparation of azide-functionalised microparticles

The previous chapter presented the fabrication of polycaprolactone microparticles by electrospraying. Here, the fabrication of azide-presenting PCL microparticles using the same method was evaluated. The initial experimental parameters were based on those used for plain PCL microparticles described in the previous chapter (see Section 4.3.1, page 134). There, the fabrication of smooth microspheres of ~7 µm by standard top-down electrospraying of 10% PCL (Mw ~45 kDa) in TFE was demonstrated. Figure 5-5 shows the optimisation of PCL-N_3 electrospraying by varying the composition of the solvent used to dissolve the polymer.

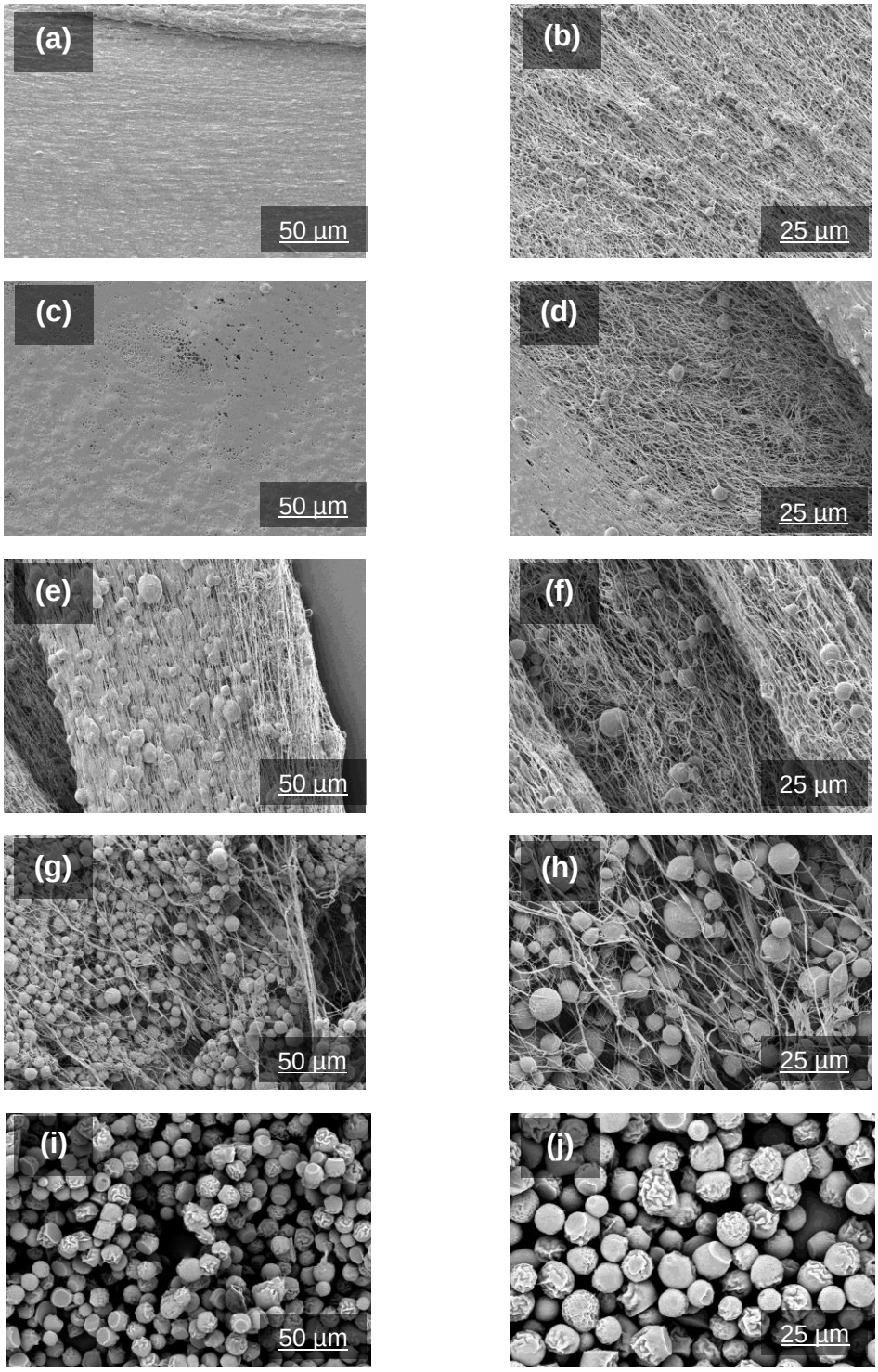

Figure 5-5: Scanning electron micrographs at 1000x (panels a,c,e,g,i) and 2000x (panels b,d,f,h,j) of the products of PCL-N_3 electrospraying. The following solvent mixtures were tested: 100% TFE (panels a and b), 75% TFE/ 25% $CHCl_3$ (panels c and d), 50% TFE/ 50% $CHCl_3$ (panels e and f), 25% TFE/ 75% $CHCl_3$ (panels g and h), 100% $CHCl_3$ (panels i and j). Increasing $CHCl_3$ content resulted in the formation of microparticles.

It became apparent that electrospraying of PCL-N_3 dissolved in TFE using the same processing conditions as previously used for PCL microparticles results in the formation of a fibrous material with an irregular structure (Figure 5-5a and b). The decision was then made to include a more volatile solvent, chloroform, in the system[113]. By varying the ratio of chloroform to TFE, it was possible to shift the process from the fabrication of fibrous products to microparticles. The gradual formation of microspheres is visible in the micrographs, with an increasing concentration of chloroform resulting in a greater number of particles formed (Figure 5-5c-h), finally reaching the target spherical morphology visible in Figure 5-5i-j at 100% $CHCl_3$.

The solvent used to manufacture unmodified PCL particles in Chapter 4, TFE, was therefore deemed unsuitable for the fabrication of PCL-N_3 microparticles and chloroform was selected instead. Although the particles had an uneven morphology, they appeared to be free flowing and separated. The rougher surface morphology could potentially provide a larger area for surface functionalisation, which could be beneficial for the proposed application of protein attachment[313].

It should be noted, however, that further process optimisation could potentially decrease the abundance of surface defects observed, such as the flattening of particles, which likely arises due to incomplete solvent evaporation during electrospraying.

The average particle size of 16 µm ± 2 µm (Figure 5-6) in diameter could potentially negatively influence the performance of these particles in *in vitro* T cell activation models as particle sizes of 1-10 µm are generally preferred (as discussed in Chapter 4).

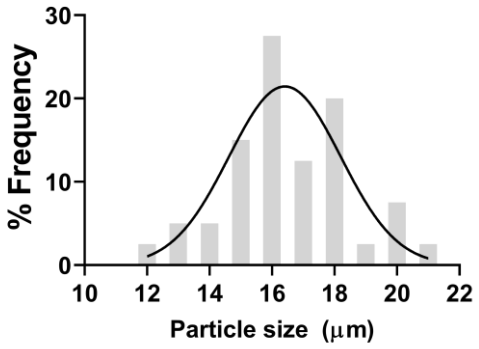

Figure 5-6: Particle size distribution of electrosprayed PCL-N_3 particles.

5.3.2. Physicochemical characterisation of PCL-N_3 particles

The next step was to characterise the fabricated PCL-N_3 particles using FTIR. The spectra of commercial PCL, electrosprayed PCL particles (prepared as described in Section 4.2.1.3, page 127), unprocessed PCL-N_3 polymer and electrosprayed PCL-N_3 particles is given in Figure 5-7.

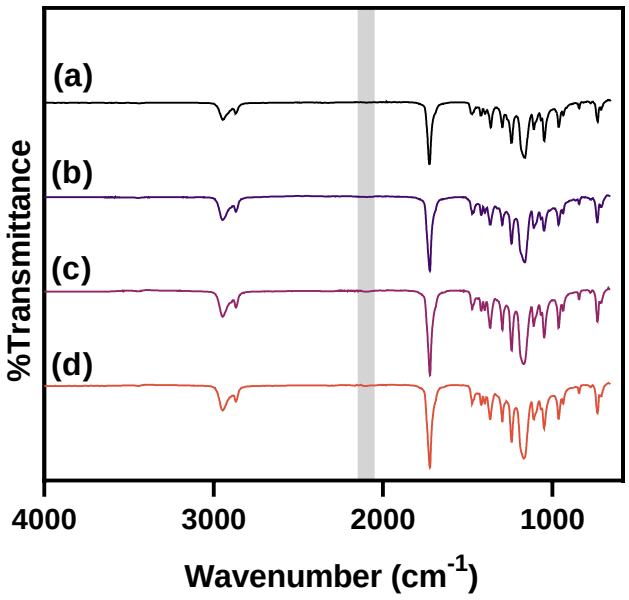

Figure 5-7: FTIR spectra of raw PCL (a), PCL particles (b), raw PCL-N_3 (c) and PCL-N_3 particles (d). Grey shading highlights the area of N=N=N stretching (2120-2160 cm^{-1}). Similar results were obtained from three independent experiments and the results of one representative experiment are shown.

The spectra of the azide-functionalised particles were identical to those of the reference samples of raw PCL polymer (Figure 5-7a) and electrosprayed PCL particles (Figure 5-7b). With both the raw PCL-N_3 polymer (Figure 5-7c) as well as the electrosprayed PCL-N_3 particles (Figure 5-7d), no signal was detected between 2120-2160 cm^{-1} where the azide stretching is typically observed[314]. It is possible that the FTIR analysis was not sensitive enough to detect the relatively small azide group (N_3) in the large polymer chain.

To characterise the fabricated particles further, a more sensitive method, XPS, was used to analyse the elemental composition of the surface (Figure 5-8). High resolution spectra for C1s, O1s and N1s were acquired, allowing for a closer analysis of chemical states of these three elements.

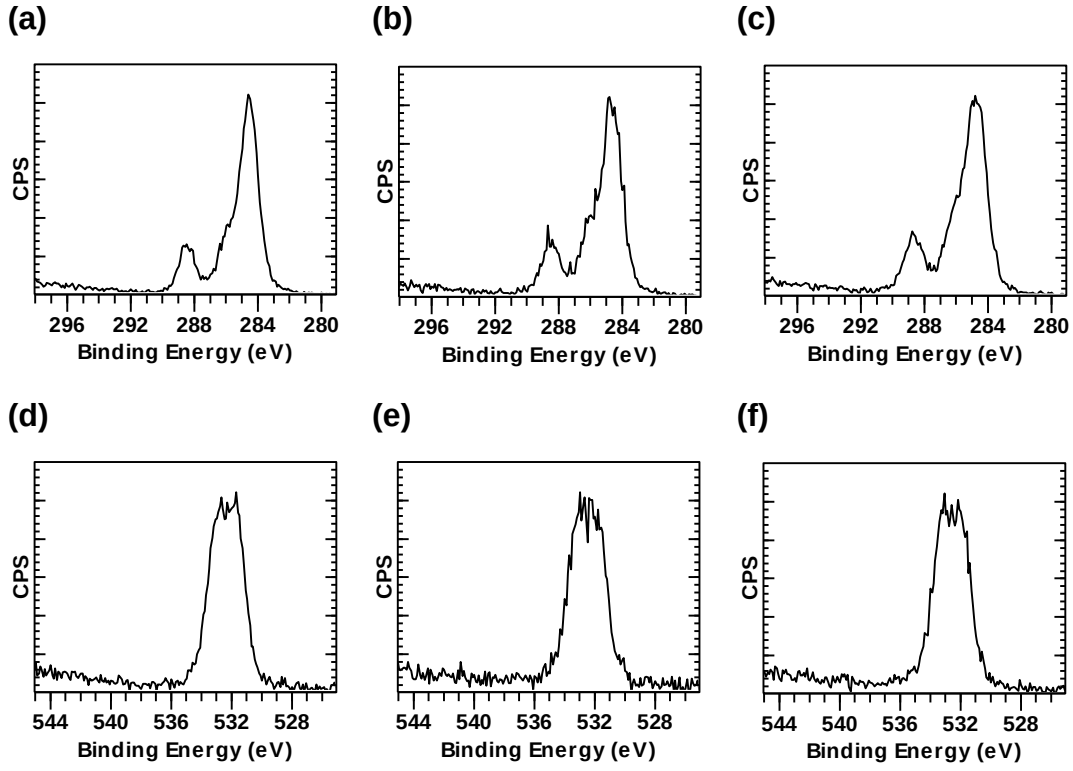

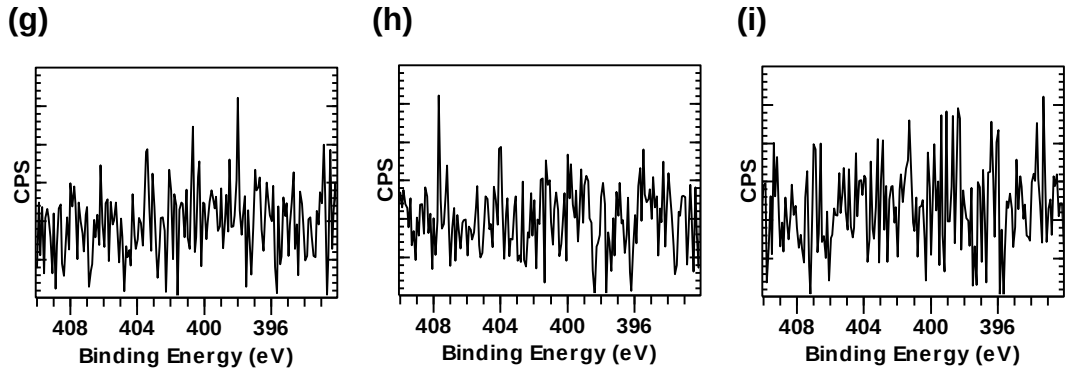

Figure 5-8: High resolution C1s (panels a-c), O1s (panels d-f) and N1s (panels g-i) XPS spectra for PCL particles (a,d,g), PCL-N_3 polymer (b,e,h) and PCL-N_3 particles (c,f,i). Similar results were obtained from three independent experiments and the results of one representative experiment are shown.

Similarly to the FTIR results (Figure 5-7), the XPS spectra for plain PCL particles, raw PCL-N_3 polymer and PCL-N_3 particles were identical. High resolution C1s (Figure 5-8a-c) and O1s (Figure 5-8d-f) spectra do not show changes to the chemical states of carbon and oxygen, respectively. Equally, no nitrogen corresponding to N_3 groups on the surface of azide-functionalised materials was detected in high resolution N1s spectra (Figure 5-8g-i).

The spectroscopic methods used for physicochemical characterisation of the produced PCL-N_3 particles thus failed to detect azide groups on the particle surface. It is possible that the large molecular weight of the PCL polymer chains overwhelmed the signal produced by relatively small azide groups. The PCL-N_3 polymer is also only end-functionalised, meaning that two azide groups would be expected per 45 kDa of PCL. An alternative explanation could be that the azide end-groups fold towards the core of the particle during electrospraying and therefore no azides are present on the surface.

An alternative method of azide detection was hence explored instead. To simplify the procedure and ascertain that the click reaction would proceed if the azide groups were available, a PCL-N_3 polymeric film was prepared by dipping a coverslip in a solution of 10% w/v PCL-N_3 in $CHCl_3$ and allowing the solvent to evaporate.

A control coverslip prepared from 10% w/v PCL in $CHCl_3$ was also prepared. Such prepared films were then incubated in a solution of fluorophore-conjugated strained-alkyne compound (Click-IT AlexaFluor® 488) for 4 hours, followed by extensive washing to remove unbound dye. If azide groups were present at the surface, they would undergo the SPAAC reaction, conjugating the fluorophore to the film surface. Figure 5-9 shows the fluorescence micrographs of the resultant films.

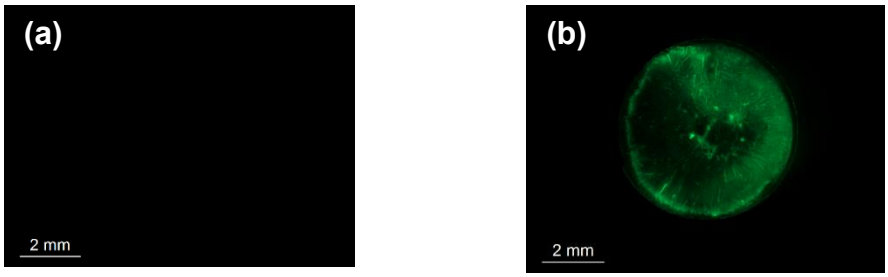

Figure 5-9: Conjugation of a fluorescently-labelled strained alkyne reagent (Click-IT AlexaFluor® 488) to PCL-N_3 polymer films. Plain PCL (panel a) showed no fluorescence, while the PCL-N_3 film (panel b) showed a bright signal, suggesting the presence of azide functional groups on the surface. Similar results were obtained from three independent experiments and the results of one representative experiment are shown.

As seen in Figure 5-9a, no fluorescence was detected in the plain PCL coverslip control, which could suggest a lack of fluorophore conjugation to the surface. In Figure 5-9b, the fluorescent regions of the coverslip can be clearly seen, proving the conjugation of Click-IT AlexaFluor® 488 to the azide groups of PCL-N_3 films. This experiment, therefore, successfully confirmed the presence of the azide groups and their reactivity with strained alkynes.

The experiment was repeated on electrosprayed PCL-N_3 particles to test whether azide groups continue to be present on the surface following the electrospraying process (Figure 5-10).

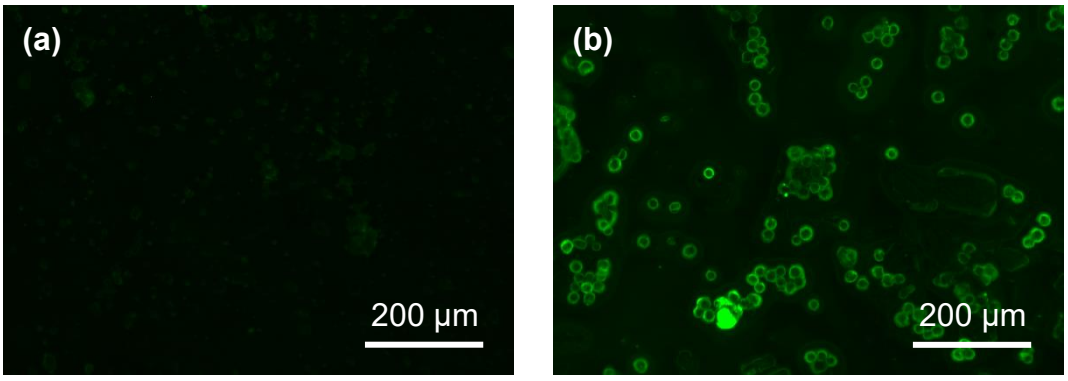

Figure 5-10: Conjugation of fluorescently-labelled strained alkyne reagent (Click-IT AlexaFluor 488) to electrosprayed PCL-N_3 particles. Plain PCL particles (panel a) showed little fluorescence, while PCL-N_3 particles (panel b) showed bright signal, suggesting the presence of azide functional groups on the surface. Similar results were obtained from three independent experiments and the results of one representative experiment are shown.

Similarly to the results obtained for polymer films (Figure 5-9), Figure 5-10a shows very low levels of fluorescence signal for PCL particle, while there appeared to be a surface coating of PCL-N_3 microparticles with the fluorescently-labelled strained alkyne reagent (Figure 5-10b). The results of this experiment are consistent with SPAAC conjugation of the dye to the PCL-N_3 particles.

5.3.3. Cytotoxicity to Jurkat cells

Soluble azide functionality is often associated with cytotoxic effects in living organisms[315]. Since the particles in this chapter are manufactured from covalently-functionalised PCL, rather than surface-coated with azide compounds, the risk of azide groups releasing into cell culture medium is relatively low. As previously mentioned, PCL-N_3 is end-functionalised, so azide groups are low abundance, therefore less likely to cause effect on cytotoxicity. Nevertheless, it was essential to establish the viability of T cells following incubation with azide-functionalised microparticles before attempting further *in vitro* testing. To do this, a human T cell line (Jurkat cells) was used, and the viability monitored using PrestoBlue assay at 1, 2, 3 and 4 days post-incubation. A range of particle concentrations was tested to investigate any dose-dependent effect on the cells. The results are depicted in Figure 5-11.

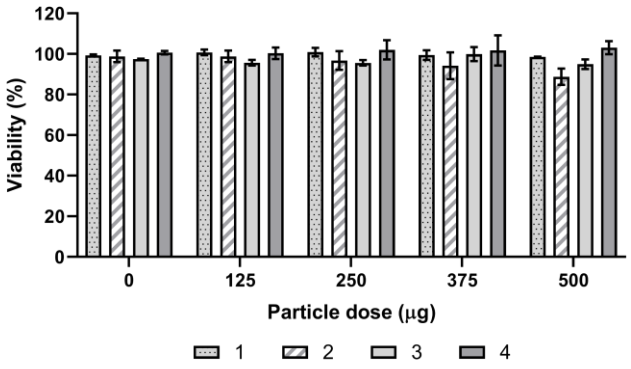

Figure 5-11: Cytotoxicity of PCL-N_3 particles following incubation for 1, 2, 3 and 4 days with Jurkat cells. Five dosing groups were tested: 0, 125, 250, 375 and 500 µg of particles per well. The cells only control was used to calculate the percentage viability. Data are shown as mean ± S.D. and are representative of three independent experiments performed on separate days, with three replicate wells per experiment.

The PCL-N_3 particles showed no cytotoxicity to Jurkat cells, with viability remaining at over 90% in all tested conditions over the period of four days, indicating that the PCL-N_3 particles can be safely used in subsequent T cell activation assays without causing harm to the cells.

Similar results were obtained by Ruizendaal et al.[316], who explored the Caco-2 cell line cytotoxicity of silicon nanoparticles functionalised with positively (amine), neutral (azide) and negatively (carboxylic acid) charged covalently attached organic monolayers. The authors found relatively low toxicity of azide-terminated silicon nanoparticles, which they attributed to the neutral nature of the azide group leading to less extensive interactions with the lipid membranes of cells.

5.3.4. DBCO modification of OKT3

Once the fabrication method of PCL-N_3 particles was established, the next step was to attempt the labelling of the target therapeutic anti-CD3 IgG, OKT3, with a strained alkyne to enable SPAAC reaction using bis-sulfone-PEG-DBCO. Changes to the molecular weight of OKT3 native antibody were monitored at each step of the conjugation reaction (Figure 5-12)

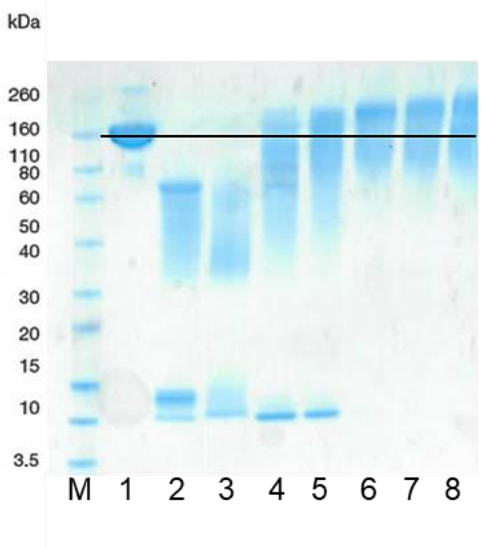

Figure 5-12: Photograph of a Novex Bis-Tris 4-12% gel showing DBCO-PEG conjugation to OKT3. M: molecular weight standard; Lane 1: native OKT3; Lane 2: unpurified DTT-OKT3 reaction mixture; Lane 3: DTT-OKT3 following purification with PD-10; Lanes 4-8 show OKT3 after reacting with varying equivalents (eq) of bis-sulfone-PEG-DBCO: 2 eq (lane 4), 4 eq (lane 5), 10 eq (lane 6), 20 eq (lane 7) and 40 eq (lane 8). Black line denotes the 150 kDa threshold.

Lane 1 shows a band at the molecular weight of the full antibody (~150 kDa). Antibody disulfide bonds were then reduced with excess DTT to expose cysteine thiols. Incubation of IgG with DTT results in dissociation of the heavy and light chains, which can be seen on SDS-PAGE as the reduction in molecular weight and appearance of additional bands[317] (lane 2). The unreacted DTT was removed by elution of the reduced antibody solution over a PD-10 column (lane 3), without causing re-oxidation of the antibody.

The reduction of the accessible disulfides was necessary for the reaction of thiols with bis-sulfone-PEG-DBCO to incorporate DBCO moiety into OKT3 (as discussed in Section 5.1.1, page 165). OKT3 is a mouse IgG_{2a} antibody with three disulfide bridges[318], therefore their reduction should yield six cysteine thiols as possible conjugation sites[319]. The native antibody exhibits molecular weight of 150 kDa[320] (lane 1). As the molecular weight of bis-sulfone-PEG-DBCO reagent used for conjugations was ~ 5 kDa, an increase in the molecular weight of the antibody to 180

kDa would suggest successful conjugation of the DBCO functionality to the native antibody (estimated 5 kDa for every thiol available, ~30 kDa in total).

To initiate the conjugation reactions, a solution of bis-sulfone-PEG-DBCO reagent was added at different molar equivalents (eq) to identify the sufficient amount of reagent needed for successful modification of OKT3 – 2 eq (lane 4), 4 eq (lane 5), 10 eq (lane 6), 20 eq (lane 7) and 40 eq (lane 8). The increase in molecular weight observed in all 5 lanes suggests the successful reformation of the disulfide bridge by *bis*-alkylation[309]. The increase in molecular weight at around 180 kDa was observed at 10 eq of bis-sulfone-PEG-DBCO per OKT3 (lane 6) and above (20 eq; lane 7, 40 eq; lane 8) and therefore this molar equivalency was chosen for future conjugations. The smudging in SDS-PAGE may suggest that further purification of the conjugate is required in future experiments. Nevertheless, the OKT3 antibody seem to have been fully reduced, and the reduced adducts from lane 2 appear to have been consumed.

To verify whether DBCO modification affected the biological activity of OKT3, both native and DBCO-labelled antibodies were tested in an *in vitro* T cell activation model in Jurkat cells. A standard 96-well plate was coated with a solution of each antibody (10 µg in PBS, 50 µL) by incubation for two hours at 37°C[223]. Following incubation with Jurkat cells for four days, IL-2 production and cell viability were measured and the results are presented in Figure 5-13.

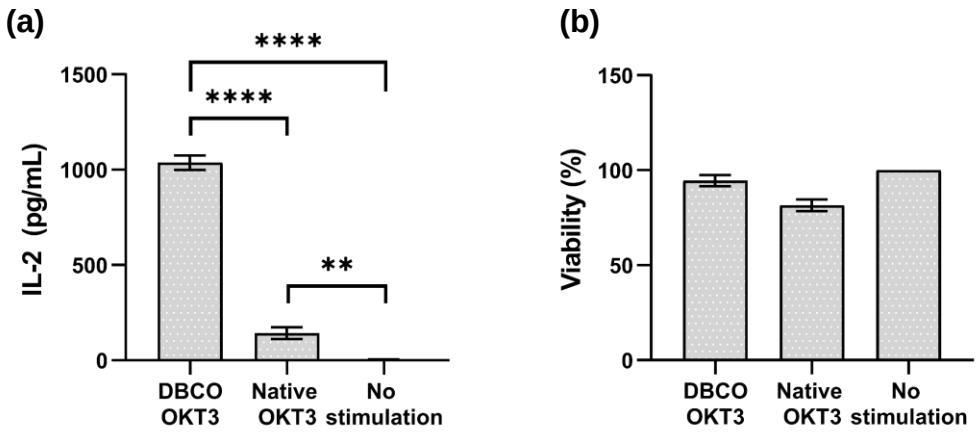

Figure 5-13: IL-2 production (panel a) and Jurkat cell viability (b) following stimulation with plate bound antibodies: DBCO-modified OKT3 (DBCO OKT3) and native OKT3. Unstimulated cells were used as a negative control (no stimulation). Data are shown as mean ± S.D. and are representative of three independent experiments performed on separate days, with three replicate wells per experiment. *Repeated measures one-way ANOVA with post hoc Tukey's test; statistical significance: ** (p-value ≤0.01), **** (p-value ≤0.0001)*.

DBCO modification of OKT3 resulted in significantly higher ($p \leq 0.0001$) stimulation of T cells as measured by IL-2 production (Figure 5-13a). The reason for this effect is unclear. One possible hypothesis is that the DBCO-PEG-modification increases the hydrophobicity of the antibody, as has been observed in antibody-drug conjugates[321]. This would potentially improve the extent and orientation of DBCO-OKT3 binding to tissue culture plastic, therefore enhancing its performance in cellular assays.

The bulky, hydrophobic, structure of the cyclooctyne component is sometimes associated with the alteration of the integrity and safety of the protein conjugates[322]. However, experiments conducted on Jurkat cells in this work did not show any negative effects on the cell viability (Figure 5-13b).

5.3.5. Conjugation of DBCO-OKT3 to PCL-N_3 particles

Once the fabrication of PCL-N_3 particles and the DBCO modification of OKT3 antibody was explored, the next step was to attempt the SPAAC reaction by incubating the modified particle and protein. In the biomedical field, the SPAAC reaction is particularly attractive as it does not require harsh conditions and can be conducted at room temperature and in aqueous solutions[176]. The effective conjugation of DBCO-modified fluorophore after four hours of incubation with PCL-N_3 microparticles is shown above (Figure 5-10, page 187). For this reason, a four-hour incubation time was selected as the initial reaction duration for DBCO-OKT3 and PCL-N_3 particle conjugation.

To determine if the successful conjugation of the antibody to the particles occurred, a fluorescence microscopy assay was developed, whereby (1) DBCO-OKT3 and PCL-N_3 particles were incubated in PBS for four hours at room temperature, followed by washing to remove unbound antibody, and then (2) a secondary antibody modified with a fluorophore was incubated for another 3 hours to allow binding to the primary DBCO-OKT3 antibody. This way, not only the spatial distribution of the antibody on the particle surface but also the retention of antibody activity (i.e. binding to primary antibody) could be observed (Figure 5-14).

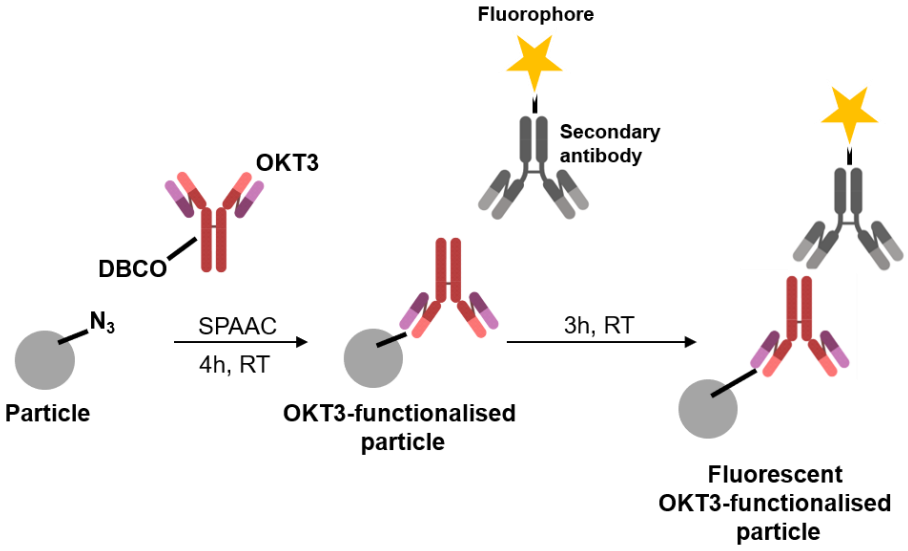

Figure 5-14: A summary of the fluorescence microscopy assay used to detect OKT3 on the PCL-N_3 particle surface. PCL-N_3 particles are first incubated with DBCO-modified OKT3 at room temperature (RT; ~25°C) to facilitate SPAAC (strain-promoted azide-alkyne cycloaddition) reaction. After washing to remove unbound antibody, the OKT3-functionalised particles are then incubated with a fluorophore-labelled secondary antibody for 3 hours at RT. If OKT3 is present on the particle surface, the particles should appear fluorescent under the microscope through primary to secondary antibody conjugation.

Figure 5-15 depicts the results of this experiment. Low levels of autofluorescence can be seen in the untreated (no antibody) control PCL-N_3 (Figure 5-15a) and PCL (Figure 5-15b) particles. In particles incubated with unmodified OKT3 (Figure 5-15c and d) the considerably greater fluorescence signal may suggest some level of OKT3 adsorbing physically to the surface, as observed in Chapter 4 (see Figure 4-9, page 152). PCL-N_3 clearly reacted with DBCO-modified OKT3 (Figure 5-15e), resulting in bright green particle staining and indicating a high ligand density on the surface. PCL particles incubated with DBCO-modified OKT3 (Figure 5-15f) also appeared fluorescent, possibly due to physical adsorption of the protein to the surface.

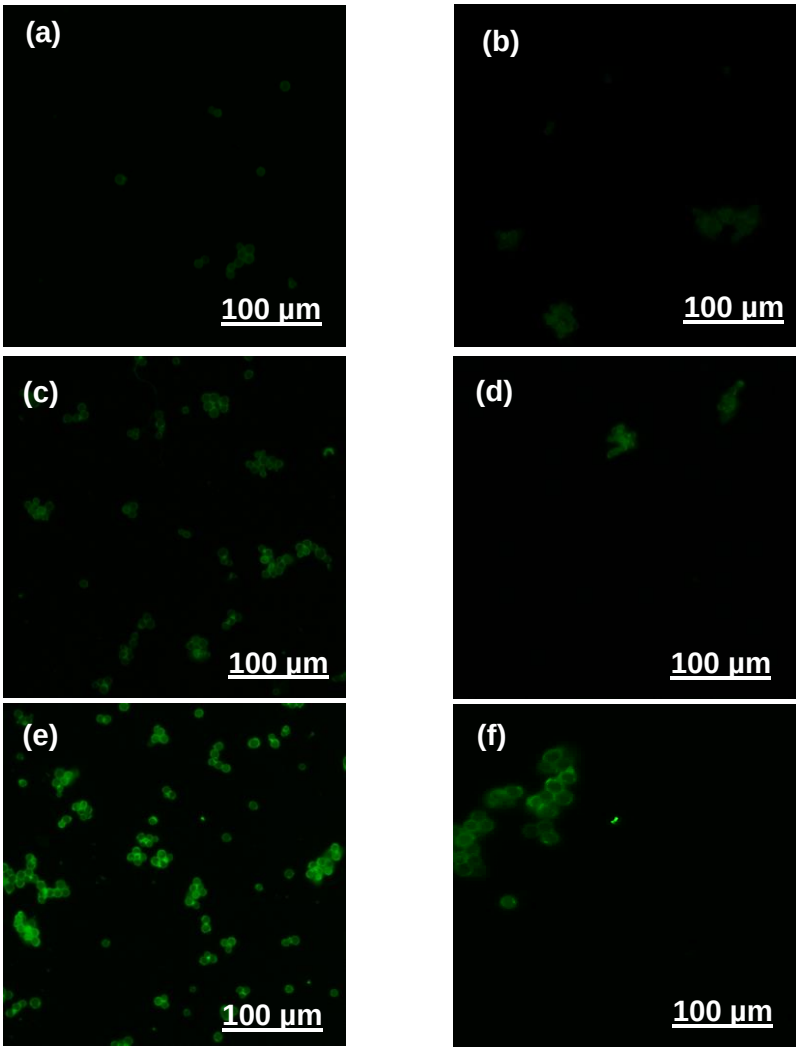

Figure 5-15: Fluorescence micrographs acquired after reacting particles with goat anti-mouse IgG conjugated to Alexa Fluor 488. Untreated PCL-N_3 (panel a) and PCL (panel b) particles were used as negative controls. Test conditions were: PCL-N_3 particles incubated with native OKT3 (panel c), PCL particles incubated with native OKT3 (panel d), PCL-N_3 incubated with DBCO-OKT3 (panel e) and PCL particle with DBCO-OKT3 (panel f).

5.3.6. T cell activation using modified PCL particles

The follow-up experiment aimed to identify the optimal dosage of particles needed to provoke a T cell-activating response in Jurkat cells, measured in terms of the release of IL-2. A similar experiment was conducted in Chapter 4 (Figure 4-7, page 146). Here, a varying amount of antibody-functionalised particles was added to each well: 125 µg, 250 µg, 375 µg and 500 µg. These dosing groups were selected based on the results of Chapter 4, where a dose of 250 µg particles functionalised with 0.5 µg OKT3

achieved the highest levels of IL-2 production. Figure 5-16 summarises the findings of this experiment.

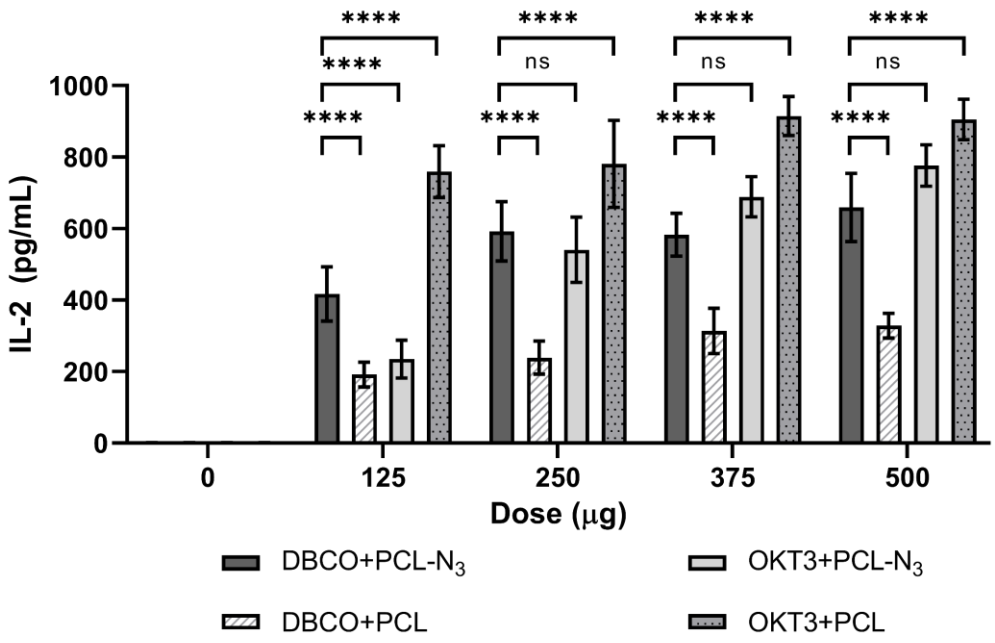

Figure 5-16: Production of IL-2 following incubation with antibody-functionalised microparticles at varying doses – 125, 250, 375 and 500 µg per well. Formulations tested were: PCL-N_3 particles incubated with DBCO-modified OKT3 (DBCO+PCL-N_3), PCL particles incubated with DBCO-modified OKT3 (DBCO+PCL), PCL-N_3 particles incubated with native OKT3 (OKT3+PCL-N_3), and PCL particles incubated with native OKT3 (OKT3+PCL). Data are shown as mean ± S.D. and are representative of three independent experiments performed on separate days, with three replicates per experiment. *Repeated measures two-way ANOVA with post hoc Tukey's test; statistical significance: ns (p-value >0.05), **** (p-value ≤0.0001)*.

The preliminary T cell activation experiment identified significant changes in the IL-2 production following particle treatments. It appears that the control group of OKT3 physically adsorbed to PCL particles (OKT3-PCL) achieved the highest T cell stimulation across all tested dosing groups, and IL-2 production was significantly higher ($p \leq 0.0001$) than in PCL-N_3 particles reacted with DBCO-OKT3. It is possible that physically adsorbed antibody quickly detaches from the particles, therefore eluting OKT3 into media, which leads to more activation on the timescale of these experiments. As the levels of IL-2 production were comparable at doses of 250 µg per well and higher, this dose was selected for further experiments to reduce

the amount of particulate material needed. The unfavourable results with DBCO-PCL-N_3 particles could suggest that the 4-hour reaction time was insufficient to achieve effective antibody conjugation to the surface. Previous attempts at protein conjugation to polymer substrates reported incubation times of 12 to 24 hours[312,323], therefore it was hypothesised that extending the reaction time to 24 hours may result in a potentiated therapeutic response in T cells. Nevertheless, at 250 µg dosage DBCO+PCL-N_3 conjugates performed better than DBCO+PCL and OKT+ PCL-N_3 controls.

5.3.7. *In vitro* performance of SPAAC antibody-particle conjugates

The effect of SPAAC reaction time (4 and 24 hours) on the therapeutic efficacy of the antibody-particle conjugates was tested in human PBMC-derived CD3+ T cells. These cells were selected over Jurkat cells to allow for a more detailed characterisation of T cell responses by quantifying three cytokines – IFN-γ, TNF-α and IL-2 (Figure 5-17).

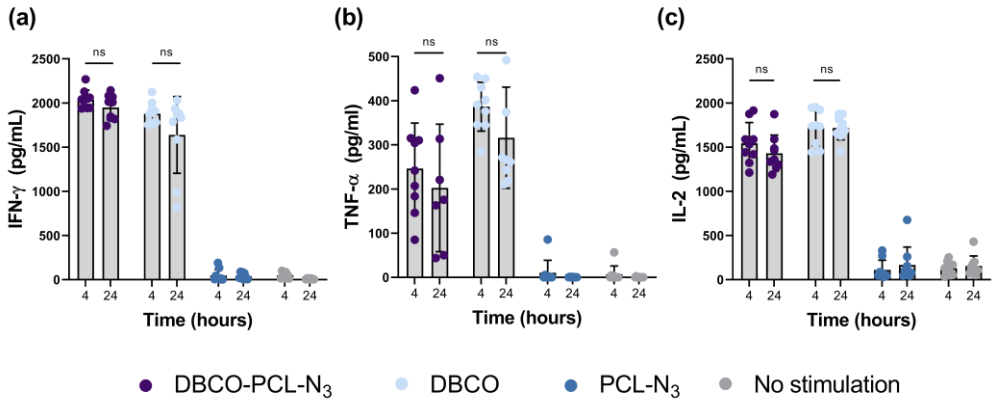

Figure 5-17: Production of IFN-γ (a), TNF-α (b) and IL-2 (c) following incubation with particles functionalised with OKT3 *via* SPAAC (DBCO-PCL-N_3). The effect of SPAAC reaction time on the therapeutic efficacy of the microparticles was investigated at 4 and 24 hours. 'DBCO' denotes plate-bound DBCO-OKT3 antibody, 'PCL-N_3' – particles without the antibody,' No stimulation' – unstimulated cells. Data are shown as mean ± S.D. and are representative of independent experiment performed on PBMCs isolated from three donors (n=3). *Repeated measures two-way ANOVA with post hoc Tukey's test; statistical significance: ns (p-value >0.05).*

The cytokine production assay data presented above indicated that prolonging the DBCO-OKT3 and PCL-N_3 incubation time from 4 to 24 hours did not result in an enhanced performance of the formulation. No statistically significant differences between these two timepoints were detected. In fact, the 4-hour reaction duration resulted in a slightly increased (although statistically insignificant) production of IFN-γ (Figure 5-17a), TNF-α (Figure 5-17b) and IL-2 (Figure 5-17c) and therefore this incubation time was selected for further experiments. For all tested outputs, delivering antibody on the surface of the microparticles resulted in enhanced cytokine production when compared to non-functionalised PCL-N_3 particles and cells only controls, while the levels of cytokine release were comparable to the positive control of plate-bound DBCO-OKT3.

Although DBCO-OKT3-PCL-N_3 conjugates stimulated PBMCs, as confirmed by the release of activation markers (Figure 5-16), it was important to compare their performance with other formulation controls. It is possible that DBCO-OKT3 was adsorbed physically to the surface, rather than covalently conjugated. To test this hypothesis, additional particle controls were included in further PBMC-derived T cell activation experiments and the performance of these formulations were measured in terms of the production of IFN-γ, TNF-α, IL-2 as well as T cell proliferation (Figure 5-18, Figure 5-19, Figure 5-20, Figure 5-22).

5.3.7.1. IFN-γ release

The analysis of IFN-γ production (Figure 5-18) following stimulation with microparticles revealed no statistically significant differences between the particulate formulations tested.

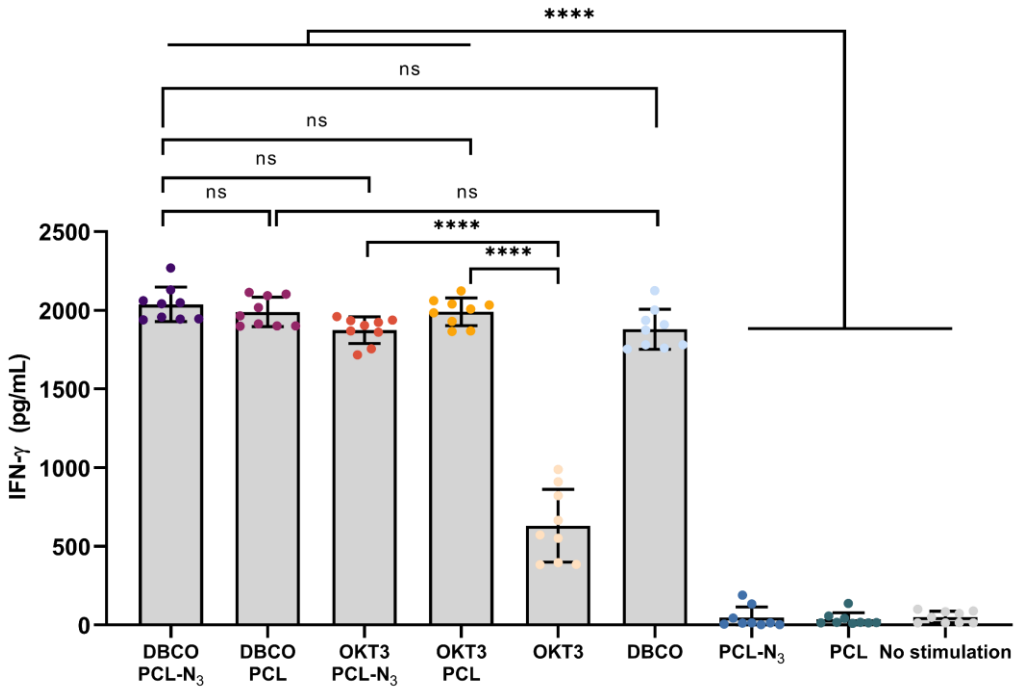

Figure 5-18: Production of IFN-γ by CD3+ T cells stimulated with antibody-coated microparticles. Formulations tested were: PCL-N_3 particles incubated with DBCO-modified OKT3 (DBCO+PCL-N_3), PCL particles incubated with DBCO-modified OKT3 (DBCO+PCL), PCL-N_3 particles incubated with native OKT3 (OKT3+ PCL-N_3), PCL particles incubated with native OKT3 (OKT3+PCL). Plate-bound OKT3 (OKT3) and DBCO-OKT3 (DBCO) were used as a positive control. Particles without antibody (PCL-N_3 and PCL) as well as unstimulated cells negative controls were included. Data are shown as mean ± S.D. and are representative of independent experiment performed on PBMCs isolated from three donors, with three replicate wells per condition tested. *Repeated measures one-way ANOVA with post hoc Tukey's test; statistical significance: ns (p-value >0.05), **** (p-value ≤0.0001)*.

In general, the results presented below give evidence for successful deposition of the antibody on the particle surface as all the antibody-loaded formulations performed significantly better than their non-antibody functionalised controls (PCL-N_3 and PCL for azide functionalised and plain PCL particles, respectively). Delivering the native OKT3 antibody on the surface of PCL particles (OKT3-PCL and OKT3-PCL-N_3) resulted in a significantly higher ($p \leq 0.001$) IFN-γ production than in plate-bound antibody control (OKT3). The same, however, was not true for the DBCO-OKT3-based formulations, where the plate-bound antibody led to very high levels of IFN-γ release (~2000 pg/mL) comparable to those of the DBCO-based particulate formulations (DBCO-PCL-N_3 and DBCO-PCL).

5.3.7.2. TNF-α release

The quantification of TNF-α release (Figure 5-19) gave findings similar to the results with IFN-γ.

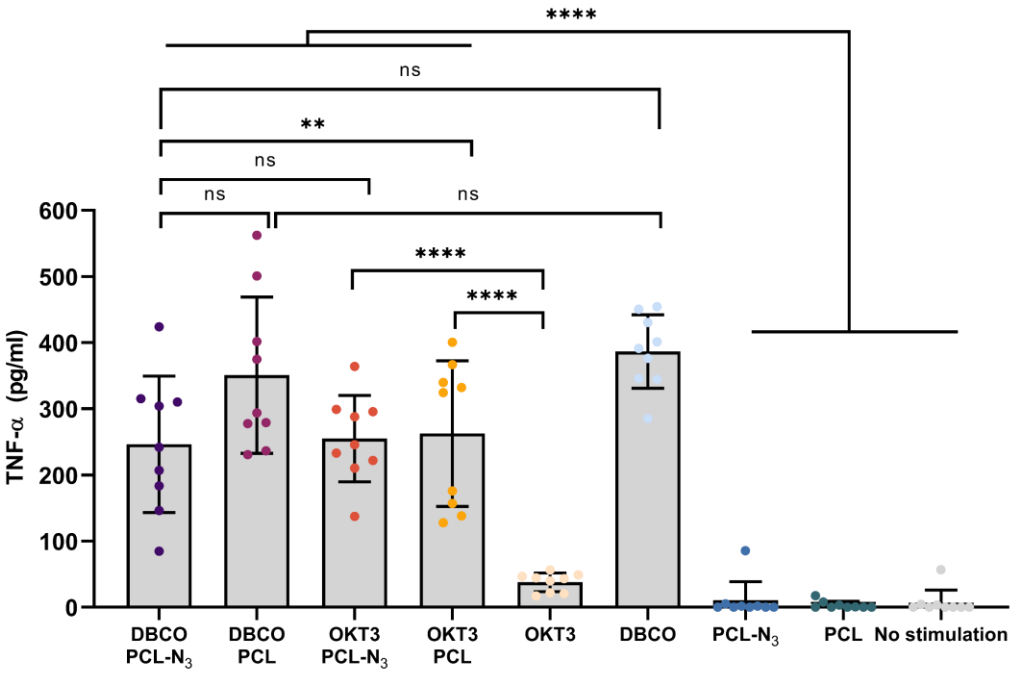

Figure 5-19: Production of TNF-α in CD3+ T cells stimulated with antibody-coated microparticles. Formulations tested were: PCL-N_3 particles incubated with DBCO-modified OKT3 (DBCO+PCL-N_3), PCL particles incubated with DBCO-modified OKT3 (DBCO+PCL), PCL-N_3 particles incubated with native OKT3 (OKT3+ PCL-N_3), PCL particles incubated with native OKT3 (OKT3+PCL). Plate-bound OKT3 (OKT3) and DBCO-OKT3 (DBCO) were used as a positive control. Particles without antibody (PCL-N_3 and PCL) as well as unstimulated cells negative controls were included. Data are shown as mean ± S.D. and are representative of independent experiment performed on PBMCs isolated from three donors, with three replicate wells per condition tested. *Repeated measures one-way ANOVA with post hoc Tukey's test; statistical significance: ns (p-value >0.05), ** (p-value ≤0.01), **** (p-value ≤0.0001)*.

Again, there were no significant differences between the DBCO-PCL-N_3 and DBCO-PCL formulations, and the overall TNF-α levels were higher (but not significantly) in non-azide functionalised particle formulation (DBCO-PCL) than in DBCO-PCL-N_3. Although the results should be interpreted with caution due to high donor-to-donor variability, the observed trend may be the effect of the differences in particle size. The PCL-N_3 particles are much larger than the PCL analogue, with an average sizes

of ~16 µm for PCL-N_3 and ~2 µm for PCL (see Chapter 4, Figure 4-8, page 148). The higher particle size for PCL-N_3 may negatively affect the interaction with T cells, as previously discussed in Chapter 4 (Section 4.1.2, page 123). This effect, however, was not observed in native OKT3-functionalised particles (OKT3-PCL-N_3 and OKT3-PCL, $p > 0.05$).

Similarly to the IFN-γ data, TNF-α production following stimulation with plate-bound DBCO-OKT3 (DBCO) was comparable to the DBCO-functionalised particulate formulations (DBCO-PCL-N_3 and DBCO-PCL). None of the differences observed were statistically significant. On the other hand, presenting native OKT3 on the surface of particles resulted in enhanced TNF-α release in both OKT3-PCL-N_3 and OKT3-PCL formulations ($p \leq 0.0001$).

5.3.7.3. IL-2 release

Figure 5-20 shows the production of IL-2 by CD3+ T cells following incubation with SPAAC antibody-particle conjugates. Some donor-to-donor variability was observed, as in the TNF-α production quantification (Figure 5-19).

Here, both DBCO- and OKT3-functionalised PCL-N_3 formulations performed worse than their PCL counterparts (DBCO-PCL and OKT3-PCL, respectively). This could potentially highlight the importance of appropriate particle size (1-10 µm, as previously described in Chapter 4) on T cell activation.

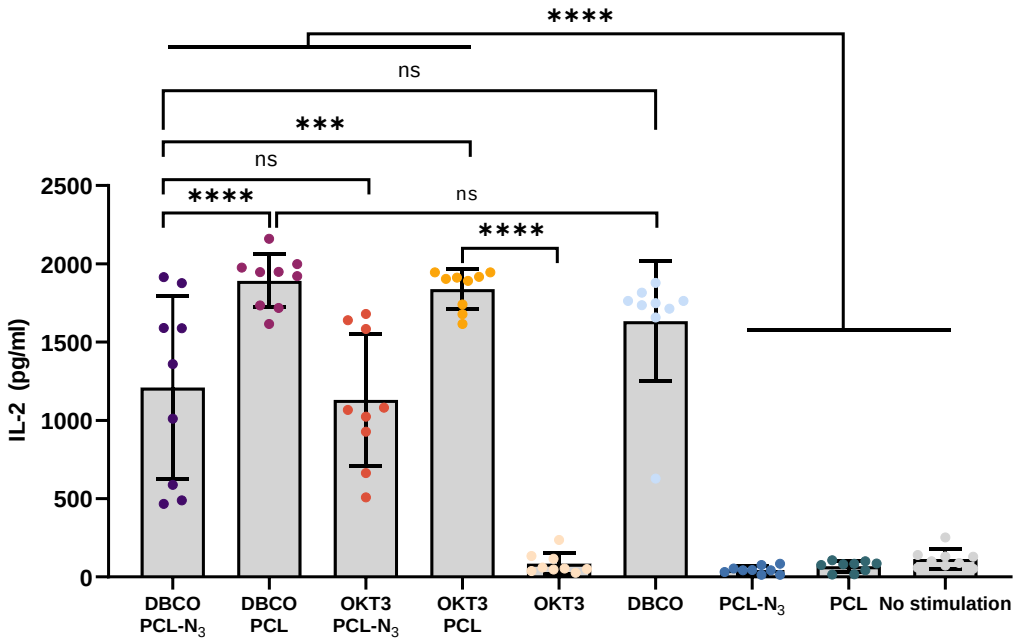

Figure 5-20: Production of IL-2 in CD3+ T cells stimulated with antibody-coated microparticles. Formulations tested were: PCL-N_3 particles incubated with DBCO-modified OKT3 (DBCO+PCL-N_3), PCL particles incubated with DBCO-modified OKT3 (DBCO+PCL), PCL-N_3 particles incubated with native OKT3 (OKT3+ PCL-N_3), PCL particles incubated with native OKT3 (OKT3+PCL). Plate-bound OKT3 (OKT3) and DBCO-OKT3 (DBCO) were used as a positive control. Particles without antibody (PCL-N_3 and PCL) as well as unstimulated cells negative controls were included. Data are shown as mean ± S.D. and are representative of independent experiment performed on PBMCs isolated from three donors (n=3). *Repeated measures one-way ANOVA with post hoc Tukey's test; statistical significance: ns (p-value >0.05), *** (p-value ≤0.001), **** (p-value ≤0.001).*

Again, no statistically significant differences were observed between DBCO delivered on tissue culture plastic (DBCO) and on the surface of the particles (DBCO-PCL-N_3 and DBCO-PCL). PCL particles delivering physically adsorbed OKT3 (OKT3-PCL) performed significantly better than plate-bound OKT3 ($p \leq 0.001$). Overall, the cytokine quantification experiments (Figure 5-18, Figure 5-19, Figure 5-20) show that the SPAAC antibody-particle conjugates are capable of inducing T cell activation as measured by cytokine production.

5.3.7.4. Proliferation and cell phenotyping

The proliferation of particle-stimulated CD3+ T cells was measured using CFSE staining as previously described in Chapter 4 (Section 4.3.7.3, page 158). The inclusion of CD4 and CD8 markers allowed for more detailed investigation of cellular behaviours by comparing the proliferation patterns for T helper cells (CD4 positive) and cytotoxic T cells (CD8 positive). An example of CD4 vs CD8 dot plots as well as the CFSE histograms obtained based on these plots is presented in Figure 5-21.

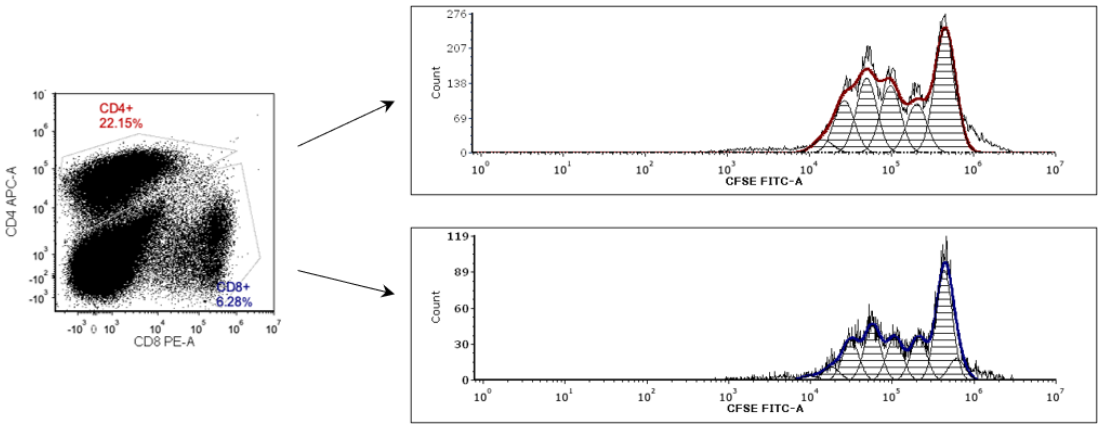

Figure 5-21: Example of results obtained in flow cytometry experiments. The inclusion of CD4 and CD8 markers allowed for the differentiation between CD4+ and CD8+ T cell populations. Then, CFSE histograms for individual populations were fitted into the proliferation modelling tool. The red line denotes peak fitting for CD4+ T cells, while the blue line shows peak fitting for CD8+ T cells.

The inclusion of CD4 and CD8 markers allowed for further differentiation of cells (either CD4 or CD8 positive) from unstained particles, as shown in the gating strategy. The proliferation index was calculated based on the proliferation model fitting into CFSE histograms, and a summary of the obtained results is presented in Figure 5-22.

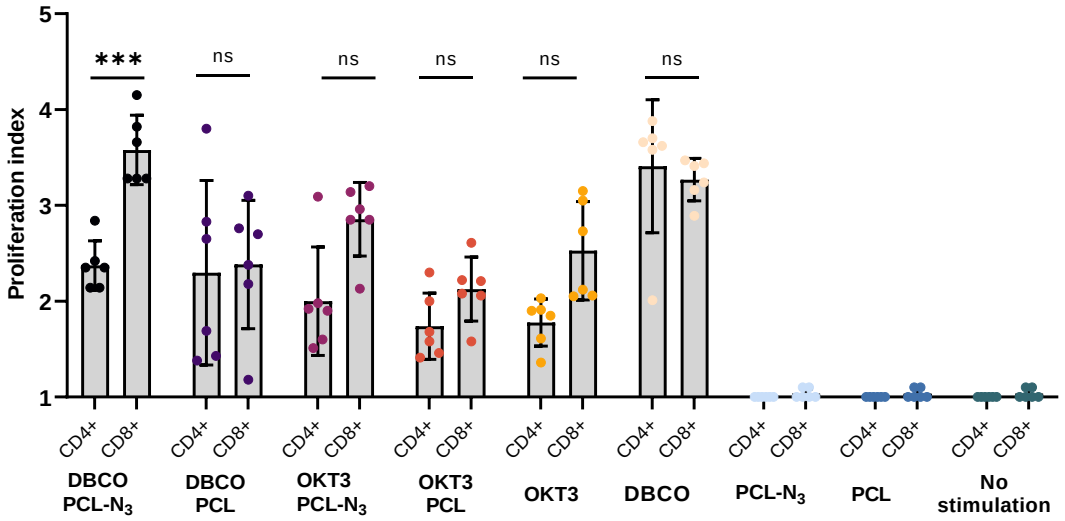

Figure 5-22: Proliferation indices of CD3+ T cells following incubation with SPAAC antibody-particle conjugates, calculated for subpopulations of CD4+ and CD8+ T cells. Formulations tested were: PCL-N_3 particles incubated with DBCO-modified OKT3 (PCL-N_3+DBCO), PCL particles incubated with DBCO-modified OKT3 (PCL+DBCO), PCL-N_3 particles incubated with native OKT3 (PCL-N_3+OKT3), PCL particles incubated with native OKT3 (PCL+OKT3). Plate-bound OKT3 (OKT3) and DBCO-OKT3 (DBCO) were used as a positive control. Particles without antibody (PCL-N_3 and PCL) as well as unstimulated cells (No stimulation) negative controls were included. Data are shown as mean ± S.D. and are representative of independent experiment performed on PBMCs isolated from three donors (n=3). *Repeated measures two-way ANOVA with post hoc Tukey's test; statistical significance: ns (p-value >0.05), *** (p-value ≤0.001).*

No proliferation was observed in non-antibody stimulated controls (non-Ab-functionalised PCL-N_3 or PCL particles and cells only wells). In general, cells stimulated with antibody-functionalised particles exhibited varying levels of proliferation, with preferential expansion of cytotoxic (CD8+) T cells. However, statistical significance was only observed in PCL-N_3-DBCO conjugates ($p \leq 0.001$). This result is particularly important for the intended application of these formulations in cancer immunotherapy, where the expansion of cytotoxic CD8+ T cells is desired[32].

When compared against the plate-bound antibody control (DBCO), PCL-N_3-DBCO resulted in significantly lower proliferation of CD4+ T cells ($p \leq 0.01$), but higher CD8+ T cell expansion ($p > 0.05$). For CD4+ T cells, the proliferation index was comparable for all particle formulations (PCL-N_3-DBCO, PCL-DBCO, PCL-N_3-OKT3, PCL-OKT3; $p > 0.05$). CD8+ T cell proliferation achieved in PCL-N_3-DBCO was significantly higher than in PCL-DBCO ($p \leq 0.001$), but comparable to PCL-N_3-OKT3 ($p > 0.05$). As observed in Jurkat cells (Figure 5-13), stimulation with DBCO-modified OKT3 resulted in a significantly higher expansion of both CD4+ ($p \leq 0.001$) and CD8+ T cells ($p \leq 0.01$) than for the unmodified OKT3 plate-bound control.

5.3.7.5. Summary of T cell activation assay results

The cytokine production assays and the calculations of proliferation index provide useful information on the biological performance of SPAAC antibody-particle conjugates. The increased proliferation and elevated production of all tested cytokines by particle-stimulated T cells suggests the successful delivery of the anti-CD3 antibody using this method. The results also confirm the superior performance of DBCO-modified antibody as compared to its unmodified state, with DBCO-OKT3 stimulating significantly higher cytokine production and proliferation of both CD4+ and CD8+ T cells. The results, however, do not conclusively confirm whether the SPAAC reaction on the particle surface was successful. The DBCO-PCL-N_3 formulation achieved results comparable to those of the particle controls (DBCO-PCL, OKT3-PCL-N_3, OKT3-PCL).

To probe for possible differences in the extent of antibody attachment to the surface, the surface composition of the particle formulations tested in the T cell activation assay was investigated with XPS. The data obtained in survey spectra allowed for the quantification of the elements present on the particle surface. The presence of the antibody on the surface can be investigated by quantifying the nitrogen content, as the

N peak can only arise from the amide and amine functionalities in the antibody. Non-antibody functionalised particle controls were used as controls. Figure 5-23 summarises the surface nitrogen percentage relative to carbon and oxygen detected on the surface.

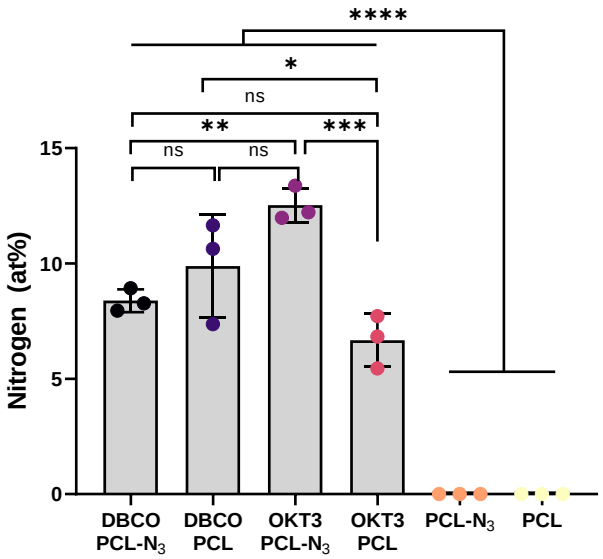

Figure 5-23: Nitrogen content (at%) at the surface of the antibody-functionalised particles after 4-hour incubation in antibody solution. Following formulations were tested: DBCO+PCL-N_3, DBCO-PCL, OKT3+PCL-N_3, OKT3+PCL. Non-functionalised particles (PCL-N_3 and PCL) were used as controls. Data are shown as mean ± standard deviation (n=3). *Repeated measures one-way ANOVA with post hoc Tukey's test; statistical significance: ns (p-value >0.05), * (p-value <0.05), ** (p-value ≤0.01), **** (p-value ≤0.0001).*

All particle formulations exhibited significantly higher surface nitrogen content than their non-antibody-functionalised controls, providing further evidence of the antibody conjugation. Nitrogen content was lowest for OKT3-PCL, followed by DBCO-PCL-N_3, DBCO-PCL and OKT3-PCL-N_3. These spectroscopic results, however, do not directly correlate to the performance of particles *in vitro*, possibly because they do not reflect on the accessibility of surface-conjugated antibodies, the elution rate and the complexity of the particle-T cell interaction.

Two parameters that potentially could be causing the inconclusive results of the *in vitro* T cell activation are (1) the difference in particle size in morphology for PCL-N_3 and PCL and (b) the biological potency of DBCO-OKT3 and OKT3. The effect of particle size on T cell activation was previously discussed in the context of electrosprayed PCL particles (Chapter 4). It is possible that the PCL-N_3 particles are inherently inferior to PCL particles due to their larger size (~16 µm). To allow a more accurate comparison, the particles should ideally exhibit the same mean diameter and morphology. Hence, further optimisation of the PCL-N_3 electrospraying process may be required.

Additionally, the plate-bound DBCO-modified OKT3 control was seen to cause significantly higher T cell activation than the native (OKT3) antibody. A more detailed characterisation of this novel DBCO-OKT3 conjugate should be performed to understand its chemistry and biological function. Further modifications to the DBCO-OKT3 conjugation protocol, for example by employing an additional purification step or by varying the molecular weight of the bis-sulfone-PEG-DBCO reagent would be interesting to explore.

Overall, the *in vitro* T cell activation results further confirm that T cell activating antibody can be safely deposited on the surface of electrosprayed particles *via* SPAAC reaction, and that such particle-antibody conjugates are capable of evoking responses in human-derived CD4+ T cells.

5.4 Conclusions

This chapter evaluated the feasibility of *in vitro* T cell activation using SPAAC antibody-particle conjugates. Azide-functionalised microparticles were prepared by electrospraying a solution of PCL-N_3. Although the process requires further optimisation to improve the morphology and decrease the diameter of the

manufactured particles, the PCL-N_3 particles showed of the ability to conjugate model DBCO compounds in fluorescence microscopy experiments.

The modification of OKT3 antibody with DBCO moieties was achieved by bis-alkylation using a bis-sulfone-PEG-DBCO reagent to yield DBCO-OKT3. The modified antibody appeared to retain biological function (as tested in a T cell activation model) and was not toxic to Jurkat cells.

Finally, the SPAAC reaction of DBCO-OKT3 and PCL-N_3 particles was attempted and achieved. The antibody delivered on the surface of the particles evoked T cell activation in PBMC-derived T cell experiments. Stimulation with the functionalised microspheres led to increased cytokine production (IFN-γ, TNF-α, IL-2) and enhanced proliferation of both CD4+ and CD8+ T cells. It is, however, unclear whether the observed effect was caused by the covalent conjugation *via* SPAAC, or simply through physical adsorption of the antibody to the particle surface. Further investigation into the individual components of the SPAAC reaction (PCL-N_3 particles, DBCO-OKT3 antibody) is needed to allow for more detailed analysis of the efficiency of this click reaction.

Chapter 6 – Implantable antibody-loaded electrospun fibres for localised delivery of immunotherapy

6.1 Introduction

Although surgical removal remains the first line treatment for most solid tumours, in some cases it is not feasible to fully resect the tumour due to its size or location. The residual tumour cells may regrow, causing cancer relapse. To prevent this, the use of implantable drug-eluting biomaterials have long been explored[324–326].

Immune checkpoint inhibitors, previously described in Section 1.2 (page 7), are showing promise in clinical trials for a variety of solid tumours. Still, the implementation of these agents into clinical treatment frameworks is often impeded by the abundance of severely debilitating immune-related adverse events. As an example, for anti-CTLA-4 antibodies, the most commonly observed side-effects include rash, pruritus, vitiligo (in 44-68% patients), and colitis (35-44%)[327]. One way to minimise the side-effects is to provide a more controlled and precisely localised release of these agents directly into the tumour site. Delivering cancer immunotherapy in a localised and sustained fashion could also decrease the amount of drug needed to elicit a therapeutic response. This could potentially lead to a decrease in the costs associated with these therapies (e.g. a £75,000 treatment course for Yervoy®[328]), which could facilitate the widespread use of these drugs in the clinic by removing the financial barriers.

Several biomaterial-assisted checkpoint inhibitor delivery systems have been proposed (as discussed in Section 1.3.1, page 16), but the field remains largely unexplored. The delicate structures of the monoclonal antibodies that comprise immune checkpoint inhibitors pose multiple challenges in the design of suitable drug delivery platforms. Many biomaterial fabrication processes may negatively impact the stability of the protein being formulated. Typical conventional encapsulation methods, such as spray-drying or hot melt extrusion, require harsh conditions (e.g. application of heat or prolonged contact with solvents) that can potentially cause protein misfolding or aggregation, and consequent loss of activity.

Electrospinning offers a simple way of manufacturing drug-loaded implantable scaffolds, the properties of which can be tuned according to the therapeutic needs. In cancer care, electrospun patches have been mostly discussed in the context of localised delivery of chemotherapeutic agents and small molecule drugs[329,330]. However, recent advancements in protein electrospinning (discussed in Section 1.4.2, page 30) could potentially widen the application of EHD processes into the cancer immunotherapy field.

Angkawinitwong et al.[112] explored coaxial electrospinning in the fabrication of bevacizumab-loaded PCL nanofibres for the treatment of age-related macular degeneration in the eye. The study provided a valuable insight into the feasibility of using coaxial electrospinning for immunotherapy delivery, highlighting the importance of the pH of the protein solution. It was found that electrospinning protein solutions at the isoelectric point of the antibody significantly enhances its in-process stability. Bevacizumab released from the optimal core-shell fibres remained intact and biologically active, confirming the appropriateness of the approach for sustained and localised delivery of antibodies. However, the encapsulation efficiency was negatively affected by electrospinning at the pI of bevacizumab, which

was attributed to the lack of electrostatic interactions driving the migration of protein towards the grounded electrode when the antibody is in its uncharged state.

Until recently, implementation of electrospinning on an industrial scale was hindered by limitations in the process scale-up. A number of high throughput ES technologies and instruments have emerged recently, making it an attractive method for the large-scale production of drug-eluting implants that can be manufactured in Good Manufacturing Practice (GMP) conditions[138,281].

6.1.1. Aims of this chapter

The delivery of therapeutic antibodies by incorporation in electrospun fibres has been largely overlooked, with only two published examples up to date[112,331]. To the best of our knowledge, electrospinning of cancer immunotherapeutics has not been attempted.

This chapter therefore aimed to prepare implantable and biodegradable electrospun formulations of an anti-CTLA-4 antibody, ipilimumab, for sustained release of this immune checkpoint inhibitors near to the tumour site. The ipilimumab-loaded fibre formulation was prepared using the core-shell EHD technology and the processing parameters were based on the previous literature in the field[112,228].

The effect of the pH of the core (antibody) solution on the stability of the electrospinning process as well as the product morphology, physical properties and drug release profile was investigated. Finally, the ipilimumab released from the fibres was tested for protein integrity to evaluate the effect of the electrospinning process on antibody stability.

6.2 Experimental details

6.2.1. Preparation of antibody-loaded fibres using co-axial electrospinning

6.2.1.1. Preparation of the shell solution

For shell solution, PCL pellets (80 kDa) were dissolved in a mixture of 2,2,2-trifluoroethanol (TFE) and deionized water (DI) (9:1 v/v) at a concentration of 10% w/v[112,228].

6.2.1.2. Preparation of the core solutions

Unused Yervoy® solution was recovered from Bart's Hospital (London, UK) and used to prepare the core solutions. For both formulations (ipilimumab at pH 8.3 named 'IPI 8.3' and and ipilimumab at pH (IPI 6.7)), the commercial antibody buffer was exchanged with Trizma® buffer (50 mM, pH 8.3 and 6.7, respectively) using a PD-10 desalting column (VWR International Ltd, UK). The resulting antibody solutions were concentrated to 12.5 mg/mL using a Vivaspin 6® centrifugal concentrator (molecular weight cut-off 30 kDa; VWR International, UK) for 3 minutes at 4000 rpm.

Concentrations of antibody solutions were calculated using two methods: by measuring absorbance at 280 nm (as described in Section 2.2.6.1, page 57) and using Bradford assay (as described in Section 2.2.6.2, page 58).

6.2.1.3. Coaxial electrospinning process

Electrospun antibody-loaded fibres were prepared using coaxial electrospinning. The details of this EHD technique are described in Section 1.4 (page 23).

Core and shell solutions were respectively loaded into 1 and 5 mL plastic syringes (Terumo, UK) immediately prior to the electrospinning process, to prevent

degradation of the antibody solution at room temperature. Afterwards, the syringes were mounted separately onto two syringe pumps (78-9100 C, Cole Parmer, UK). The syringe containing the core solution was tipped with a nested feeding channel on a coaxial spinneret (inner / outer internal diameters: 0.5 /1.0 mm) whereas the shell syringe was connected to a silicone tube which attached to the outer channel of the spinneret. The positive electrode of a high voltage DC power supply was connected to the metal tip of the coaxial spinneret while the grounded electrode was connected to a metal plate collector wrapped with baking paper. The core and shell fluids were then simultaneously fed through the spinneret at a fixed flow rate. EHD was performed under ambient conditions (temperature 25 ± 2 °C and relative humidity 35 ± 10%). Coaxial electrospinning was performed for 2 hours (spinning 3 mL of shell and 0.6 mL of core solution). The fibre mats were collected onto a collector. Afterwards, each sample was carefully removed from the baking paper using a scalpel and stored at 2-8 ºC prior to further experiments. Three batches of each fibre formulations were produced. Table 6-1 summarises the electrospinning parameters used.

Table 6-1: Summary of coaxial ES parameters used to prepare ipilimumab-loaded fibres.

Parameters	**IPI 8.3**	**IPI 6.7**
Core solution	Yervoy® (ipilimumab) solution in Trizma® buffer (12.5 mg/mL, pH 8.3)	Yervoy® (ipilimumab) solution in Trizma® buffer (12.5 mg/mL, pH 6.7)
Shell solution	10% w/v PCL in 9:1 v/v TFE:deionized water	
Core : shell flow rates	0.3 mL h^{-1} : 1.5 mL h^{-1}	
Spinneret to collector distance	16 cm	
Voltage	20-22 kV	

6.2.2. Physicochemical characterisation

The morphology and physicochemical properties of the produced fibres were evaluated with SEM, FTIR, XPS, DSC and XRD as described in Sections 2.2.2 (page 54) and 2.2.3 (page 55).

6.2.3. Confirmation of antibody encapsulation

6.2.3.1. Transmission electron microscopy

The core-shell structure of antibody-loaded electrospun fibres was investigated with transmission electron microscopy (TEM). A small amount of sample was collected by electrospinning directly onto the TEM grid (TAAB, UK). The samples were then analysed by Dr Andrew Weston using a FEI CM 120 Bio-Twin TEM (Philips/FEI, USA).

6.2.3.2. FITC-ipilimumab conjugation

FITC-conjugated ipilimumab (FITC-IPI) was prepared to visualize the distribution of ipilimumab in the fibres. Briefly, the core solutions prepared in Section 6.2.1.2 (page 211) were diluted with PBS (pH 7.4) to 1 mg/mL (1 mL). NHS-fluorescein (NHS-FITC; Sigma-Aldrich, UK) was dissolved in DMSO (10 mg/mL, 100 µL) immediately before the reaction. Afterwards, 4.7 µL of NHS-FITC solution was added into a reaction tube containing 1 mL of a 1 mg/mL ipilimumab solution. NHS-FITC was used in molar excess (15 equivalents) to ipilimumab, as per the manufacturer's recommendations. The reaction was incubated for 1 h at room temperature under gentle stirring and protected from light. Thereafter, the reaction mixture (ca. 1 mL) was loaded onto a PD-10 desalting column (VWR International Ltd, UK) and eluted with Trizma® buffer (ca. 4 mL; pH 8.3 and pH 6.7 for FITC-IPI-8.3 and FITC-IPI-6.7, respectively). The washing and elution steps were repeated to finish purification of the

whole mixture. The final concentration of FITC-labelled antibody was measured using the formula below (Equation (6.1)):

$$FITC - IPI\ concentration\ (M) = \frac{A_{280} - A_{493} \times CF}{\varepsilon_{protein}} \times dilution\ factor \qquad (6.1)$$

where A_{280}= absorbance at 280 nm, A_{493}= absorbance at 493 nm, CF=correction factor (0.3), $\varepsilon_{protein}$= extinction coefficient for ipilimumab (210000 M^{-1} cm^{-1} for IgG).

The FITC-IPI solution was then concentrated to 12.5 mg/mL using a Vivaspin 6® centrifugal concentrator (molecular weight cut-off 30 kDa; VWR International, UK) and used in the electrospinning experiment in place of unlabeled IPI. A small amount of fibres was collected onto a glass microscope slide and visualized with an EVOS XL Cell Imaging System digital inverted microscope (ThermoFisher Scientific, UK) set to green fluorescent protein (GFP) filter.

6.2.3.3. Determination of encapsulation efficiency

Fibre samples were extracted using a modified method from the literature[112]. Approximately 10 mg of fibres were dissolved in 1 mL DMSO and gently agitated for one hour. A solution (5 mL) of NaOH (0.05 M) and sodium dodecyl sulfate (SDS; 0.05% w/v in PBS) was then added to the sample solution, which was left under constant shaking at 100 rpm for another hour at room temperature. The resulting solution was collected and filtered through 0.22 μm Millex-GP syringe filter units (Fisher Scientific, UK) prior to quantification with microBCA™ as previously described (Section 2.2.6.3, page 58). Each formulation was tested in triplicate.

6.2.4. *In vitro* release study

6.2.4.1. Cumulative release

Approximately 50 mg of each formulation was placed in a 28 mL glass vial and filled with PBS (5.0 mL, pH 7.4), supplemented with 0.05% w/v sodium azide and 0.5% v/v

Tween® 80. The samples were then placed in a shaking incubator (Incu-Shake MINI, SciQuip, UK) set to 37 °C and 120 rpm. Aliquots (0.5 mL) were collected from the release medium at predetermined timepoints, and the release medium replenished with same volume of fresh medium. Protein content was measured using microBCA™ as previously described (Section 2.2.6.3, page 58) and the results are presented as cumulative release (calculated using Equation (3.2), page 78). Each formulation was tested in triplicate.

6.2.4.2. Antibody stability

The stability of the ipilimumab released from both formulations (IPI 8.3 and IPI 6.7) was studied using SDS-PAGE. Protein aliquots (20 μL) collected from the *in vitro* release study were filtered with 0.22 μm Millex-GP syringe filter unit (Fisher Scientific, UK) before running SDS-PAGE, followed by Coomasie blue staining (see Section 2.2.5.1, page 57).

6.3 Results and discussion

The electrospinning parameters used for the fabrication of ipilimumab-loaded fibres were chosen based on existing literature[112]. The effect of the pH of the core solution became apparent from the onset of the electrospinning process, where the formulation with the core solution at the isoelectric point of ipilimumab (IPI 8.3) resulting in the formation of a distinct Taylor cone, clearly visible in Figure 6-1a, and the electrospinning process remaining stable throughout the experiment (2 hours). In contrast, when the core solution at pH 6.7 (IPI 6.7) was spun, the process was rather unstable, with the Taylor cone splitting as observed in Figure 6-1b. The tip of the coaxial needle required frequent cleaning to prevent the clogging of the outlet, due to a build-up of semi-solid polymer residue resulting from the unstable electrospinning process.

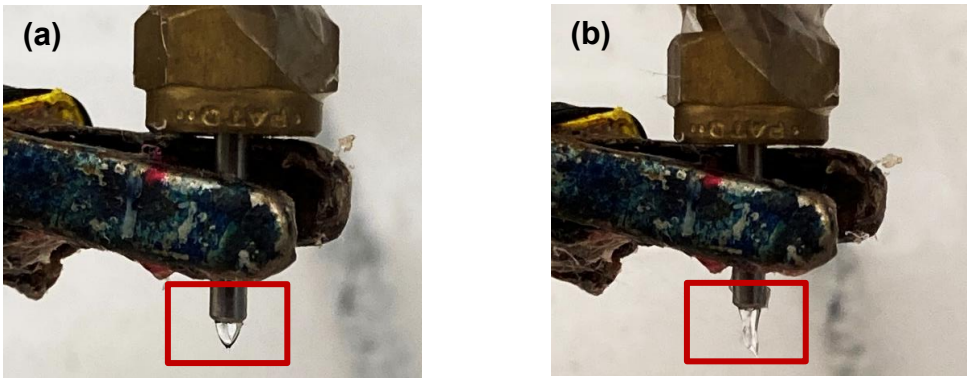

Figure 6-1: Photographs presenting the stability of a Taylor cone when electrospinning IPI 8.3 (panel a) and IPI 6.7 (panel b).

6.3.1. Fibre size and morphology

The morphology and size distribution of the electrospun fibres was investigated with SEM (Figure 6-2).

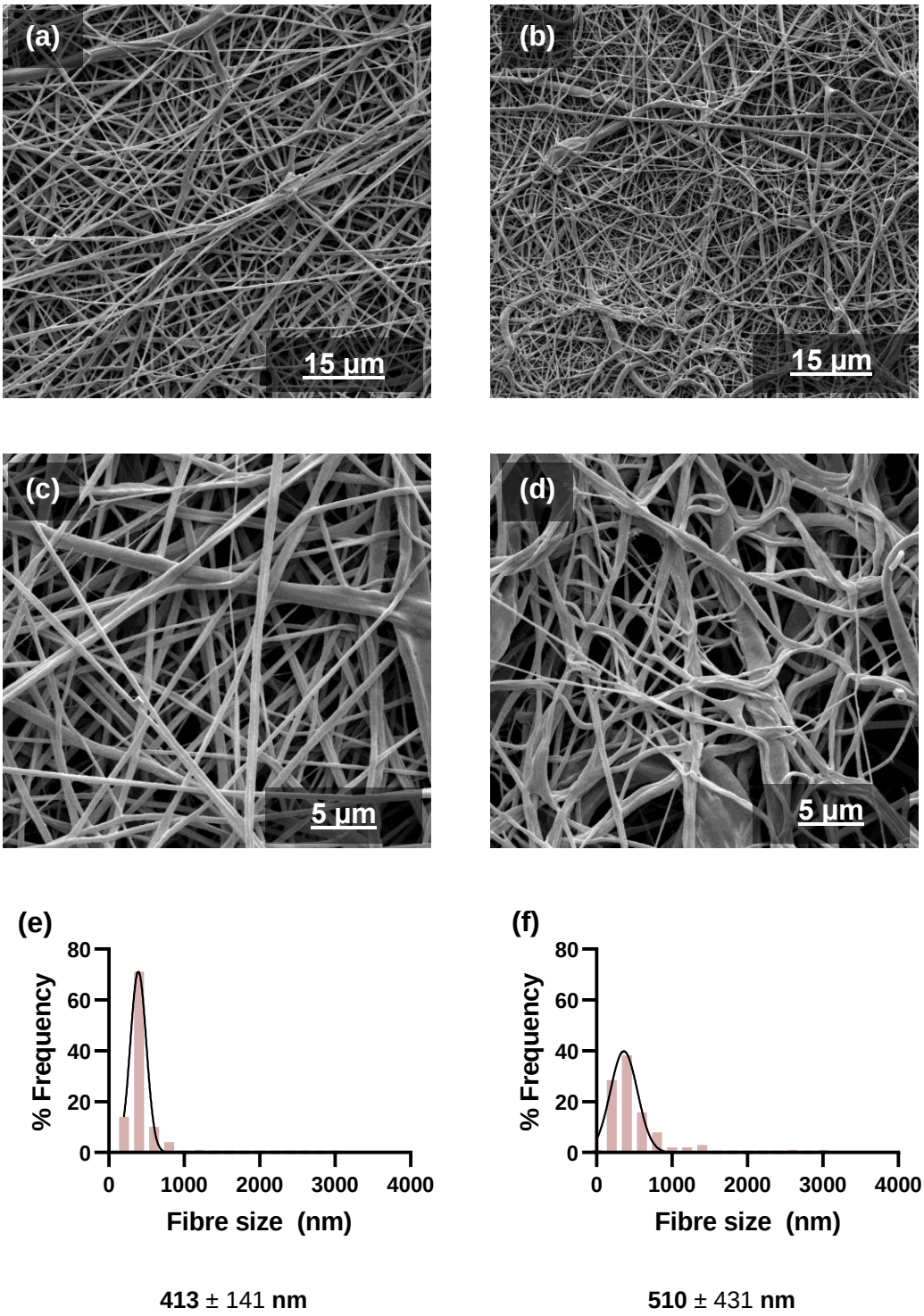

413 ± 141 **nm**

510 ± 431 **nm**

Figure 6-2: Scanning electron micrographs of ipilimumab-loaded fibres at two magnifications: 4000x (a,b) and 10 000x (c,d). Panels (a) and (c) show IPI 8.3, while panels (b) and (d) represent IPI 6.7. Size distributions as well as mean ± S.D. fibre diamaters were calculated from micrographs for IPI 8.3 (panel e) and IPI 6.7 (panel f). Similar results were obtained from three independent experiments and the results of one representative experiment are shown.

Both formulations generated bead-free fibres, although their morphology differed. Samples prepared from a solution at the isoelectric point of ipilimumab (IPI 8.3) formed relatively uniform and smooth strands (Figure 6-2a and c) of 413 ± 141 nm (Figure 6-2e). Conversely, the IPI 6.7 formulation showed a branched and tangled structure (Figure 6-2b and d). The diameter of the individual strands varied widely, with a mean of 510 ± 430 nm (Figure 6-2f). The relatively distorted structure of the fibres spun at pH 6.7 could be the result of the unstable electrospinning process discussed above (Figure 6-1).

6.3.2. Physicochemical characterisation

FTIR analysis of ipilimumab-loaded fibres (Figure 6-3) did not reveal any clear evidence for the presence of the antibody. The spectra in Figure 6-3 for the IPI-loaded formulations are identical to that of PCL. It is possible that the PCL signal dominated due to the low antibody loading, and this being confined within the core of the fibre. Similar results were obtained for bevacizumab-loaded fibres prepared using the same electrospinning parameters[228].

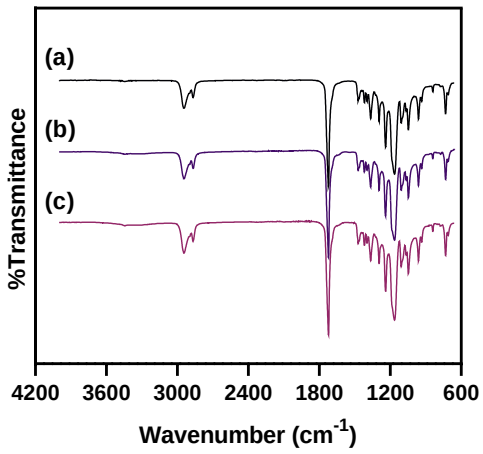

Figure 6-3: FTIR spectra of ipilimumab-loaded fibres. The following samples were measured: a) plain PCL fibre, and ipilimumab-loaded fibres spun at b) pH 6.7 and c) pH 8.3. No structural differences between plain and antibody-loaded fibres were observed. Similar results were obtained from all three independent experiments and the results of one representative experiment are shown.

XPS was used to investigate the elemental composition at the surface of the antibody-loaded fibres. Since PCL does not contain nitrogen in its structure (Figure 1-8, page 26), any signal from nitrogen will indicate the presence of amide and amine functional groups within the protein structure. High resolution N1s XPS spectra are presented in Figure 6-4.

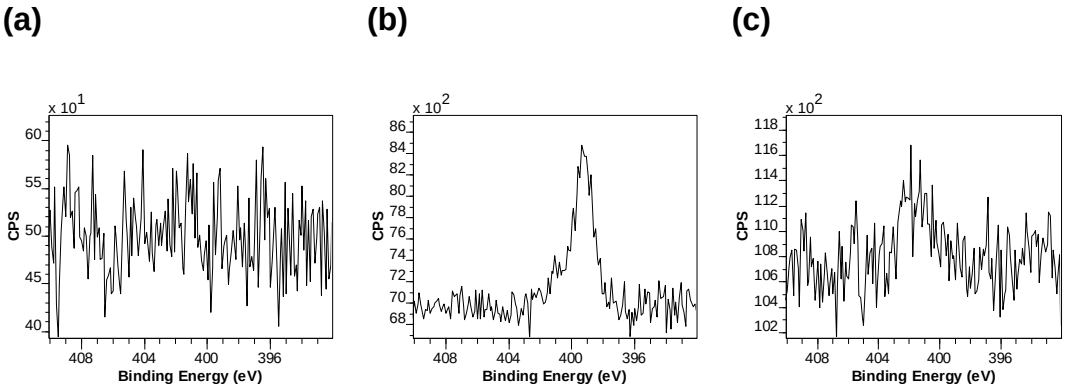

Figure 6-4: High resolution N1s XPS spectra for (a) plain PCL fibres, and ipilimumab-loaded fibre spun at b) pH 6.7 and c) pH 8.3. Similar results were obtained from three independent experiments and the results of one representative experiment are shown.

A control blank PCL fibre sample (Figure 6-4a) showed no signal between 408-396 eV, indicating no nitrogen present on the surface. In contrast, a nitrogen peak was detected in ipilimumab-loaded fibres spun at both pH 6.7 (Figure 6-4b) and pH 8.3 (Figure 6-4c). The survey spectra obtained for these samples were used to quantify the elemental composition at the surface, and the results are presented in Table 6-2.

Table 6-2: Elemental composition of the fibre surfaces. Data are shown as mean ± standard deviation (n=3).

Formulation	Surface C (at%)	Surface O (at%)	Surface N (at%)
PCL fibre	76.38 ± 0.74	23.62 ± 0.71	0
IPI 6.7	75.05 ± 0.31	23.44 ± 0.44	1.51 ± 0.15
IPI 8.3	76.76 ± 0.05	22.63 ± 0.06	0.62 ± 0.10

Since the penetration depth of the X-ray beam in the XPS instrument is 10 nm, it can be assumed that the nitrogen signal observed in the antibody-loaded fibres corresponds to the protein present either on or near to the surface of the scaffold. This

could indicate that some protein has become encapsulated in the fibre shell, or that the thickness of the shell is less than 10 nm. The increased surface N percentage of IPI 6.7 could potentially accelerate the release of the therapeutic antibody from this formulation. It has been previously hypothesised that, under the electric field applied during the electrospinning process, easily polarisable charged macromolecules such as proteins may migrate from the core to the shell fluid. At the isoelectric point of ipilimumab (pH ~8.3), the antibody possesses no charge and migration to the fibre surface is unlikely to occur, while at pH 6.7 it is positively charged and therefore more prone to migration towards the shell via dielectrophoretic movements[228]. This could potentially explain the increased nitrogen percentage detected on the surface of IPI 6.7.

6.3.3. Confirmation of antibody presence within electrospun scaffolds

The localisation of ipilimumab within the fibres was explored with FITC-conjugated ipilimumab, electrospun under the same processing conditions used to prepare IPI 8.3 and IPI 6.7. The fibre structure was investigated with fluorescence microscopy and the results are presented in Figure 6-5. The light microscopy images (Figure 6-5a and b) were acquired to map the electrospun fibres on the microscope slide. The presence of fluorescence (Figure 6-5c and d) in both samples tested, at comparable intensity levels, indicates the successful encapsulation of the antibody within the fibres. The fluorescence is easily observed in the fibre strands of the larger diameter.

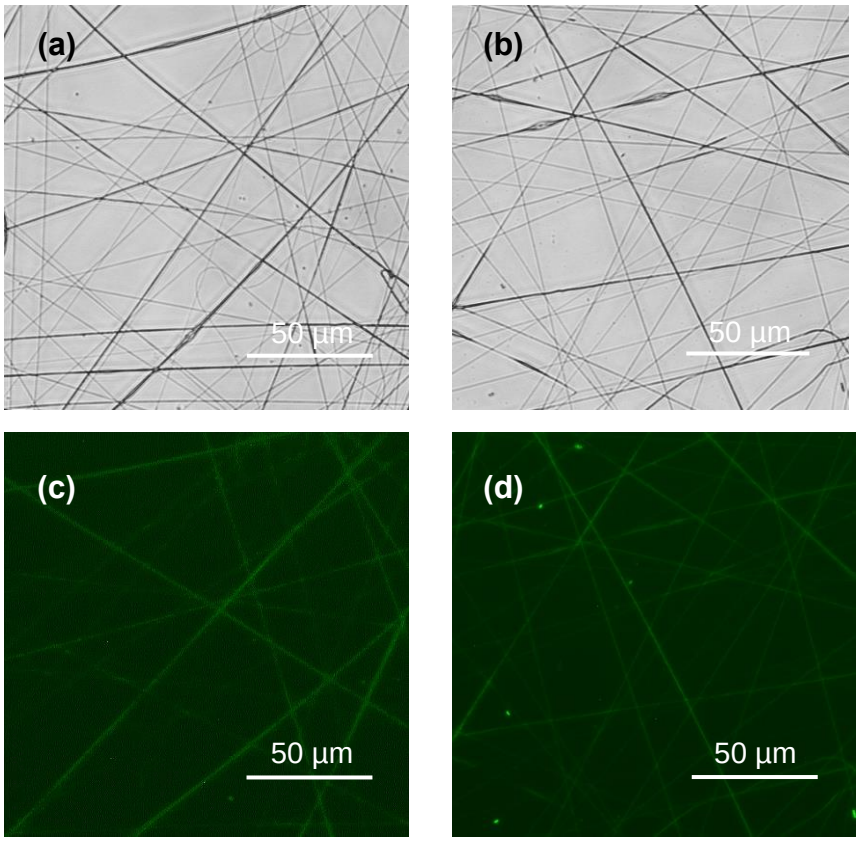

Figure 6-5: Light (a,b) and fluorescence (c,d) micrographs of electrospun ipilimumab-loaded nanofibres magnified 10x. The following formulations are presented: IPI 8.3 (a,c) and IPI 6.7 (b,d). Similar results were obtained from three independent experiments and the results of one representative experiment are shown.

Further information on the core-shell structure of the electrospun fibres was obtained with TEM (Figure 6-6). In TEM micrograph of IPI 8.3, (Figure 6-6a), the darker core is embedded within the lighter shell, as indicated by arrows. The TEM images of IPI 6.7 show a poorly defined core-shell structure, with irregularities observed in Figure 6-6b that may suggest non-uniform distribution of the antibody within the fibre. In contrast to Figure 6-6c (IPI 8.3), where the core-shell structure is clearly defined, it appears that the thickness of the shell is much smaller for the IPI 6.7 fibres (Figure 6-6d), and/or that the mixing of the core and shell solutions during electrospinning occurred. As discussed above in the context of XPS results, the migration of a charged protein towards the surface of the fibre under the electric field may occur. Both the XPS and TEM results support the hypothesis that electrospinning near the isoelectric

point of a protein results in accumulation of the drug cargo within the core with little or no migration to the surface visible, and are consistent with previous literature in the field[112].

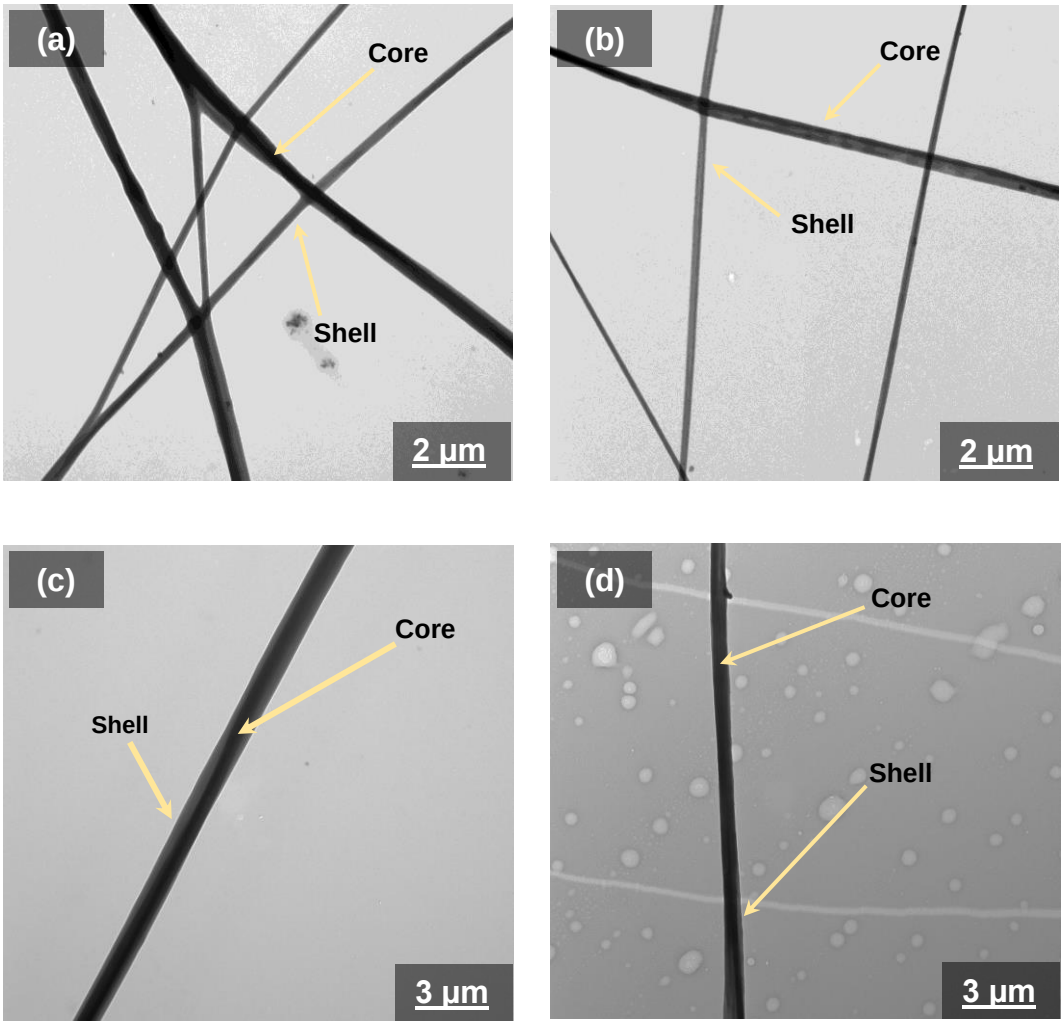

Figure 6-6: Transmission electron micrographs of electrospun fibres. The following formulations are presented: IPI 8.3 (a,c) and IPI 6.7 (b,d). Similar results were obtained from three independent experiments and the results of one representative experiment are shown.

6.3.3.1. Preliminary *in vitro* ipilimumab release study

The release of ipilimumab from IPI 8.3 and IPI 6.7 was observed over 16 days (Figure 6-7).

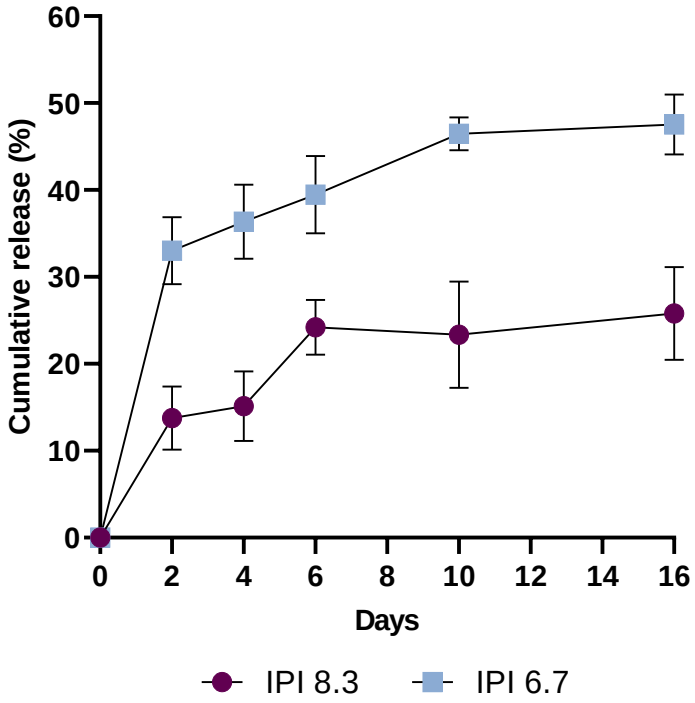

Figure 6-7: Cumulative release profiles of ipilimumab from antibody-loaded PCL fibres. Formulations tested were: IPI 8.3 and IPI 6.7. Data are presented as mean ± SD (n=6).

The fibres spun with a core solution at the isoelectric point of ipilimumab (IPI 8.3) showed a 13.8 ± 3.2% burst release at day 2, followed by a period of sustained release for the next 8 days, reaching 23.3 ± 5.5% at day 10. On the other hand, the IPI 6.7 fibres exhibited a burst of 32.5 ± 6.7% release at day 2, accelerating to 46.6 ± 1.9% at day 10. For both formulations the release seems to plateau after day 10, showing only a modest increase from 23.3 ± 5.5% to 25.8 ± 4.8% for IPI 8.3 and 46.6 ± 1.9% to 47.5 ± 3.2% for IPI 6.7 These results are consistent with the previously presented hypothesis that the morphological defects and irregular distribution of the antibody in the IPI 6.7 formulation may result in an accelerated and less controlled release of the therapeutic agent from the fibre. The release profile of IPI 8.3, on the other hand, shows promise for the sustained delivery of ipilimumab. It should be noted, however, that neither of the formulations released their complete drug cargo within 16 days and therefore long-term release profiles should be established to characterise the release

kinetics more accurately. Here, a nonionic surfactant (Tween® 80) was added to the release medium to enhance wetting of the hydrophobic PCL shell. This will have accelerated fibre degradation and antibody release, allowing quantification within a relatively short timeframe of two weeks. Future experiments should include further optimisation of the protein release study to mimic the tumour microenvironment more accurately and exclude the need for detergent supplementation of the release medium.

Ipilimumab released from the fibres was analysed with SDS-PAGE, followed by Coomasie staining to investigate the protein stability (Figure 6.8).

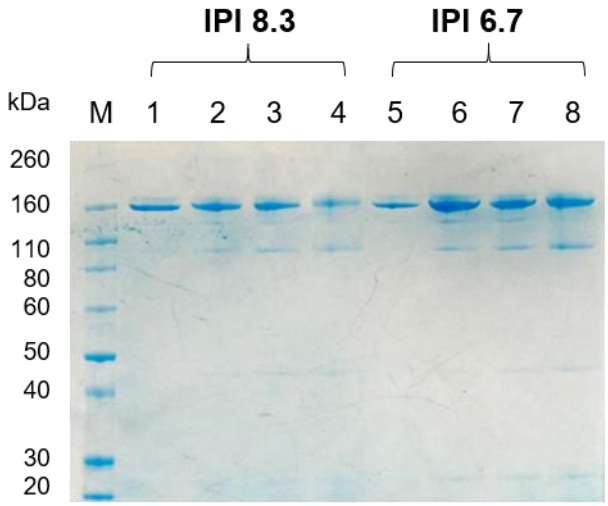

Figure 6-8: Photograph of a Novex Bis-Tris 4-12% gel showing ipilimumab collected from the release studies. Lanes are labelled as follows: M - molecular weight standard; Lane 1: control ipilimumab solution at pH 8.3; lanes 2, 3, 4 – supernatant of IPI 8.3 release at days 2, 6, 10 respectively; lane 5 – control ipilimumab solution at pH 6.7; lanes 6, 7, 8 - supernatant of IPI 6.7 release at days 2, 6, 10 respectively. Similar results were obtained from three batches of each fibre formulation, and the results of one representative experiment are shown.

Lanes 1 and 5 serve as controls for IPI 8.3 and IPI 6.7, respectively, and show the intact ipilimumab solutions used for the fabrication of the loaded electrospun fibres. Lanes 2-4 show the supernatant of IPI8.3 release study at days 2, 6, and 10. A large proportion of the intact antibody is still present, with bright blue lines visible at around ~150 kDa. However, the appearance of faint bands at 110 and 50 kDa may suggest some level of antibody fragmentation[332]. A similar trend is observed for IPI 6.7 release

supernatants (lanes 6-8 for days 2, 6, 10, respectively), however, the extent of protein fragmentation is considerably higher than in IPI 8.3.

The antibody fragmentation observed in the release study supernatants could also be a result of the inclusion of a nonionic surfactant, Tween® 80, in the release medium. Although the addition of Tween® 20 or Tween® 80 at low concentrations (0.01-0.05%) has been associated with protection against aggregation in protein solutions, at higher concentrations the detergents may cause protein unfolding.[333]

Due to limited literature on the localised delivery of anti-CTLA-4 antibodies, it is difficult to estimate the preferred duration of action of such implants at the tumour resection site. Previous publications explored the antibody release over 60 days[80] or 2 weeks[81]. Future *in vitro* CTLA-4 blockade experiments could potentially aid the selection of a favourable antibody release profile by establishing the therapeutic window needed to elicit responses in immune cells. As the core-shell electrospinning process described above can be easily tweaked to increase or decrease antibody loading, the release profiles may be tuned to match the intended application.

6.4 Conclusions

The results presented in this chapter suggest successful fabrication of ipilimumab-eluting electrospun PCL fibres that could potentially be used for sustained delivery of checkpoint inhibitors at the tumour site. PCL scaffolds were prepared using coaxial electrospinning, and the effect of the pH of the aqueous antibody core solution on the fabrication process and material performance was investigated.

It became apparent that adjusting the pH to the isoelectric point of ipilimumab results in the formation of uniform fibres with a clear core-shell structure. On the other hand, a core solution at lower pH (6.7) destabilises the electrospinning process, causing

irregular morphology of the fibres and migration of the antibody towards the polymer shell, as observed with TEM and XPS.

The release of ipilimumab from both formulations was compared in a 16-day study. The formulation spun at pH 8.3 showed more sustained release, reaching ~30% at day 10. Further investigation of long-term release profiles should be performed in a more biorelevant dissolution model to allow for further analysis of the release kinetics. Nevertheless, in these preliminary studies, the electrospun ipilimumab-loaded PCL scaffolds show promise for sustained and controlled delivery of immunotherapeutics, with little or no damage to the encapsulated monoclonal antibody being evident.

Chapter 7 – Conclusions and future work

7.1 Summary of research findings

The work described in this thesis explores the feasibility of using antibody-functionalised biomaterials to address critical issues associated with modern cancer immunotherapies. In recent years there has been growing interest in harnessing the immune system for fighting cancer. In particular, adoptive T cell therapy has been widely explored. A common obstacle to the widespread use of cell therapies is the manufacturing complexity associated with them. To overcome this, a number of approaches have been applied and the existing literature in the field suggests that it is possible to potentiate T cell responses directly *in vivo*, without the need for *ex vivo* processing of T cells in a laboratory setting. In nature, T cells become activated upon contact with antigen presenting cells, and it may be possible to mimic this interaction using biomaterials surface-functionalised with T cell stimulating molecules, such as anti-CD3 antibodies.

Therefore, Chapter 3 explored the feasibility of surface functionalisation of electrospun PCL nanoscaffolds with antibodies using perfluorophenyl azide chemistry. This method of surface modification is relatively unexplored, hence extensive optimisation experiments were carried out before attempting the attachment of the target (OKT3) antibody. The work presented addresses several knowledge gaps in the field, for example by testing the potential cytotoxicity of PFPA-NHS in Caco-2 cells and by exploring the effect of PFPA-NHS functionalisation on the biological

activity of the protein being conjugated. A model enzyme, catalase, was successfully attached to the surface of PCL fibres using PFPA-NHS with no negative impact on its activity, as measured by catalase activity assay. The covalently conjugated catalase released from the fibres at a much slower rate than physically adsorbed catalase, revealing this approach to be suitable for safe and effective attachment of proteins to hydrocarbon-based biomaterials.

For the first time, the conjugation of antibodies *via* PFPA-NHS was next attempted. The PFPA-NHS chemistry was used to attach a model (infliximab) and the target T cell-activating antibody (OKT3) to the surface of electrospun PCL patches. Such an antibody-decorated scaffold could be implanted at the tumour resection site for promoting T cell activation and proliferation. However, the scaffolds did not stimulate T cell activation as effectively as the positive control of plate-bound antibody. It is possible that the conjugated antibody was buried deep into the nanofibrous mesh and therefore inaccessible for T cells to interact with. It was then hypothesised that using a biomaterial resembling T cells in size and shape may lead to a better performance *in vitro* and, subsequently, *in vivo.*

To address this, two chapters of this thesis explored the development of polymeric microparticles surface-functionalised with OKT3. The particles were fabricated by electrospraying of biodegradable polymers and functionalised using either perfluorophenyl azide chemistry (Chapter 4) or strain-promoted azide-alkyne cycloaddition (Chapter 5). The morphological and physicochemical properties of particle-antibody conjugates were extensively characterised using SEM, FTIR and XPS. In Chapter 4, PCL microparticles were prepared by electrospraying. The standard method of top-down electrospraying generated aggregated microspheres and therefore several modifications of the electrospraying setup were explored to yield separated particles. The method of electrospraying into liquid nitrogen

was conceptually interesting, but further improvements to the experimental design need to be introduced to increase the yield of produced particles.

PFPA-NHS was undetectable with FTIR and only trace amounts of fluorine and nitrogen were found in XPS survey spectra, which suggests that the extent of the surface functionalisation was rather low. However, the visual confirmation of surface antibody attachment conducted using fluorescently-labelled reagents confirmed the results previously obtained for PFPA-NHS functionalised fibres (Chapter 3). Surface protein loading was successfully quantified by depletion. Finally, *in vitro* T cell behaviour following stimulation with antibody-functionalised microparticles was explored in both cell line (Jurkat cells) and human PBMC-derived T cell activation models.

In human PBMC-derived CD3+ T cell studies conducted in Chapter 4, the screening of three activation markers and proliferation showed superior results when the antibody was delivered on the surface of spherical electrosprayed particles, as opposed to the tissue culture plastic flat substrate. The effect of particle size was investigated, showing enhanced T cell activation when smaller (~2 μm) and separated microparticles were used, as opposed to larger (~ 7 μm) and more aggregated ones. It should be noted that the flow cytometry experiments were severely affected by the interference of the microparticles which could not be safely separated from the cells and therefore created noise in forward scatter vs side scatter plots.

In Chapter 5, conjugation of the anti-CD3 OKT3 antibody to polymeric particles using strain-promoted azide-alkyne cycloaddition (SPAAC) was successfully achieved. Azide-bearing PCL particles capable of undergoing SPAAC with fluorescently-labelled model molecules were prepared using electrospraying and showed no cytotoxicity in Jurkat cells. It was, however, impossible to confirm the azide groups presence using spectroscopical methods. Additionally, the OKT3 antibody was

successfully modified by bis-sulfone-PEG-DBCO conjugation, with no detriment to biological activity. Both components of the SPAAC reaction were developed using novel protocols, with no precedence in current literature. The antibody-particle conjugates were extensively tested in human PBMC-derived CD3+ T cells and showed a positive effect on T cell proliferation and cytokine production.

Taken together, the results of Chapter 4 and Chapter 5 show that it is possible to conjugate antibodies to the surface of electrosprayed PCL particles, and that such antibody-particle conjugates are capable of potentiating the activation and proliferation of human CD3+ T cells.

The final experimental chapter of this thesis tackled another commonly encountered challenge in cancer immunotherapy. Checkpoint inhibitor monoclonal antibodies, although capable of reducing tumour sizes, are associated with serious immune-related side-effects when administered intravenously. The off-target toxicity profile often prevents these agents from reaching the market. Chapter 6 therefore aimed to prepare implantable and biodegradable electrospun formulations of an anti-CTLA-4 antibody, ipilimumab, for sustained release of this immune checkpoint inhibitors near to the tumour site. The ipilimumab-loaded fibre formulation was prepared using the core-shell electrospinning technology. This study built on the existing literature, confirming that electrospinning monoclonal antibodies near to their isoelectric point leads to improved process stability and enhanced protein encapsulation. Moreover, such formulated antibody retains its structural integrity and releases from the scaffold in a sustained fashion. On the other hand, the formulation prepared from a solution at a lower pH (~ 6.7) resulted in the formation of irregular fibres with an unfavourable release profile. At the isoelectric point proteins carry zero net charge, therefore limiting protein migration from the core to the shell solution. This protects the delicate protein cargo from accidental damage due to solvent exposure during the electrospinning process. The results of this chapter suggest that core-shell

electrospinning technology can be used for the formulation of pharmaceutically relevant monoclonal antibodies within implantable and biodegradable scaffolds for a safe and localised protein delivery.

7.2 Future work

The results presented in this thesis provide information on the development of protein-bearing biomaterials for various pharmaceutical applications. Nevertheless, further experiments are required to further optimise the developed formulations.

The PFPA-NHS functionalisation approach could be of great potential in applications where a prolonged presentation of protein on the surface is required, for example in the design of growth factor-decorated implantable scaffolds. Therefore, it would be interesting to explore the attachment of growth factors to the surface of electrospun PCL patches, e.g. for applications in nerve regeneration.

The antibody-functionalised particles developed in Chapter 4 showed promise in a PBMC-derived T cell activation model, but the particles were incubated with cells for a relatively short period of time (4 days). Within this timeframe it was impossible to distinguish between the efficacy of physisorbed and covalently attached antibody-particle formulations. It is anticipated that the covalently attached antibody will be presented on the particle surface for a prolonged period of time, therefore eliciting an extended response in T cells. To test this hypothesis, a long-term (14-21 days) T cell activation experiment should be conducted, taking into account possible T cell exhaustion caused by prolonged overstimulation of naïve T cells.

Chapter 5 reported a study on the preparation of azide-bearing PCL microparticles *via* electrospraying. However, further process optimisation is required to improve the size and morphology of the fabricated microparticles. For the intended application in T cell activation, a mean particle diameter of below 10 μm would be of benefit.

Moreover, the DBCO modification of the target antibody (OKT3) could be improved by introducing further purification steps, for example using ion exchange chromatography. Further investigation into the structure of DBCO-OKT3 (e.g. by circular dichroism) is needed to characterise the conjugate. Taken together, the knowledge gained in further experiments will allow for more accurate analysis of the efficiency of the SPAAC reaction occurring between the PCL-N_3 particle and DBCO-OKT3 antibody.

In Chapter 6, further investigation of long-term release profiles should be performed in a more biorelevant dissolution model to allow for further analysis of the release kinetics. The retention of biological activity of the formulated antibodies could be tested using surface plasmon resonance (SPR) or ELISA. The ipilimumab-loaded fibres could also be tested in *in vitro* and *in vivo* experiments. For example, a commercially available CTLA-4 blockade bioassay could be used to measure the potency and stability of CTLA-4 targeting antibodies in an assay using two engineered cell lines (CTLA-4 effector cells and aAPC/Raji cells). If successful, the formulation could be tested further in human PBMC-derived co-culture T cell suppression assays.

The feasibility of core-shell electrospinning as a platform technology for the encapsulation of monoclonal antibodies for various pharmaceutical applications is further verified in this work. Fibre fabrication and the characterisation of protein release and stability could be performed using additional model antibodies, for example nivolumab (anti-PD-1) or infliximab (anti-TNF-α). The project would also benefit from an investigation into the process scale-up. This could be achieved by using a climate-controlled Bioinicia Fluidnatek LE-50 electrospinning machine which resembles the equipment used by Bioinicia in their GMP facility, allowing for an immediate transition into scalable clinical-grade GMP manufacture if the antibody-loaded scaffolds show promise in pre-clinical studies.

Bibliography

1. Finn, O. J. Immuno-oncology: understanding the function and dysfunction of the immune system in cancer. *Ann. Oncol.* **23**, viii6–viii9 (2012).

2. Hanahan, D. & Weinberg, R. A. The hallmarks of cancer. *Cell* **100**, 57–70 (2000).

3. Hanahan, D. & Weinberg, R. A. Hallmarks of cancer: The next generation. *Cell* **144**, 646–674 (2011).

4. Fridman, W. H., Pagès, F., Sautès-Fridman, C. & Galon, J. The immune contexture in human tumours: Impact on clinical outcome. *Nat. Rev. Cancer* **12**, 298–306 (2012).

5. Dempke, W. C. M., Fenchel, K., Uciechowski, P. & Dale, S. P. Second- and third-generation drugs for immuno-oncology treatment-The more the better? *Eur. J. Cancer* **74**, 55–72 (2017).

6. Strokotov, D. I. *et al.* Is there a difference between T- and B-lymphocyte morphology? *J. Biomed. Opt.* **14**, 1–12 (2009).

7. Banchereau, J. & Steinman, R. M. Dendritic cells and the control of immunity. *Nature* **392**, 245–252 (1998).

8. Sharpe, M. & Mount, N. Genetically modified T cells in cancer therapy: opportunities and challenges. *Dis. Model. Mech.* **8**, 337–350 (2015).

9. Esensten, J. H., Helou, Y. A., Chopra, G., Weiss, A. & Bluestone, J. A. CD28 costimulation: from mechanism to therapy (Author Manuscript). *Immunity* **30**, 6347–6358 (2016).

10. Andersen, M. H., Schrama, D., Thor Straten, P. & Becker, J. C. Cytotoxic T cells. *J. Invest. Dermatol.* **126**, 32–41 (2006).

11. Vinay, D. S. & Kwon, B. S. 4-1BB (CD137), an inducible costimulatory receptor, as a specific target for cancer therapy. *BMB Rep.* **47**, 122–129 (2014).

12. Mescher, M. F. Surface contact requirements for activation of cytotoxic T lymphocytes. *J. Immunol.* **149**, 2402 LP – 2405 (1992).

13. Curtsinger, J. M. *et al.* Inflammatory cytokines provide a third signal for activation of naive CD4+ and CD8+ T cells. *J. Immunol.* **162**, 3256–62 (1999).

14. Kim, J. V., Latouche, J. B., Rivière, I. & Sadelain, M. The ABCs of artificial antigen presentation. *Nat. Biotechnol.* **22**, 403–410 (2004).

15. Hombach, A. *et al.* T-cell activation by recombinant receptors: CD28 costimulation is required for interleukin 2 secretion and receptor-mediated T-cell proliferation but does not affect receptor-mediated target cell lysis. *Cancer Res.* **61**, 1976–1982 (2001).

16. Mougiakakos, D., Choudhury, A., Lladser, A., Kiessling, R. & Johansson, C. C. Chapter 3 - Regulatory T Cells in Cancer. in (eds. Vande Woude, G. F. & Klein, G. B. T.-A. in C. R.) vol. 107 57–117 (Academic Press, 2010).

17. Yang, L., Pang, Y. & Moses, H. L. TGF-β and immune cells: an important regulatory axis in the tumor microenvironment and progression. *Trends Immunol.* **31**, 220–227 (2010).

18. Oft, M. IL-10: Master Switch from Tumor-Promoting Inflammation to Antitumor Immunity. *Cancer Immunol. Res.* **2**, 194 LP – 199 (2014).

19. Mellman, I., Coukos, G. & Dranoff, G. Cancer immunotherapy comes of age. *Nature* **480**, 480–489 (2011).

20. Dougan, M. & Dranoff, G. Immune Therapy for Cancer. *Annu. Rev. Immunol.* **27**, 83–117 (2009).

21. Eggermont, A. & Finn, O. Advances in immuno-oncology. Foreword. *Annals of oncology : official journal of the European Society for Medical Oncology* vol. 23 Suppl 8 viii5 (2012).

22. Couzin-Frankel, J. Cancer Immunotherapy. *Science (80-.).* **342**, 1432 LP – 1433 (2013).

23. Pardoll, D. M. The blockade of immune checkpoints in cancer immunotherapy. *Nat. Rev. Cancer* **12**, 252–264 (2012).

24. Munn, D. H. & Bronte, V. Immune suppressive mechanisms in the tumor microenvironment. *Curr. Opin. Immunol.* **39**, 1–6 (2016).

25. Alsaab, H. O. *et al.* PD-1 and PD-L1 Checkpoint Signaling Inhibition for Cancer Immunotherapy: Mechanism, Combinations, and Clinical Outcome. *Front. Pharmacol.* **8**, 561 (2017).

26. Somasundaram, R. & Herlyn, M. Nivolumab in combination with ipilimumab for the treatment of melanoma. *Expert Rev. Anticancer Ther.* **15**, 1135–1141 (2015).

27. Xie, Y.-Q., Wei, L. & Tang, L. Immunoengineering with biomaterials for enhanced cancer immunotherapy. *WIREs Nanomedicine and Nanobiotechnology* **10**, e1506 (2018).

28. Ribas, A. & Wolchok, J. D. Cancer immunotherapy using checkpoint blockade. *Science (80-.).* **359**, 1350 LP – 1355 (2018).

29. Francis, D. M. & Thomas, S. N. Progress and opportunities for enhancing the delivery and efficacy of checkpoint inhibitors for cancer immunotherapy. *Adv. Drug Deliv. Rev.* **114**, 33–42 (2017).

30. Riley, R. S., June, C. H., Langer, R. & Mitchell, M. J. Delivery technologies for cancer immunotherapy. *Nat. Rev. Drug Discov.* **18**, 175–196 (2019).

31. Chambers, C. A., Kuhns, M. S., Egen, J. G. & Allison, J. P. CTLA-4-mediated inhibition in regulation of T cell responses: mechanisms and manipulation in tumor immunotherapy. *Annu. Rev. Immunol.* **19**, 565–594 (2001).

32. Phan, G. Q. *et al.* Cancer regression and autoimmunity induced by cytotoxic T lymphocyte-associated antigen 4 blockade in patients with metastatic melanoma. *Proc. Natl. Acad. Sci.* **100**, 8372 LP – 8377 (2003).

33. Farkona, S., Diamandis, E. P. & Blasutig, I. M. Cancer immunotherapy: the beginning of the end of cancer? *BMC Med.* **14**, 73 (2016).

34. Postow, M. A., Sidlow, R. & Hellmann, M. D. Immune-Related Adverse Events Associated with Immune Checkpoint Blockade. *N. Engl. J. Med.* **378**, 158–168 (2018).

35. Hodi, F. S. *et al.* Improved survival with ipilimumab in patients with metastatic melanoma. *N. Engl. J. Med.* **363**, 711–723 (2010).

36. Francisco, L. M. *et al.* PD-L1 regulates the development, maintenance, and function of induced regulatory T cells. *J. Exp. Med.* **206**, 3015–3029 (2009).

37. Keir, M. E., Butte, M. J., Freeman, G. J. & Sharpe, A. H. PD-1 and its ligands in tolerance and immunity. *Annu. Rev. Immunol.* **26**, 677–704 (2008).

38. Topalian, S. L. *et al.* Safety, Activity, and Immune Correlates of Anti–PD-1 Antibody in Cancer. *N. Engl. J. Med.* **366**, 2443–2454 (2012).

39. Wolchok, J. D. *et al.* Nivolumab plus ipilimumab in advanced melanoma. *N. Engl. J.*

Med. **369**, 122–133 (2013).

40. Larkin, J. *et al.* Combined Nivolumab and Ipilimumab or Monotherapy in Untreated Melanoma. *N. Engl. J. Med.* **373**, 23–34 (2015).

41. AstraZeneca.com. Imfinzi and tremelimumab granted Orphan Drug Designation in the US for liver cancer. https://www.astrazeneca.com/media-centre/press-releases/2020/imfinzi-and-tremelimumab-granted-orphan-drug-designation-in-the-us-for-liver-cancer-20012020.html.

42. Boutros, C. *et al.* Safety profiles of anti-CTLA-4 and anti-PD-1 antibodies alone and in combination. *Nat. Rev. Clin. Oncol.* **13**, 473–486 (2016).

43. Kourie, H. R. & Klastersky, J. A. Side-effects of checkpoint inhibitor-based combination therapy. *Curr. Opin. Oncol.* **28**, (2016).

44. Jiang, W. *et al.* Designing nanomedicine for immuno-oncology. *Nat. Biomed. Eng.* **1**, 29 (2017).

45. Guedan, S., Ruella, M. & June, C. H. Emerging Cellular Therapies for Cancer. *Annu. Rev. Immunol.* **37**, 145–171 (2018).

46. Scheetz, L. *et al.* Engineering patient-specific cancer immunotherapies. *Nat. Biomed. Eng.* **3**, 768–782 (2019).

47. Approved Cellular and Gene Therapy Products. https://www.fda.gov/vaccines-blood-biologics/cellular-gene-therapy-products/approved-cellular-and-gene-therapy-products.

48. Gilboa, E., Nair, S. K. & Lyerly, H. K. Immunotherapy of cancer with dendritic-cell-based vaccines. *Cancer Immunol. Immunother.* **46**, 82–87 (1998).

49. Wong, K. K., Li, W. A., Mooney, D. J. & Dranoff, G. Chapter Five - Advances in Therapeutic Cancer Vaccines. in *Tumor Immunology* (ed. Schreiber, R. D. B. T.-A. in I.) vol. 130 191–249 (Academic Press, 2016).

50. Garg, A. D., Coulie, P. G., Van den Eynde, B. J. & Agostinis, P. Integrating Next-Generation Dendritic Cell Vaccines into the Current Cancer Immunotherapy Landscape. *Trends Immunol.* **38**, 577–593 (2017).

51. Palucka, K. & Banchereau, J. Dendritic-Cell-Based Therapeutic Cancer Vaccines. *Immunity* **39**, 38–48 (2013).

52. Anassi, E. & Ndefo, U. A. Sipuleucel-T (provenge) injection: the first immunotherapy

agent (vaccine) for hormone-refractory prostate cancer. *P T* **36**, 197–202 (2011).

53. Kantoff, P. W. *et al.* Sipuleucel-T Immunotherapy for Castration-Resistant Prostate Cancer. *N. Engl. J. Med.* **363**, 411–422 (2010).

54. Excellence, N. I. for H. and C. Sipuleucel-T for treating asymptomatic or minimally symptomatic metastatic hormone-relapsed prostate cancer. 1–60 (2015).

55. Conry, R. M., Westbrook, B., McKee, S. & Norwood, T. G. Talimogene laherparepvec: First in class oncolytic virotherapy. *Hum. Vaccin. Immunother.* **14**, 839–846 (2018).

56. Melcher, A., Parato, K., Rooney, C. M. & Bell, J. C. Thunder and lightning: immunotherapy and oncolytic viruses collide. *Mol. Ther.* **19**, 1008–1016 (2011).

57. Choi, I.-K. *et al.* Oncolytic adenovirus co-expressing IL-12 and IL-18 improves tumor-specific immunity via differentiation of T cells expressing IL-12Rβ2 or IL-18Rα. *Gene Ther.* **18**, 898–909 (2011).

58. Huang, J.-H. *et al.* Therapeutic and Tumor-specific Immunity Induced by Combination of Dendritic Cells and Oncolytic Adenovirus Expressing IL-12 and 4-1BBL. *Mol. Ther.* **18**, 264–274 (2010).

59. European Medicines Agency. First oncolytic immunotherapy medicine recommended for approval. **44**, (2015).

60. Kohlhapp, F. J. & Kaufman, H. L. Molecular Pathways: Mechanism of Action for Talimogene Laherparepvec, a New Oncolytic Virus Immunotherapy. *Clin. Cancer Res.* **22**, 1048 LP – 1054 (2016).

61. Clinicaltrials.gov search of 'oncolytic virus'. https://clinicaltrials.gov/ct2/results?term=oncolytic+virus&Search=Apply&recrs=b&recrs=a&recrs=d&age_v=&gndr=&type=&rslt=.

62. Zheng, M., Huang, J., Tong, A. & Yang, H. Oncolytic Viruses for Cancer Therapy: Barriers and Recent Advances. *Mol. Ther. - Oncolytics* **15**, 234–247 (2019).

63. Kaufman, H. L., Kohlhapp, F. J. & Zloza, A. Oncolytic viruses: a new class of immunotherapy drugs. *Nat. Rev. Drug Discov.* **14**, 642–662 (2015).

64. Ruella, M. & Kalos, M. Adoptive immunotherapy for cancer. *Immunol. Rev.* **257**, 14–38 (2014).

65. Weber, J. S., Yang, J. C., Atkins, M. B. & Disis, M. L. Toxicities of immunotherapy for the practitioner. *J. Clin. Oncol.* **33**, 2092–2099 (2015).

66. Sadelain, M., Brentjens, R. & Riviere, I. The basic principles of chimeric antigen receptor (CAR) design. *Cancer Discov.* **3**, 388–398 (2013).

67. Dunn, Z. S., Mac, J. & Wang, P. T cell immunotherapy enhanced by designer biomaterials. *Biomaterials* **217**, 119265 (2019).

68. Levine, B. L., Miskin, J., Wonnacott, K. & Keir, C. Global Manufacturing of CAR T Cell Therapy. *Mol. Ther. Methods Clin. Dev.* **4**, 92–101 (2016).

69. Yarchoan, M., Hopkins, A. & Jaffee, E. M. Tumor Mutational Burden and Response Rate to PD-1 Inhibition. *N. Engl. J. Med.* **377**, 2500–2501 (2017).

70. Sambi, M., Bagheri, L. & Szewczuk, M. R. Current Challenges in Cancer Immunotherapy: Multimodal Approaches to Improve Efficacy and Patient Response Rates. *J. Oncol.* **2019**, 4508794 (2019).

71. Goldberg, M. S. Improving cancer immunotherapy through nanotechnology. *Nat. Rev. Cancer* **19**, 587–602 (2019).

72. Dellacherie, M. O., Seo, B. R. & Mooney, D. J. Macroscale biomaterials strategies for local immunomodulation. *Nat. Rev. Mater.* **4**, 379–397 (2019).

73. Cheung, A. S. & Mooney, D. J. Engineered materials for cancer immunotherapy. *Nano Today* **10**, 511–531 (2015).

74. Gu, L. & Mooney, D. J. Biomaterials and emerging anticancer therapeutics: engineering the microenvironment. *Nat. Rev. Cancer* **16**, 56–66 (2015).

75. Meyer, R. A., Sunshine, J. C. & Green, J. J. Biomimetic particles as therapeutics. *Trends Biotechnol.* **33**, 514–524 (2015).

76. Ben-Akiva, E., Est Witte, S., Meyer, R. A., Rhodes, K. R. & Green, J. J. Polymeric micro- and nanoparticles for immune modulation. *Biomater. Sci.* **7**, 14–30 (2019).

77. Ben-Akiva, E., Meyer, R. A., Wilson, D. R. & Green, J. J. Surface engineering for lymphocyte programming. *Advanced Drug Delivery Reviews* (2017) doi:10.1016/j.addr.2017.05.005.

78. Riley, R. S., June, C. H., Langer, R. & Mitchell, M. J. Delivery technologies for cancer immunotherapy. *Nat. Rev. Drug Discov.* **18**, 175–196 (2019).

79. Vonderheide, R. H. *et al.* Clinical activity and immune modulation in cancer patients treated with CP-870,893, a novel CD40 agonist monoclonal antibody. *J. Clin. Oncol. Off. J. Am. Soc. Clin. Oncol.* **25**, 876–883 (2007).

80. Rahimian, S. *et al.* Polymeric microparticles for sustained and local delivery of antiCD40 and antiCTLA-4 in immunotherapy of cancer. *Biomaterials* **61**, 33–40 (2015).

81. Wang, C., Ye, Y., Hochu, G. M., Sadeghifar, H. & Gu, Z. Enhanced Cancer Immunotherapy by Microneedle Patch-Assisted Delivery of Anti-PD1 Antibody. *Nano Lett.* **16**, 2334–2340 (2016).

82. Wang, C., Ye, Y. & Gu, Z. Local delivery of checkpoints antibodies. *Hum. Vaccin. Immunother.* **13**, 245–248 (2017).

83. Li, Y. *et al.* Hydrogel dual delivered celecoxib and anti-PD-1 synergistically improve antitumor immunity. *Oncoimmunology* **5**, e1074374–e1074374 (2015).

84. Ali, O. A., Huebsch, N., Cao, L., Dranoff, G. & Mooney, D. J. Infection-mimicking materials to program dendritic cells in situ. *Nat. Mater.* **8**, 151–158 (2009).

85. Kim, J., Li, W. A., Sands, W. & Mooney, D. J. Effect of pore structure of macroporous poly(lactide-co-glycolide) scaffolds on the in vivo enrichment of dendritic cells. *ACS Appl. Mater. Interfaces* **6**, 8505–8512 (2014).

86. Ali, O. A., Lewin, S. A., Dranoff, G. & Mooney, D. J. Vaccines Combined with Immune Checkpoint Antibodies Promote Cytotoxic T-cell Activity and Tumor Eradication. *Cancer Immunol. Res.* **4**, 95–100 (2016).

87. Clinicaltrials.gov. Dendritic Cell Activating Scaffold in Melanoma. https://clinicaltrials.gov/ct2/show/NCT01753089?term=WDVAx&draw=2&rank=1.

88. Kim, J. *et al.* Injectable, spontaneously assembling, inorganic scaffolds modulate immune cells in vivo and increase vaccine efficacy. *Nat. Biotechnol.* **33**, 64–72 (2015).

89. Qiu, F. *et al.* Poly(propylacrylic acid)-peptide nanoplexes as a platform for enhancing the immunogenicity of neoantigen cancer vaccines. *Biomaterials* **182**, 82–91 (2018).

90. Cui, L., Osada, K., Imaizumi, A., Kataoka, K. & Nakano, K. Feasibility of a subcutaneously administered block/homo-mixed polyplex micelle as a carrier for DNA vaccination in a mouse tumor model. *J. Control. Release* **206**, 220–231 (2015).

91. Keller, S. *et al.* Neutral polymer micelle carriers with pH-responsive, endosome-releasing activity modulate antigen trafficking to enhance CD8+ T cell responses. *J. Control. Release* **191**, 24–33 (2014).

92. Tjomsland, V. *et al.* Semi mature blood dendritic cells exist in patients with ductal pancreatic adenocarcinoma owing to inflammatory factors released from the tumor. *PLoS One* **5**, e13441–e13441 (2010).

93. Deicher, A. *et al.* Targeting dendritic cells in pancreatic ductal adenocarcinoma. *Cancer Cell Int.* **18**, 85 (2018).

94. Curiel, T. J. *et al.* Blockade of B7-H1 improves myeloid dendritic cell–mediated antitumor immunity. *Nat. Med.* **9**, 562–567 (2003).

95. Wang, H. & Mooney, D. J. Biomaterial-assisted targeted modulation of immune cells in cancer treatment. *Nat. Mater.* **17**, 761–772 (2018).

96. Stephan, S. B. *et al.* Biopolymer implants enhance the efficacy of adoptive T-cell therapy. *Nat Biotech* **33**, 97–101 (2015).

97. Stephan, M. T., Moon, J. J., Um, S. H., Bershteyn, A. & Irvine, D. J. Therapeutic cell engineering with surface-conjugated synthetic nanoparticles. *Nat Med* **16**, 1035–1041 (2010).

98. Zhang, F. *et al.* Nanoparticles That Reshape the Tumor Milieu Create a Therapeutic Window for Effective T-cell Therapy in Solid Malignancies. *Cancer Res.* **78**, 3718–3730 (2018).

99. Zheng, Y. *et al.* In vivo targeting of adoptively transferred T-cells with antibody- and cytokine-conjugated liposomes. *J. Control. Release* **172**, 426–435 (2013).

100. Coon, M. E., Stephan, S. B., Gupta, V., Kealey, C. P. & Stephan, M. T. Nitinol thin films functionalized with CAR-T cells for the treatment of solid tumours. *Nat. Biomed. Eng.* **4**, 195–206 (2020).

101. Abastado, J. P., Lone, Y. C., Casrouge, A., Boulot, G. & Kourilsky, P. Dimerization of soluble major histocompatibility complex-peptide complexes is sufficient for activation of T cell hybridoma and induction of unresponsiveness. *J. Exp. Med.* **182**, 439–447 (1995).

102. Ge, Q. *et al.* Soluble peptide–MHC monomers cause activation of CD8+ T cells through transfer of the peptide to T cell MHC molecules. *Proc. Natl. Acad. Sci.* **99**, 13729 LP – 13734 (2002).

103. Hamad, A. R. *et al.* Potent T cell activation with dimeric peptide-major histocompatibility complex class II ligand: the role of CD4 coreceptor. *J. Exp. Med.* **188**, 1633–1640 (1998).

104. Hasan, A. N., Selvakumar, A. & O'Reilly, R. J. Artificial Antigen Presenting Cells: An Off the Shelf Approach for Generation of Desirable T-Cell Populations for Broad Application of Adoptive Immunotherapy. *Adv. Genet. Eng.* **4**, 130 (2015).

105. Fadel, T. R. *et al.* A carbon nanotube-polymer composite for T-cell therapy. *Nat. Nanotechnol.* **9**, 639–647 (2014).

106. Perica, K. *et al.* Nanoscale artificial antigen presenting cells for T cell immunotherapy. *Nanomedicine Nanotechnology, Biol. Med.* **10**, 119–129 (2014).

107. van der Weijden, J., Paulis, L. E., Verdoes, M., van Hest, J. C. M. & Figdor, C. G. The right touch: design of artificial antigen-presenting cells to stimulate the immune system. *Chem. Sci.* **5**, 3355–3367 (2014).

108. Siefert, A. L., Fahmy, T. M. & Kim, D. Artificial Antigen-Presenting Cells for Immunotherapies BT - Cancer Nanotechnology: Methods and Protocols. in (ed. Zeineldin, R.) 343–353 (Springer New York, 2017). doi:10.1007/978-1-4939-6646-2_21.

109. Wang, C., Ye, Y., Hu, Q., Bellotti, A. & Gu, Z. Tailoring Biomaterials for Cancer Immunotherapy: Emerging Trends and Future Outlook. *Adv. Mater.* **29**, 1606036 (2017).

110. Xie, J., Jiang, J., Davoodi, P., Srinivasan, M. P. & Wang, C.-H. Electrohydrodynamic atomization: A two-decade effort to produce and process micro-/nanoparticulate materials. *Chem. Eng. Sci.* **125**, 32–57 (2015).

111. Chiu, Y.-J. *et al.* The Effect of Solvent Vapor Annealing on Drug-Loaded Electrospun Polymer Fibers. *Pharmaceutics* vol. 12 (2020).

112. Angkawinitwong, U., Awwad, S., Khaw, P. T., Brocchini, S. & Williams, G. R. Electrospun formulations of bevacizumab for sustained release in the eye. *Acta Biomater.* **64**, 126–136 (2017).

113. Williams, G. R., Raimi-Abraham, B. T. & Luo, C. J. *Nanofibres in Drug Delivery*. (UCL Press, 2018).

114. Yarin, A. L., Koombhongse, S. & Reneker, D. H. Taylor cone and jetting from liquid droplets in electrospinning of nanofibers. *J. Appl. Phys.* **90**, 4836–4846 (2001).

115. Yu, D.-G., Li, J.-J., Zhang, M. & Williams, G. R. High-quality Janus nanofibers prepared using three-fluid electrospinning. *Chem. Commun.* **53**, 4542–4545 (2017).

116. Frizzell, H., Ohlsen, T. J. & Woodrow, K. A. Protein-loaded emulsion electrospun fibers optimized for bioactivity retention and pH-controlled release for peroral delivery of biologic therapeutics. *Int. J. Pharm.* **533**, 99–110 (2017).

117. Makadia, H. K. & Siegel, S. J. Poly Lactic-co-Glycolic Acid (PLGA) as Biodegradable

Controlled Drug Delivery Carrier. *Polymers (Basel).* **3**, 1377–1397 (2011).

118. Gentile, P., Chiono, V., Carmagnola, I. & Hatton, P. V. An overview of poly(lactic-co-glycolic) Acid (PLGA)-based biomaterials for bone tissue engineering. *Int. J. Mol. Sci.* **15**, 3640–3659 (2014).

119. Anderson, J. M. & Shive, M. S. Biodegradation and biocompatibility of PLA and PLGA microspheres. *Adv. Drug Deliv. Rev.* **64**, 72–82 (2012).

120. Labet, M. & Thielemans, W. Synthesis of polycaprolactone: a review. *Chem. Soc. Rev.* **38**, 3484–3504 (2009).

121. Fu, K., Pack, D. W., Klibanov, A. M. & Langer, R. Visual Evidence of Acidic Environment Within Degrading Poly(lactic-co-glycolic acid) (PLGA) Microspheres. *Pharm. Res.* **17**, 100–106 (2000).

122. Houchin, M. L. & Topp, E. M. Chemical Degradation of Peptides and Proteins in PLGA: A Review of Reactions and Mechanisms. *J. Pharm. Sci.* **97**, 2395–2404 (2008).

123. Castilla-Cortázar, I. *et al.* Hydrolytic and enzymatic degradation of a poly(ε-caprolactone) network. *Polym. Degrad. Stab.* **97**, 1241–1248 (2012).

124. Luo, C. J., Nangrejo, M. & Edirisinghe, M. A novel method of selecting solvents for polymer electrospinning. *Polymer (Guildf).* **51**, 1654–1662 (2010).

125. Shenoy, S. L., Bates, W. D., Frisch, H. L. & Wnek, G. E. Role of chain entanglements on fiber formation during electrospinning of polymer solutions: good solvent, non-specific polymer–polymer interaction limit. *Polymer (Guildf).* **46**, 3372–3384 (2005).

126. Fridrikh, S. V, Yu, J. H., Brenner, M. P. & Rutledge, G. C. Controlling the Fiber Diameter during Electrospinning. *Phys. Rev. Lett.* **90**, 144502 (2003).

127. Ekaputra, A. K., Prestwich, G. D., Cool, S. M. & Hutmacher, D. W. The three-dimensional vascularization of growth factor-releasing hybrid scaffold of poly (e{open}-caprolactone)/collagen fibers and hyaluronic acid hydrogel. *Biomaterials* **32**, 8108–8117 (2011).

128. Seif, S., Planz, V. & Windbergs, M. Delivery of Therapeutic Proteins Using Electrospun Fibers—Recent Developments and Current Challenges. *Arch. Pharm. (Weinheim).* **350**, 1–8 (2017).

129. Awwad, S. & Angkawinitwong, U. Overview of antibody drug delivery. *Pharmaceutics* **10**, 83 (2018).

130. Ye, C. & Chi, H. A review of recent progress in drug and protein encapsulation: Approaches, applications and challenges. *Mater. Sci. Eng. C* **83**, 233–246 (2018).

131. Buzgo, M., Mickova, A., Rampichova, M. & Doupnik, M. 11 - Blend electrospinning, coaxial electrospinning, and emulsion electrospinning techniques. in *Woodhead Publishing Series in Biomaterials* (eds. Focarete, M. L. & Tampieri, A. B. T.-C.-S. N. for D. D. and T.) 325–347 (Woodhead Publishing, 2018). doi:https://doi.org/10.1016/B978-0-08-102198-9.00011-9.

132. Mickova, A. *et al.* Core/Shell Nanofibers with Embedded Liposomes as a Drug Delivery System. *Biomacromolecules* **13**, 952–962 (2012).

133. Vysloužilová, L. *et al.* Needleless coaxial electrospinning: A novel approach to mass production of coaxial nanofibers. *Int. J. Pharm.* **516**, 293–300 (2017).

134. Nikmaram, N. *et al.* Emulsion-based systems for fabrication of electrospun nanofibers: food, pharmaceutical and biomedical applications. *RSC Adv.* **7**, 28951–28964 (2017).

135. Furtmann, B. *et al.* Electrospray Synthesis of Poly(lactide-co-glycolide) Nanoparticles Encapsulating Peptides to Enhance Proliferation of Antigen-Specific CD8+ T Cells. *J. Pharm. Sci.* **106**, 3316–3327 (2017).

136. Briggs, T. & Arinzeh, T. L. Examining the formulation of emulsion electrospinning for improving the release of bioactive proteins from electrospun fibers. *J. Biomed. Mater. Res. Part A* **102**, 674–684 (2014).

137. McClellan, P. & Landis, W. J. Recent Applications of Coaxial and Emulsion Electrospinning Methods in the Field of Tissue Engineering. *BioResearch open access* vol. 5 212–227 (2016).

138. Moreira, A. *et al.* Protein encapsulation by electrospinning and electrospraying. *J. Control. Release* (2020) doi:https://doi.org/10.1016/j.jconrel.2020.10.046.

139. Chen, X. *et al.* Mussel-inspired polydopamine-assisted bromelain immobilization onto electrospun fibrous membrane for potential application as wound dressing. *Mater. Sci. Eng. C* **110**, 110624 (2020).

140. Yoshida, M., Langer, R., Lendlein, A. & Lahann, J. From Advanced Biomedical Coatings to Multi-Functionalized Biomaterials. *J. Macromol. Sci. Part C* **46**, 347–375 (2006).

141. Norde, W. & Haynes, C. A. Reversibility and the Mechanism of Protein Adsorption. in *Proteins at Interfaces II* vol. 602 2–26 (American Chemical Society, 1995).

142. Mathes, J. M. Protein Adsorption to Vial Surfaces – Quantification , Structural and Mechanistic Studies. *Adsorpt. J. Int. Adsorpt. Soc.* 1–233 (2010).

143. Tsai, T., Mehta, R. C. & DeLuca, P. P. Adsorption of peptides to poly (D , L-lactide-co-glycolide): 2 . Effect of solution properties on the adsorption. *Int. J. Pharm.* **5173**, (1996).

144. Rabe, M., Verdes, D. & Seeger, S. Understanding protein adsorption phenomena at solid surfaces. *Adv. Colloid Interface Sci.* **162**, 87–106 (2011).

145. Van Der Veen, M., Norde, W. & Stuart, M. C. Electrostatic interactions in protein adsorption probed by comparing lysozyme and succinylated lysozyme. *Colloids Surfaces B Biointerfaces* **35**, 33–40 (2004).

146. Tanaka, R. *et al.* A novel enhancement assay for immunochromatographic test strips using gold nanoparticles. *Anal. Bioanal. Chem.* **385**, 1414–1420 (2006).

147. Bölgen, N., Vargel, İ., Korkusuz, P., Menceloğlu, Y. Z. & Pişkin, E. In vivo performance of antibiotic embedded electrospun PCL membranes for prevention of abdominal adhesions. *J. Biomed. Mater. Res. Part B Appl. Biomater.* **81B**, 530–543 (2007).

148. Xia, B. & Lv, Y. Dual-delivery of VEGF and NGF by emulsion electrospun nanofibrous scaffold for peripheral nerve regeneration. *Mater. Sci. Eng. C* **82**, 253–264 (2018).

149. Grafahrend, D., Heffels, K. H., Möller, M., Klee, D. & Groll, J. Electrospun, biofunctionalized fibers as tailored in vitro substrates for keratinocyte cell culture. *Macromol. Biosci.* **10**, 1022–1027 (2010).

150. Diaz-Gomez, L. *et al.* Biodegradable electrospun nanofibers coated with platelet-rich plasma for cell adhesion and proliferation. *Mater. Sci. Eng. C* **40**, 180–188 (2014).

151. Mitragotri, S., Burke, P. A. & Langer, R. Overcoming the challenges in administering biopharmaceuticals: formulation and delivery strategies. *Nat. Rev. Drug Discov.* **13**, 655–672 (2014).

152. Sivaram, A. J., Wardiana, A., Howard, C. B., Mahler, S. M. & Thurecht, K. J. Recent Advances in the Generation of Antibody–Nanomaterial Conjugates. *Adv. Healthc. Mater.* **7**, 1700607 (2018).

153. Yoo, H. S., Kim, T. G. & Park, T. G. Surface-functionalized electrospun nanofibers for tissue engineering and drug delivery. *Adv. Drug Deliv. Rev.* **61**, 1033–1042 (2009).

154. Rim, N. G. *et al.* Mussel-inspired surface modification of poly(l-lactide) electrospun fibers for modulation of osteogenic differentiation of human mesenchymal stem cells.

Colloids Surfaces B Biointerfaces **91**, 189–197 (2012).

155. Ku, S. H. & Park, C. B. Human endothelial cell growth on mussel-inspired nanofiber scaffold for vascular tissue engineering. *Biomaterials* **31**, 9431–9437 (2010).

156. Lin, C.-C. & Fu, S.-J. Osteogenesis of human adipose-derived stem cells on poly(dopamine)-coated electrospun poly(lactic acid) fiber mats. *Mater. Sci. Eng. C* **58**, 254–263 (2016).

157. Cheng, L. *et al.* Surface biofunctional drug-loaded electrospun fibrous scaffolds for comprehensive repairing hypertrophic scars. *Biomaterials* **83**, 169–181 (2016).

158. Liu, Y. *et al.* Polydopamine-modified poly(l-lactic acid) nanofiber scaffolds immobilized with an osteogenic growth peptide for bone tissue regeneration. *RSC Adv.* **9**, 11722–11736 (2019).

159. Hermanson, G. T. Chapter 3 - The Reactions of Bioconjugation. in (ed. Hermanson, G. T. B. T.-B. T. (Third E.) 229–258 (Academic Press, 2013). doi:https://doi.org/10.1016/B978-0-12-382239-0.00003-0.

160. Martínez-Jothar, L. *et al.* Insights into maleimide-thiol conjugation chemistry: Conditions for efficient surface functionalization of nanoparticles for receptor targeting. *J. Control. Release* **282**, 101–109 (2018).

161. Bai, M.-Y. & Liu, S.-Z. A simple and general method for preparing antibody-PEG-PLGA sub-micron particles using electrospray technique: An in vitro study of targeted delivery of cisplatin to ovarian cancer cells. *Colloids Surfaces B Biointerfaces* **117**, 346–353 (2014).

162. Hermanson, G. T. Chapter 2 - The Chemistry of Reactive Groups. in (ed. Hermanson, G. T. B. T.-B. T. (Second E.) 169–212 (Academic Press, 2008). doi:https://doi.org/10.1016/B978-0-12-370501-3.00002-3.

163. Hermanson, G. T. *Enzyme Modification and Conjugation*. *Bioconjugate Techniques* (2013). doi:10.1016/B978-0-12-382239-0.00022-4.

164. Keleştemur, S., Altunbek, M. & Culha, M. Influence of EDC/NHS coupling chemistry on stability and cytotoxicity of ZnO nanoparticles modified with proteins. *Appl. Surf. Sci.* **403**, 455–463 (2017).

165. Hermanson, G. T. Chapter 14 - Microparticles and Nanoparticles. in (ed. Hermanson, G. T. B. T.-B. T. (Third E.) 549–587 (Academic Press, 2013). doi:https://doi.org/10.1016/B978-0-12-382239-0.00014-5.

166. Staros, J. V. Membrane-impermeant crosslinking reagents: probes of the structure and dynamics of membrane proteins. *Acc. Chem. Res.* **21**, 435–441 (1988).

167. Hermanson, G. T. Zero-length crosslinkers. *Bioconjugate Tech.* **3**, 259–273 (2013).

168. Li, W. *et al.* Electrospun nanofibers immobilized with collagen for neural stem cells culture. *J. Mater. Sci. Mater. Med.* **19**, 847–854 (2008).

169. Guex, A. G. *et al.* Covalent immobilisation of VEGF on plasma-coated electrospun scaffolds for tissue engineering applications. *Colloids Surfaces B Biointerfaces* **123**, 724–733 (2014).

170. Sadeghi, A. R. *et al.* Surface modification of electrospun PLGA scaffold with collagen for bioengineered skin substitutes. *Mater. Sci. Eng. C* **66**, 130–137 (2016).

171. Schaub, N. J. *et al.* The Effect of Surface Modification of Aligned Poly-L-Lactic Acid Electrospun Fibers on Fiber Degradation and Neurite Extension. *PLoS One* **10**, e0136780–e0136780 (2015).

172. Mattanavee, W. *et al.* Immobilization of Biomolecules on the Surface of Electrospun Polycaprolactone Fibrous Scaffolds for Tissue Engineering. *ACS Appl. Mater. Interfaces* **1**, 1076–1085 (2009).

173. Boyer, C., Huang, X., Whittaker, M. R., Bulmus, V. & Davis, T. P. An overview of protein–polymer particles. *Soft Matter* **7**, 1599–1614 (2011).

174. Kolb, H. C., Finn, M. G. & Sharpless, K. B. Click Chemistry: Diverse Chemical Function from a Few Good Reactions. *Angew. Chemie Int. Ed.* **40**, 2004–2021 (2001).

175. Kolb, H. C., Finn, M. G. & Sharpless, K. B. Click Chemistry: Diverse Chemical Function from a Few Good Reactions. *Angew. Chemie - Int. Ed.* **40**, 2004–2021 (2001).

176. Kolb, H. C. & Sharpless, K. B. The growing impact of click chemistry on drug discovery. *Drug Discov. Today* **8**, 1128–1137 (2003).

177. Hein, C., Liu, X.-M. & Wang, D. Click Chemistry, a Powerful Tool for Pharmaceutical Sciences. *Pharm Res* **25**, 2216–2230 (2009).

178. Lu, J., Shi, M. & Shoichet, M. S. Click Chemistry Functionalized Polymeric Nanoparticles Target Corneal Epithelial Cells through RGD-Cell Surface Receptors. *Bioconjug. Chem.* **20**, 87–94 (2009).

179. Shokeen, M. *et al.* Evaluation of Multivalent, Functional Polymeric Nanoparticles for Imaging Applications. *ACS Nano* **5**, 738–747 (2011).

180. Kamphuis, M. M. J. *et al.* Targeting of Cancer Cells Using Click-Functionalized Polymer Capsules. *J. Am. Chem. Soc.* **132**, 15881–15883 (2010).

181. Bhaskar, S., Roh, K.-H., Jiang, X., Baker, G. L. & Lahann, J. Spatioselective Modification of Bicompartmental Polymer Particles and Fibers via Huisgen 1,3-Dipolar Cycloaddition. *Macromol. Rapid Commun.* **29**, 1655–1660 (2008).

182. Chen, R. T. *et al.* Fabrication of asymmetric 'Janus' particles via plasma polymerization. *Chem. Commun. (Camb).* **46**, 5121–5123 (2010).

183. Wang, Q. *et al.* Bioconjugation by Copper(I)-Catalyzed Azide-Alkyne [3 + 2] Cycloaddition. *J. Am. Chem. Soc.* **125**, 3192–3193 (2003).

184. Thirumurugan, P., Matosiuk, D. & Jozwiak, K. Click Chemistry for Drug Development and Diverse Chemical–Biology Applications. *Chem. Rev.* **113**, 4905–4979 (2013).

185. Hong, V., Steinmetz, N. F., Manchester, M. & Finn, M. G. Labeling Live Cells by Copper-Catalyzed Alkyne−Azide Click Chemistry. *Bioconjug. Chem.* **21**, 1912–1916 (2010).

186. Such, G. K., Johnston, A. P. R., Liang, K. & Caruso, F. Synthesis and functionalization of nanoengineered materials using click chemistry. *Prog. Polym. Sci.* **37**, 985–1003 (2012).

187. Moses, J. E. & Moorhouse, A. D. The growing applications of click chemistry. *Chem. Soc. Rev.* **36**, 1249–1262 (2007).

188. Pitt, C. G., Chasalow, F. I., Hibionada, Y. M., Klimas, D. M. & Schindler, A. Aliphatic polyesters. I. The degradation of poly(ϵ-caprolactone) in vivo. *J. Appl. Polym. Sci.* **26**, 3779–3787 (1981).

189. Chen, G., Ito, Y. & Imanishi, Y. Photo-immobilization of epidermal growth factor enhances its mitogenic effect by artificial juxtacrine signaling. *Biochim. Biophys. Acta - Mol. Cell Res.* **1358**, 200–208 (1997).

190. Zhang, Y., Ouyang, H., Lim, C. T., Ramakrishna, S. & Huang, Z.-M. Electrospinning of gelatin fibers and gelatin/PCL composite fibrous scaffolds. *J. Biomed. Mater. Res. Part B Appl. Biomater.* **72B**, 156–165 (2005).

191. Rim, N. G., Shin, C. S. & Shin, H. Current approaches to electrospun nanofibers for tissue engineering. *Biomed. Mater.* **8**, (2013).

192. Cheng, Q., Lee, B. L.-P., Komvopoulos, K., Yan, Z. & Li, S. Plasma Surface Chemical Treatment of Electrospun Poly(l-Lactide) Microfibrous Scaffolds for Enhanced Cell

Adhesion, Growth, and Infiltration. *Tissue Eng. Part A* **19**, 1188–1198 (2013).

193. Siri, S., Wadbua, P., Amornkitbamrung, V., Kampa, N. & Maensiri, S. Surface modification of electrospun PCL scaffolds by plasma treatment and addition of adhesive protein to promote fibroblast cell adhesion. *Mater. Sci. Technol.* **26**, 1292–1297 (2010).

194. Liu, W. *et al.* Effects of plasma treatment to nanofibers on initial cell adhesion and cell morphology. *Colloids Surfaces B Biointerfaces* **113**, 101–106 (2014).

195. Nandakumar, A. *et al.* Surface modification of electrospun fibre meshes by oxygen plasma for bone regeneration. *Biofabrication* **5**, 15006 (2012).

196. Abbasi, N., Soudi, S., Hayati-Roodbari, N., Dodel, M. & Soleimani, M. The Effects of Plasma Treated Electrospun Nanofibrous Poly (ε-caprolactone) Scaffolds with Different Orientations on Mouse Embryonic Stem Cell Proliferation. *Cell J.* **16**, 245–254 (2014).

197. Zandén, C. *et al.* Stem cell responses to plasma surface modified electrospun polyurethane scaffolds. *Nanomedicine Nanotechnology, Biol. Med.* **10**, e949–e958 (2014).

198. Sankar, D., Shalumon, K. T., Chennazhi, K. P., Menon, D. & Jayakumar, R. Surface Plasma Treatment of Poly(caprolactone) Micro, Nano, and Multiscale Fibrous Scaffolds for Enhanced Osteoconductivity. *Tissue Eng. Part A* **20**, 1689–1702 (2013).

199. Pritchard, D. J., Morgan, H. & Cooper, J. M. Micron-Scale Patterning of Biological Molecules. *Angew. Chemie Int. Ed. English* **34**, 91–93 (1995).

200. Hengsakul, M. & Cass, A. E. G. Protein Patterning with a Photoactivatable Derivative of Biotin. *Bioconjug. Chem.* **7**, 249–254 (1996).

201. Gérard, E. *et al.* Surface modification of poly(butylene terephthalate) nonwoven by photochemistry and biofunctionalization with peptides for blood filtration. *J. Polym. Sci. Part A Polym. Chem.* **49**, 5087–5099 (2011).

202. Yang, Y. *et al.* Homogeneous synthesis of GRGDY grafted chitosan on hydroxyl groups by photochemical reaction for improved cell adhesion. *Carbohydr. Polym.* **80**, 733–739 (2010).

203. Li, B., Chen, J. & Wang, J. H.-C. RGD peptide-conjugated poly(dimethylsiloxane) promotes adhesion, proliferation, and collagen secretion of human fibroblasts. *J. Biomed. Mater. Res. Part A* **79A**, 989–998 (2006).

204. Nakajima, H. *et al.* Photochemical Immobilization of Protein on Inner Wall of Microchannel. *Chem. Lett.* **34**, 358–359 (2005).

205. Ito, Y., Kondo, S., Chen, G. & Imanishi, Y. Patterned artificial juxtacrine stimulation of cells by covalently immobilized insulin. *FEBS Lett.* **403**, 159–162 (1997).

206. Xie, S., Sundhoro, M., Houk, K. N. & Yan, M. Electrophilic Azides for Materials Synthesis and Chemical Biology. *Acc. Chem. Res.* (2020) doi:10.1021/acs.accounts.0c00046.

207. Norberg, O., Lee, I. H., Aastrup, T., Yan, M. & Ramström, O. Photogenerated lectin sensors produced by thiol-ene/yne photo-click chemistry in aqueous solution. *Biosens. Bioelectron.* **34**, 51–56 (2012).

208. Norberg, O., Deng, L., Yan, M. & Ramstrom, O. Photo-click immobilization of carbohydrates on polymeric surfaces--a quick method to functionalize surfaces for biomolecular recognition studies. *Bioconjug. Chem.* **20**, 2364–2370 (2009).

209. Kong, N., Park, J., Yang, X., Ramström, O. & Yan, M. Carbohydrate Functionalization of Few-Layer Graphene through Microwave-Assisted Reaction of Perfluorophenyl Azide. *ACS Appl. Bio Mater.* **2**, 284–291 (2019).

210. Yan, M., Cai, S. X., Wybourne, M. N. & Keana, J. F. W. N-Hydroxysuccinimide Ester Functionalized Perfluorophenyl Azides as Novel Photoactive Heterobifunctional Crosslinking Reagents. The Covalent Immobilization of Biomolecules to Polymer Surfaces. *Bioconjug. Chem.* **5**, 151–157 (1994).

211. Maalouli, N. *et al.* Comparison of photo- and Cu(i)-catalyzed “click” chemistries for the formation of carbohydrate SPR interfaces. *Analyst* **138**, 805–812 (2013).

212. Noy, J.-M., Li, Y., Smolan, W. & Roth, P. J. Azide–para-Fluoro Substitution on Polymers: Multipurpose Precursors for Efficient Sequential Postpolymerization Modification. *Macromolecules* **52**, 3083–3091 (2019).

213. Keana, J. F. W. & Xiong Cai, S. Functionalized Perfluorophenyl Azides: New Reagents for Photoaffinity Labeling. *J. Fluor. Chem.* **43**, 151–154 (1989).

214. Wentrup, C. Chemical Activation in Azide and Nitrene Chemistry:
Methyl Azide, Phenyl Azide, Naphthyl Azides, Pyridyl Azides, Benzotriazoles, and Triazolopyridines. *Aust. J. Chem.* **66**, 852–863 (2013).

215. Siegmann, K., Inauen, J., Villamaina, D. & Winkler, M. Photografting of perfluoroalkanes onto polyethylene surfaces via azide/nitrene chemistry. *Appl. Surf.*

Sci. **396**, 672–680 (2017).

216. Liu, L. & Yan, M. Functionalization of pristine graphene with perfluorophenyl azides. 3273–3276 (2011) doi:10.1039/c0jm02765k.

217. Cai, S. X., Glenn, D. J., Kanskar, M., Wybourne, M. N. & Keana, J. F. W. Development of Highly Efficient Deep-UV and Electron Beam Mediated Cross-Linkers: Synthesis and Photolysis of Bis(perfluorophenyl) Azides. *Chem. Mater.* **6**, 1822–1829 (1994).

218. Park, J. & Yan, M. Covalent Functionalization of Graphene with Reactive Intermediates. *Acc. Chem. Res.* **46**, 181–189 (2013).

219. Poe, R., Schnapp, K., Young, M. J. T., Grayzar, J. & Platz, M. S. Chemistry and kinetics of singlet pentafluorophenylnitrene. *J. Am. Chem. Soc.* **114**, 5054–5067 (1992).

220. Liu, L.-H. & Yan, M. Perfluorophenyl Azides: New Applications in Surface Functionalization and Nanomaterial Synthesis. *Acc. Chem. Res.* **43**, 1434–1443 (2010).

221. Luetzow, K. *et al.* Perfluorophenyl azide functionalization of electrospun poly(para-dioxanone). *Polym. Adv. Technol.* **30**, 1165–1172 (2019).

222. Johansson, L. H. & Håkan Borg, L. A. A spectrophotometric method for determination of catalase activity in small tissue samples. *Anal. Biochem.* **174**, 331–336 (1988).

223. EBioscience. In Vitro T cell activation protocol. 4–7 http://tools.thermofisher.com/content/sfs/manuals/t-cell-activation-in-vitro.pdf (2013).

224. Abdelrazek, E. M., Hezma, A. M., El-khodary, A. & Elzayat, A. M. Spectroscopic studies and thermal properties of PCL/PMMA biopolymer blend. *Egypt. J. Basic Appl. Sci.* **3**, 10–15 (2016).

225. Ndugire, W., Wu, B. & Yan, M. Synthesis of carbohydrate-grafted glycopolymers using a catalyst-free, perfluoroarylazide-mediated fast staudinger reaction. *Molecules* **24**, 1–11 (2019).

226. Smith, M. T. Advances in Understanding Benzene Health Effects and Susceptibility. *Annu. Rev. Public Health* **31**, 133–148 (2010).

227. Cao, H., Mchugh, K., Chew, S. Y. & Anderson, J. M. The topographical effect of electrospun nanofibrous scaffolds on the in vivo and in vitro foreign body reaction. *J. Biomed. Mater. Res. Part A* **93A**, 1151–1159 (2010).

228. Angkawinitwong, U. Novel biopharmaceutical formulations from electrohydrodynamic

atomisation. (University College London, 2018).

229. Arnarson, T. S. & Keil, R. G. Organic–mineral interactions in marine sediments studied using density fractionation and X-ray photoelectron spectroscopy. *Org. Geochem.* **32**, 1401–1415 (2001).

230. Turner, N. H., Dunlap, B. I. & Colton, R. J. Surface analysis: x-ray photoelectron spectroscopy, Auger electron spectroscopy and secondary ion mass spectrometry. *Anal. Chem.* **56**, 373–416 (1984).

231. Zorn, G. *et al.* X-ray Photoelectron Spectroscopy Investigation of the Nitrogen Species in Photoactive Perfluorophenylazide-Modified Surfaces. *J. Phys. Chem. C* **118**, 376–383 (2014).

232. Li, L., Li, J., Kulkarni, A. & Liu, S. Polyurethane (PU)-derived photoactive and copper-free clickable surface based on perfluorophenyl azide (PFPA) chemistry. *J. Mater. Chem. B* **1**, 571–582 (2013).

233. Lee, S. Human serum albumin: A nanomedicine platform targeting breast cancer cells. *J. Drug Deliv. Sci. Technol.* **52**, 652–659 (2019).

234. Campos, A., Marconcini, J. M., Martins-Franchetti, S. M. & Mattoso, L. H. C. The influence of UV-C irradiation on the properties of thermoplastic starch and polycaprolactone biocomposite with sisal bleached fibers. *Polym. Degrad. Stab.* **97**, 1948–1955 (2012).

235. Chamouard, P. *et al.* Circulating cell-derived microparticles in Crohn's disease. *Dig. Dis. Sci.* **50**, 574–580 (2005).

236. Minor, D. R., Chin, K. & Kashani-Sabet, M. Infliximab in the Treatment of Anti-CTLA4 Antibody (Ipilimumab) Induced Immune-Related Colitis. *Cancer Biother. Radiopharm.* **24**, 321–325 (2009).

237. Montfort, A. *et al.* Anti-TNF, a magic bullet in cancer immunotherapy? *J. Immunother. Cancer* **7**, 303 (2019).

238. Yanai, S., Nakamura, S. & Matsumoto, T. Nivolumab-Induced Colitis Treated by Infliximab. *Clin. Gastroenterol. Hepatol.* **15**, e80–e81 (2017).

239. Hadwan, M. H. Simple spectrophotometric assay for measuring catalase activity in biological tissues. *BMC Biochem.* **19**, 7 (2018).

240. Li, Y. & Schellhorn, H. E. Rapid kinetic microassay for catalase activity. *J. Biomol. Tech.* **18**, 185–187 (2007).

241. Absolom, D. R., Zingg, W. & Neumann, A. W. Protein adsorption to polymer particles: Role of surface properties. *J. Biomed. Mater. Res.* **21**, 161–171 (1987).

242. Ogueri, K. S., Jafari, T., Escobar Ivirico, J. L. & Laurencin, C. T. Polymeric Biomaterials for Scaffold-Based Bone Regenerative Engineering. *Regen. Eng. Transl. Med.* **5**, 128–154 (2019).

243. Im, J. S., Yun, J., Lim, Y.-M., Kim, H.-I. & Lee, Y.-S. Fluorination of electrospun hydrogel fibers for a controlled release drug delivery system. *Acta Biomater.* **6**, 102–109 (2010).

244. Niino, H., Koga, Y. & Yabe, A. Surface reaction of organic materials by laser ablation of matrix-isolated photoreactive aromatic azido compound. *J. Photochem. Photobiol. A Chem.* **106**, 9–13 (1997).

245. Malikmammadov, E., Tanir, T. E., Kiziltay, A., Hasirci, V. & Hasirci, N. PCL and PCL-based materials in biomedical applications. *J. Biomater. Sci. Polym. Ed.* **29**, 863–893 (2018).

246. Guerra, A. J., Cano, P., Rabionet, M., Puig, T. & Ciurana, J. Effects of different sterilization processes on the properties of a novel 3D-printed polycaprolactone stent. *Polym. Adv. Technol.* **29**, 2327–2335 (2018).

247. Pavlova, E. R. *et al.* Poly(hydroxybutyrate-co-hydroxyvalerate) and bovine serum albumin blend prepared by electrospinning. *J. Appl. Polym. Sci.* **134**, 45090 (2017).

248. Wang, J. & Windbergs, M. Controlled dual drug release by coaxial electrospun fibers – Impact of the core fluid on drug encapsulation and release. *Int. J. Pharm.* **556**, 363–371 (2019).

249. Gian, B., Gaetani, F., Kirkman, H. N., Mangerini, R. & Ferraris, A. M. Importance of Catalase in the Disposal of Hydrogen Peroxide Within Human Erythrocytes. **84**, 325–330 (1994).

250. Cheung, A. S., Zhang, D. K. Y., Koshy, S. T. & Mooney, D. J. Scaffolds that mimic antigen-presenting cells enable ex vivo expansion of primary T cells. *Nat. Biotechnol.* **36**, 160–169 (2018).

251. Zhang, D. K. Y., Cheung, A. S. & Mooney, D. J. Activation and expansion of human T cells using artificial antigen-presenting cell scaffolds. *Nat. Protoc.* **15**, 773–798 (2020).

252. Hirano, B. Y. & Mooney, D. J. Peptide and Protein Presenting Materials for Tissue Engineering **. 17–25 (2004) doi:10.1002/adma.200300383.

253. Cope, A. P. *et al.* Chronic exposure to tumor necrosis factor (TNF) in vitro impairs the activation of T cells through the T cell receptor/CD3 complex; reversal in vivo by anti-TNF antibodies in patients with rheumatoid arthritis. *J. Clin. Invest.* **94**, 749–760 (1994).

254. Gamero, A. M. & Larner, A. C. Signaling via the T cell antigen receptor induces phosphorylation of Stat1 on Serine 727. *J. Biol. Chem.* **275**, 16574–16578 (2000).

255. Steenblock, E. R. & Fahmy, T. M. A comprehensive platform for ex vivo T-cell expansion based on biodegradable polymeric artificial antigen-presenting cells. *Mol. Ther.* **16**, 765–772 (2008).

256. Meyer, R. A. *et al.* Biodegradable Nanoellipsoidal Artificial Antigen Presenting Cells for Antigen Specific T-Cell Activation. *Small* **11**, 1519–1525 (2015).

257. Sawawi, M., Wang, T. Y., Nisbet, D. R. & Simon, G. P. Scission of electrospun polymer fibres by ultrasonication. *Polymer (Guildf).* **54**, 4237–4252 (2013).

258. Deniz, A. E., Celebioglu, A., Kayaci, F. & Uyar, T. Electrospun polymeric nanofibrous composites containing TiO2 short nanofibers. *Mater. Chem. Phys.* **129**, 701–704 (2011).

259. Chung, H. J. & Park, T. G. Surface engineered and drug releasing pre-fabricated scaffolds for tissue engineering. *Adv. Drug Deliv. Rev.* **59**, 249–262 (2007).

260. Ma, Z., Gao, C., Gong, Y. & Shen, J. Cartilage tissue engineering PLLA scaffold with surface immobilized collagen and basic fibroblast growth factor. *Biomaterials* **26**, 1253–1259 (2005).

261. FDA. FDA webpage entry on Kymriah. https://www.fda.gov/BiologicsBloodVaccines/CellularGeneTherapyProducts/ApprovedProducts/ucm573706.htm.

262. FDA. FDA webpage entry on Yeskarta. https://www.fda.gov/biologicsbloodvaccines/cellulargenetherapyproducts/approvedproducts/ucm581222.htm.

263. Eggermont, L. J., Paulis, L. E., Tel, J. & Figdor, C. G. Towards efficient cancer immunotherapy: Advances in developing artificial antigen-presenting cells. *Trends Biotechnol.* **32**, 456–465 (2014).

264. Sunshine, J. C. & Green, J. J. Nanoengineering approaches to the design of artificial antigen-presenting cells. *Nanomedicine (Lond).* **8**, 1173–1189 (2013).

265. Sunshine, J. C., Perica, K., Schneck, J. P. & Green, J. J. Particle shape dependence of CD8+ T cell activation by artificial antigen presenting cells. *Biomaterials* **35**, 269–277 (2014).

266. Perica, K., Kosmides, A. K. & Schneck, J. P. Linking form to function: Biophysical aspects of artificial antigen presenting cell design. *Biochim. Biophys. Acta - Mol. Cell Res.* **1853**, 781–790 (2015).

267. Kosmides, A. K. *et al.* Biomimetic biodegradable artificial antigen presenting cells synergize with PD-1 blockade to treat melanoma. *Biomaterials* **118**, 16–26 (2017).

268. Durai, M. *et al.* In vivo functional efficacy of tumor-specific T cells expanded using HLA-Ig based artificial antigen presenting cells (aAPC). *Cancer Immunol. Immunother.* **58**, 209–220 (2009).

269. Wang, W. *et al.* A biodegradable killer microparticle to selectively deplete antigen-specific T cells in vitro and in vivo . *Oncotarget; Vol 7, No 11* (2016).

270. Ben-Akiva, E., Est Witte, S., Meyer, R. A., Rhodes, K. R. & Green, J. J. Polymeric micro- and nanoparticles for immune modulation. *Biomater. Sci.* **7**, 14–30 (2019).

271. Meyer, R. A., Sunshine, J. C. & Green, J. J. Biomimetic particles as therapeutics. *Trends Biotechnol.* **33**, 514–524 (2015).

272. Rudolf, D. *et al.* Potent costimulation of human CD8 T cells by anti-4-1BB and anti-CD28 on synthetic artificial antigen presenting cells. *Cancer Immunol. Immunother.* **57**, 175–183 (2008).

273. Steenblock, E. R., Fadel, T., Labowsky, M., Pober, J. S. & Fahmy, T. M. An artificial antigen-presenting cell with paracrine delivery of IL-2 impacts the magnitude and direction of the T cell response. *J. Biol. Chem.* **286**, 34883–34892 (2011).

274. Zhang, L. *et al.* An Artificial Antigen-Presenting Cell Delivering 11 Immune Molecules Expands Tumor Antigen–Specific CTLs in Ex Vivo and In Vivo Murine Melanoma Models. *Cancer Immunol. Res.* **7**, 1188 LP – 1201 (2019).

275. Curtsinger, J., Deeths, M. J., Pease, P. & Mescher, M. F. Artificial cell surface constructs for studying receptor-ligand contributions to lymphocyte activation. *J. Immunol. Methods* **209**, 47–57 (1997).

276. Mescher, M. F. *et al.* Signals required for programming effector and memory development by CD8+ T cells. *Immunol. Rev.* **211**, 81–92 (2006).

277. Tasnim, H. *et al.* Quantitative Measurement of Naïve T Cell Association With Dendritic Cells, FRCs, and Blood Vessels in Lymph Nodes . *Frontiers in Immunology* vol. 9 1571 (2018).

278. Dumortier, H. *et al.* Antigen Presentation by an Immature Myeloid Dendritic Cell Line Does Not Cause CTL Deletion In Vivo, but Generates CD8⁺ Central Memory-Like T Cells That Can Be Rescued for Full Effector Function. *J. Immunol.* **175**, 855 LP – 863 (2005).

279. Fahmy, T. M., Samstein, R. M., Harness, C. C. & Saltzman, W. M. Surface modification of biodegradable polyesters with fatty acid conjugates for improved drug targeting. *Biomaterials* **26**, 5727–5736 (2005).

280. Fifis, T. *et al.* Size-Dependent Immunogenicity: Therapeutic and Protective Properties of Nano-Vaccines against Tumors. *J. Immunol.* **173**, 3148 LP – 3154 (2004).

281. Busolo M.A. A4 - Torres-Giner, S. A4 - Prieto, C. A4 - Lagaron, J.M., M. A. A.-B. Electrospraying assisted by pressurized gas as an innovative high-throughput process for the microencapsulation and stabilization of docosahexaenoic acid-enriched fish oil in zein prolamine. *Innov. food Sci. Emerg. Technol.* **v. 51**, 12-19–2019 v.51 (2019).

282. Express, F. Proliferation Statistics. https://fcsexpressdownloads.s3.amazonaws.com/manual/manual_IVD/index.html?proliferation_statistics.htm.

283. Champion, J. A., Katare, Y. K. & Mitragotri, S. Particle shape: A new design parameter for micro- and nanoscale drug delivery carriers. *J. Control. Release* **121**, 3–9 (2007).

284. Zhou, F.-L., Hubbard Cristinacce, P. L., Eichhorn, S. J. & Parker, G. J. M. Preparation and characterization of polycaprolactone microspheres by electrospraying. *Aerosol Sci. Technol.* **50**, 1201–1215 (2016).

285. Kostakova, E., Seps, M., Pokorny, P. & Lukas, D. Study of polycaprolactone wet electrospinning process. *Express Polym. Lett.* **8**, 554–564 (2014).

286. Zhou, F.-L., Chirazi, A., Gough, J. E., Hubbard Cristinacce, P. L. & Parker, G. J. M. Hollow Polycaprolactone Microspheres with/without a Single Surface Hole by Co-Electrospraying. *Langmuir* **33**, 13262–13271 (2017).

287. Wright, B., Parmar, N., Bozec, L., Aguayo, S. D. & Day, R. M. A simple and robust method for pre-wetting poly (lactic-co-glycolic) acid microspheres. *J. Biomater. Appl.* **30**, 147–159 (2015).

288. Huang, Y. X., Ren, J., Chen, C., Ren, T. B. & Zhou, X. Y. Preparation and properties of poly(lactide-co-glycolide) (PLGA)/ Nano-Hydroxyapatite (NHA) scaffolds by thermally induced phase separation and rabbit MSCs culture on scaffolds. *J. Biomater. Appl.* **22**, 409–432 (2008).

289. Liu, G., Miao, X., Fan, W., Crawford, R. & Xiao, Y. Porous PLGA Microspheres Effectively Loaded with BSA Protein by Electrospraying Combined with Phase Separation in Liquid Nitrogen. *J. Biomimetics, Biomater. Tissue Eng.* **6**, 1–18 (2010).

290. Sahay, R., Thavasi, V. & Ramakrishna, S. Design Modifications in Electrospinning Setup for Advanced Applications. *J. Nanomater.* **2011**, 317673 (2011).

291. Prieto, C. & Lagaron, J. M. Nanodroplets of docosahexaenoic acid-enriched algae oil encapsulated within microparticles of hydrocolloids by emulsion electrospraying assisted by pressurized gas. *Nanomaterials* **10**, (2020).

292. Bartelt, R. R., Cruz-Orcutt, N., Collins, M. & Houtman, J. C. D. Comparison of T Cell Receptor-Induced Proximal Signaling and Downstream Functions in Immortalized and Primary T Cells. *PLoS One* **4**, e5430 (2009).

293. Guerin, T. F., Mondido, M., McClenn, B. & Peasley, B. Application of resazurin for estimating abundance of contaminant-degrading micro-organisms. *Lett. Appl. Microbiol.* **32**, 340–345 (2001).

294. Shipkova, M. & Wieland, E. Surface markers of lymphocyte activation and markers of cell proliferation. *Clin. Chim. Acta* **413**, 1338–1349 (2012).

295. Saraiva, M. *et al.* Interleukin-10 Production by Th1 Cells Requires Interleukin-12-Induced STAT4 Transcription Factor and ERK MAP Kinase Activation by High Antigen Dose. *Immunity* **31**, 209–219 (2009).

296. Carcaboso, A. M. *et al.* Potent, long lasting systemic antibody levels and mixed Th1/Th2 immune response after nasal immunization with malaria antigen loaded PLGA microparticles. *Vaccine* **22**, 1423–1432 (2004).

297. Tau, G. Z., Cowan, S. N., Weisburg, J., Braunstein, N. S. & Rothman, P. B. Regulation of IFN-gamma signaling is essential for the cytotoxic activity of CD8(+) T cells. *J. Immunol.* **167**, 5574–5582 (2001).

298. Santis, A. G. *et al.* Tumor necrosis factor-α production induced in T lymphocytes through the AIM/CD69 activation pathway. *Eur. J. Immunol.* **22**, 1253–1259 (1992).

299. Sethi, G., Sung, B. & Aggarwal, B. B. TNF: a master switch for inflammation to cancer.

Front. Biosci. **13**, 5094–5107 (2008).

300. Ross, S. H. & Cantrell, D. A. Signaling and Function of Interleukin-2 in T Lymphocytes. *Annu. Rev. Immunol.* **36**, 411–433 (2018).

301. Hilchey, S. P. & Bernstein, S. H. Use of CFSE to Monitor Ex Vivo Regulatory T-cell Suppression of CD4+ and CD8+ T-cell Proliferation within Unseparated Mononuclear Cells from Malignant and Non-Malignant Human Lymph Node Biopsies. *Immunol. Invest.* **36**, 629–648 (2007).

302. Fulcher, D. A. & Wong, S. W. J. Carboxyfluorescein succinimidyl ester-based proliferative assays for assessment of T cell function in the diagnostic laboratory. *Immunol. Cell Biol.* **77**, 559–564 (1999).

303. Pattanapanyasat, K., Kyle, D. E., Tongtawe, P., Yongvanitchit, K. & Fucharoen, S. Flow cytometric immunophenotyping of lymphocyte subsets in samples that contain a high proportion of non-lymphoid cells. *Cytometry* **18**, 199–208 (1994).

304. Ten Brinke, A. *et al.* Monitoring T-Cell Responses in Translational Studies: Optimization of Dye-Based Proliferation Assay for Evaluation of Antigen-Specific Responses . *Frontiers in Immunology* vol. 8 1870 (2017).

305. Konigsberg, W. B. T.-M. in E. [13] Reduction of disulfide bonds in proteins with dithiothreitol. in *Enzyme Structure, Part B* vol. 25 185–188 (Academic Press, 1972).

306. Khalili, H., Godwin, A., Choi, J., Lever, R. & Brocchini, S. Comparative binding of disulfide-bridged PEG-Fabs. *Bioconjug. Chem.* **23**, 2262–2277 (2012).

307. Brocchini, S. *et al.* Disulfide bridge based PEGylation of proteins. *Adv. Drug Deliv. Rev.* **60**, 3–12 (2008).

308. Badescu, G. *et al.* Bridging disulfides for stable and defined antibody drug conjugates. *Bioconjug. Chem.* **25**, 1124–1136 (2014).

309. Balan, S. *et al.* Site-specific PEGylation of protein disulfide bonds using a three-carbon bridge. *Bioconjug. Chem.* **18**, 61–76 (2007).

310. Jung, S. & Yi, H. Facile Strategy for Protein Conjugation with Chitosan-Poly(ethylene glycol) Hybrid Microparticle Platforms via Strain-Promoted Alkyne–Azide Cycloaddition (SPAAC) Reaction. *Biomacromolecules* **14**, 3892–3902 (2013).

311. Lallana, E., Fernandez-Megia, E. & Riguera, R. Surpassing the Use of Copper in the Click Functionalization of Polymeric Nanostructures: A Strain-Promoted Approach. *J. Am. Chem. Soc.* **131**, 5748–5750 (2009).

312. Walden, G. *et al.* Synthesis and Fabrication of Surface-Active Microparticles Using a Membrane Emulsion Technique and Conjugation of Model Protein via Strain-Promoted Azide–Alkyne Click Chemistry in Physiological Conditions. *Bioconjug. Chem.* (2019) doi:10.1021/acs.bioconjchem.8b00868.

313. Blaker, J. J., Knowles, J. C. & Day, R. M. Novel fabrication techniques to produce microspheres by thermally induced phase separation for tissue engineering and drug delivery. *Acta Biomater.* **4**, 264–272 (2008).

314. Sigma-Aldrich. IR spectrum table. https://www.sigmaaldrich.com/technical-documents/articles/biology/ir-spectrum-table.html.

315. Jones, J. A., Starkey, J. R. & Kleinhofs, A. Toxicity and mutagenicity of sodium azide in mammalian cell cultures. *Mutat. Res. Toxicol.* **77**, 293–299 (1980).

316. Ruizendaal, L. *et al.* Synthesis and cytotoxicity of silicon nanoparticles with covalently attached organic monolayers. *Nanotoxicology* **3**, 339–347 (2009).

317. Khalili, H. *et al.* Fab-PEG-Fab as a Potential Antibody Mimetic. *Bioconjug. Chem.* **24**, 1870–1882 (2013).

318. Chatenoud, L. *et al.* Restriction of the human in vivo immune response against the mouse monoclonal antibody OKT3. *J. Immunol.* **137**, 830 LP – 838 (1986).

319. Pabst, M. *et al.* Modulation of drug-linker design to enhance in vivo potency of homogeneous antibody-drug conjugates. *J. Control. Release* **253**, 160–164 (2017).

320. Vidarsson, G., Dekkers, G. & Rispens, T. IgG subclasses and allotypes: from structure to effector functions. *Front. Immunol.* **5**, 520 (2014).

321. Bryant, P. *et al.* In Vitro and In Vivo Evaluation of Cysteine Rebridged Trastuzumab–MMAE Antibody Drug Conjugates with Defined Drug-to-Antibody Ratios. *Mol. Pharm.* **12**, 1872–1879 (2015).

322. Braun, A. C., Gutmann, M., Lühmann, T. & Meinel, L. Bioorthogonal strategies for site-directed decoration of biomaterials with therapeutic proteins. *J. Control. Release* **273**, 68–85 (2018).

323. Nogueira, J. C. F. *et al.* Functionalised thermally induced phase separation (TIPS) microparticles enabled for “click” chemistry. *Org. Biomol. Chem.* **18**, 2215–2218 (2020).

324. Leach, D. G., Young, S. & Hartgerink, J. D. Advances in immunotherapy delivery from implantable and injectable biomaterials. *Acta Biomater.* **88**, 15–31 (2019).

325. Brudno, Y. *et al.* Replenishable drug depot to combat post-resection cancer recurrence. *Biomaterials* **178**, 373–382 (2018).

326. Chew, S. A. & Danti, S. Biomaterial-Based Implantable Devices for Cancer Therapy. *Adv. Healthc. Mater.* **6**, 1600766 (2017).

327. Hu, D. *et al.* Improving safety of cancer immunotherapy via delivery technology. *Biomaterials* **265**, 120407 (2021).

328. NICE. Ipilimumab for previously treated advanced (unresectable or metastatic) melanoma. https://www.nice.org.uk/guidance/ta268 (2020).

329. Khodadadi, M. *et al.* Recent advances in electrospun nanofiber-mediated drug delivery strategies for localized cancer chemotherapy. *J. Biomed. Mater. Res. Part A* **108**, 1444–1458 (2020).

330. Abid, S., Hussain, T., Raza, Z. A. & Nazir, A. Current applications of electrospun polymeric nanofibers in cancer therapy. *Mater. Sci. Eng. C* **97**, 966–977 (2019).

331. Gandhi, M., Srikar, R., Yarin, A. L., Megaridis, C. M. & Gemeinhart, R. A. Mechanistic Examination of Protein Release from Polymer Nanofibers. *Mol. Pharm.* **6**, 641–647 (2009).

332. Vlasak, J. & Ionescu, R. Fragmentation of monoclonal antibodies. *MAbs* **3**, 253–263 (2011).

333. Daugherty, A. L. & Mrsny, R. J. Formulation and delivery issues for monoclonal antibody therapeutics. *Adv. Drug Deliv. Rev.* **58**, 686–706 (2006).

334. CAR-T cell therapy ClinicalTrials.gov search. *clinicaltrials.gov* https://www.clinicaltrials.gov/ct2/results/details?term=car-t+cell.